5-18-2007

Flow-Transport Modeling and Quantification

Karim El Kheiashy
University of New Orleans

Flow-Transport Modeling and Quantification of the Periodic Nature of Bed Forms in the Lower Mississippi River

A Dissertation

Submitted to the Graduate Faculty of the
University of New Orleans
in partial fulfillment of the
requirements for the degree of

Doctor of Philosophy
in
Engineering and Applied Science

by

Karim El Kheiashy

B.S. Ain Shams University, 2000
M.S. University of Louisiana at Lafayette, 2003

May 2007

ACKNOWLEDGMENT

First and foremost I would like to thank my advisor Prof. Alex McCorquodale for his never ended support that made this research possible. I would also like to thank Dr. Ioannis Georgiou, for his continuing help and being always present for discussions. I gratefully acknowledge all the efforts that Dr. Ehab Meselhe had done for me, from providing the data needed for the research and giving me a space to do my research in Lafayette at the Center of Louisiana Inland Water Studies. Special Thanks go to all my PhD committee members, Dr. Donald Barbe, Dr. Alim Hannoura and Dr. Denise Reed for their valuable input on this research.

Special thanks go to the United States Army Corps of Engineers for providing the data needed for this research.

Special thanks go to the Danish Hydraulic Institute (DHI) and Hay & Company consultants (HAYCO) for providing their proprietary models (MIKE 3 & H3D respectively), and HydroQual who developed the ECOMSED model.

I owe special thanks to my fiancée Heidi for her patience, love, and encouragement during these years of my studies. Special thanks for my mom and dad, without their prayers, I could not have done this. I would also like to thank my uncle and aunt for their support during my stay in Lafayette. Thanks God for Everything.

TABLE OF CONTENTS

LIST OF FIGURES

LIST OF TABLES

ABSTRACT

Several research investigations have been conducted on the flow and sediment transport over bed forms in alluvial rivers (e.g. mean flow field, turbulence, shear partitioning, bed load transport and bed form geometry). Much of this work was either laboratory studies or small scale field investigations. Recently, advances in technology have improved the way data are collected and analyzed, e.g. flow data, velocity data and detailed bathymetric information that provide greater knowledge about the bed form geometry. Recent advances in computing power have also reduced the computational restrictions on using three dimensional numerical models in modeling flow applications to predict the temporal and spatial changes of flow and sediment environments.

The work performed in this research quantified the periodic nature of bed forms types and geometries along the Lower Mississippi River. Correlations were performed relating the hydrodynamics of the river to the bed form types and geometries. The research work showed the inability of hydrostatic numerical modeling systems to accurately predict flow separation at the bed form crest but indicated that these models could reasonably predict the out of phase relationship between the bed form and the water surface profile. Furthermore the hydrostatic models predicted the total bed resistance as adequately as the non-hydrostatic models. It was found that non-hydrostatic models are required to properly simulate flow separation at bed form crests. Models such as MIKE 3 with constant z-level vertical discretization failed to capture the observed boundary layers unless very fine grids are used. A new procedure was developed as a part of this research, in which relations and dependencies between the hydrodynamic resistance and the bed form dimensions relative to the numerical model spatial scale were derived. This procedure can be used to aid in numerical riverine model calibration and to provide a better representation of flow resistance in hydrodynamic modeling codes.

CHAPTER 1
INTRODUCTION

There is a dynamic relationship between the hydrodynamics and the morphology of mobile bed in rivers with non-cohesive bed material. The interaction of flow and sediment results in a variety of undulations of the bed which in turn affect the nature of the flow. Consider a flat and even, stationary bed consisting of loose, non-cohesive, and mobile solid particles of uniform size. Once flow is introduced, bed forms will start to form by the action of the water on the bed material. The changing geometry of these molded bed forms depends on various flow parameters and in turn these various flow parameters are influenced by the bed forms resulting in a very complex flow-sediment environment.

The goal of this research is to understand the relationship between flow and bed form geometry in alluvial rivers. All data used in this study were collected from the Lower Mississippi River.

1.1 THE MISSISSIPPI RIVER

The Mississippi River has the third largest drainage basin in the world, exceeded in size only by the watersheds of the Amazon and Congo Rivers. It drains 41 percent of the 48 contiguous states of the United States. The basin covers more than 1,245,000 square miles, includes all or parts of 31 states and two Canadian provinces.

The Lower Mississippi River Basin (Mississippi Alluvial Valley) (Figure 1.1) extends 954 river miles from the confluence of the Ohio and Mississippi rivers at Cairo, Illinois to the Gulf of Mexico.

The Mississippi Alluvial Valley covers a portion of six states: Mississippi, Tennessee, Kentucky, Missouri, Arkansas and Louisiana. The area consists of over 115 counties. The alluvial valley ranges from 30 to 110 miles wide and encompasses approximately 22 million acres. Wetlands comprise 28% of the total surface area. Agriculture, aquaculture and commercial fisheries at the coastal wetlands are the major land uses.

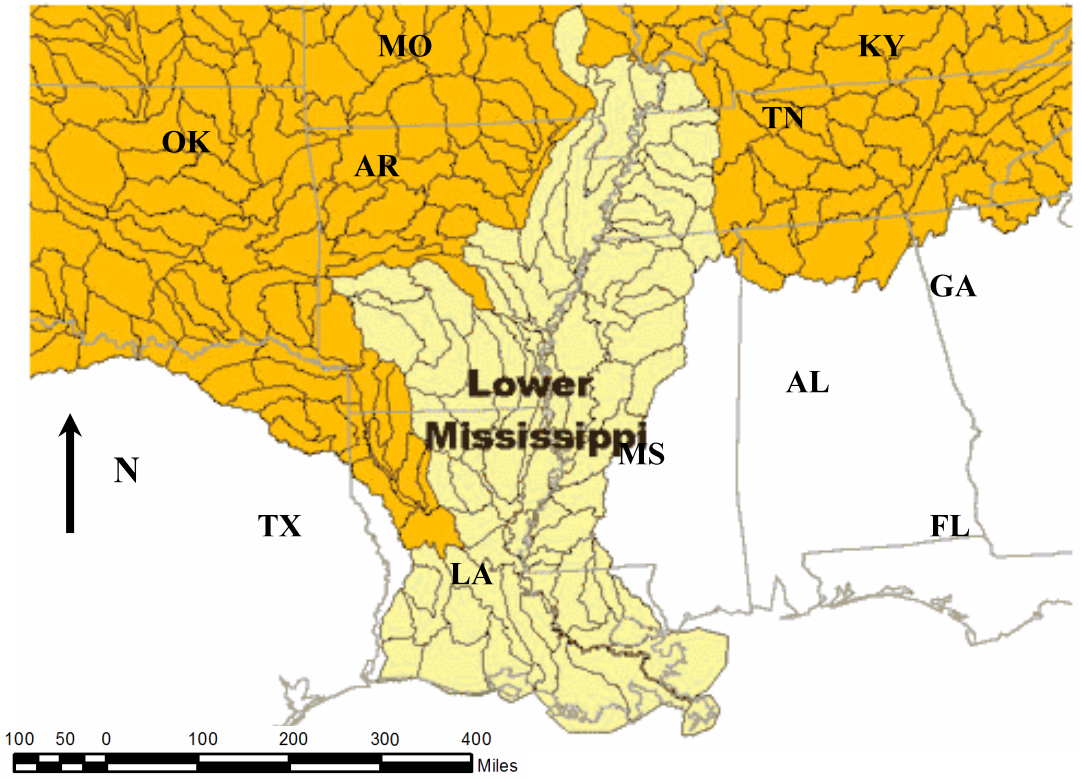

Figure 1.1 Lower Mississippi River basin (adapted from Daigle, D., 2006)

1.2 BED FORMS OF ALLUVIAL RIVERS

An alluvial river like the Mississippi River is defined as a stream that transports gravel, sands or/and clays. Alluvial rivers normally have an aspect ratio (width to depth) of 10 or greater (Yalin and da Silva, 2001).

One of the major characteristics of alluvial rivers is that their channel geometry is not only affected by the magnitude of the discharge, but also by the amount of sediment being transported. The river discharge causes a change in the river sediment transport and in turn, the channel bed geometry responds to this change. This causes a change in the water level elevation and thus another change in the sediment transport. The resulting bed forms appear in two flow regimes, lower-flow regime and upper-flow regime.

Bed forms in the lower-flow regimes, with Froude number ($Fr = \frac{U}{\sqrt{gh}}$, where, U is the mean velocity; g is the acceleration of gravity; h is the mean flow depth) generally less than 1, are as follows: ripples, dunes, washed out dunes (also called transition dunes). With higher velocities, the lower-flow regime transitions into the upper flow regime (Froude number near or greater than 1), which has the following bed forms: plane bed, anti-dunes, and chutes and pools (Simons and Richardson, 1966).

Once bed forms appear, streamlines near the bed may not conform to the bed surface, especially in the case of ripples and dunes where the flow separates at the crest of the bed form so that there is a pressure gradient between the downstream and upstream faces of the bed form. The net force thus produced is the form resistance of the bed form. As a major component of resistance, form resistance changes as the flow conditions change. Hence, the effective 'friction' factor in an alluvial river varies with flow conditions.

During the transformation of a sand bed from a flat bed to ripples, and subsequently to dunes, the resistance to flow tends to increase. Then resistance decreases as the dunes are washed out at higher discharges. At even higher velocities, nearly symmetrical sand waves (anti-dunes) form

with little or no flow separation at the crests. Therefore, the form resistance is smaller than that for dunes. The energy loss is more than that for a plane bed, because the breaking of the sand waves generates a strong local turbulence that dissipates part of the flow energy. Energy must also be expended to transport the increased bed material load. Flow separation occurs near the crest of the bed forms followed by a reattachment of the flow on the next downstream bed form. At the reattachment point, a new internal boundary layer begins to grow within the wake region. The formation of bed forms, and concurrent effects on flow, result in an additional resistance component termed form resistance.

1.3. PRESENT STUDY

1.3.1. RESEARCH NEEDS AND MOTIVATIONS

Extensive research has been conducted on the flow and sediment transport over bed forms in alluvial rivers (e.g. mean flow field, turbulence, shear partitioning, bed load transport, bed form geometry) as outlined in Chapter Two. Much of this work was either laboratory studies or small scale field investigations. Recently (1990s), advances in technology have improved the way data are collected and analyzed, e.g. flow data, velocity data and detailed bathymetric information, providing greater knowledge about the bed form geometry, which permits a more intensive study of the issues raised by a number of researchers, such as:

Kennedy and Karim (1990) stated the following about the necessity of more detailed data when modeling flow and transport over bed forms: "*models that are significantly more accurate than those that have already been developed, including those presented herein, likely will not be*

forthcoming until more accurate and more comprehensive field and laboratory data are available".

American Society of Civil Engineers (ASCE) Task Committee on Flow and Transport over Dunes (2002) reported the following conclusions *"Field studies with detailed measurements of not only dune characteristics but also flow and transport are valuable and daunting for the same reason: they indicate the complexity of the real problem, which together with practical constrains on field measurements, make more difficult the analysis and interpretation of the data".*

Technological advances in river bottom mapping and data collection devices such as multi-dimensional surveys of the riverbed (also called Multibeam Bathymetric Surveys) and advanced velocity measurements (Acoustic Doppler Current Profiler- ADCP) represent an opportunity for researchers to overcome some of these hurdles, as they can provide information that could have never been acquired with older technology. In addition, advances in computing power have also eased the restrictions of utilizing three dimensional numerical models in modeling flow applications. Riverine numerical models can be used to predict the temporal changes of flow and sediment environments providing valuable information to researchers.

Riverine modeling applications can be grouped into 1-D (cross-sectionally averaged), 2-D (depth-averaged), 3-D (hydrostatic) and 3-D (non-hydrostatic) models. Lane et al. (1999) stated that a 3-D model is necessary for predicting sediment erosion and deposition whenever

significant secondary currents exist or the ratio of vertical flows to the horizontal flows is significant, such as in river bends, flow over bed forms, crossings, distributaries, or diversions.

Olsen and Stokseth (1995) carried out a 3-D simulation of an 80-m long reach of the river Sokna in Norway. The model successfully predicted the flow features and the results were in good agreement with observed data. Sinha et al. (1998) performed a comprehensive numerical study of flow through a 4-km reach of the Columbia River. They modeled both rapidly varying bed topography and the presence of multiple islands. Their results agreed well with experiments and field measurements.

Bradbrook et al. (2000) modeled the flow in a natural river channel confluence. The model simulated periodic flow features in river confluences and agreed well with experimental data. Gesseler et al. (1999) applied the U.S. Army Corps of Engineers code CH3D-SED to the Deep Draft Navigation project on the lower Mississippi River. The code predicted the sediment deposition in the river matching with the observations in the field.
Holly and Spasojevic (1994) applied the CH3D-SED code to study water and sediment diversion at the Old River Control complex on the lower Mississippi river.

1.3.2. HYPOTHESES

The following *hypotheses* are proposed in this dissertation:

HYPOTHESIS ONE: The resistance to the flow in alluvial rivers such as the Lower Mississippi River is a function of the bed form geometry and varies by River Mile;

HYPOTHESIS TWO: Three dimensional hydrostatic numerical models are capable of simulating the resistance to flow past bed forms;

HYPOTHESIS THREE: The scale of bed forms relative to the spatial resolution in a numerical model affects the hydrodynamic resistance in the model.

1.3.3 GOALS AND OBJECTIVES OF THIS STUDY

The main task in this research is to investigate the complex nature of bed forms in a large alluvial river such as the Lower Mississippi River for the purpose of establishing appropriate relations and dependencies between the hydraulics of the river and its ability to transport sediment.
The following specific objectives are proposed to test the hypotheses of this dissertation:

1. Quantifying the periodic nature of bed forms types and geometries along the route of the river.
2. Quantifying the effect of bed forms geometries on the hydrodynamics and the transport capacities of the river and not vice versa.
3. Evaluating the applicability of hydrostatic and non-hydrostatic numerical modeling systems to accurately predict the flow resistance and transport environment over bed forms.
4. Developing a new procedure intended to aid in numerical riverine models calibration and providing a better representation of flow resistance in hydrodynamic and sediment transport modeling codes.

1.4. ORGANIZATION OF THE DISSERTATION

Chapter Two (Literature Review and Theoretical Background) presents a comprehensive review of the literature related to the topic of bed form and resistance in alluvial rivers, **Chapter Three (Data Analysis and Assessment)** describes in details the methodology used to capture and characterize the periodic character of bed forms in the Lower Mississippi River and the effect of bed form types and geometries on the hydrodynamics properties of the river**, Chapter Four (Numerical Modeling of Flow and Transport over Bed Forms)** addresses the applicability of several numerical modeling systems to correctly predict the flow and transport structure over bed forms**, Chapter Five (Applications and Correlations)** details the methodology followed in the generation of a calibration tool to better represent the flow resistance in hydrodynamics and sediment transport modeling codes. **Chapter Six (Discussions and Recommendations)** presents detailed discussions of the results obtained in the previous chapters and presents recommendations for future work. **Chapter Seven (Conclusions)** presents closing remarks and final conclusions for the research presented in this study.

CHAPTER 2
LITERATURE REVIEW AND THEORETICAL BACKGROUND

2.1 INTRODUCTION

Simons et al. (1965) proposed a classification system for bed forms, shown in Table 2.1 and Figure 2.1. Their data were based on an extensive dataset of laboratory studies on bed forms performed by the U.S. Geological Survey at Colorado State University in the 1950s and 1960s. They compared the bed form geometry to the flow regime (Froude number) where the bed forms exist as shown in Table 2.1.

However later field studies by Simons showed that the use of Froude number as a classification method was not the optimum decision due to the variable nature of the Froude number across the channel cross section.

Flow regime	Bed form type	Bed material concentrations, ppm	Mode of sediment transport	Type of roughness	Roughness, $\frac{C}{\sqrt{g}}$
Lower regime	Ripples Ripples on dunes Dunes	10-200 100-1,200 200-2,000	Discrete steps	Form roughness predominates	7.8-12.4 -- 7.0-13.2
Transition	Washed-out dunes	1,000-3,000		Variable	7.0-20.0
Upper regime	Plane beds Antidunes Chutes and pools	2,000-6,000 >2,000 >2,000	Continuous	Grain roughness predominates	16.3-20 10.8-20 9.4-10.7

Table 2.1 Classification of bed forms and other information [Simons and Richardson (1966)]

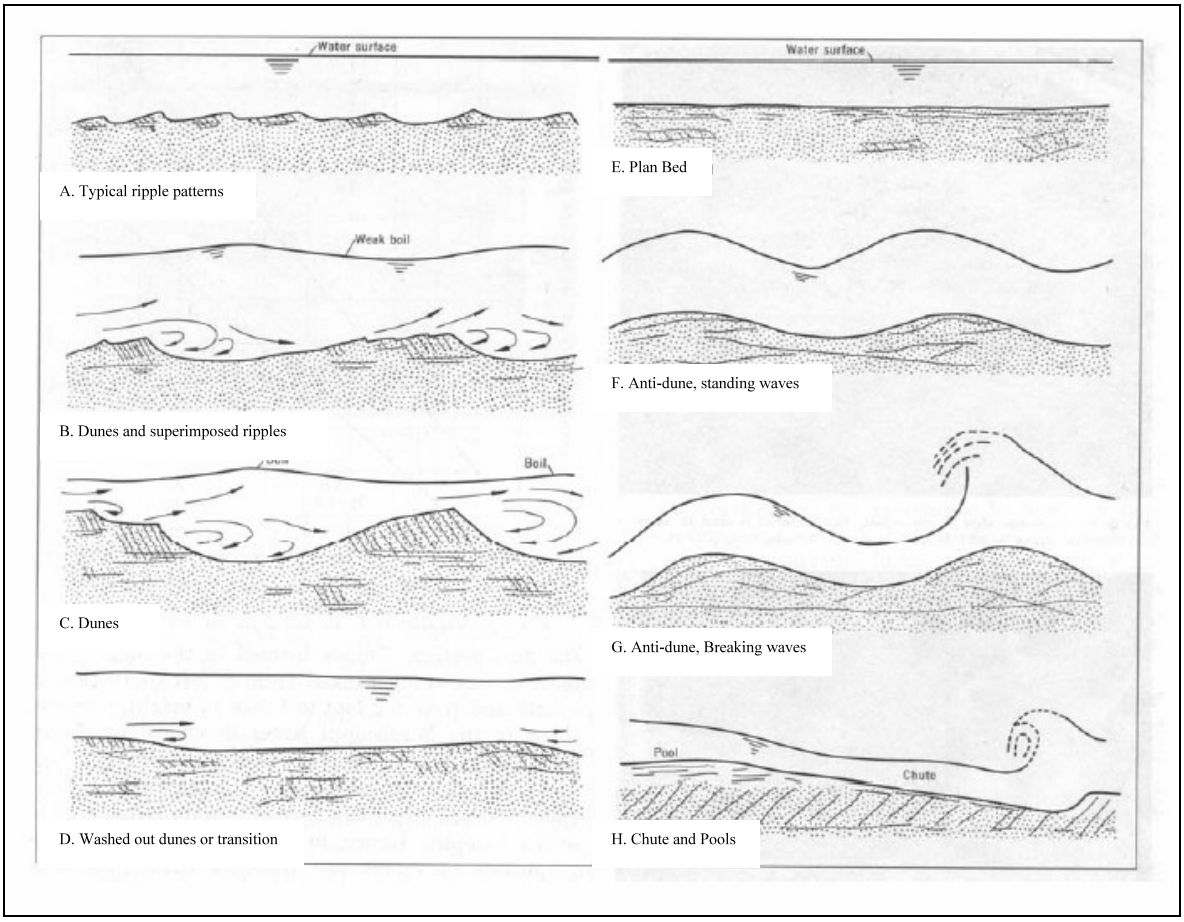

Figure 2.1 Bed forms in alluvial channels (after Simons and Richards (1966)

Vanoni (1975) provided a detailed summary of descriptions and definitions adopted from the American Society of Civil Engineers (ASCE) (1966) report from the task force on bed forms. These definitions are adopted in Table 2.2.

Van Rijn (1984) reported that lower and transitional flow regimes are the most important in field scale environments. Yalin and da Silva (2001) produced similar results stating that dunes lengths correlates with bed form depths, while bars lengths correlates with flow widths.

Bed form Configuration	Dimensions	Shape	Behavior and Occurrence
Ripples	Wave length less than approx. 1ft, height less than approx. 0.1ft	Roughly triangular in profile, with gentle, slightly convex upstream slopes and downstream slopes nearly equal to the angle of repose, generally short-crested and three dimensional	Move downstream with velocity much less than that of the flow, generally do not occur in sediment coarser than about 0.6 mm
Bars	Lengths comparable to the channel width. Height comparable to mean flow depth	Profile similar to ripples. Plan form variable	Four types of bars are distinguished: (1) Point; (2) alternating; (3) Transverse; and (4) Tributary. Ripples may occur on upstream slopes
Dunes	Wavelength and height greater than ripples but less than bars	Similar to ripples	Upstream slopes of dunes may be covered with ripples. Dunes migrate downstream in manner similar to ripples
Transition	Vary widely	Vary widely	A configuration consisting of a heterogeneous array of bed forms, primarily low-amplitude ripples and dunes interspersed with flat regions
Flat Bed	-------	-------	A bed surface devoid of bed forms. May not occur for some ranges of depth and sand size
Anti-dunes	Wave length = approx. $\frac{2\pi V^2}{g}$. Height depends on depth and velocity of flow	Nearly sinusoidal in profile. Crest length comparable to wave-length	In phase with and strongly interact with gravity water-surface waves. May move upstream, downstream, or remain stationary, depending on properties of flow and sediment

Table 2.2 Bed forms configurations (after ASCE 1966)

Exner (1925) analyzed the bed forms by using a perturbation stability theory as mentioned in Kennedy and Odgaard (1991). His analysis showed the transition of bed forms from symmetric features into non-symmetrical skewed features as ripples and dunes.

Engelund (1982) reported that ripples and dunes have different geometric scales. Ripples heights are smaller than dunes heights and significantly smaller than and independent of the flow depth. Ripple lengths depends on the sediment size and has no relation to the flow depth, while the dune height is highly dependent on the flow depth. Dune length is longer than the height but still proportional to flow depth as stated in Van Rijn (1984).

According to Simons (1965) dunes and ripples have a similar geometrical shape; they both have a mild slope on the upstream face and a steeper slope on the downstream face as shown in Figure 2.2.

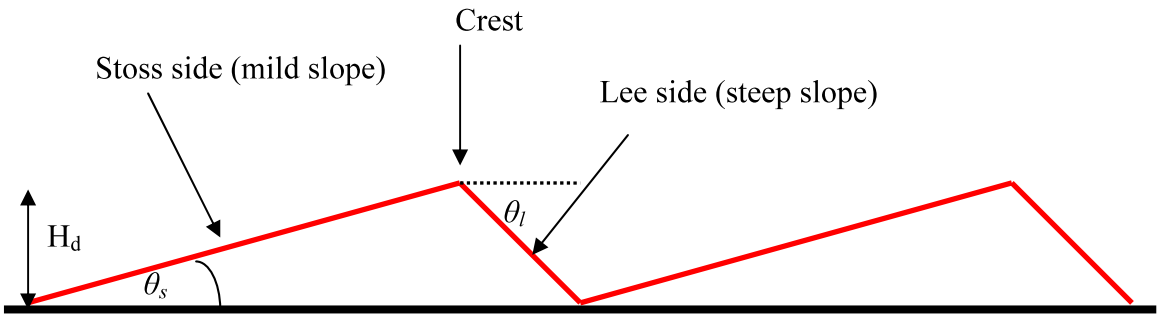

Figure 2.2 Dunes morphology

Bennet and Best (1995) reported that dunes are classified into equilibrium dunes and non-equilibrium dunes, where equilibrium dunes have the following properties:

- A non symmetric appearance ($L_s/L_l > 1$), where L_s, L_l are the lengths of the stoss and the lee side of the dune as shown in Figure 2.2.
- Gradual stoss slope (θ_s) leading to a crest then to a sharp lee slope (θ_l), roughly equal to the angle of repose of the bed material (φ_{max}) = 30°
- The height and the wavelength of the bed form are proportional to the flow depth ($H_d \approx 1/6$ H, $\lambda \approx 2\pi H$)

Kennedy and Odgaard (1991) grouped all research done on bed forms into the following categories

1- Analytical models

This group relied on the perturbation stability theory mentioned earlier and included research studies from Exner (1925), Anderson (1953), Kennedy (1963), Kennedy (1969), Hayashi (1970), Engelund (1970), Gill (1971), Fredsoe (1974), Richards (1980), Fredsoe (1982), Haque and Mahmood (1985).

2- Empirical relations

This group attempted to establish empirical relations between bed forms geometry and stream dimensions (flow Depth and height) and included research studies from Garde and Anderson (1959), Yalin (1964), Ranga Raju and Soni (1976), Yalin and Karahan (1979), Jaeggi (1984), Ikeda (1984), Van Rijn (1984), Menduni and Paris (1986).

3- Statistical Analysis

This group utilized statistical techniques to predict bed form types and geometries; it included studies from Nordin and Algert (1966), Hino (1968), Annambhotla, Sayre and Livesay (1972), and Jain and Kennedy (1974).

2.2. BED FORM MORPHOLOGY

Garcia (1999) mentioned that the bed in sand bed streams is initially flat, and then once velocity is imposed, the bed remains flat for some time, and once the imposed velocity reaches a higher critical value, ripples start to form. As the imposed velocity continues to increase, ripples transforms into dunes. When the velocity reaches a higher critical value in the Froude number spectrum (greater than 1), the dunes are washed out and flat bed forms back once more. This is known as the upper regime (supercritical). Yalin and da Silva (2001) in their research on bed forms reported that internal non-uniformities of the flow caused by turbulent bursts converts the initially flat bed into dunes as shown in Figure 2.3. This bursting process transforms small eddies in the areas of large shear stresses near the bed into large scale turbulence eddies. The small eddies develop due to the fluctuation in shear stress near the bed. Once they form, small eddies are transported by the flow downstream, moving away from the boundary, and coming together to become larger and less in quantity. These burst-forming eddies grow with the increase in the flow depth until they break. Once the large eddies break out, their breaking entrain sediment and form small new eddies to repeat the cycle.

Yalin and da Silva (2001) reported that ripple geometry is not dependent on the overall flow dimensions and in return it is unlikely that ripples are affected by the bursting process, with a viscous layer near the bed preventing the bed from interacting with the bursts.

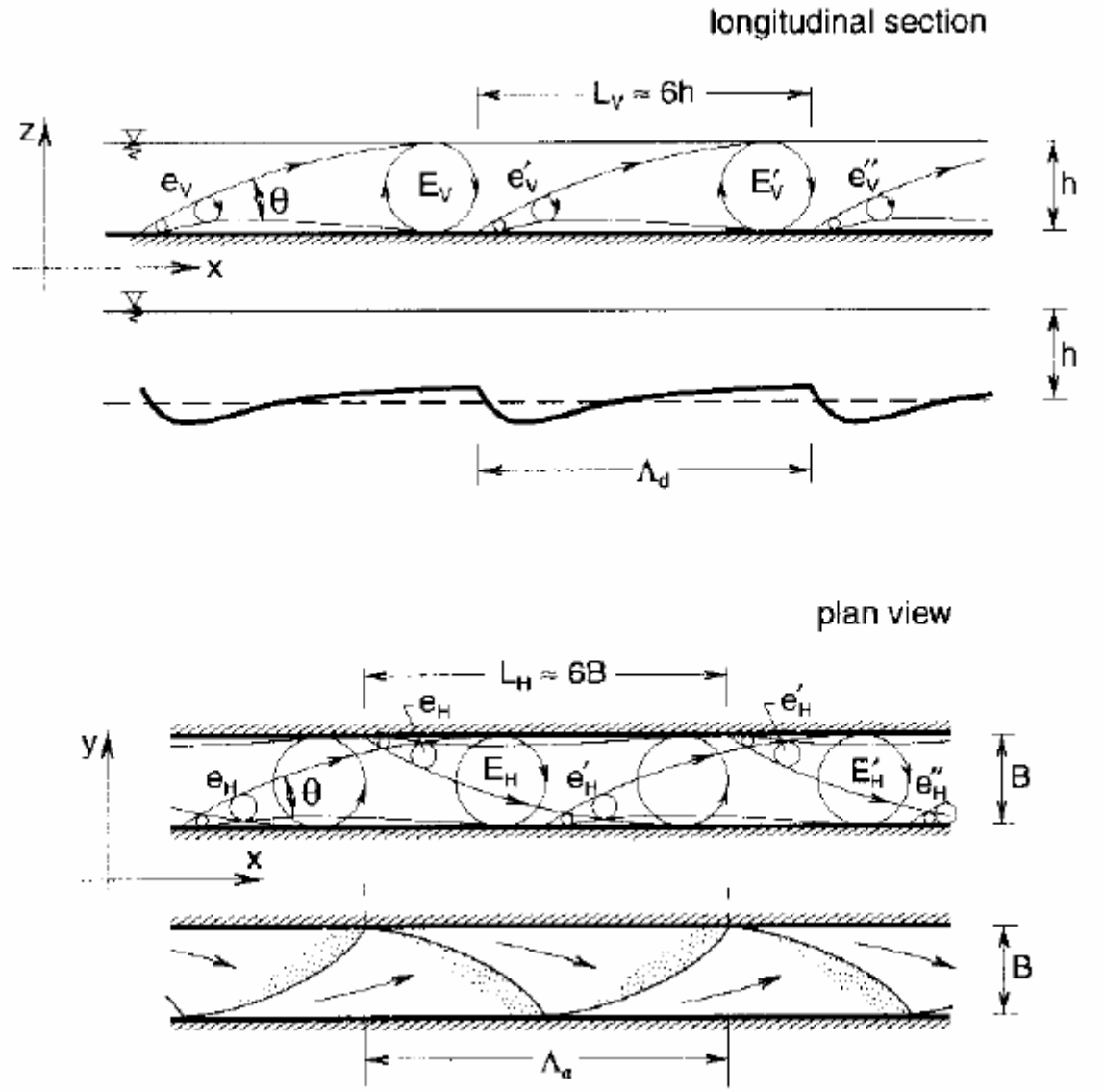

Figure 2.3 Evolution of eddies [after Yalin and da Silva (2001)]

where e_V= "burst-forming" vertical eddies, e_H= "burst-forming" horizontal eddies; E_V=large scale vertical eddies; E_H=large scale horizontal eddies; h=flow depth; B=width; L_V=vertical burst length; L_H=horizontal burst length; Λ_d=dune length; Prime symbol designates new eddies

2.2.1 BED FORM CONFIGURATIONS

Bed form types and geometries have been the topic of several research studies in the last fifty years or so. Many investigators have proposed relations to predict the bed form type and dimensions: bed form height (H_d), bed form length (λ) and bed form steepness (H_d/ λ).

Simons and Richardson (1966) proposed a dimensional plot of stream power (bed shear stress x mean velocity) versus median grain size to predict the bed form type (Figure 2.4). Vanoni (1975) mentioned that data from Rio Grande agreed well with the graph (Figure 2.4), however data from Jordan (1965) from the Mississippi River with smaller magnitude velocities and large scale depths did not agree with the plot in Figure 2.4. Shen (1978) also reported that data from Missouri River did not agree with this plot (Figure 2.4).

Simons and Richardson (1966) reported that they used data from laboratory investigations, along with some field data from Middle Loup River, Nebraska, Rio Grande, New Mexico which are in a way are smaller rivers in magnitude with shallower depths when compared with the Mississippi or the Missouri Rivers.

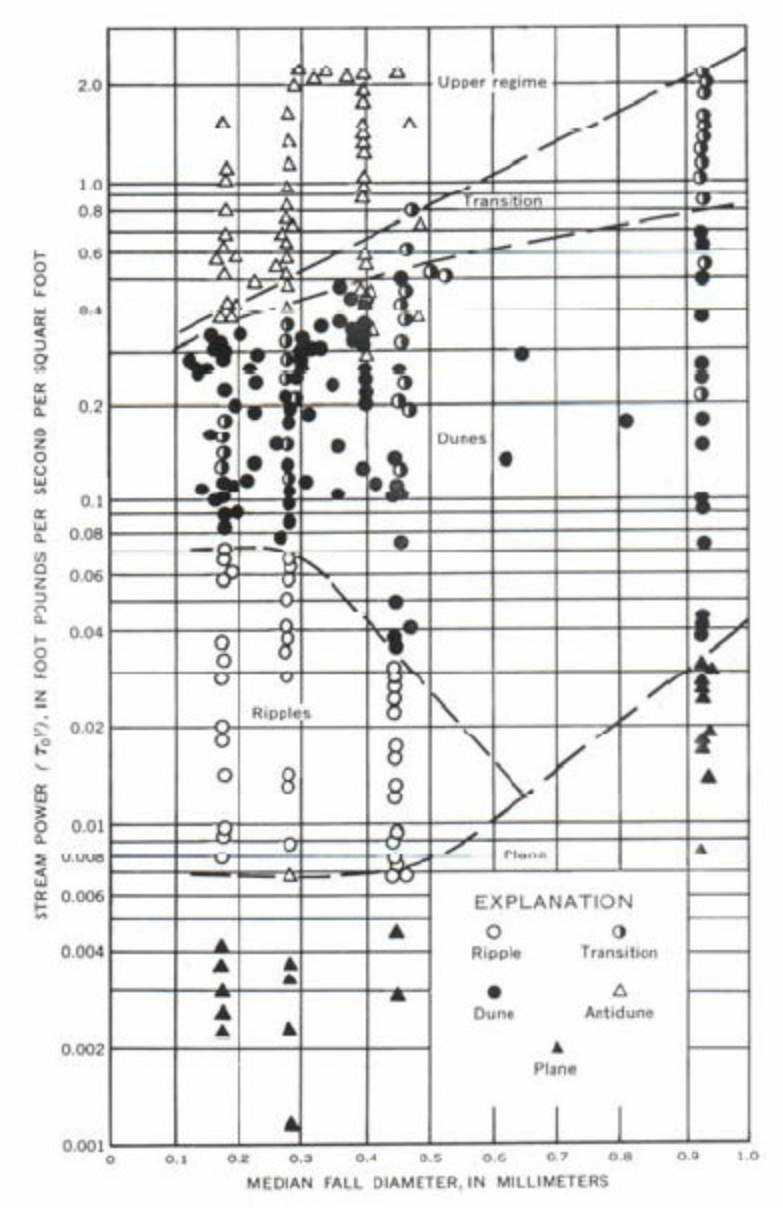

Figure 2.4 Prediction of bed forms [After Simons and Richardson (1966)]

Liu (1957) proposed another dimensionless plot for shear velocity versus shear velocity-Reynolds numbers to delineate zones of different bed form types shown in Figure 2.5. Simons and Sentruk (1977) reported that field data does not agree well with this plot and they attributed that to the limited field data that were used to generate this plot.

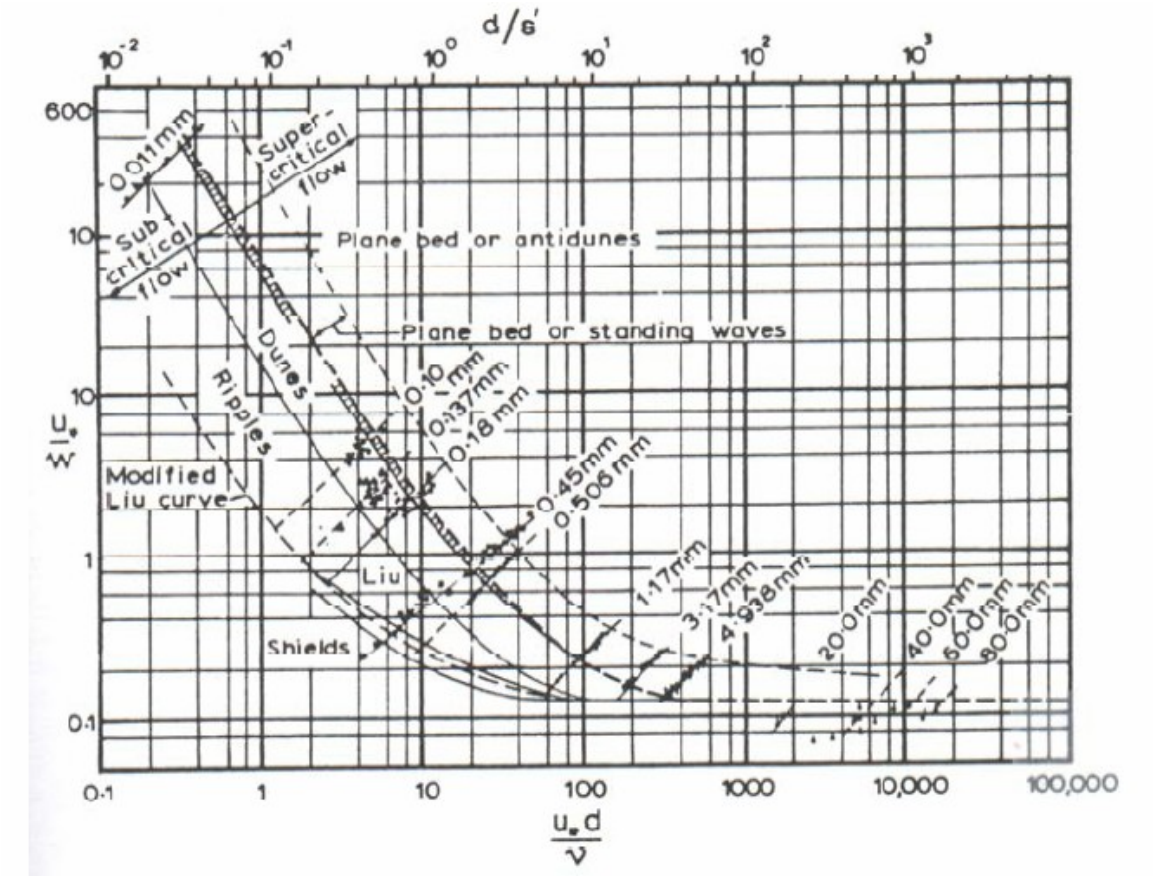

Figure 2.5 Bed form prediction [After Liu (1957)]

Kennedy (1969) presented another graph shown in Figure 2.6 based on his two-dimensional potential flow model and experimental data to predict the bed form based on Froude number and J, where J is the ratio between the lag distance δ (phase shift between local sediment transport rate and local mean velocity) and the depth of flow H.

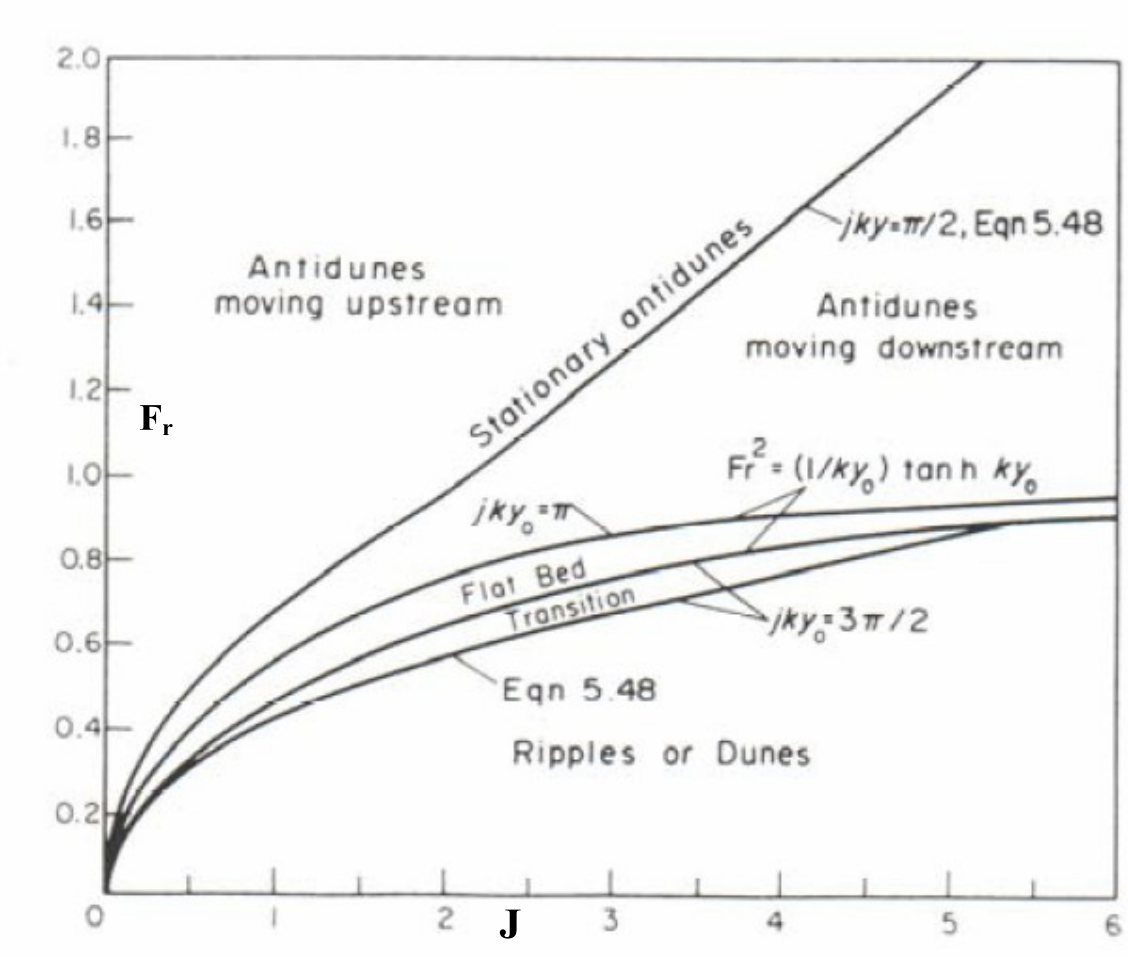

Figure 2.6 Bed form prediction [After Kennedy (1969)] where F_r = Froude number; λ = wavelength of bed form; $j = \delta/y_0$; y_0 = flow depth; δ = lag distance of the local sediment transport rate and the local velocity.

Znameskaya (1969) proposed another plot for Froude number versus dimensionless mean velocity shown in Figure 2.7.

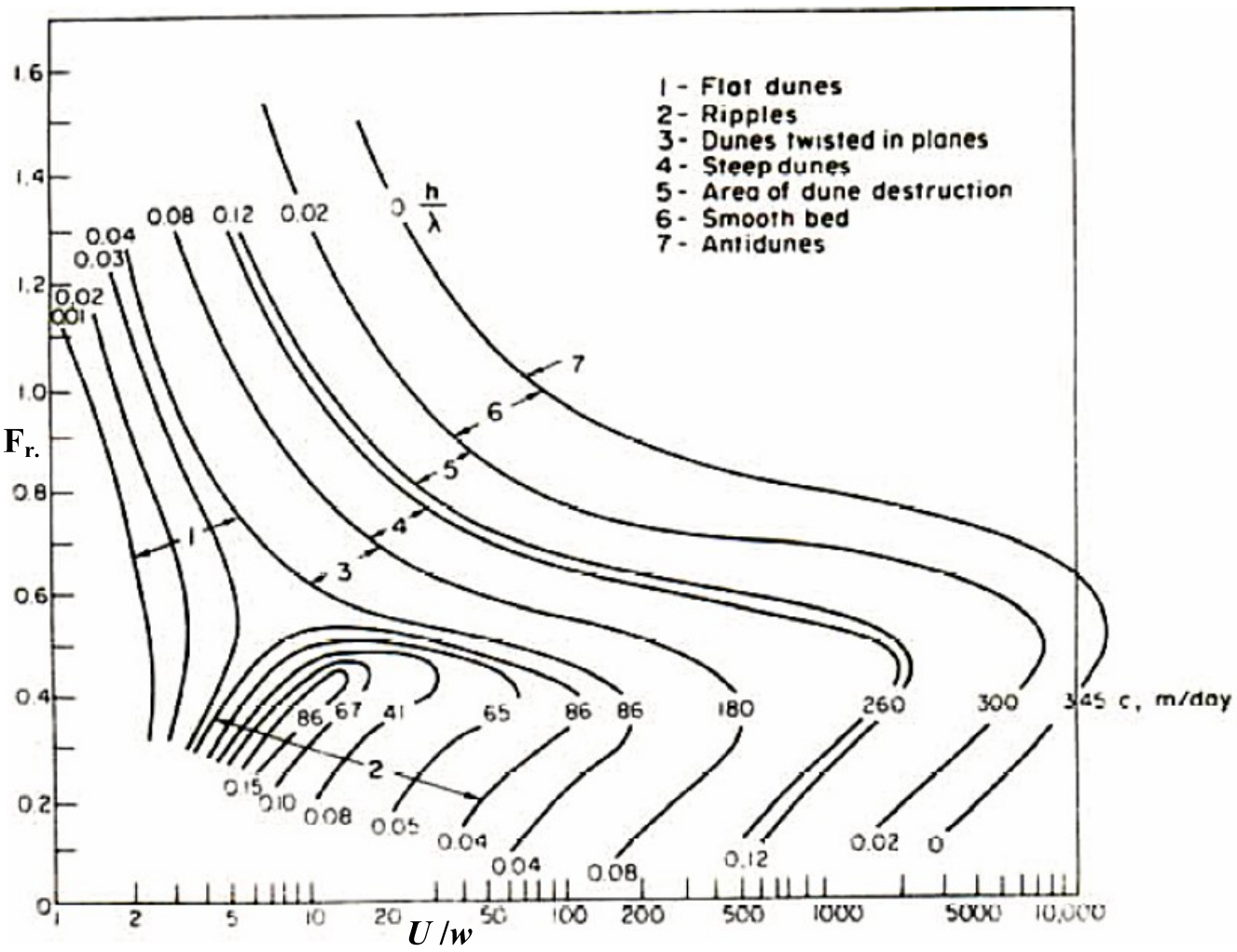

Figure 2.7 Bed form prediction [After Znamenskaya (1969)] where F_r = Froude number; U=mean velocity; w=fall velocity of sediment; h = dune height; λ=dune wavelength; c=dune translation velocity.

2.2.2. BED FORM GEOMETRY

2.2.2.1 ANALYTICAL MODELS

These models used linear stability analysis to determine the stability of sinusoidal bed features. Kennedy (1963) used a potential flow formulation of free surface flow over a sinusoidal bed to derive an equation for the dune wavelength as follows

$$\mathrm{Fr}^2 = \frac{U^2}{gH} = \frac{1 + kH\tanh(kh) + k\delta\cot(k\delta)}{(kH)^2 + (2 + k\delta\cot(k\delta))kH\tanh(kH)} \qquad [2.1]$$

where F_r is the Froude number; K is the wave number ($2\pi\backslash\lambda$); λ is the wavelength; δ is the phase shift between the local sediment discharge and local near-bed velocity.

Fredsoe (1982) gave an equation for the phase shift as follows:

$$\delta = \frac{\varepsilon U_b}{v_s^2} \qquad [2.2]$$

where U_b is slip velocity at the bed, which is approximately equal to shear velocity u_*, ε is the eddy viscosity taken as constant over the depth = $0.077\, u_* H$, v_s is fall velocity.

However, Kennedy (1991) acknowledged that since this method was developed using linearized (small wave amplitude) theory; it is of a limited value when studying fully developed bed forms. Fredsoe (1982) equated the dune dimensions (wavelength and height) to sediment transport, shear stress and water depth to come up with the following equation for bed form height as shown in Figure 2.8

$$\frac{H_d / H}{(1 - \frac{H_d}{2H})} = \frac{\Phi_b}{2\theta\left(\left(\frac{d\Phi_b}{d\theta}\right) + \left(\frac{d\Phi_s}{d\theta}\right)\right)} \qquad [2.3]$$

where Φ_s is the dimensionless suspended sediment transport; θ is the bed shear stress near the top of the dune (which he assumed equal to grain shear stress τ'_*).

$$\Phi_b = \frac{q_b}{\sqrt{RgD^3}} \quad [2.4]$$

$$\Phi_s = \frac{q_s}{\sqrt{RgD^3}} \quad [2.5]$$

$$\tau'_* = \frac{\tau'_0}{\rho RgD} \quad [2.6]$$

$$\Phi_s = f(\tau'_*) \quad [2.7]$$

where q_b is the bed load transport; q_s is the suspended sediment transport; R is the submerged specific gravity; ρ is the water density; D is the median grain diameter.

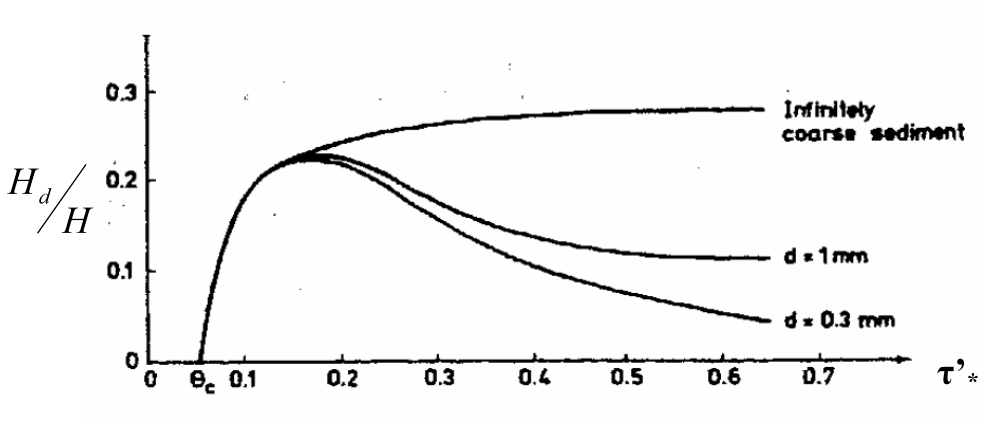

Figure 2.8 Bed shear stress and dune height relation [After Fredsoe (1982)]

Fredsoe also proposed the following equation for the dune wavelength as shown in Figure 2.9.

$$\lambda = \frac{[16H_d q_b + (16H_d + \delta)q_s}{(q_b + q_s)} \quad [2.8]$$

where δ is the phase shift.

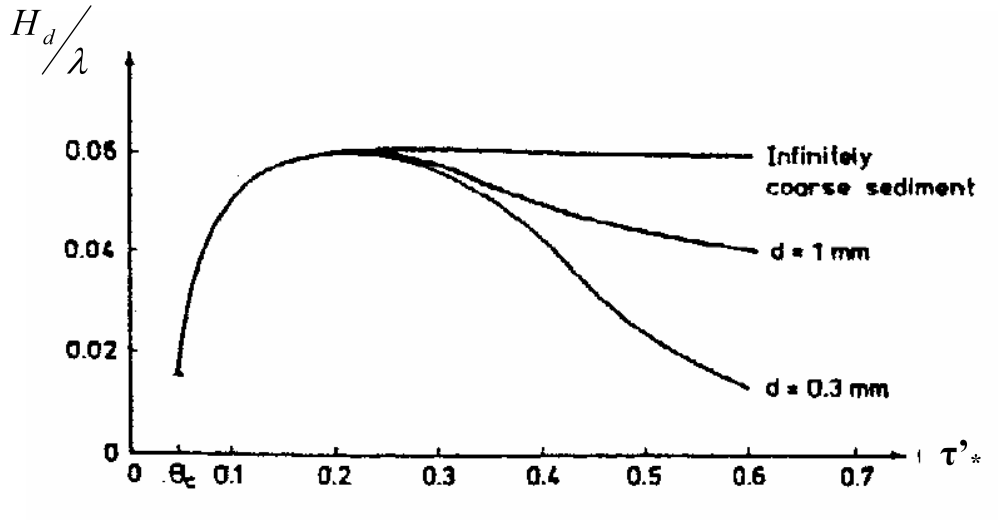

Figure 2.9 Bed shear stress and dune steepness relation [After Fredsoe (1982)]

Kennedy and Odgaard (1991) proposed an analytical equation in the following form

$$\frac{H_d}{H} = 1/2\{\frac{1.2A\alpha f_0}{8C_D} + [(\frac{1.2A\alpha f_0}{8C_D})^2 + \frac{2\pi Fr^2 f_0}{C_D C_1}(\frac{f}{f_0} - \frac{1.2A}{2})]^{\frac{1}{2}}\} \qquad [2.9]$$

where f_0 is the rigid flat bed Darcy-Weisbach friction factor

$$f_0 = \frac{8}{\left\{6.25 + 2.5\ln(\frac{H}{2.5D_{50}})\right\}^2} \qquad [2.10]$$

where f is the Darcy-Weisbach friction factor; F_r is the Froude number; $A = 1.0$; $C_D = 1.0$; $\alpha = 5$; $C_1 = 0.25$. These two equations were derived by equating the energy slope because of the form drag to head loss across an abrupt expansion in a conduit.

Karim (1999) followed Kennedy and Odgaard (1991) and related the energy losses because of form drag to head loss across a sudden expansion in an open channel to come up with the following equation:

$$\frac{H_d}{H} = [\frac{\{S_e - 0.0168(\frac{D_{50}}{H})^{0.33} Fr^2\}(\frac{\lambda}{H})^{1.20}}{0.47 Fr^2}]^{0.73} \quad [2.11]$$

where S_e is the energy slope.

2.2.2.2 EMPIRICAL RELATIONS

In this category of studies, several investigators attempted to use some flow characteristics as will be mention next to characterize bed form height and bed form length. Some of these characteristics included:

Flow depth (H), Shields Stress or bed shear stress, $\tau_* = \frac{\tau}{\rho RgD}$, Grain Size (D), Water viscosity (υ), Submerged specific gravity ($R = \frac{\rho_s - \rho}{\rho}$), Bed porosity (p).

Yalin (1977) proposed relations to characterize the bed form geometries as follows:

- Ripples

$$\frac{\lambda}{D} = f[\frac{u_* D}{\nu}) \quad [2.12]$$

$$\frac{H_d}{\lambda} = f[\frac{\tau_*}{\tau_{cr}}) \quad [2.13]$$

- Dunes

$$\frac{\lambda}{H} = f[\frac{u_* D}{\nu}, \frac{H}{D}) \quad [2.14]$$

$$\frac{H_d}{\lambda} = f[\frac{\tau_*}{\tau_{cr}}, \frac{u_* D}{\nu}, \frac{H}{D}) \quad [2.15]$$

where $\frac{u_* D}{\nu}$ is the boundary Reynolds number (Re_*).

Yalin (1964) proposed the following formula for bed form height

$$\frac{H_d}{H} = \frac{1}{6}[1 - \frac{H_{cr}}{H}) \quad [2.16]$$

where H_{cr} is the critical water depth where motion starts to take place.

Garcia (1999) reported that $\frac{H_d}{H}$ can not exceed 1/6, however Nordin and Algert (1965) reported that this fraction should be equal to 1/3 based on their field data collected from the Rio Grande dunes.

Yalin (1964) also reported that wavelength of ripples can be calculated as follows:

$$\lambda = 1000\ D \qquad [2.17]$$

While, Richards (1980) proposed the following formula for ripple wavelength

$$203\ D < \lambda < 4050\ D \qquad [2.18]$$

Yalin (1964) proposed an equation for dunes wavelengths as follows:

$$\lambda = 2\ \pi\ H \qquad [2.19]$$

Hino (1968) estimated dune wavelength to:

$$\lambda = 7\ H \qquad [2.20]$$

Allen (1970) proposed a formula for dune wavelength for deep flows as follows: (where H is greater than 10m)

$$\lambda = 1.16\ H^{1.55} \qquad [2.21]$$

Yalin (1977) also proposed two plots for the steepness of ripples and dunes as shown in Figure 2.10 and 2.11. He plotted the steepness $\frac{H_d}{\lambda}$ versus shields stress and critical shields stress.

Yalin (1977) determined that for dunes to occur, Re_* has to be greater than 31.62 and H/D greater than 100, while for ripples Re_* has to be less than 10 and H/D greater than 400

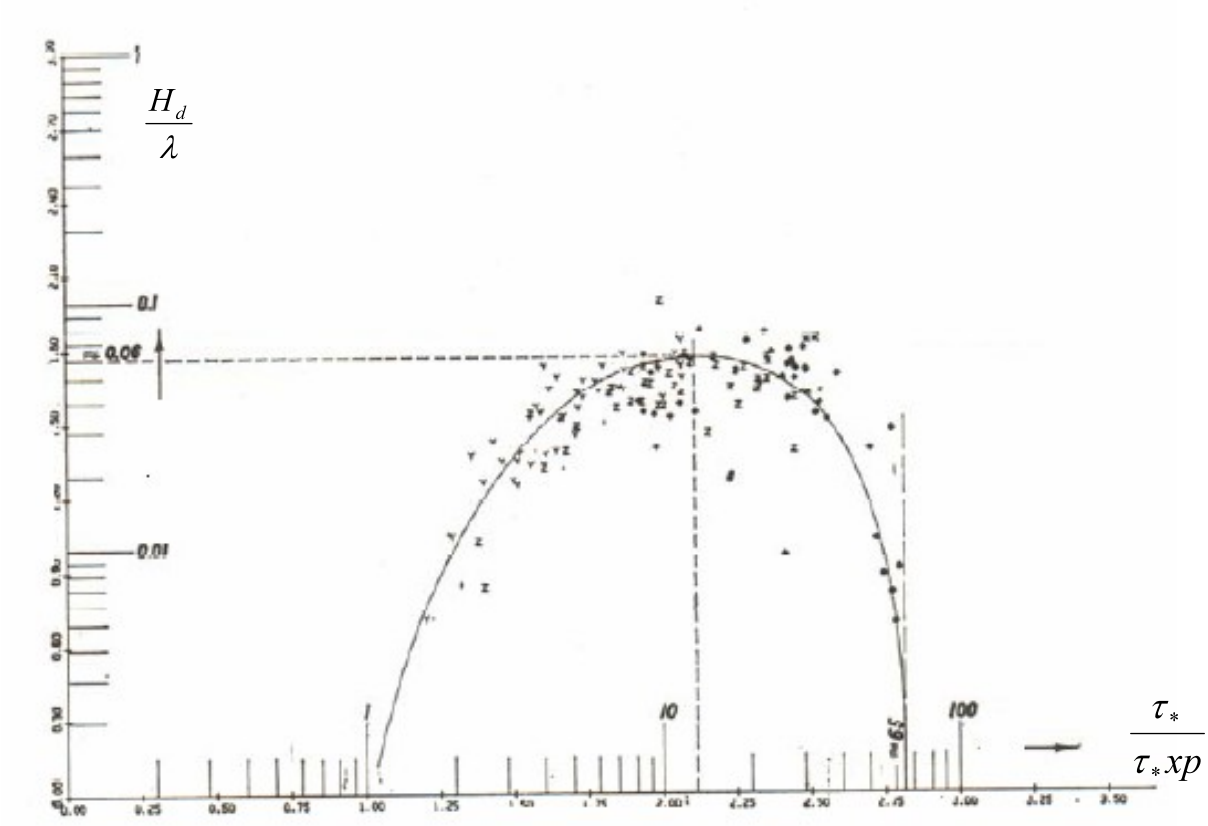

Figure 2.10 Dune steepness prediction [after Yalin (1977)]

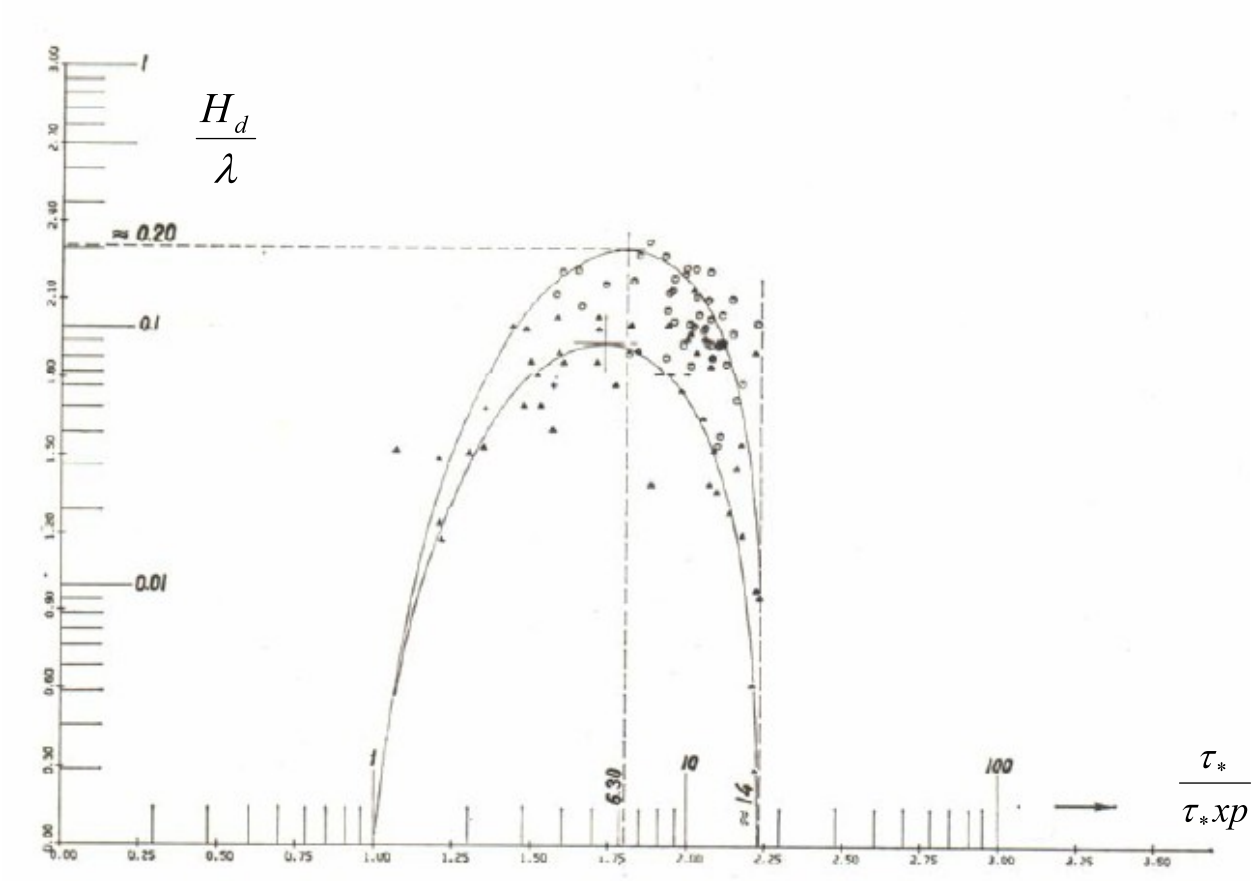

Figure 2.11 Ripple steepness prediction [after Yalin (1977)]

Van Rijn (1984) utilized flume experiments data in addition to field scale river data to produce the following equations as shown in Figure 2.12 and 2.13.

$$\frac{H_d}{H} = 0.11(\frac{D_{50}}{H})^{0.3}(1-e^{-0.5T})(25-T) \qquad [2.22]$$

$$\frac{H_d}{\lambda} = 0.015(\frac{D_{50}}{H})^{0.3}(1-e^{-0.5T})(25-T) \qquad [2.23]$$

where T is the transport stage parameter = $\frac{u_*^{'2} - u_{*cr}^{\ 2}}{u_{*cr}^{\ 2}}$ [2.24]

Bed form length can then be estimated as λ = 7.3 H

	source	flow velocity $\bar{u}$ (m/s)	flow depth d (m)	particle size D_{50} (μm)	temperature Te (°C)
flume data	o Guy et al	0.34 - 1.17	0.16 - 0.32	190	8 - 34
	x Guy et al	0.41 - 0.65	0.14 - 0.34	270	8 - 34
	▲ Guy et al	0.47 - 1.15	0.16 - 0.32	280	8 - 34
	◔ Guy et al	0.77 - 0.98	0.16	330	8 - 34
	□ Guy et al	0.48 - 1.00	0.10 - 0.25	450	8 - 34
	♀ Guy et al	0.53 - 1.15	0.12 - 0.34	930	8 - 34
	● Williams	0.54 - 1.06	0.15 - 0.22	1350	25 - 28
	◪ Delft Hydr. Lab.	0.45 - 0.87	0.28 - 0.49	790	12 - 18
	◔ Stein	0.52 - 0.95	0.24 - 0.31	400	20 - 26
	♂ Znamenskaya	0.53 - 0.80	0.11 - 0.21	800	–
field data	● Dutch Rivers	0.85 - 1.55	4.4 - 9.5	490 - 3600	5 - 20
	◪ Rio Parana	1.0	12.7	400	–
	◆ Japanese Channels	0.53 - 0.89	0.25 - 0.88	1100 - 2300	–
	■ Mississippi River	1.35 - 1.45	6 - 16	350 - 550	–

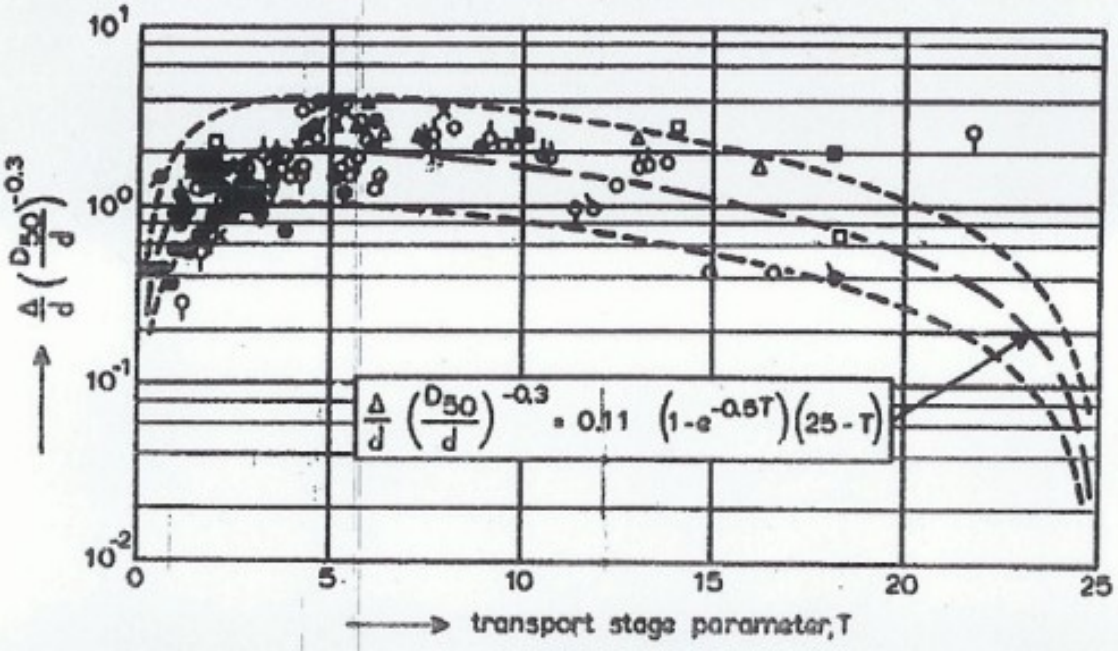

Figure 2.12 Bed form height prediction [(after Van Rijn (1984)]

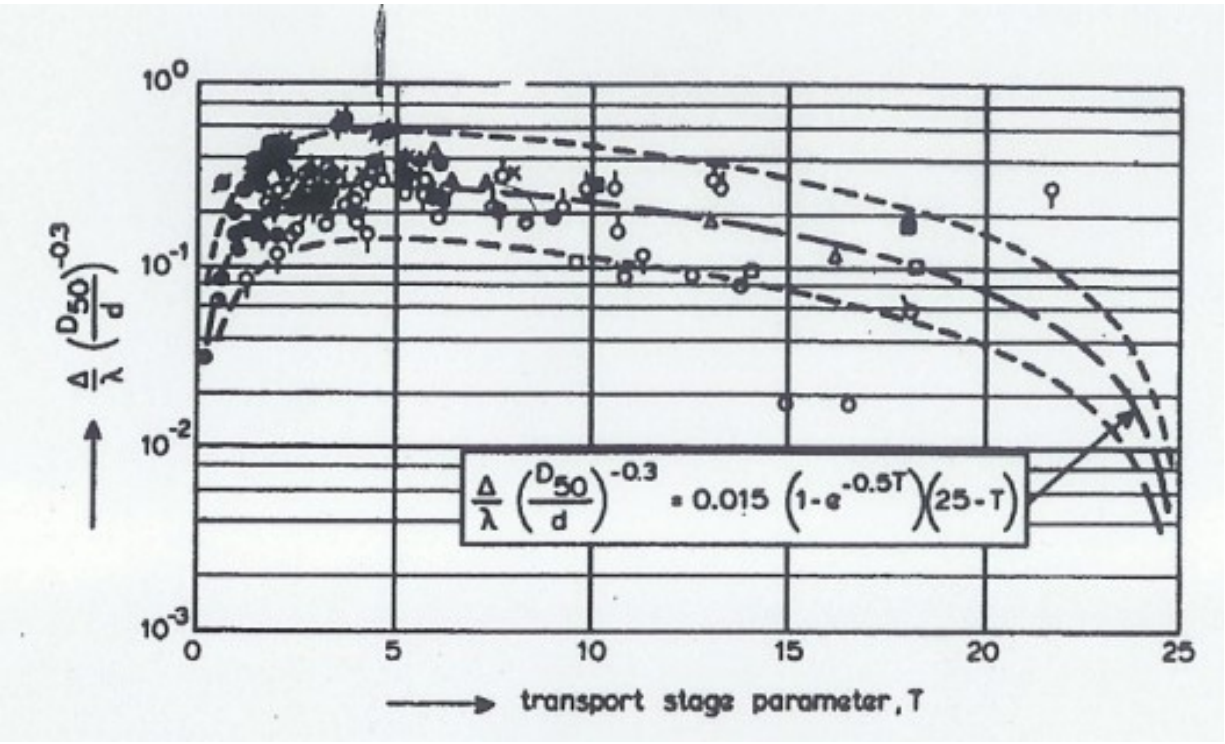

Figure 2.13 Bed form steepness prediction [(after Van Rijn (1984)]

2.3 BED FORM HYDRAULICS

As mentioned before, alluvial channels have a distinct characteristic, which is their ability to change their morphology with different flow conditions.

Giratalla (1977) studied the flow over natural and artificial ripples. He used film technology to measure the Reynolds stresses and velocities over the ripples. He used a finite element model based stream function – vorticity to develop a two dimensional laterally averaged model. His analysis indicated that the shear stress variation along the ripple surface could be accounted for by a rapid increase in shear immediately downstream of the point of reattachment (Figure 2.14); a tendency for shear to decrease as the boundary layer develops; and a compensating increase in

shear due to the increase in velocity near the bed resulting from the flow contracting from the due to the ripple form (Griatalla 1977).

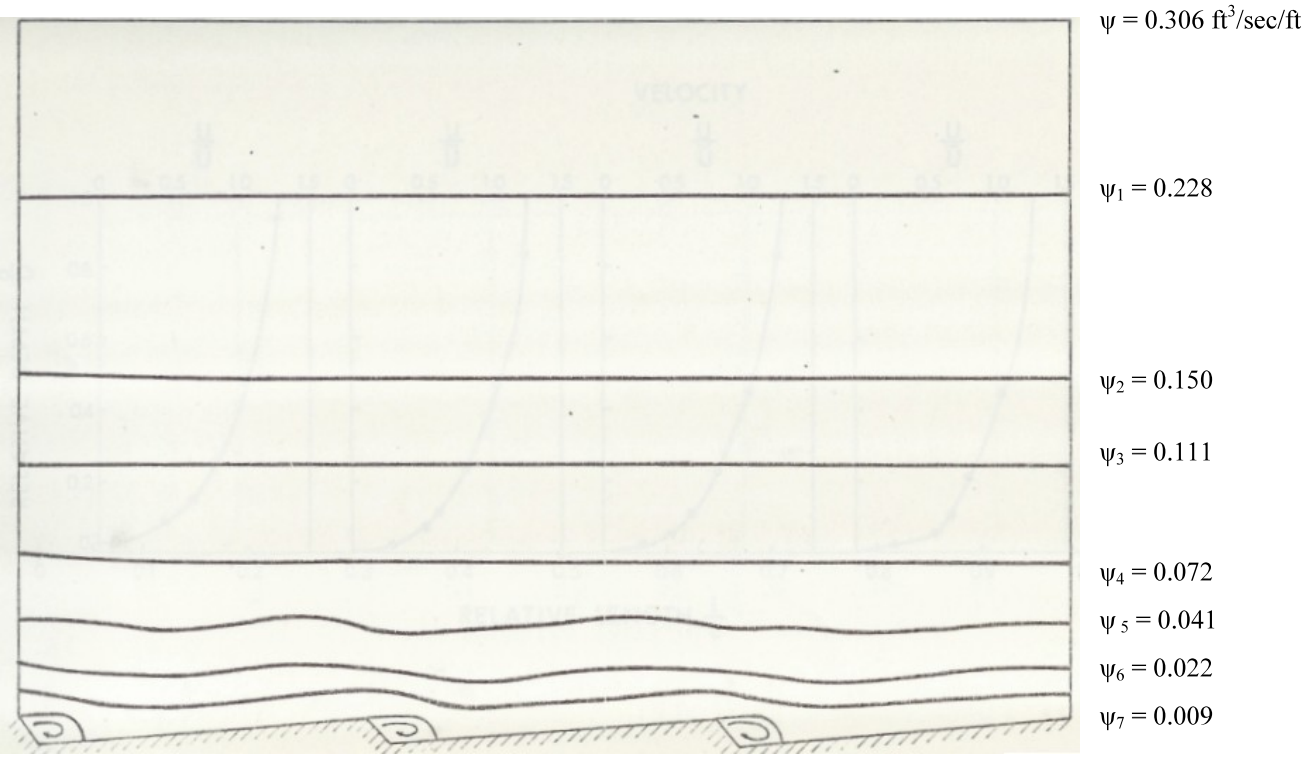

Figure 2.14 Finite element solution of the stream function (ψ) for turbulent flow ψ = 0.306 ft^3/sec/ft (Adapted from Giratalla 1977)

Shen (1990) reported that flow separation and reattachment properties creates a region of adverse pressure gradient that makes the velocity near the bed to be closer to zero or even creates a region of flow reversal as shown in Figure 2.15.

Nelson (1993) (Figure 2.16) reported that a momentum defect region is formed over bed forms. A region of flow separation and wake formation is formed at the downstream side of the bed form. The separation occurs at some point close to the crest of the bed form and then reattachment occurs again at some point along the downstream side of the next bed form.

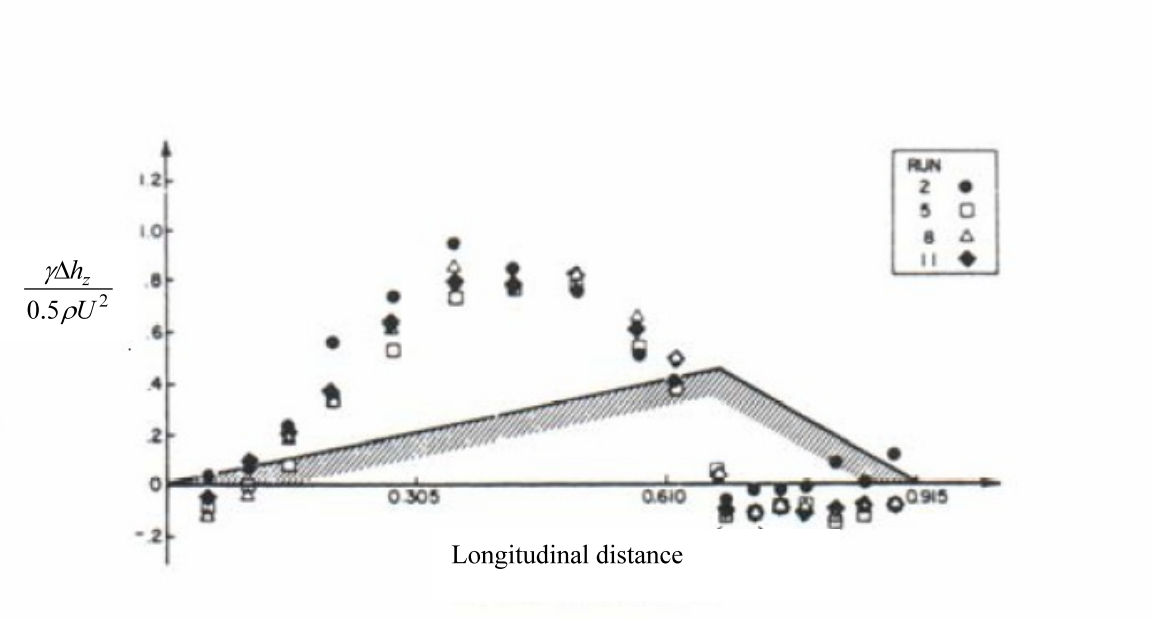

Figure 2.15 Pressure distribution over bed form [After Shen et al (1990)]

In normal flow conditions where the bed of the channel is a flat immobile bed, the velocity profile along the vertical can be approximated with a logarithmic curve according to Vanoni (1975). Reynolds stresses follow an opposite logarithmic curve, with the highest value near the bed decreasing until it reaches zero near the water surface in equilibrium conditions (Vanoni 1975). This is not the case for beds with superimposed bed forms. According to Nelson (1993) the velocity profiles along the vertical still follow the logarithmic curve but with two different slopes and these two slopes meet where the flow separation occurs as shown in Figure 2.16. This separation point corresponds to the maximum Reynolds stress as shown in Figure 2.18.

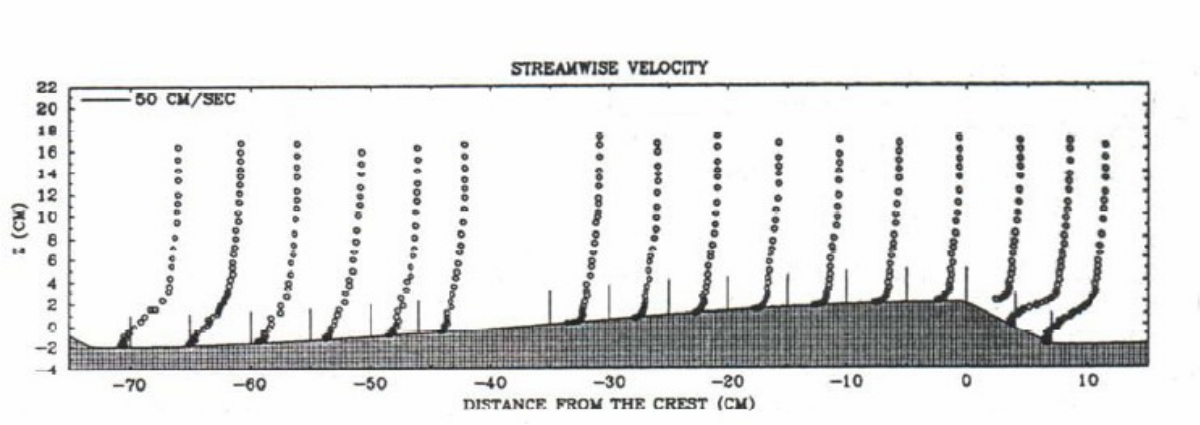

Figure 2.16 Stream-wise vertical velocity distribution over bed form in linear scale [After Nelson (1993)]

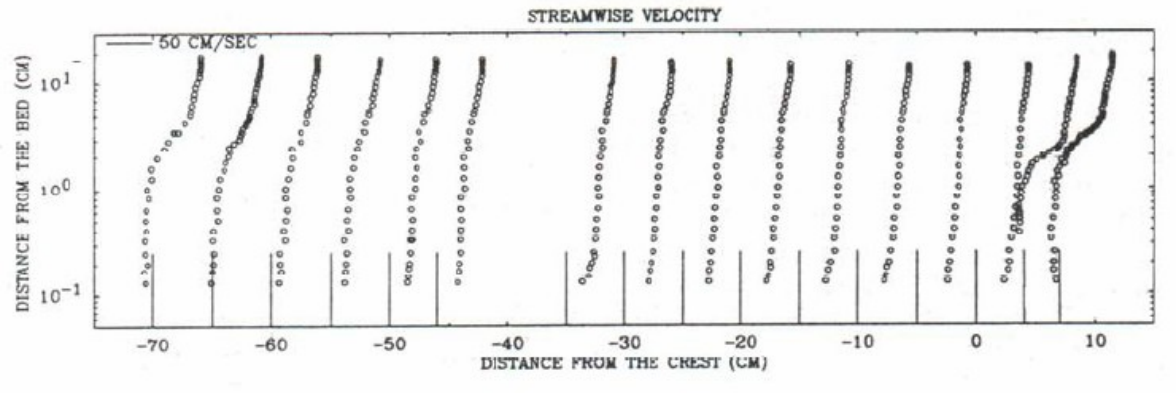

Figure 2.17 Stream-wise vertical velocity distribution over bed form in logarithmic scale [After Nelson (1993)]

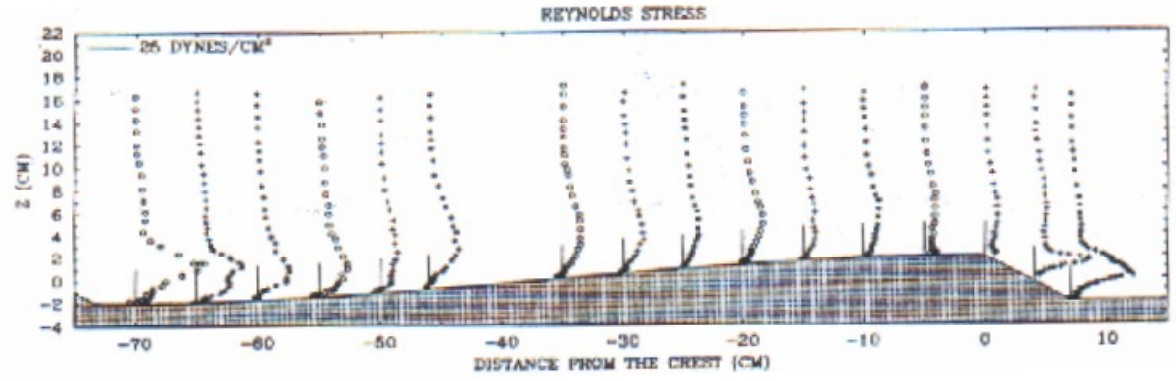

Figure 2.18 Reynolds stresses distribution over bed form in logarithmic scale [After Nelson (1993)]

As mentioned in Chapter One, the resistance to the flow in alluvial channels with bed forms is divided into two categories, one being the grain resistance which exists in any natural channel, while the second component of the resistances results from the presence of the bed form and is called form resistance.

Einstein (1950) put this into an equation as follows:

$$\tau_0 = \tau_{0'} + \tau_{0''} \qquad [2.25]$$

where τ_0 is the total shear stress; $\tau_{0'}$ is the grain or surface shear stress; $\tau_{0''}$ is the form or drag shear stress. Equation 2.25 could be rewritten as follows:

$$\tau_0 = \gamma S (R'_h + R''_h) \qquad [2.26]$$

where R'_h is the hydraulic radius due to grain roughness; R''_h is the hydraulic radius due to bed form roughness. Furthermore, if we used the shear velocity relationships in Equation 1.4, we could reach the following equation:

$$u_*^2 = u'^2_* + u''^2_* \qquad [2.27]$$

where, u_*^2 is the total shear velocity; u'^2_* is the grain or surface shear velocity; u''^2_* is the form or drag shear velocity.

The next section discusses the flow resistance in alluvial channels in more detail.

2.3.1 FLOW RESISTANCE IN ABSENCE OF BED FORMS

The resistance to steady uniform flow is commonly expressed with the Weisbach-Darcy relation as follows:

$$S = \frac{h_l}{L} = f \frac{1}{4R_h} \frac{\bar{u}^2}{2g} \quad [2.28]$$

where S is the slope, L is the channel length; h_l is the head loss across the length L; f is the Weisbach-Darcy friction factor; $\bar{u}$ is the mean average velocity

According to Graf (1984), a relationship exists between the shear velocity and mean velocity as follows:

$$\frac{\bar{u}}{u_*} = \sqrt{\frac{8}{f}} \quad [2.29]$$

where $\bar{u}$ can be derived using the Manning's formula of flow

$$\bar{u} = \frac{1}{n} R_h^{\frac{2}{3}} S^{\frac{1}{2}} \quad [2.30]$$

and in turn

$$n = R_h^{\frac{1}{6}} \sqrt{\frac{f}{8g}} \quad [2.31]$$

Einstein (1950) gave another relation between shear velocity and resistance to flow as follows:

$$\frac{\bar{u}}{u_*} = 5.75 \log(12.27 \frac{R'_h x}{k_s}) \quad [2.32]$$

where the apparent roughness $\frac{k_s}{x}$ can be obtained from Figure 2.18

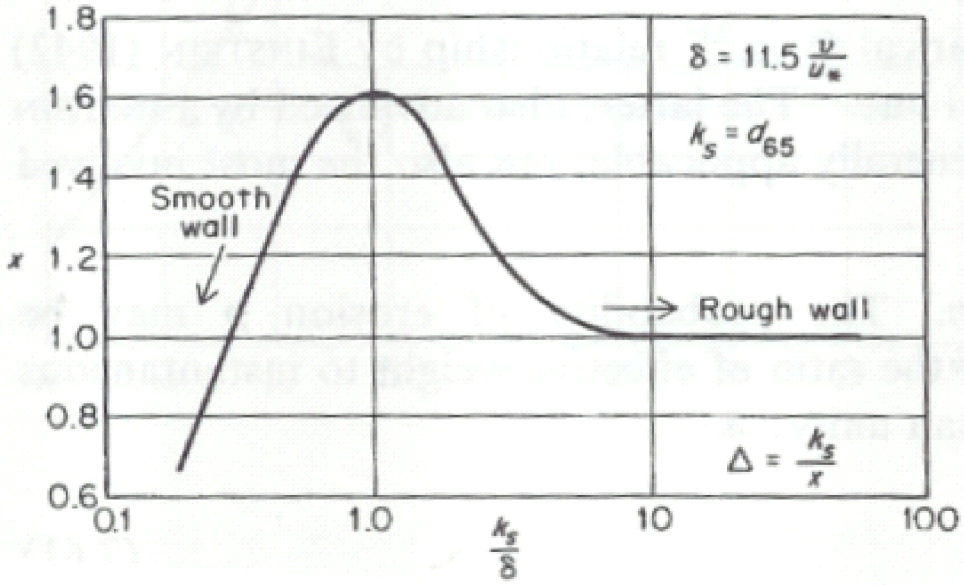

Figure 2.19 Correction factor in the logarithmic velocity distribution [After Einstein (1950)]

where x is a correction factor incorporating the smooth-transition-rough-wall; k_s can be approximated to be equal to d_{65}.

2.3.2 FLOW RESISTANCE IN PRESENCE OF BED FORMS

Bed form flow resistance can be expressed in terms of friction velocity or in terms of friction factor as explained next.

2.3.2.1 FLOW RESISTANCE EXPRESSED WITH FRICTION VELOCITY

Einstein and Barbarosa (1952) suggested a relation between the intensity of shear on bed particles and flow resistance due to bed forms as follows and as shown in Figure 2.20

$$\frac{\bar{u}}{u''_*} = Fn(\psi_{35}) \qquad [2.33]$$

where Ψ_{35} is the intensity of shear on representative particles $= \frac{\rho_s - \rho}{\rho} x \frac{d_{35}}{R'_h S}$; d_{35} is the sieve size in the bed material of which 35 percent is finer

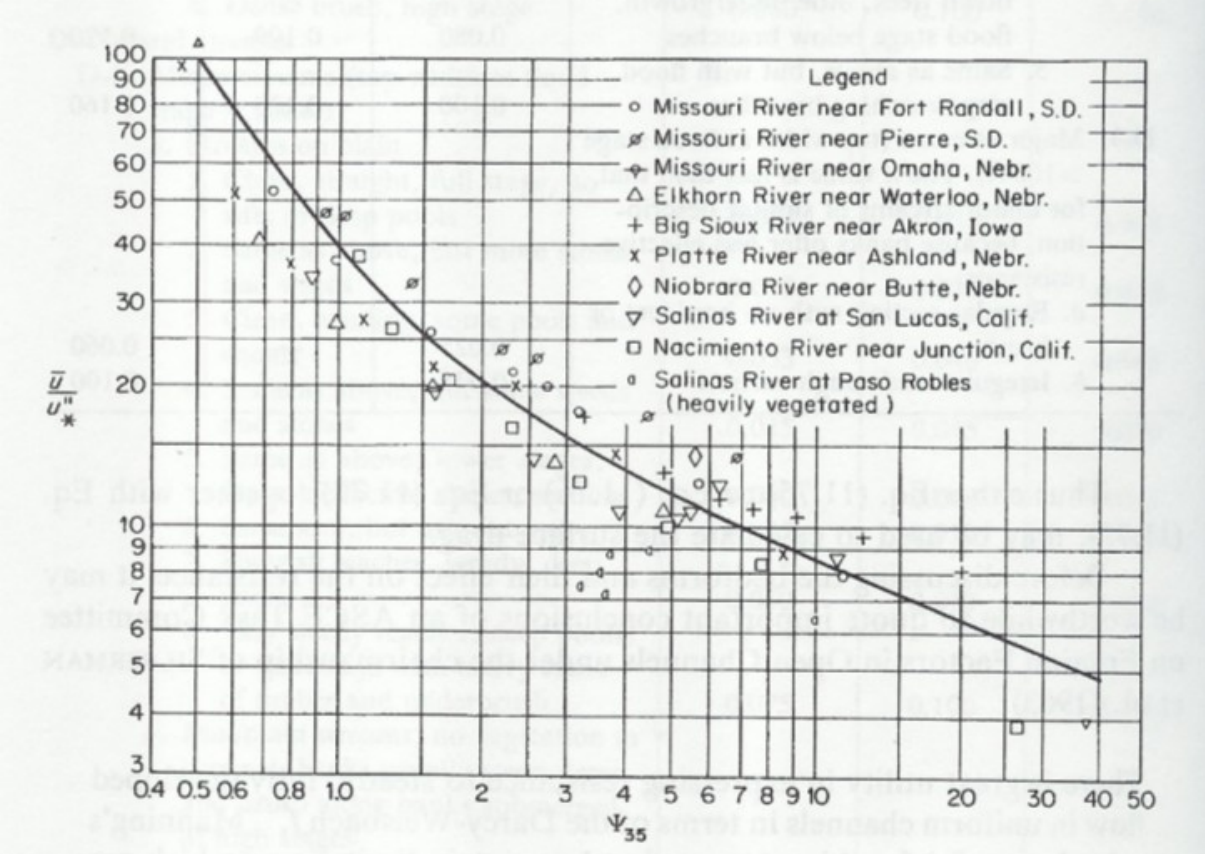

Figure 2.20 Flow resistance due to bed forms [After Einstein (1952)]

In his analysis of Figure 2.20, Einstein reported that:

> *The effect of irregularities (Bed forms) is to distort the flow pattern. When the discharge is least, the distortion of the flow pattern is greatest; as the discharge increases and hence the sediment transport along the bed also increases, the distortion of the flow pattern becomes less and less because the alignment of flow becomes progressively straighter.*

Consequently, one may expect that the additional friction loss, u''_*,

diminishes as the discharge increases.

Shen (1962) suggested another alternative to Equation 2.33 as follows and plotted it as shown in Figure 2.21

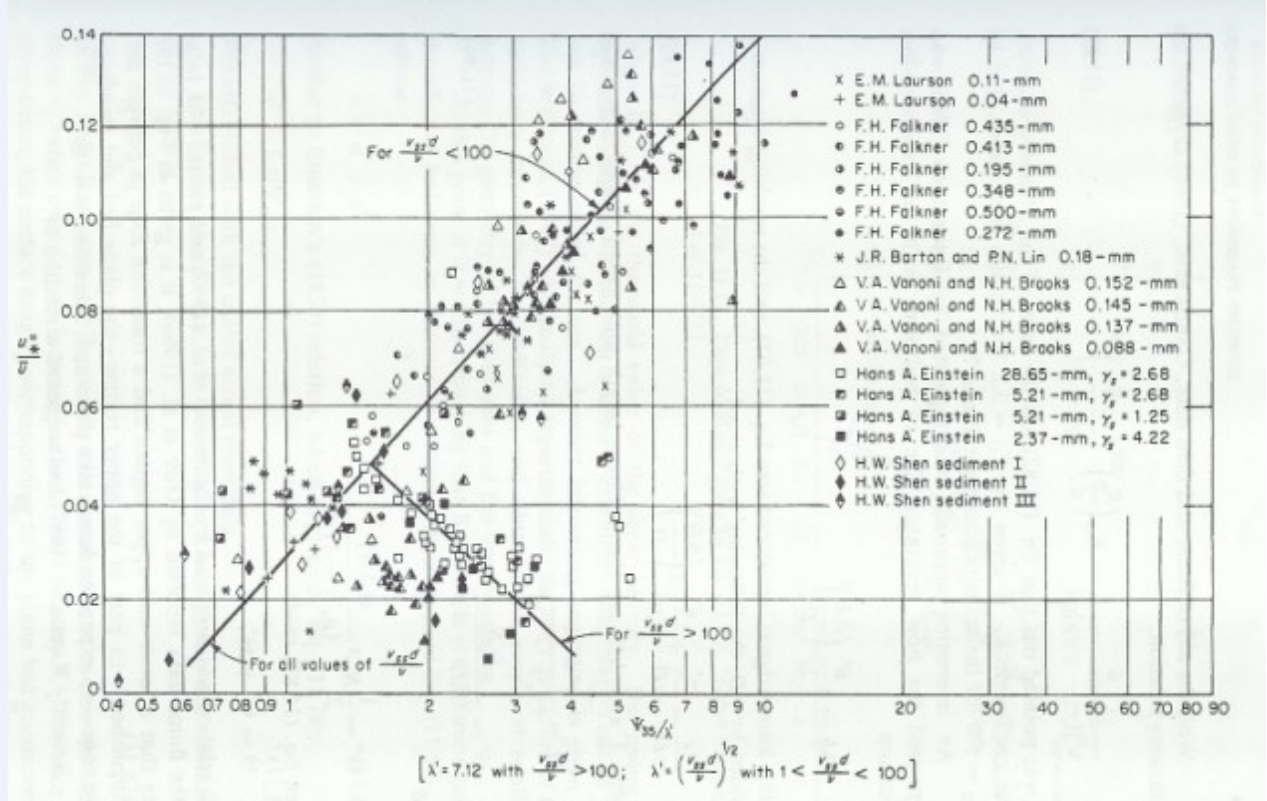

Figure 2.21 Flow resistance due to bed forms [After Shen (1962)]

Shen (1962) included the term $\frac{v_{ss}d}{\nu}$ in the equation as follow:

$$\frac{\bar{u}}{u''_*} = Fn(\psi_{35}, \frac{v_{ss}d}{\nu}) \qquad [2.34]$$

where $\frac{v_{ss}d}{\nu}$ is the Reynolds number in terms of settling velocity

2.3.2.2 FLOW RESISTANCE EXPRESSED WITH FRICTION FACTOR:

Raudkivi (1967) on his research on bed forms presented a plot shown in Figure 2.22.

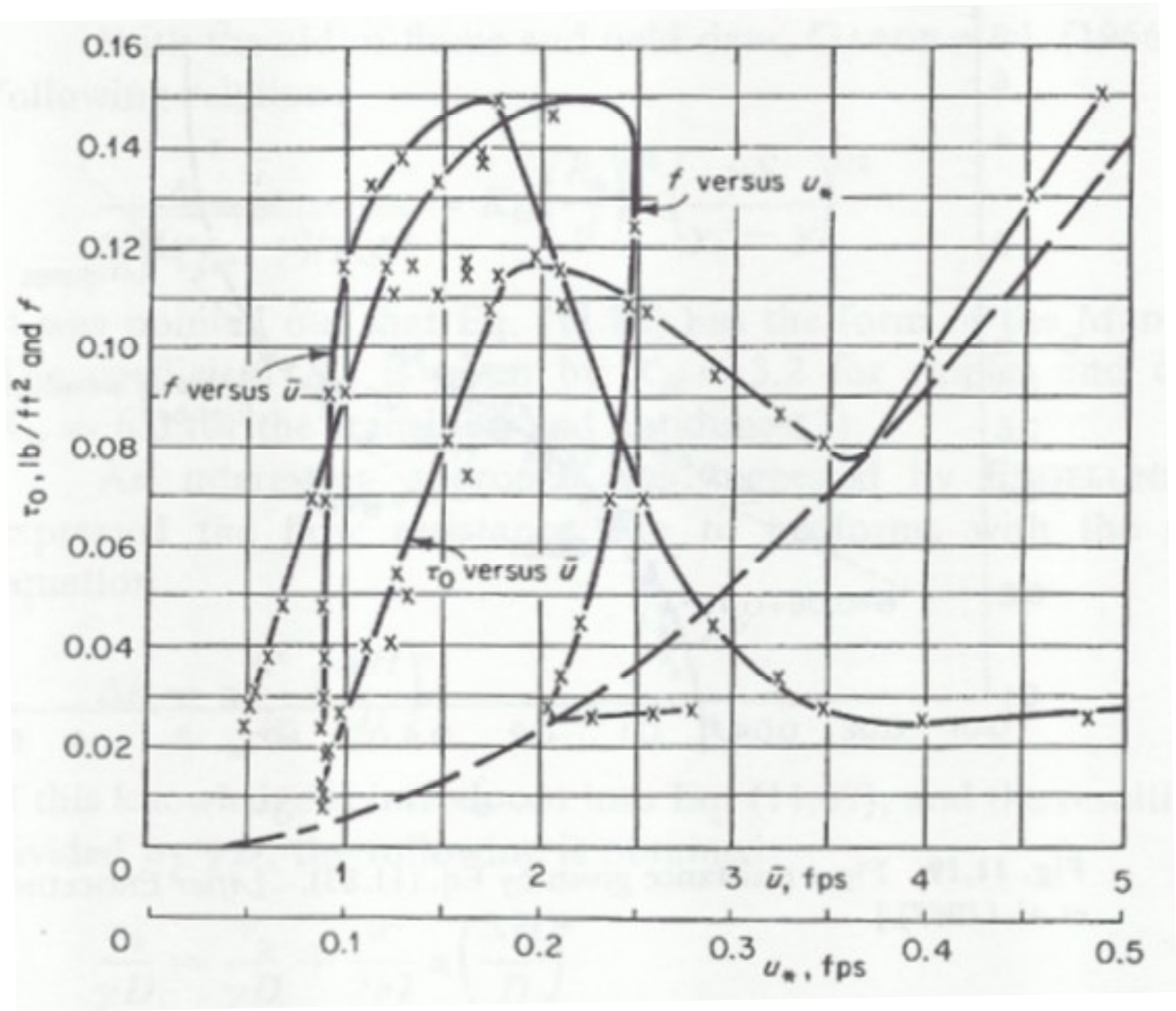

Figure 2.22 Flow resistance due to bed forms [After Raudkivi (1967)]

Figure 2.22 shows that the *f* value increases rapidly once bed forms are created and then decreases as the bed forms are washed out. In the transition region, the friction factor *f* is as low as it was at the initiation of the bed material motion, and increases slightly when the bed forms of

the upper regime are formed. This trend is noticed in f vs. mean velocity $\bar{u}$ and f *vs. shear velocity* u_* relationships.

Nelson and Smith, according to Nelson and others (1993) introduced an expression for the form drag force as follows:

$$D_f = B\frac{1}{2}\rho C_d H_d U_r^{\,2} \qquad [2.35]$$

where D_f is the form drag force; B is the channel width; C_d is the drag coefficient (0.21-0.23), H_d is the bed form height; U_r is a reference velocity that corresponds to a mean velocity between z = k_s and z = H_d if bed form was not present; z = distance from the bed

Thus, the shear stress can be calculated by dividing by the area of the bed over which the force is acting upon as follows:

$$\tau_0" = \frac{1}{2}\rho C_d \frac{H_d}{\lambda} U_r^{\,2} \qquad [2.36]$$

where λ is the bed form wavelength. This means that once the bed form geometry is known; the surface shear stress, form shear stress and the total shear stress can be calculated. Applications of this procedure will be demonstrated in Chapter Three.

2.4 BOUNDARY LAYER THEORY

This section explains the relation of the flow separation phenomena to the boundary layer theory. When a fluid flows over a stationary boundary, e.g. the bed of a river or the wall of a pipe, the fluid touching the surface is brought to rest by the shear stress at the boundary. The velocity increases from the boundary to a maximum in the main stream of the flow as shown in Figure 2.23.

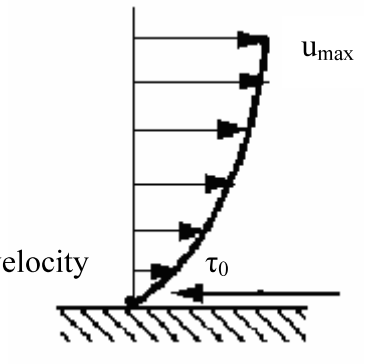

Figure 2.23 Vertical velocity profile [after Douglas (1994)]

This profile must build up gradually from the point where the fluid starts to flow past the surface which in the case of a pipe for example is when it enters a pipe.

In a flat plate in the middle of a fluid, the build up of the velocity profile as the fluid moves over the plate is shown in Figure 2.24. Upstream the velocity profile is uniform, (free stream flow) while a long distance downstream the velocity profile is known as fully developed flow. This region, where there is a velocity profile in the flow due to the shear stress at the boundary is called the boundary layer. The stages of the formation of the boundary layer are shown Figure 2.24:

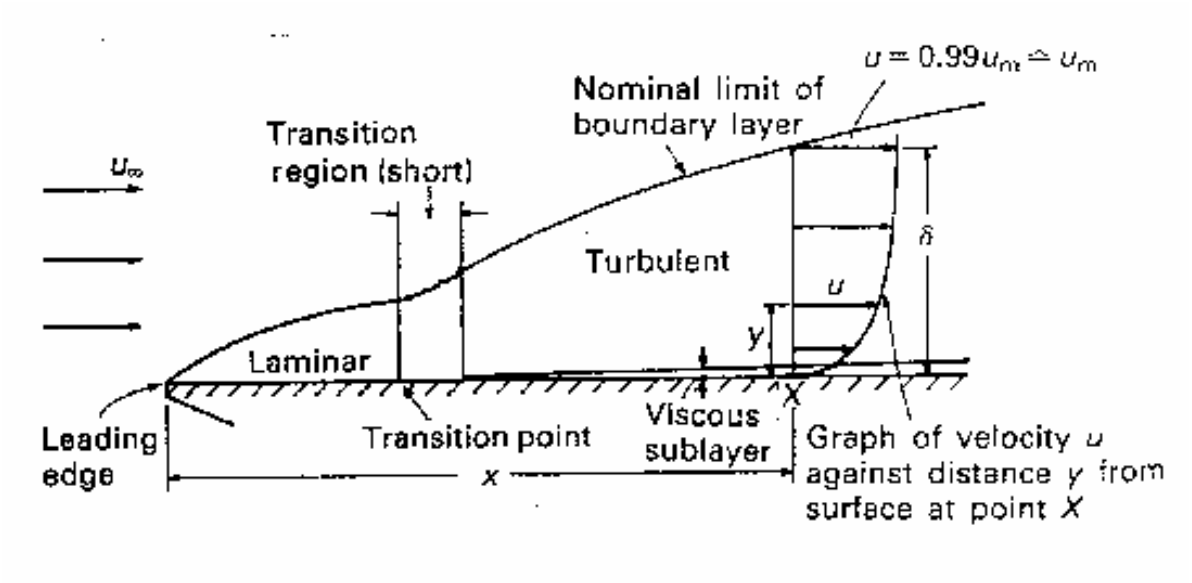

Figure 2.24 Stages of the formation of the boundary layer (after Douglas (1994))

In Figure 2.24, δ is the boundary layer thickness; d = distance from boundary to point where $u = 0.99u_{mainstream.}$ The thickness of this boundary layer is the distance from the boundary to the point where the velocity is 99% of the "free stream" velocity, the velocity in the middle of the river (Douglas 1994). The value of d will increase with the horizontal distance from the point where the fluid first starts to pass over the boundary (x in Figure 2.24). It increases to a maximum in fully developed flow. Correspondingly, the total drag force D on the fluid due to shear stress at the wall increases from zero at the start of the plate to a maximum in the fully developed flow region where it remains constant (Douglas 1994); however, the shear stress decreases with increasing distance along the developing boundary layer.

2.4.1 FORMATION OF THE BOUNDARY LAYER

2.4.1.1 LAMINAR BOUNDARY LAYER

According to Douglas (1994) the boundary layer grows from zero when a fluid starts to flow over a solid surface. As it passes over a greater length more fluid is slowed by friction between the fluid layers close to the boundary. Hence the thickness of the slower layer increases.
The fluid near the top of the boundary layer is dragging the fluid nearer to the solid surface along. The mechanism for this drag may be one of two types:

The first type occurs when the normal viscous forces (the forces which hold the fluid together) are large enough to exert drag effects on the slower moving fluid close to the solid boundary. If the boundary layer is thin then the velocity gradient normal to the surface $\frac{du}{dy}$ is large and in turn the shear stress is also large. The corresponding force may then be large enough to exert drag on the fluid close to the surface.

The second type occurs when the boundary layer thickness becomes greater, the velocity gradient become smaller and the shear stress decreases until it is no longer enough to drag the slow fluid near the surface along. Up to this point the flow has been laminar. This part of the boundary layer is known as the laminar boundary layer.

2.4.1.2 TURBULENT BOUNDARY LAYER

The viscous shear stresses have held the fluid particles in a constant motion within layers. These stresses become small as the boundary layer increases in thickness and the velocity gradient gets

smaller (Douglas 1994). Eventually they are no longer able to hold the flow in layers and the fluid starts to rotate as shown in Figure 2.25.

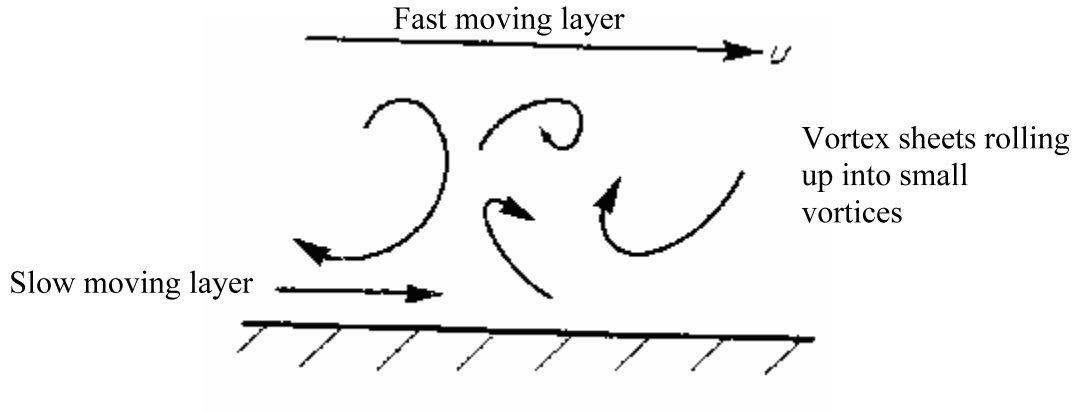

Figure 2.25 Transition between the laminar and turbulent boundary layers [After Douglas (1994)]

This causes the fluid motion to rapidly become turbulent. Fluid from the fast moving region moves to the slower zone transferring momentum and thus maintaining the fluid near the wall in motion. Conversely, slow moving fluid moves to the faster moving region slowing it down. The net effect is an increase in momentum in the boundary layer and thus this region of the boundary layer is called the turbulent boundary layer.

At points very close to the boundary the velocity gradients become very large with the viscous shear forces again becoming large enough to maintain the fluid in laminar motion. This region is known as the laminar sub-layer, in this region, the velocity profile is logarithmic. According to Schilichting (1979), the depth of this layer is given as follows:

$$\delta_v = X \frac{v}{u_*} \qquad [2.37]$$

where X ranges from 5 to 12.6 according to many investigators

2.4.2 SURFACE ROUGHNESS EFFECT

Despite its thinness, the laminar sub-layer can play a vital role in the friction characteristics of the surface. In a turbulent flow structure, a roughness height (k_s) is greater than the thickness of the laminar sub-layer increases the amount of turbulence and energy losses in the flow. If the height of roughness (k_s) is less than the thickness of the laminar sub-layer the flow is said to be hydraulically smooth and it has little effect on the boundary layer. Table 2.3 summarizes different flow regimes with respect to the Reynolds number. In Table 2.3 Reynolds number = vR/υ; v is the mean fluid velocity; R is the hydraulic radius; υ is the kinematics viscosity.

Type of Flow	**Reynolds Number**
Laminar	< 500
Transition	500-1000
Turbulent	>1000

Table 2.3 Types of flow regimes and the corresponding Reynolds number [After Graf (1994)]

Outside the viscous sublayer, another region referred to the outer region exists. In this region the velocity profile is also logarithmic, however it has a different scaling than the laminar sublayer scaling.

Various investigations of the different regions of flows based on the turbulent structure of the flow have been performed over the history. Nezu and Nakagawa (1993) divided the regions as follows:

- Wall region $\left(0 \leq \frac{z}{H} \leq 0.15\text{-}0.20\right)$

Velocities in this region are proportional to the shear velocity (u_*), while lengths are proportional to $\frac{v}{u_*}$.

- Intermediate region

An intermediary layer between the wall and the free surface region, velocities in this region are proportional to the shear velocity (u_*), while lengths are proportional to the flow depth.

- Free surface region ($0.6 \leq \frac{z}{H} \leq 1.0$)

Velocities in this region are proportional to the maximum velocity U_{max} ($U_{mainstream}$) and lengths are proportional to the flow depth.

2.4.3 BOUNDARY LAYER SEPARATION

When the pressure increases (as shown in Figure 2.26) in the direction of flow, the fluid outside the boundary layer has enough momentum to overcome this pressure which is trying to push it backwards. The fluid within the boundary layer has so little momentum that it will very quickly be brought to rest, and possibly reversed in direction. If this reversal occurs it lifts the boundary layer away from the surface as shown in Figure 2.27.

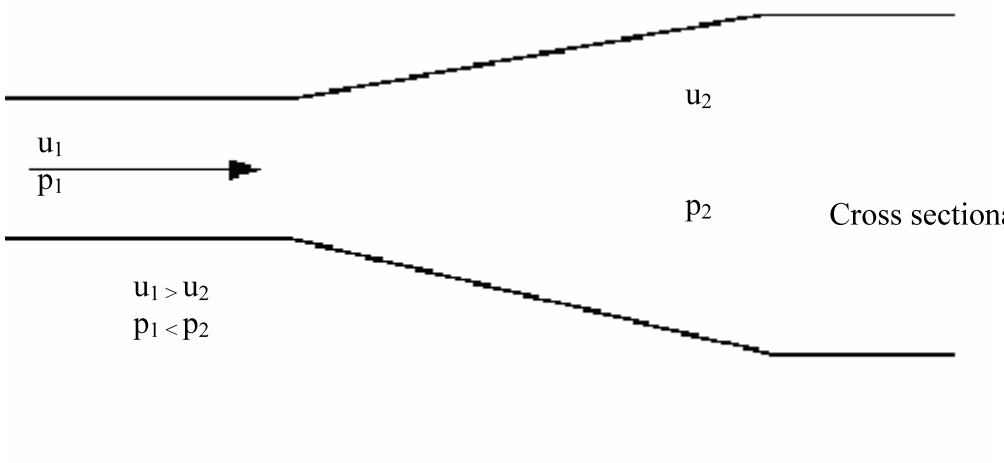

Figure 2.26 Divergent flows [After Douglas (1994)]

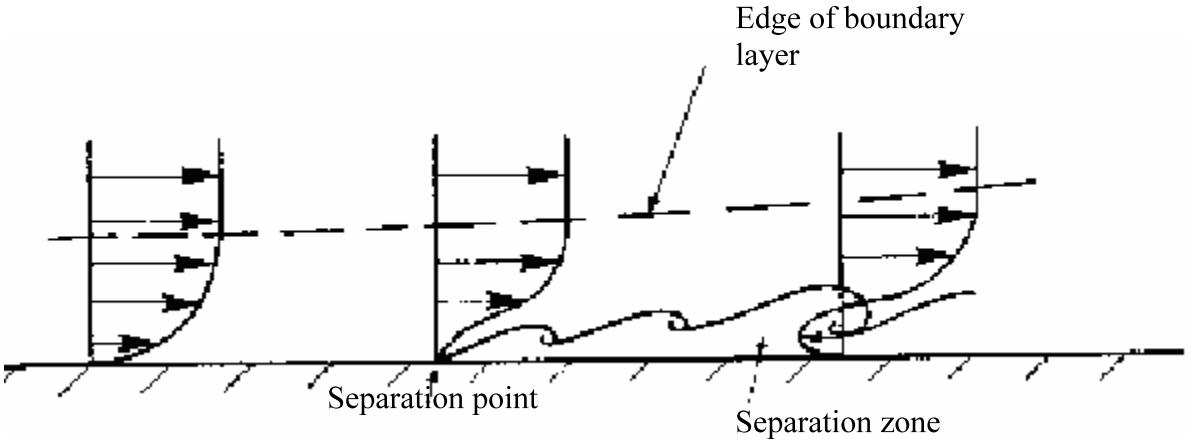

Figure 2.27 Boundary layer separation [After Douglas (1994)]

This phenomenon is known as boundary layer separation (Douglas 1994). At the edge of the separated boundary layer, where the velocities change direction, a line of vortices occur (known as a vortex sheet). This happens because fluid to either side is moving in the opposite direction as shown in Figure 2.28.

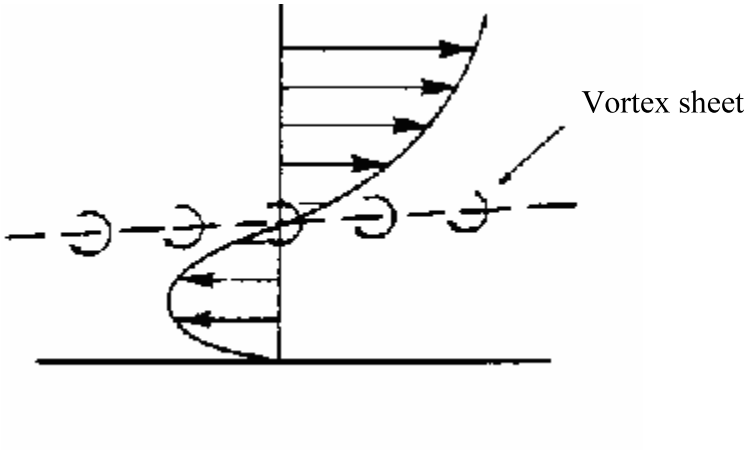

Figure 2.28 Boundary layer separation (Vortex Shear) [After Douglas (1994)]

This boundary layer separation increases the turbulence because of the vortices and results in very large energy losses in the flow. These separating / divergent flows are inherently unstable and far more energy is lost than in parallel or convergent flow. Detailed discussions of the separation phenomenon and its application in the current study are presented in Chapter Three and Four.

2.5. LITERATURE REVIEW SUMMARY

Several studies in the current literature attempted to address ***Hypothesis One*** mentioned in Chapter One which assumes that the resistance to the flow is a function of the bed form geometry and varies by River Mile. However previous research on bed forms was primarily based laboratory studies or small scale field investigations. All the field investigations represented snap shots of the bed form geometry with no indications of extent of the bed forms in the river.

The literature review also revealed the lack of field investigations that addressed the three-dimensional nature of bed forms in alluvial rivers, and how this affect the turbulent structure on the surface of bed forms. Also, the review revealed the lack of any investigations in the suspended sediment concentration profiles on top of the bed forms, several investigators have studied the erosion, deposition and migration rates of bed forms, but these studies failed to address the effect of the suspended sediment concentration on the turbulent structure on top of the bed forms and how the sediment concentration profiles vary from at the crest, lee and developing side of the bed form. All laboratory flume experiments presented in the literature represented controlled flow conditions unlike the flow environments in natural alluvial rivers where seasonal flow and wash load variations occur.

Although several three dimensional numerical models have and continue to be developed for the simulation of flow and transport in alluvial rivers, this literature review revealed the absence of any research that has addressed in details ***Hypothesis Two*** and ***Hypothesis Three.***

The resistance in numerical codes familiar to the author is represented as a skin friction coefficient with some additional modification for the bed form resistance based on the numerical modeler's experience. This additional modification is used as a calibration parameter without correlating the bed form geometry to the grid spacing of the river simulation model. Chapter Five and Six, respectively, address these hypotheses.

CHAPTER 3
DATA ANALYSIS AND ASSESSMENT

This portion of the study discusses ***Hypothesis One*** which assumes that the resistance to the flow is a function of the bed form geometry and varies by River Mile.

3.1. GEOMETRIC CHARACTERISTICS OF BED FORMS IN THE LOWER MISSISSIPPI RIVER

The geometric characteristics of bed forms are irregular in nature and therefore the notion of average bed form wave length and average bed form wave amplitude is not sufficient to describe the geometry of the bed forms; alternative statistical indicators are introduced in this study.

3.1.1. SPECTRAL ANALYSIS

The approach in this study was to apply spectral analysis to the multibeam bathymetric survey data. Spectral analysis is a powerful tool to examine periodicity in natural phenomena such as periodicities in bed forms sequences. Spectral analysis belongs to a family of time series analytic techniques whose aim is to uncover trends or patterns in a sequence of data over time. By extending the temporal methods and substituting space for time, one dimensional spatial data can also be analyzed by these techniques (Granger, 1969; Bennet 1979; Richards, 1981).

Examples of this application are the determination of objective wavelengths in meanders (Speight, 1965, 1967; Chang and Toebes, 1970; Ferguson, 1975; Hokke, 1984), pools and riffles (Richards, 1976), bed forms (Naden 1987, Nordin 1971), and pools caused by coarse woody

debris (Nakamura and Swanson, 1996). These successful applications suggest that spectral analysis may be a useful test for the periodicity in bed forms in the Lower Mississippi River. Spectral analysis partitions the variation in a time (or spatial) series into components according to the duration or length of the intervals within which the variation occurs. The analysis is based on the Fourier theory that almost any function of a real variable can be represented as the sum of sine and cosine functions.

Any wave form, regardless of how complex, can be described by an expression of the Fourier relationship:

$$Y = a[k] \cos (k\theta) + b[k] \sin (k\theta) \qquad [3.1]$$

where a[k] is the amplitude; k is the phase angle; θ is the angle, and b[k] is the harmonic number, or the number of cycles per basic interval. Since the sum of all the sinusoids is equal to the original time (or spatial) series, the sum of the variation in all of the sinusoids represents the total variation in the series. Spectral analysis isolates the harmonic present and partitions the variance according to frequency. The results are summarized in a power spectrum (spectral density function) which indicates the variance accounted for by the fluctuations at the different frequencies. Rayner (1971) and Davis (1986) provide more detailed explanations of spectral analysis for geologic research. This analysis adopts the standard terminology used to describe sinusoidal curves (Rayner, 1971). The term wave length refers to the distance between similar points on the curve (for example, from crest to crest or trough to trough) (Figure3.1).

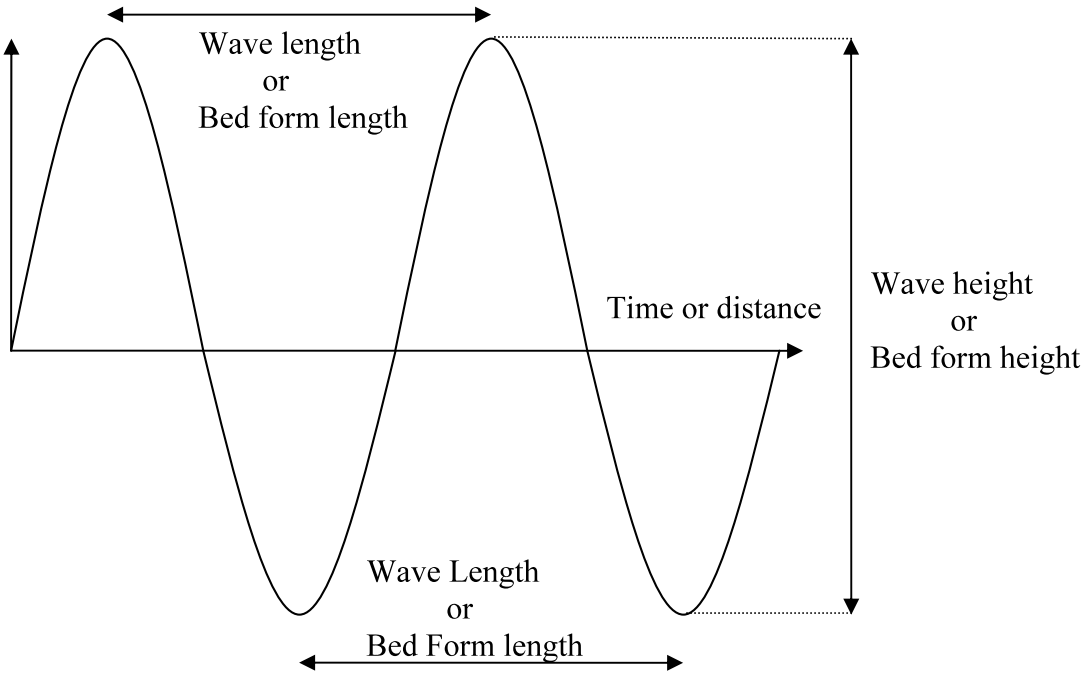

Figure 3.1: Bed Form Terminology

3.1.2. METHODOLOGY

Spectral analysis was applied in this study to the multibeam bathymetric survey data collected by the U.S. Army Corps of Engineer in the Lower Mississippi River in the period of June 2003 to September 2003. These data were provided to the author as a part of a hydrodynamic and ecological modeling study of the Lower Mississippi River. Meselhe et al (2005) presented a more detailed explanation of the study.

Multibeam data were collected from River Mile (RM) Zero (Head of Passes, LA) up to RM 234 (Baton Rouge, LA). Figure 3.2 shows the location of the multibeam data collected. A sample three dimensional view of a multibeam dataset collected at RM 223 is shown in Figure 3.3.

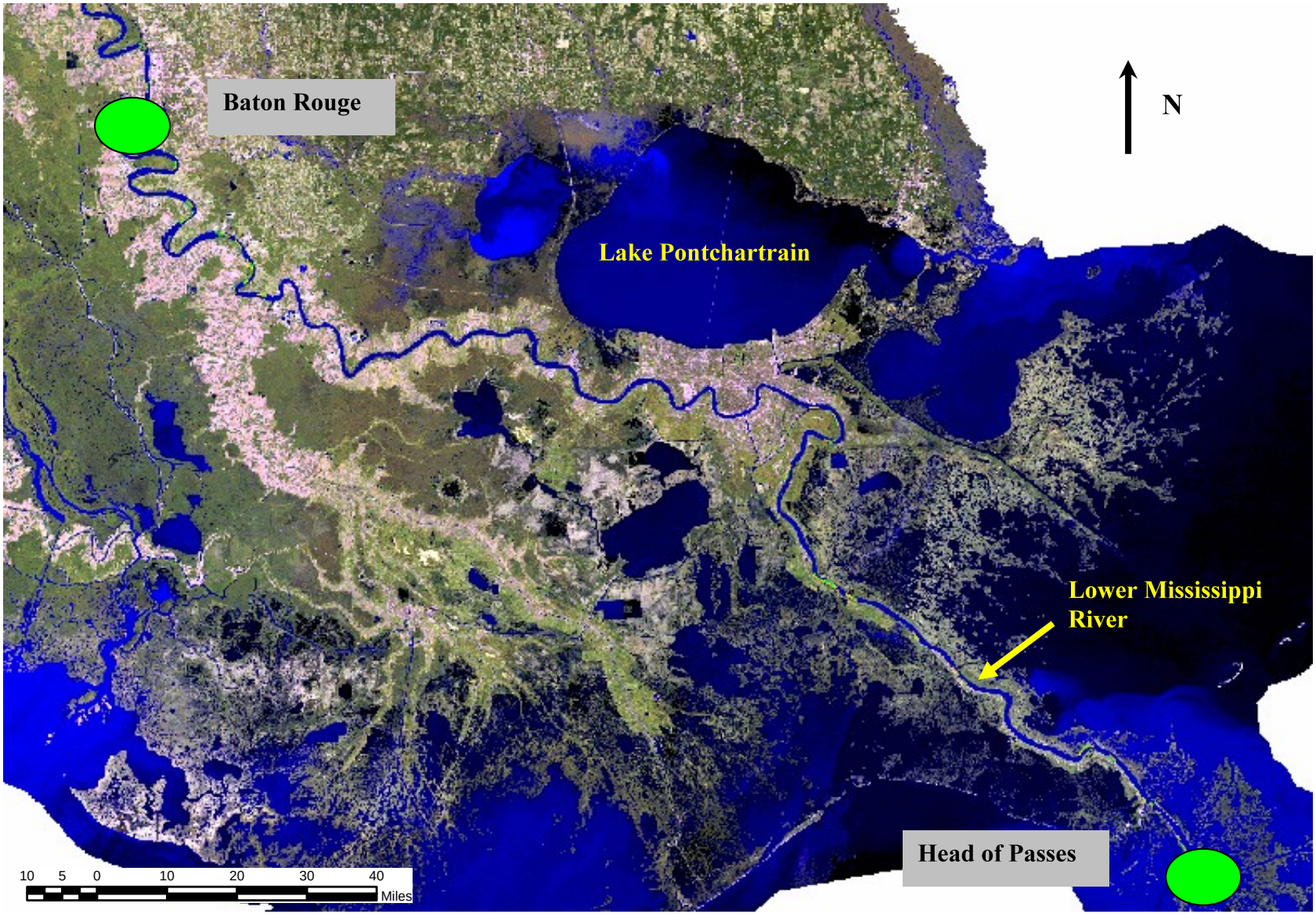

Figure 3.2: Range of multibeam bathymetric data collected by USACE (between Baton Rouge, LA and Head of Passess, LA)

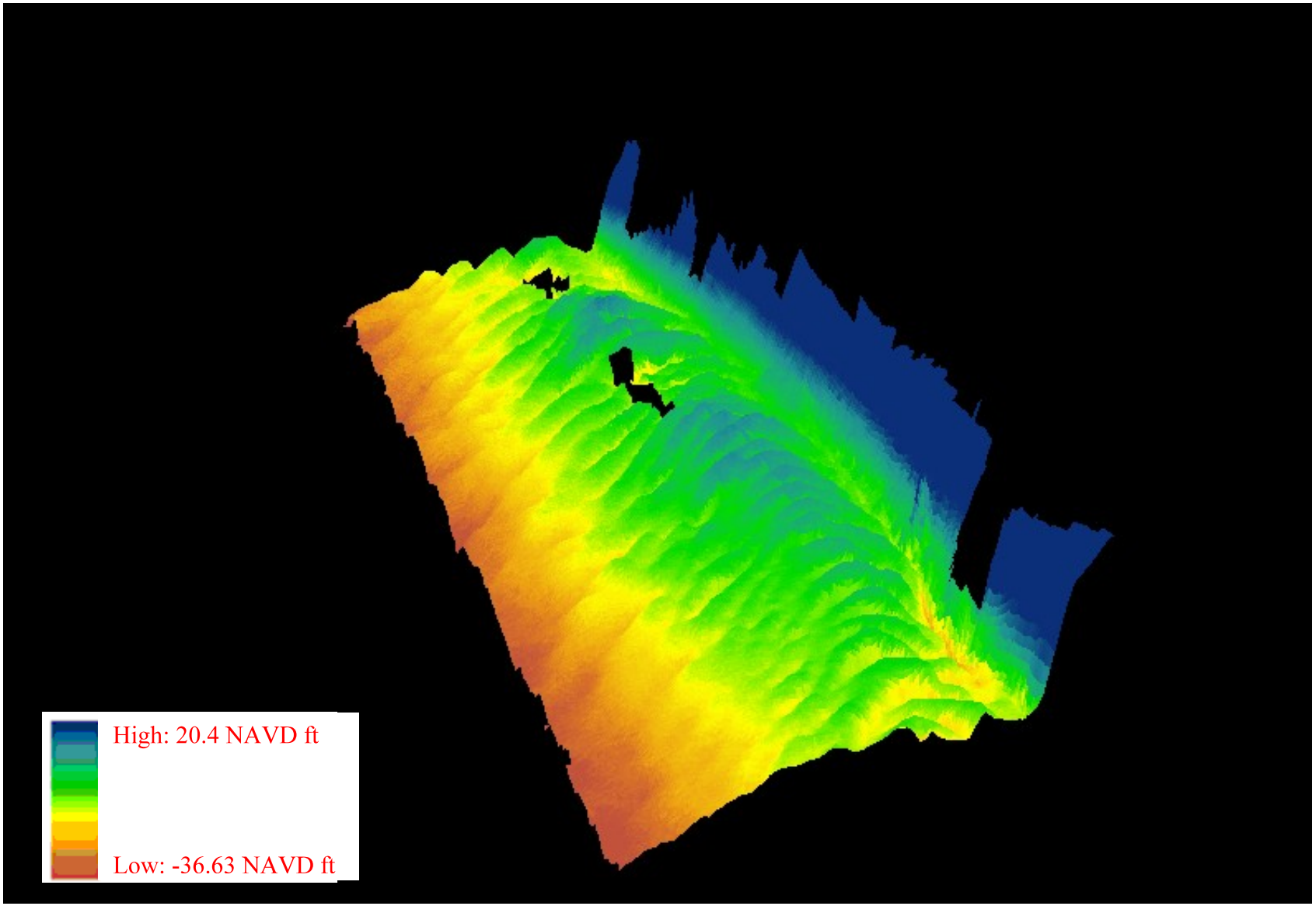

Figure 3.3: 3D view of a multibeam data collected in RM 223

A total of 31 Multibeam datasets were acquired and three longitudinal profiles were extracted from each data set. The profile locations were carefully selected such that they cover the total width of each dataset, one on each side and one in the middle of the dataset in an attempt to cover the three-dimensional nature of the observed bed form. Spectral analysis was then applied to the extracted profiles.

3.1.3. RESULTS

A sample extracted profile from multibeam dataset at RM 223 (Figure 3.4 and 3.5) is shown in Figure 3.6, while spectral analysis results of the same profile are shown in Figure 3.7. Multibeam surfaces images are included in Appendix 1

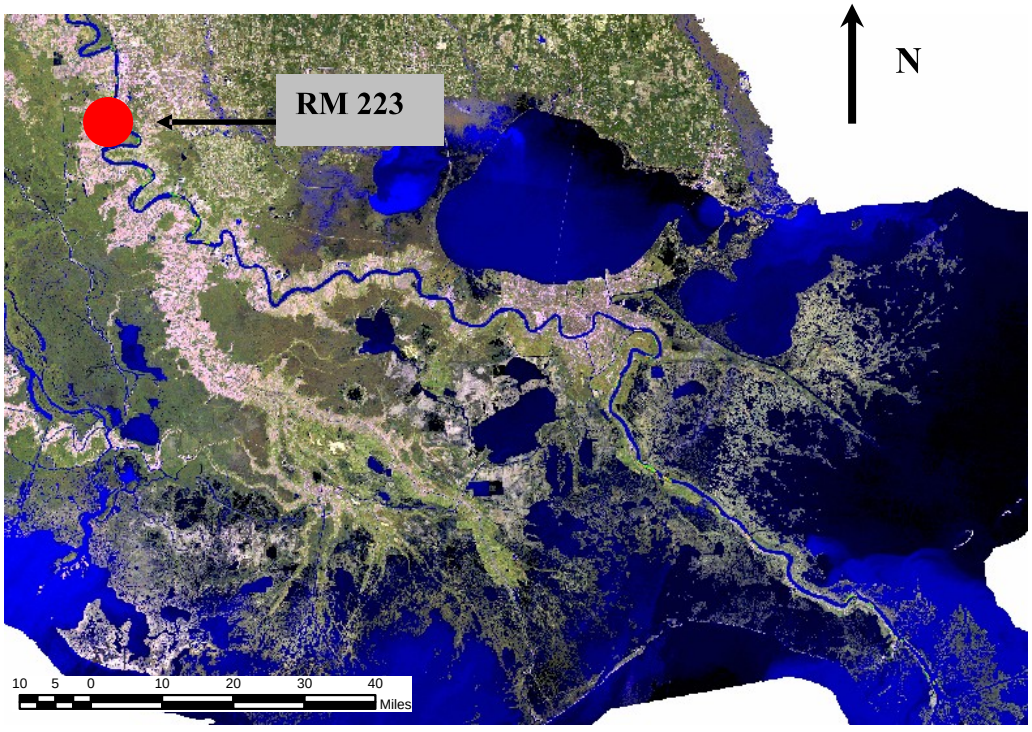

Figure 3.4: Location of RM 223 along the Lower Mississippi River (near Baton Rouge, LA)

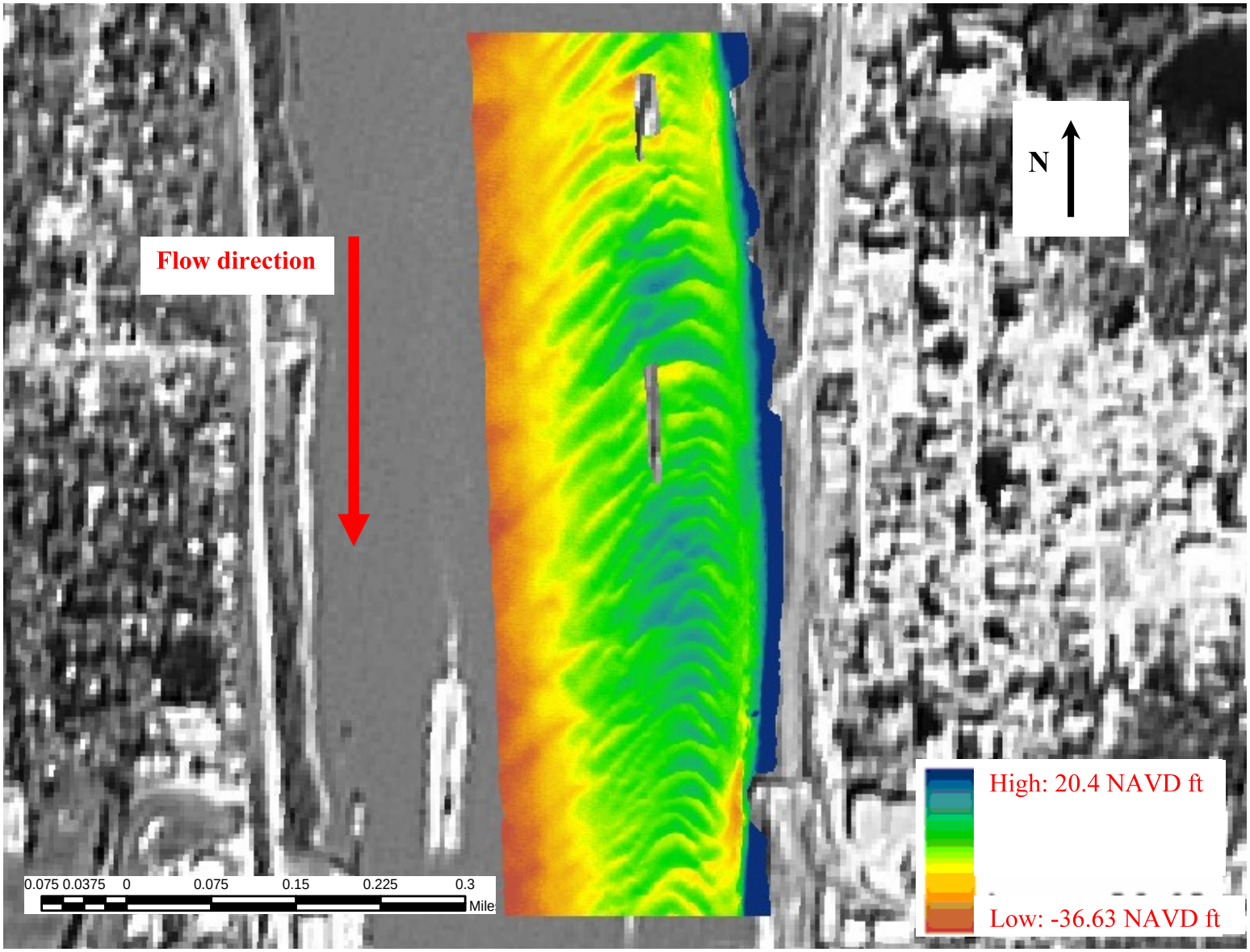

Figure 3.5: Plan view of multibeam dataset at RM 223

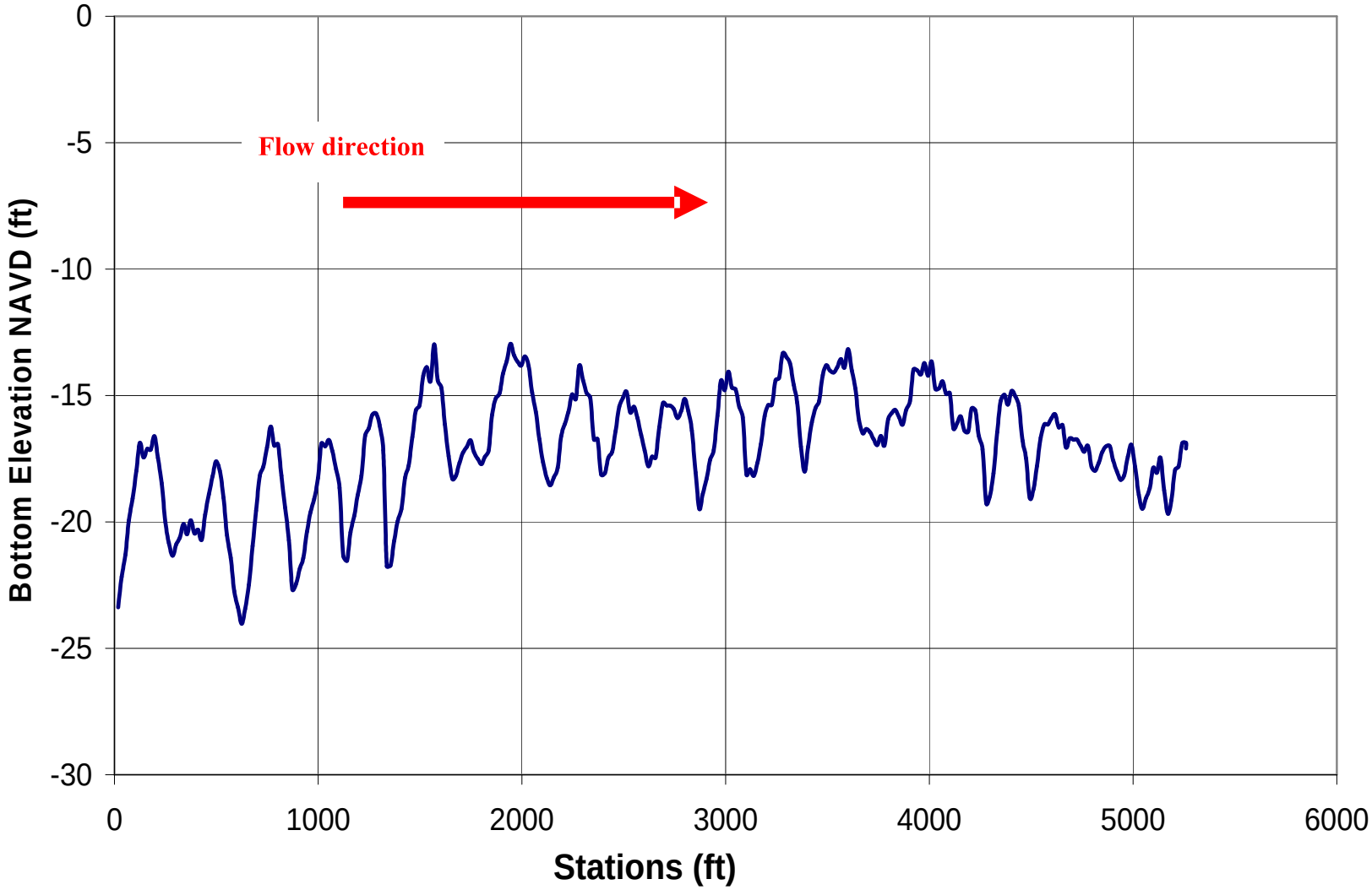

Figure 3.6: Extracted profile at RM 223

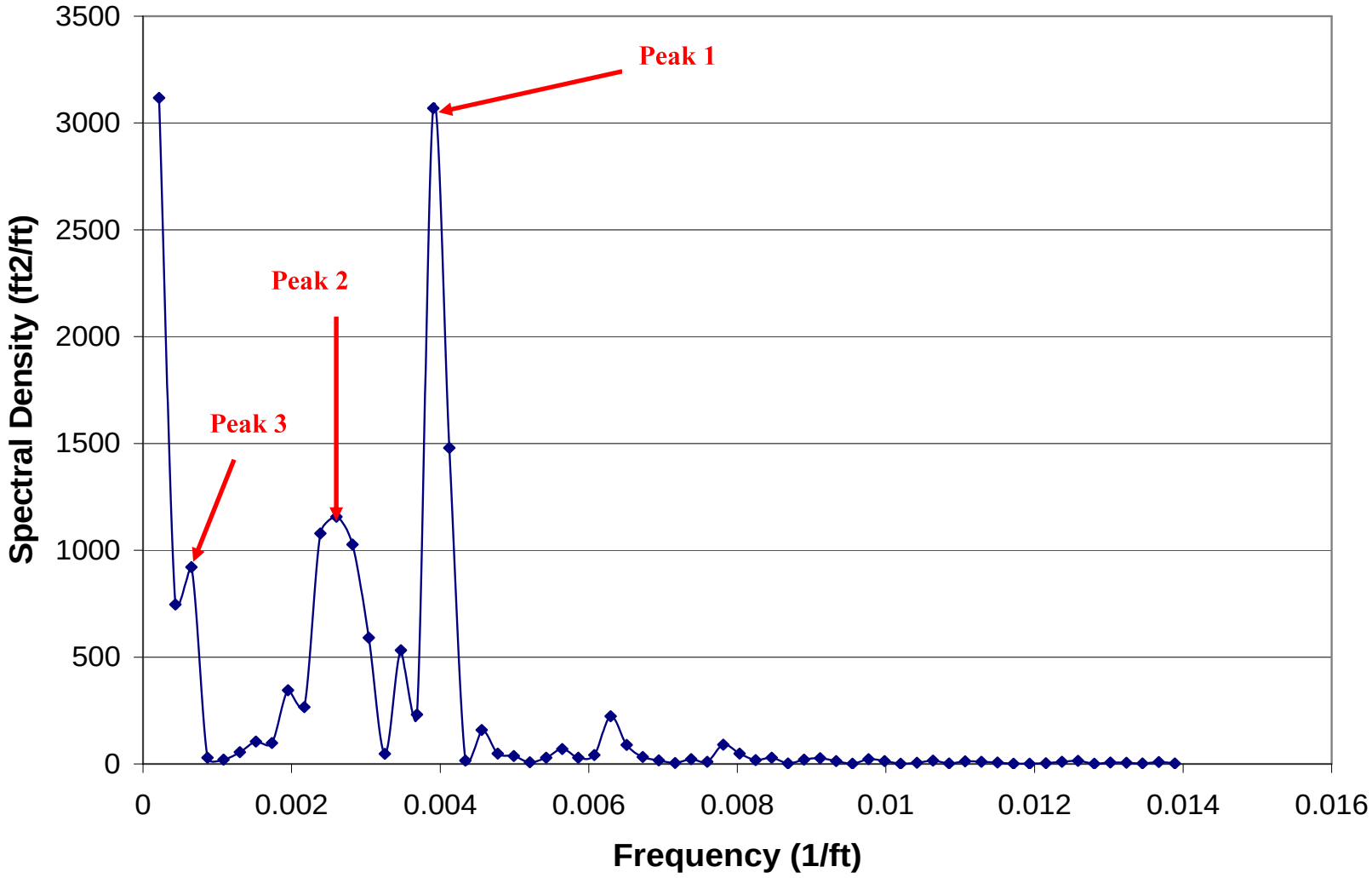

Figure 3.7: Spectral analysis results at RM 223 showing the three highest peaks

Results of the spectral analysis show a distinct periodic character in the longitudinal bed profiles in the sampled datasets. Several spectral peaks were detected in all of the datasets; several reaches exhibit more than one peak as shown in Figure 3.7.

Three highest spectral peaks were noted for each profile (Figure 3.7) as an attempt to eliminate some of the uncertainties associated with the spectral analysis and then the corresponding bed form wave lengths (≈ 1/frequency), heights (≈ $\sqrt[3]{Spectral.Density}$) and steepness (height/wavelength) were calculated as shown below in Table 3.1. The calculated bed form geometry was then checked against the observed bed form to eliminate any erroneous bed form dimensions that might have resulted from the spectral analysis.

Spectral Peak No.	**Bed form length (ft)**	**Bed form height (ft)**	**Bed form steepness**
Peak 1	1/0.0041 = 243.9	$\sqrt[3]{3102} = 14.58$	14.58/243.9 = 0.059
Peak 2	1/0.0031 = 322.5	$\sqrt[3]{1092} = 10.29$	10.29/322.5 = 0.031
Peak 3	1/ 0.0015 = 666.6	$\sqrt[3]{989} = 9.96$	9.96/666.6 = 0.015

Table 3.1 Calculation of bed form length, height and steepness for RM 223

The calculated wave lengths, heights and steepness for the entire length of the studied reach are shown in Figure 3.8, 3.9 and 3.10. Figure 3.11 shows a spatial series for the bed form height divided by the depth.

Figure 3.8 shows that the calculated bed form wave lengths on average ranged from 50ft to 500ft (15m to 152m) in the downstream section of the studied reach while an increase in the wave

length was observed in the upstream section of the reach where the bed form wave length on average ranged from 250ft – 1000ft (76m to 305m).

The same pattern was also observed in the bed form height (Figure 3.9) where the heights on average ranged from 1ft to 7ft (0.3m to 2 m) in the downstream reaches of the River, while in the upstream reaches they ranged from 4ft to 15ft (1.2m to 4.5m). However, a clear pattern was not observed for the steepness case.

Figure 3.11 shows that the majority of the data have a ratio of bed form height to depth of less than 0.16 (1/6) which agrees with Garcia (1999) results mentioned in Chapter Two. At the same time some higher ratios extended up to 0.3 (1/3) validating the results of Nordin (1965) also mentioned in Chapter Two.

Although Figures 3.8 to 3.10 reveal some valuable information about the bed form geometry in the studied reach of the Lower Mississippi River, they also clearly show that presenting the spectral results alone as spatial series plots is not adequate to represent the results. In the next section, statistical characterization of the bed form geometries will be performed using statistical summary tables, histogram plots and box plots.

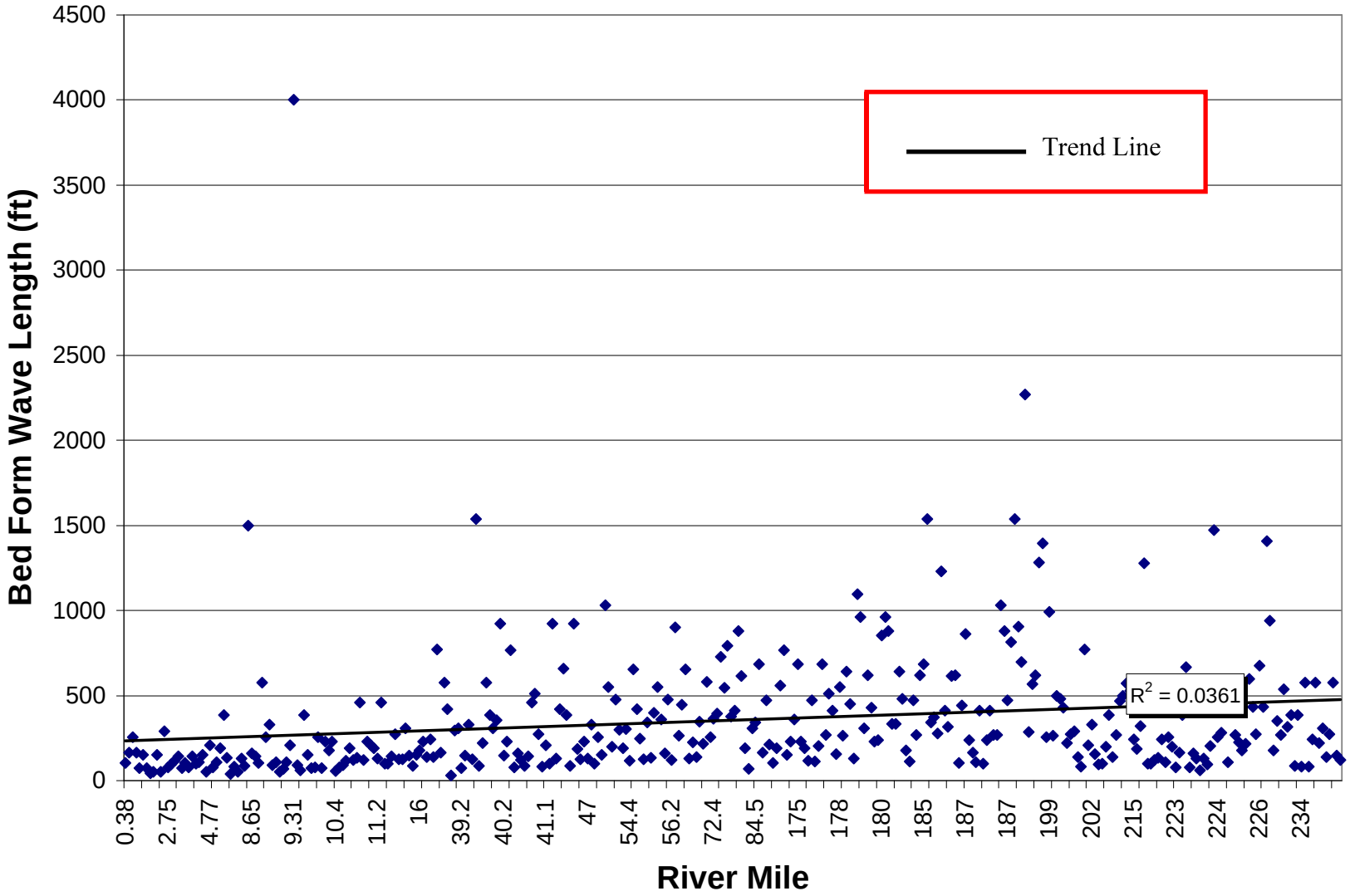

Figure 3.8: Spatial series of bed form wave length for Lower Mississippi River between RM 0.00 and RM 234 (349 observations).

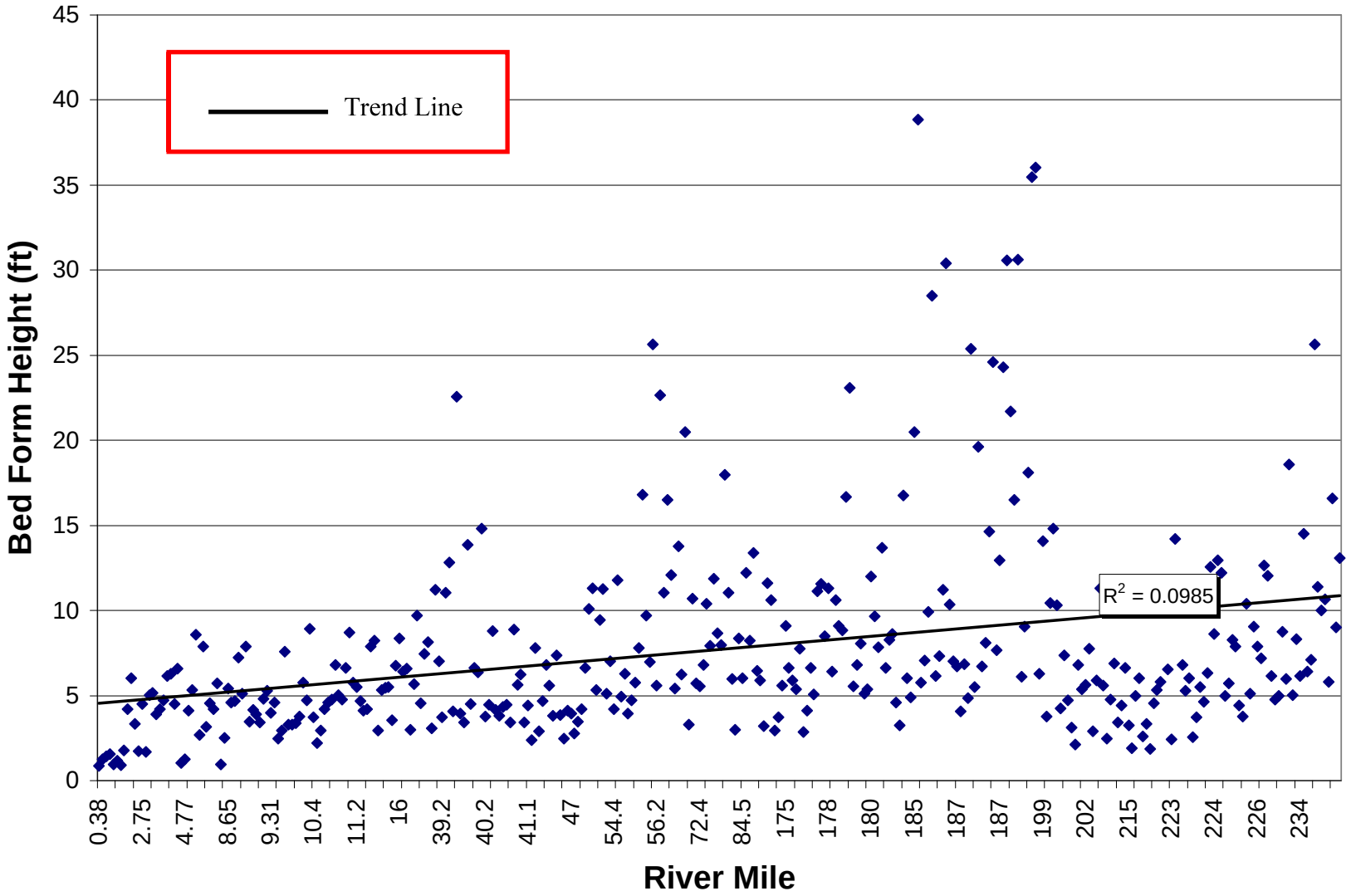

Figure 3.9: Spatial series of bed form height for Lower Mississippi River between RM 0.00 and RM 234 (349 observations).

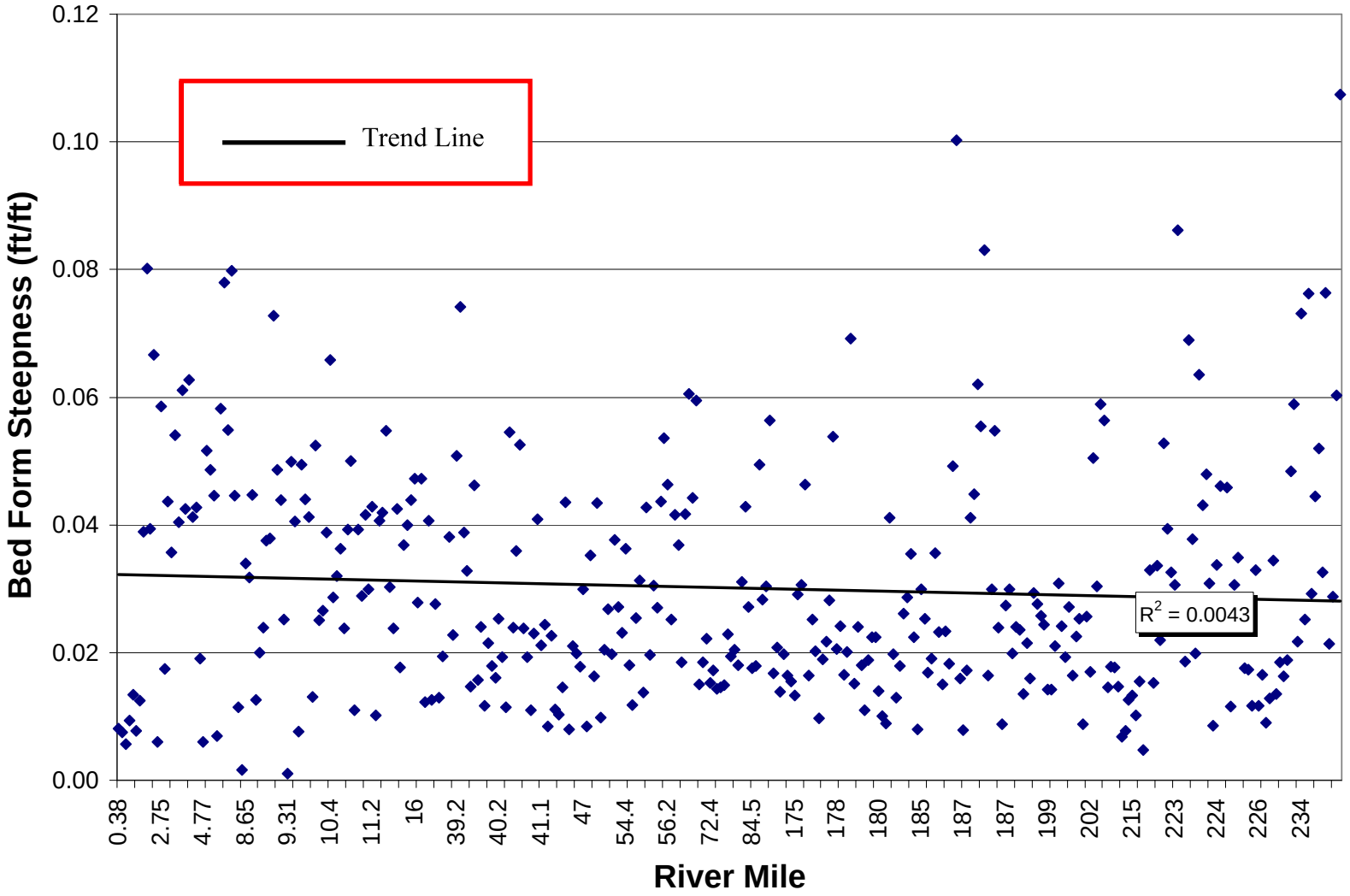

Figure 3.10: Spatial series of bed form steepness for Lower Mississippi River between RM 0.00 and RM 234 (349 observations).

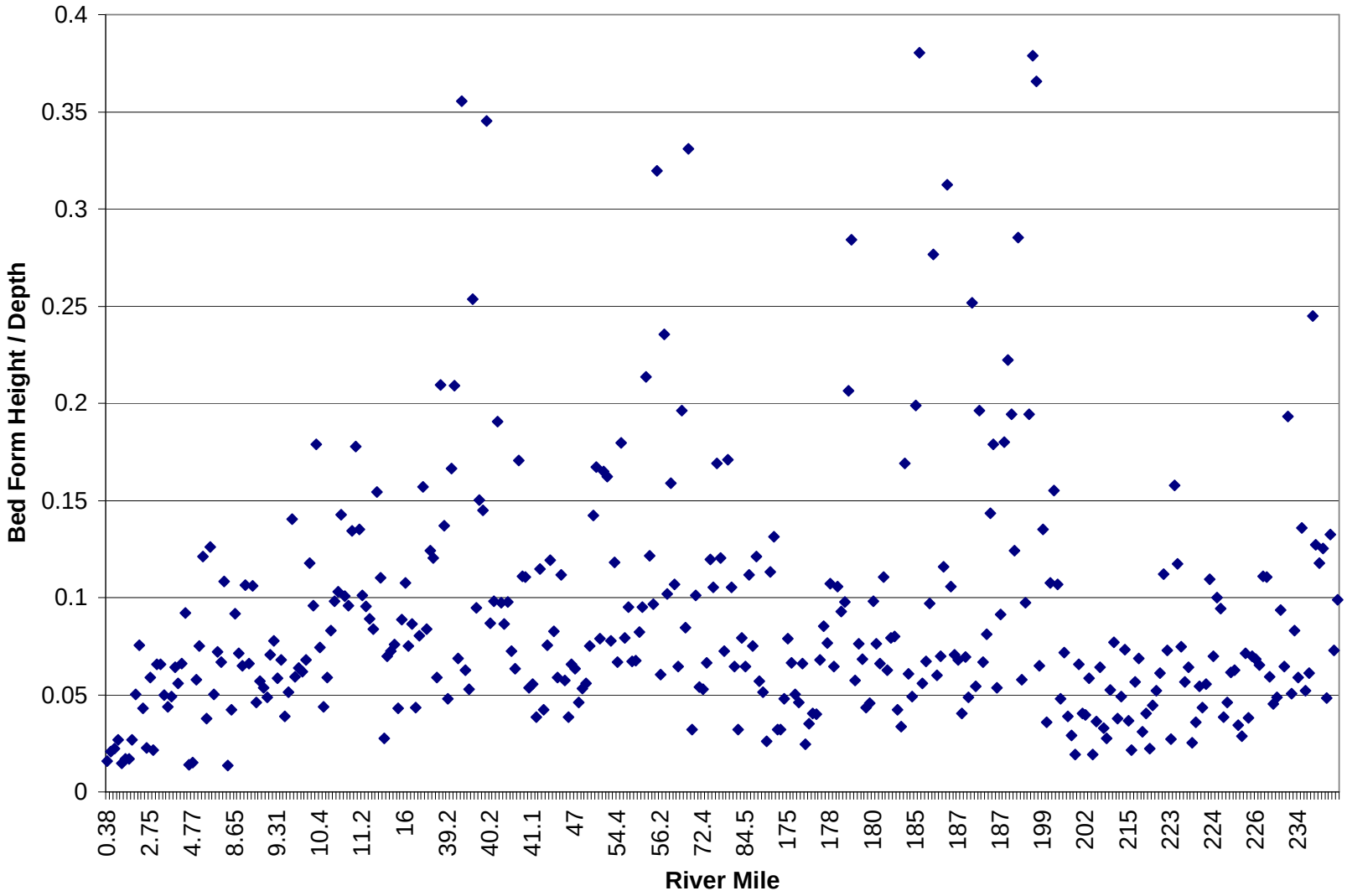

Figure 3.11: Spatial series of bed form height/depth for Lower Mississippi River between RM 0.00 and RM 234 (349 observations).

Table 3.1 summarizes additional statistical analysis performed on the spectral results obtained from the survey. The data included the three spectral peaks surveyed at each river mile.

Bed Form Geometry Summary			
	Bed form length (m)	**Bed form Height (m)**	**Steepness (m/m)**
Mean	108.1	2.35	0.03011
Std. Dev.	112.3	1.78	0.01821
Median	73.97	1.82	0.02520
Minimum	8.97	0.25	0.00100
Maximum	1227.12	11.84	0.10742
Range (Max-Min)	1210.2	11.58	0.10642
Skewness	4.06	2.40	1.23

Table 3.2 Bed form geometry summary of the spectral results

The statistical measures summarized in Table 3.2 reveal the high variability present in this natural system; the bed form standard deviation is of the same order of magnitude as the mean suggesting that the bed form data are following a skewed probability density function. Frequency histograms for the bed form wave lengths, heights and steepness were constructed (Figure 3.12, 3.13 and 3.14) to illustrate the degree of skewness present in the bed form data. The data included the three spectral peaks surveyed at each river mile. These frequency plots list the number of observations of each variable (length, height and steepness) in different classes. The dataset were divided into ten classes where each class boundary is presented at the mid point of the class. Sample size (N) was equal to 349 observations.

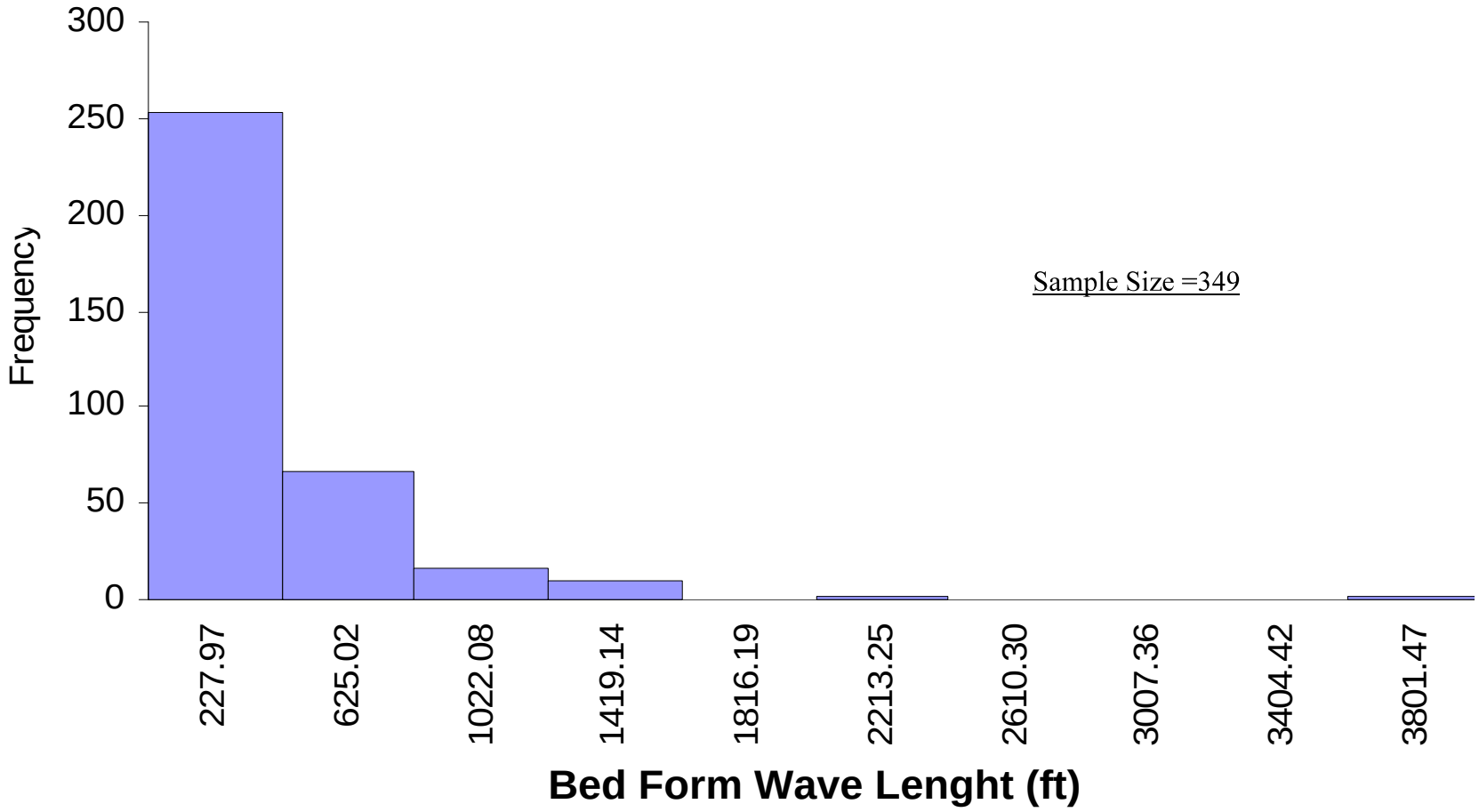

Figure 3.12 Histogram of the bed form wave length for Lower Mississippi River between RM 0.00 and RM 234 (349 observations).

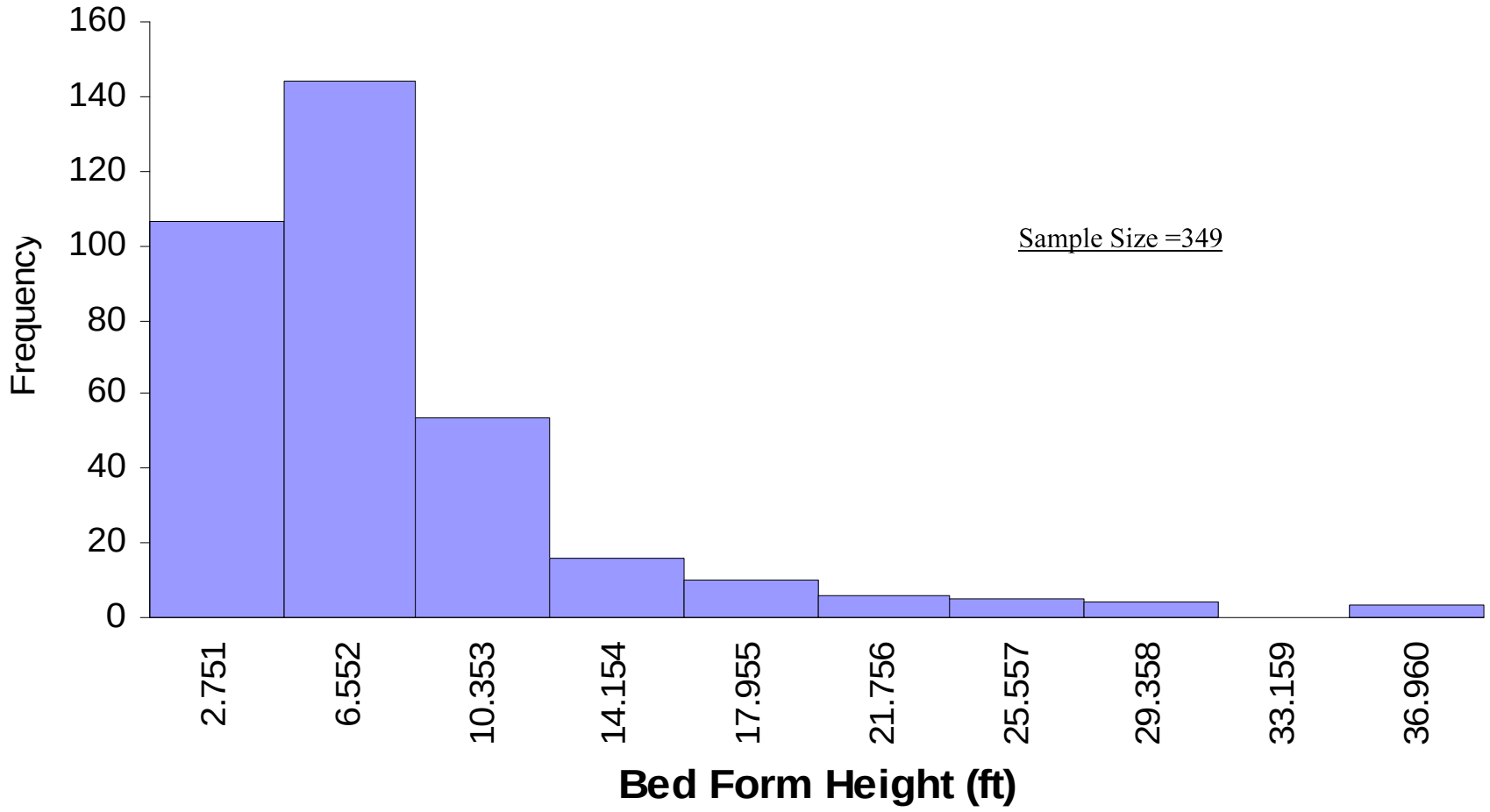

Figure 3.13 Histogram of the bed form height for Lower Mississippi River between RM 0.00 and RM 234 (349 observations).

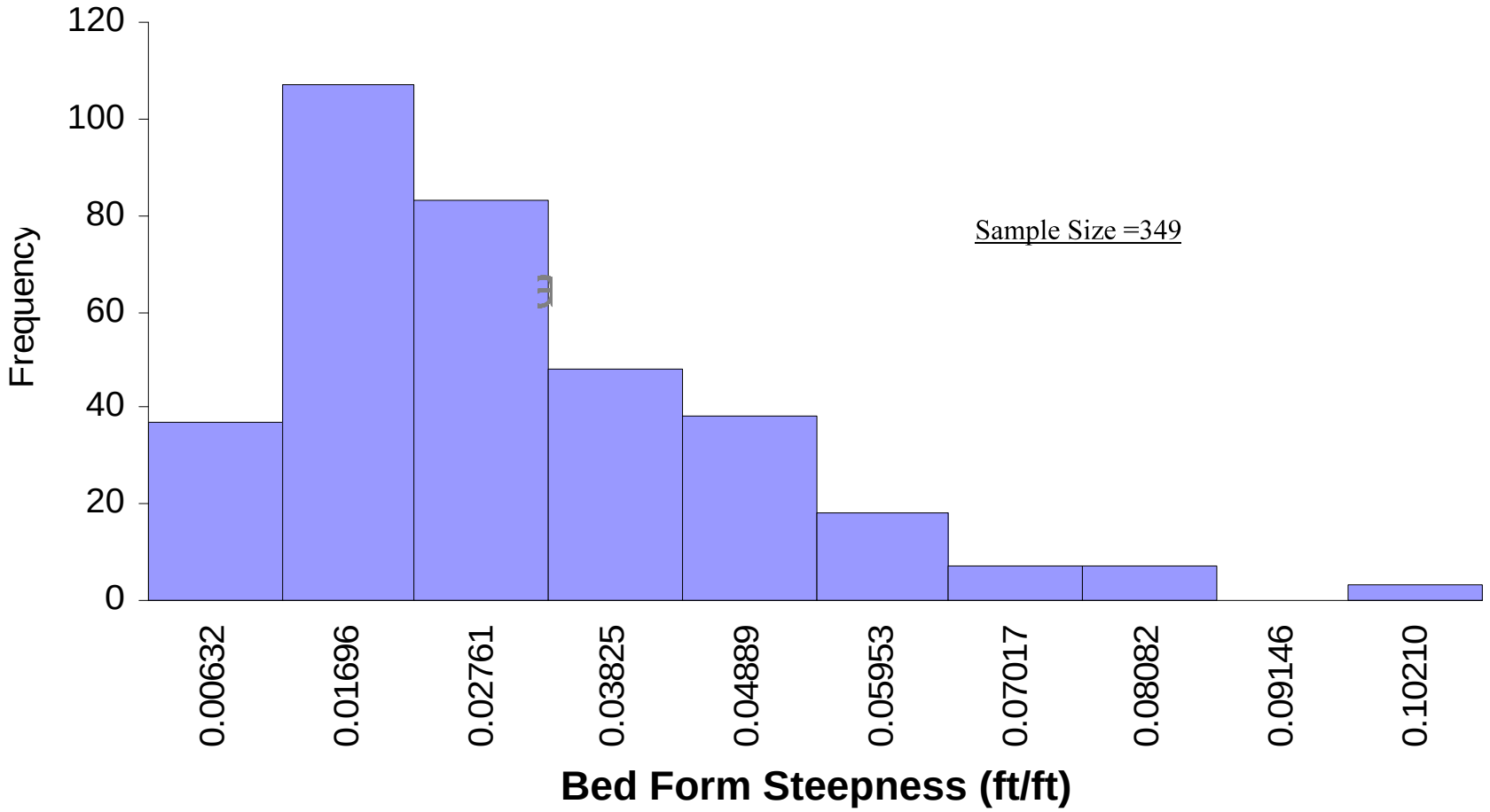

Figure 3.14 Histogram of the bed form steepness for Lower Mississippi River between RM 0.00 and RM 234 (349 observations).

The histogram shapes confirm the skewness observed in the bed form geometry summary presented in Table 3.1. The histograms plots showed skewness to the right with a single peak. For bed form wave lengths (Figure 3.12), the majority of the calculated wave lengths are in the 250 -500ft (76m – 152m) range, while for bed form height (Figure 3.13), the majority of the values are in the range of 6 - 8 ft (1.82m – 2.43m); the steepness was in the range of 0.01 to 0.03 (Figure 3.14).

Box plots were also constructed as a way of summarizing the bed form data on an interval scale. The data included the three spectral peaks surveyed at each river mile. A box plot is a type of graph which is used to show the shape of the distribution, its central value, and spread. The plot produced consists of the most extreme values in the data set (maximum and minimum values), the lower and upper quartiles, and the median.

Box plots are used for indicating whether a distribution is skewed and whether there are any unusual observations (outliers) in the data set.

The quartiles separate the data into 25 percent intervals. The first quartile is the value under which 25% of the data lie and the third quartile is the value over which 25% of the data are found. First quartile is the median of the lower half of the data. Third quartile is the median of the upper half of the data. Inter-quartile range (IQR) is the distance between and the first and the third quartile. Whiskers extend to the furthest observations that are no more than 1.5 IQR from the edges of the box. Mild outliers are observations between 1.5 IQR and 3 IQR from the edges of the box. Extreme outliers are greater than 3 IQR from the edges of the box.

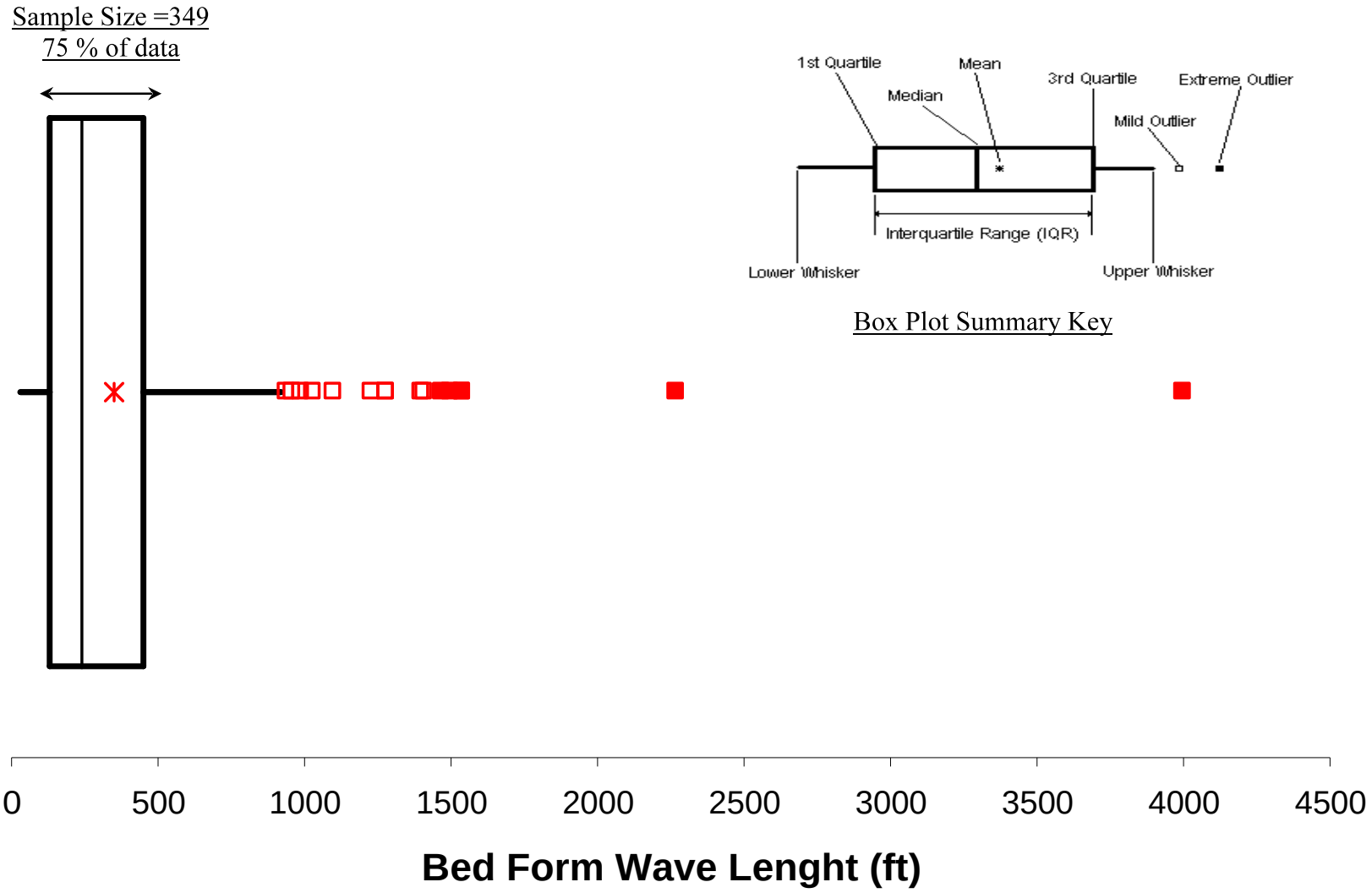

Figure 3.15 Box plot of bed form wave length for Lower Mississippi River between RM 0.00 and RM 234 (349 observations).

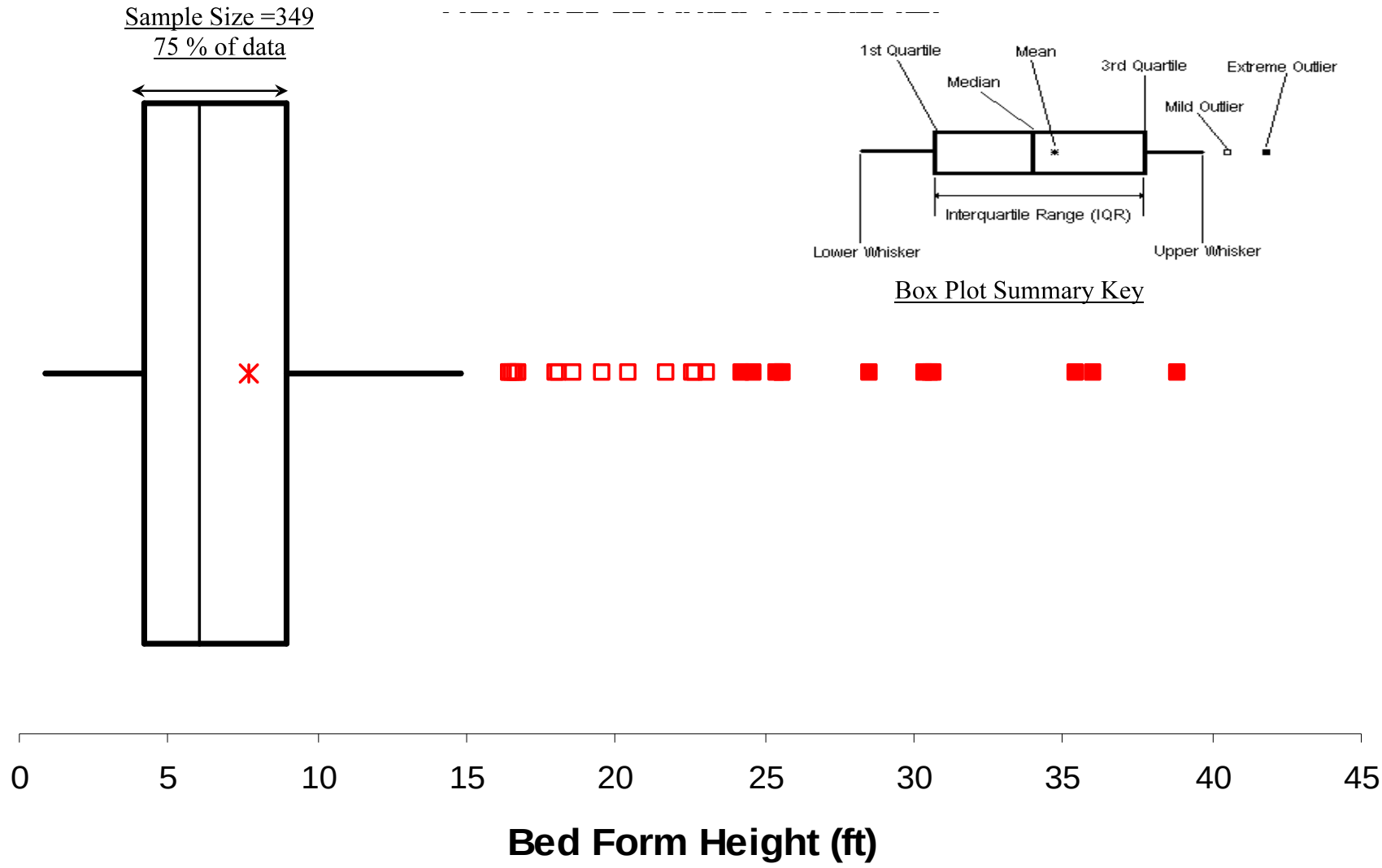

Figure 3.16 Box plot of bed form height for Lower Mississippi River between RM 0.00 and RM 234 (349 observations).

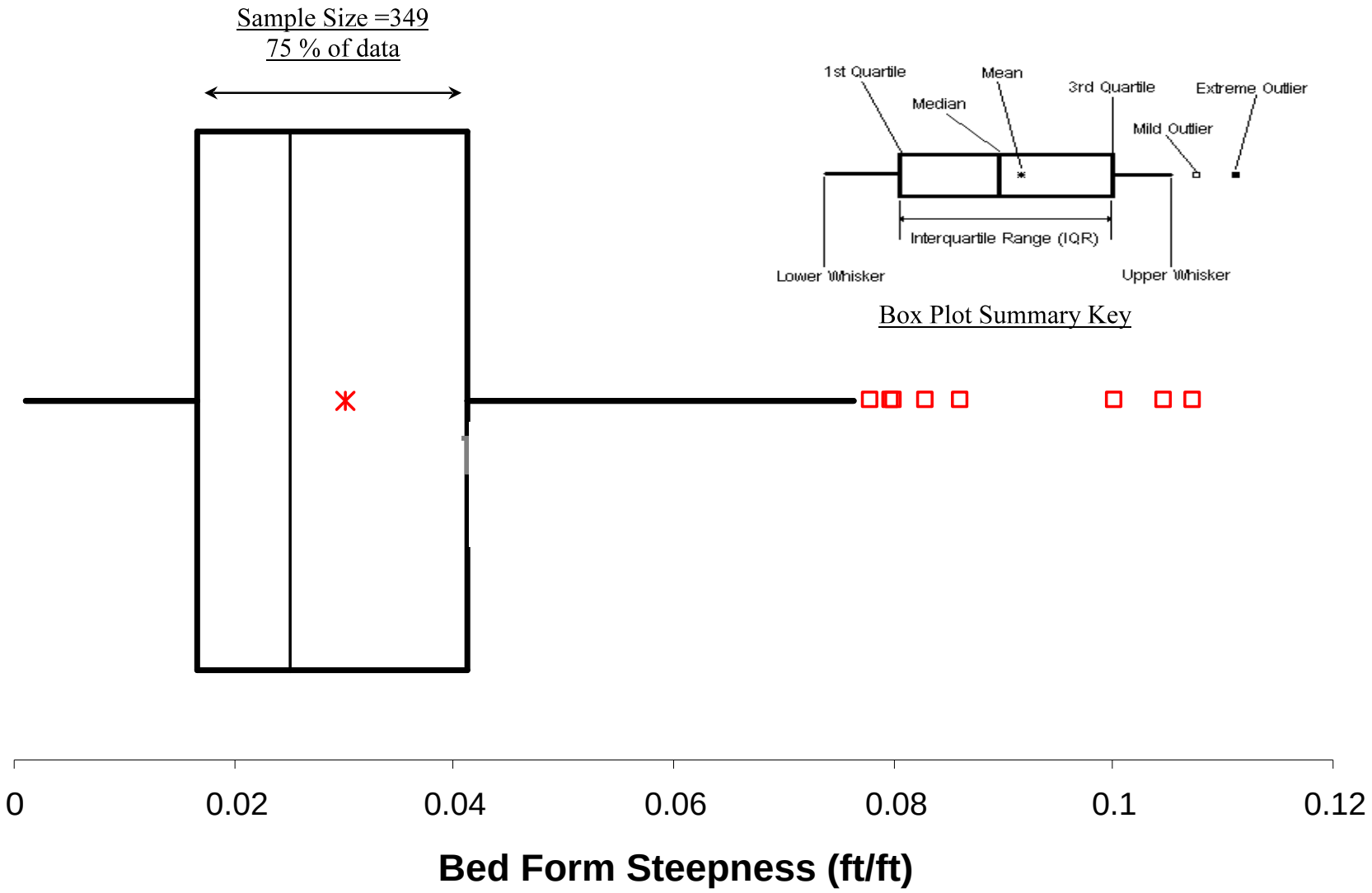

Figure 3.17 Box plot of bed form steepness for Lower Mississippi River between RM 0.00 and RM 234 (349 observations).

The results of the box plot suggests that although a large proportion of the data (length, height and steepness) lies in the lower magnitude ranges, the variability in the data is high as can be seen in the several outliers points to the right of each box plot. These outlier points, show that the extreme peaks while present in the natural system, they do not represent the majority of the data. These outliers are shown in the time series as higher peaks and in the histogram as small frequency categorizes on the right of the charts.

3.2. BED FORMS HYDRAULICS IN THE LOWER MISSISSIPPI RIVER

The bed form geometries presented above were then correlated with certain hydrodynamic features that resulted from an undergoing hydrodynamic modeling study of the Lower Mississippi River described in Meselhe et al (2005).

3.2.1 ONE DIMENSIONAL NUMERICAL MODEL RESULTS

Hydrodynamic model results for the period between June 2003 and September 2003 (same period when the multibeam data were collected) were obtained from a calibrated one-dimensional model for the Lower Mississippi River. The Danish Hydraulic Institute (DHI) MIKE 11 model was used in the study. The model extends from Tarbert Landing, MS RM 306, to the Head of Passes, LA RM Zero (Meselhe et al 2005). Figure 3.18 shows river discharges for the studied period. The use of the model results are discussed in Section 3.3. Model data that were used included: Average velocity (U), Total Average Hydraulic Radius (R_h), Energy Slope (S) values at several points along the study reach. The data for this time interval were then averaged to obtain a single value along the route of the studied reach of the river. Figure 3.19 thought 3.23 shows the averaged of depth, velocity, total hydraulic radius, energy slope and total bed shear stress respectively.

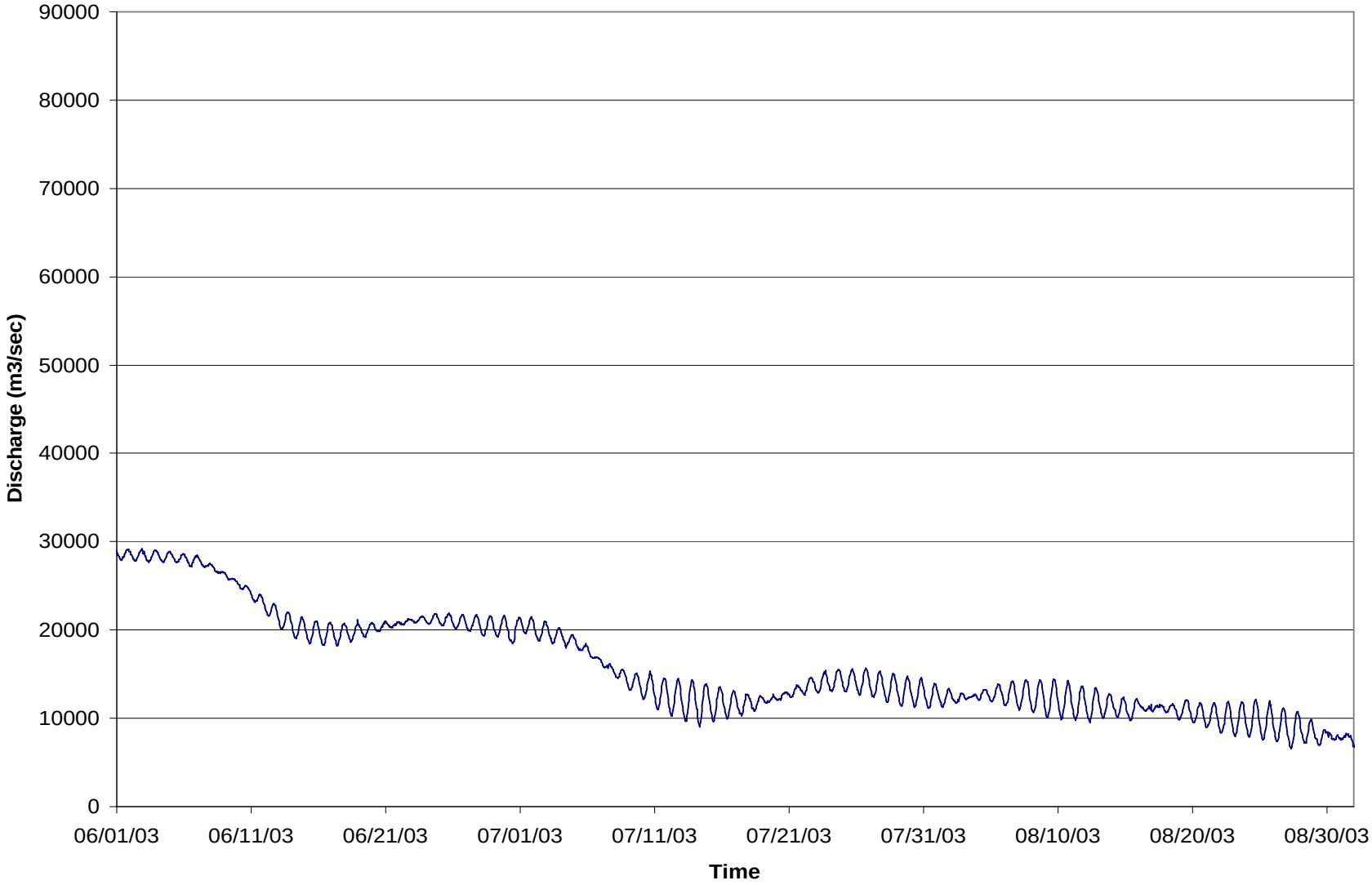

Figure 3.18 Time series of river discharges at the Head of Passes, LA, the Lower Mississippi River (June 2003 – September 2003)

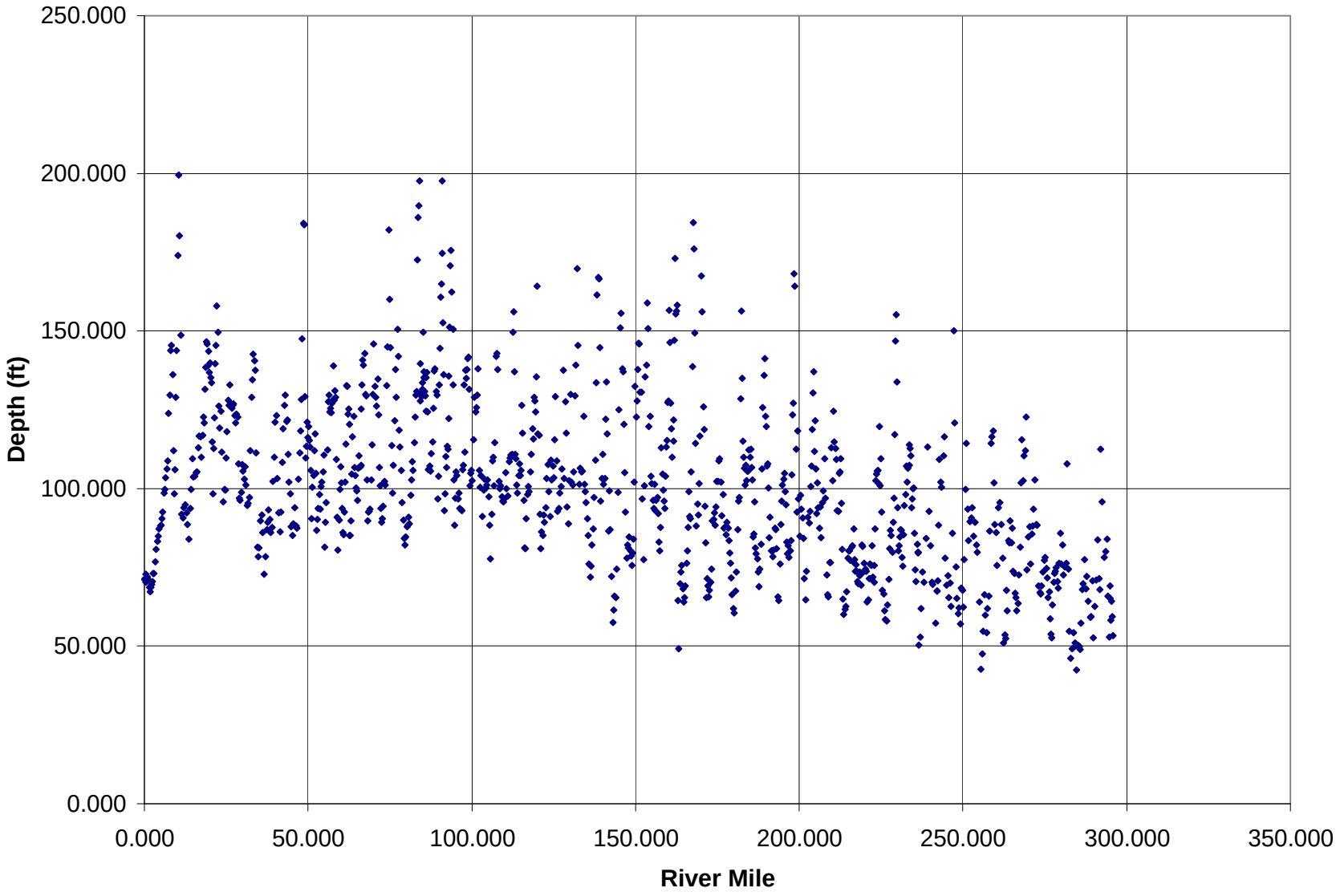

Figure 3.19 Maximum depth along the Lower Mississippi River from RM 0.00 to RM 300.00 (June 2003 – September 2003)

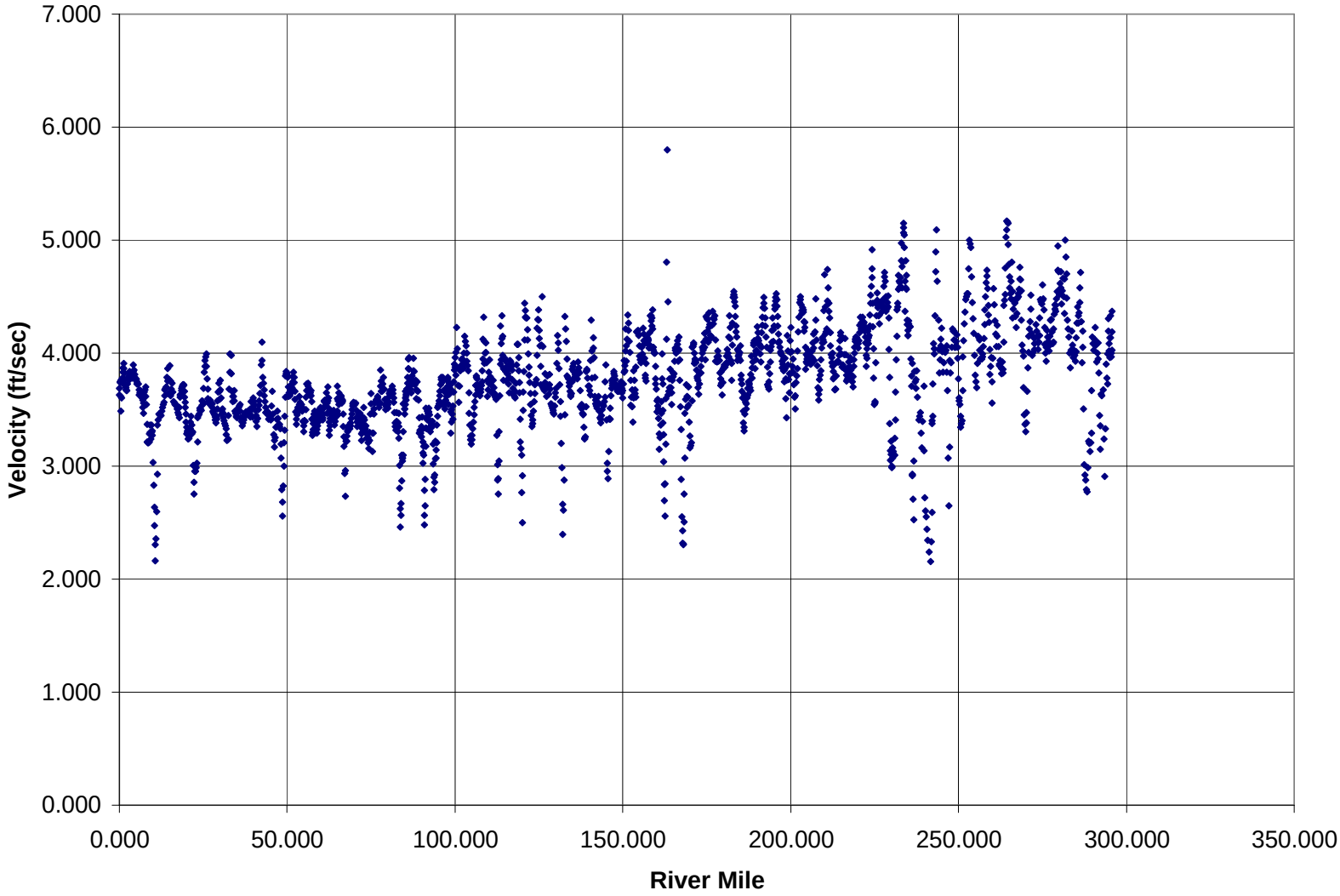

Figure 3.20 Average cross-sectional velocity along the Lower Mississippi River from RM 0.00 to RM 300.00 (June 2003 – September 2003)

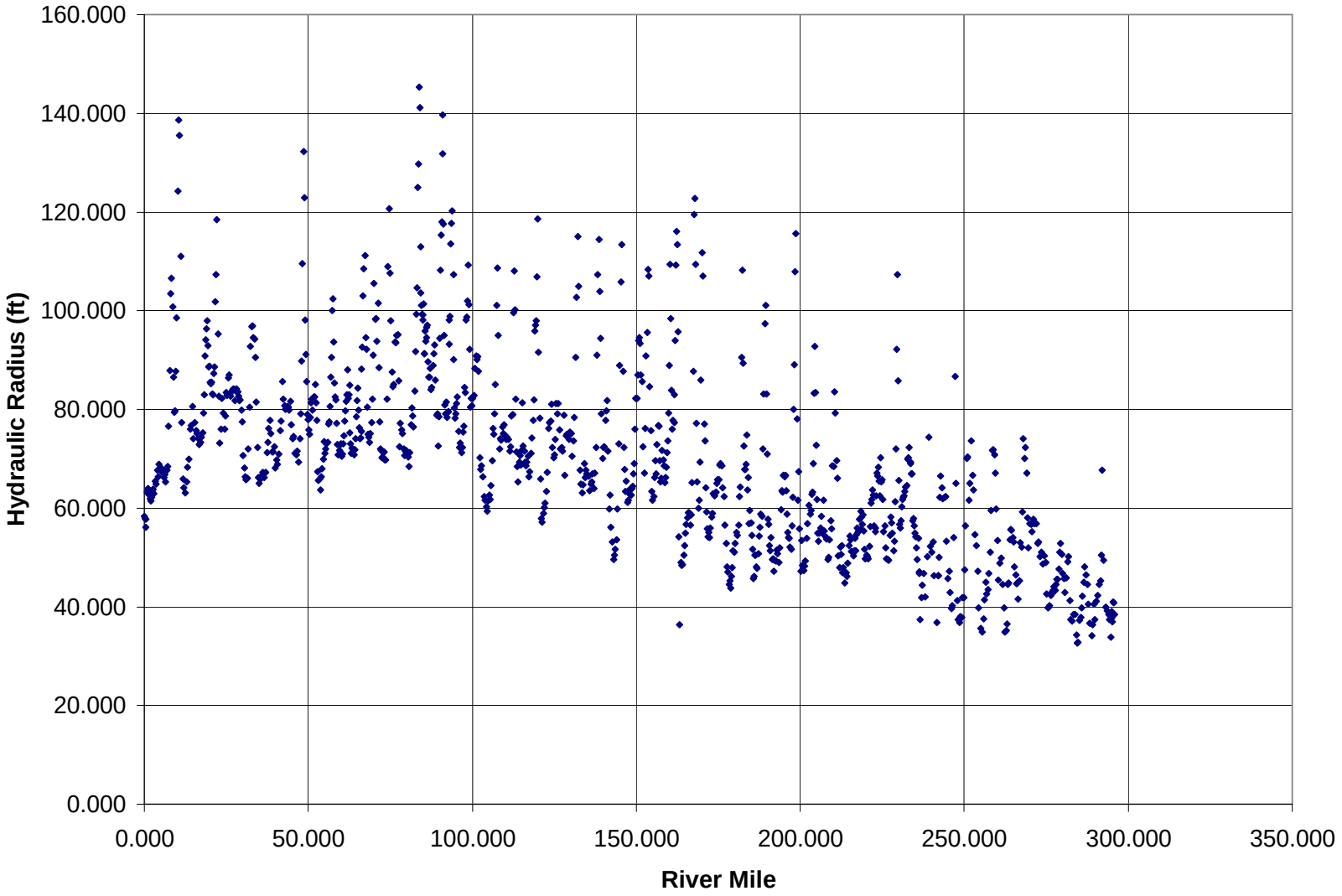

Figure 3.21 Average hydraulic radius along the Lower Mississippi River from RM 0.00 to RM 300.00 (June 2003 – September 2003)

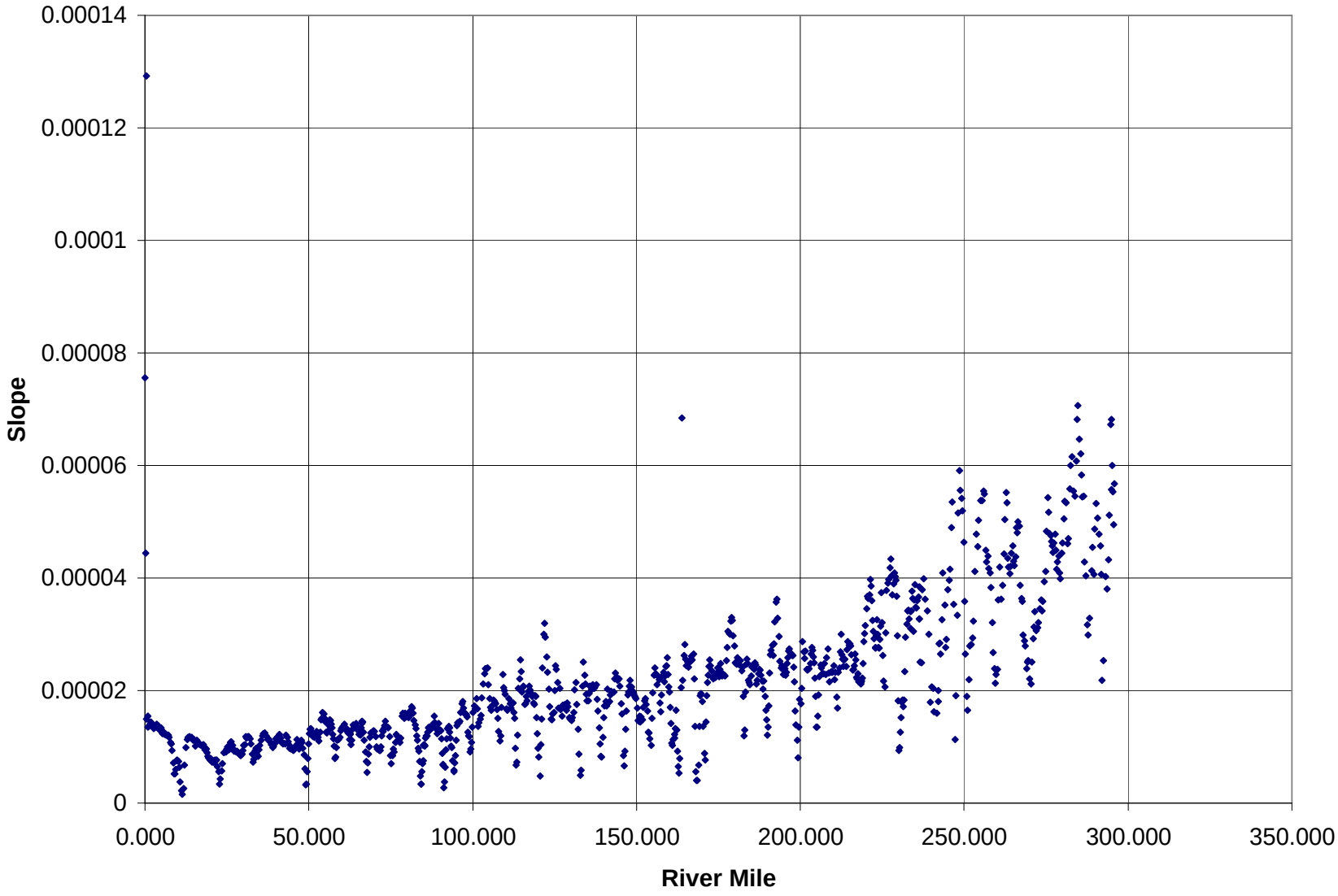

Figure 3.22 Average energy slope along the Lower Mississippi River from RM 0.00 to RM 300.00 (June 2003 – September 2003)

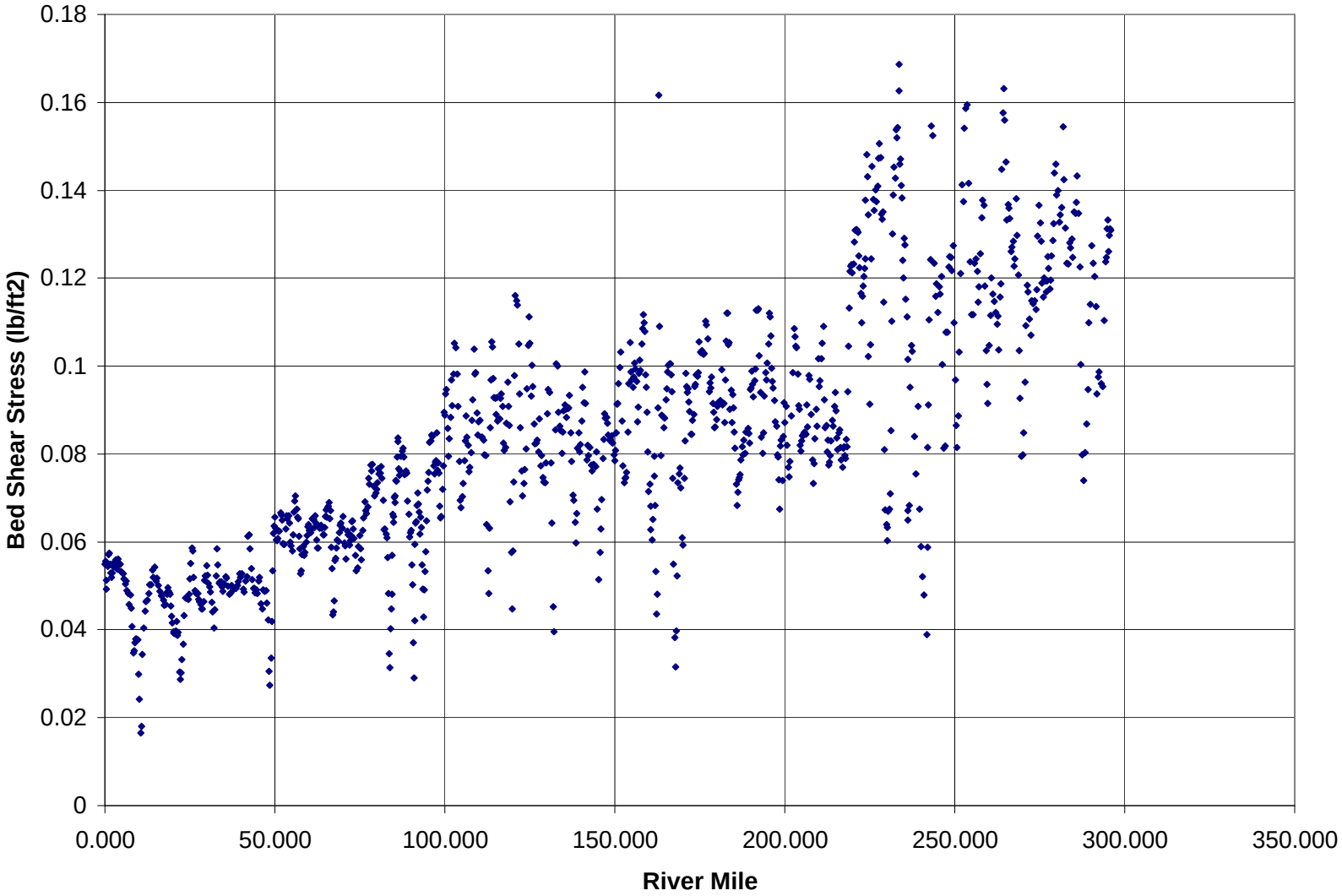

Figure 3.23 Average total bed shear stress along the Lower Mississippi River from RM 0.00 to RM 300.00 (June 2003 – September 2003)

3.2.2. ACOUSTIC DOPPLER CURRENT PROFILER (ADCP) OBSERVATION

In addition to the one dimensional model results, several ADCP surveys for the river were provided to the author by the hydro-ecological modeling team currently studying the Lower Mississippi River (Meselhe et al 2005). ADCP data covered several locations along the river, but only one ADCP survey completely overlapped with the multibeam survey (RM 11.55 near Venice, LA) as shown in Figure 3.24 and 3.25. Only this ADCP data set was included in the study. Although the use of ADCP surveys to characterize the vertical velocity profile on top of bed forms is beyond the scope of the current study, the results presented here can assist in future field investigations of flow properties on top of bed forms in the Lower Mississippi River.

In spite of the scatter in the ADCP data (example shown in Figure 3.26), the data revealed some interesting properties of the velocity profile as will be mentioned later. The ADCP survey covered the whole width of the river for eight times- 4 complete cycles, while the bathymetric survey covered only a portion of the width as shown in Figure 3.24 and 3.25. Figure 3.25 shows a 3D view of the bathymetry survey.

The bathymetry survey showed the existence of a dredge channel on the side of the river and accordingly, this portion was excluded when performing the spectral analysis; ADCP data on top of the dredge channel was also disregarded to eliminate any uncertainties in the ADCP data that might have been produced by the different flow conditions in the dredge channel. There was no information to the author if this dredge channel was recent or a more historical channel and therefore it was disregarded from the analysis.

Several velocity vertical profiles were extracted from the ADCP survey and then averaged to obtain one profile. The profiles showed that the logarithmic velocity profile possess three different slopes as shown in Figure 3.27. The same phenomenon was observed by Fedele and Garcia (2001) as shown in Figure 3.28; however Fedele and Garcia (2001) predicted two slopes.

Fedele (2001) referred to the point where the slopes change as the equilibrium layer where the maximum shear stress is nearly equal to the form stress (maximum flow separation). Detailed ADCP instruments with very fine measuring resolutions are required in order to fully study this effect. However these instruments were not available to the author at the time of study.

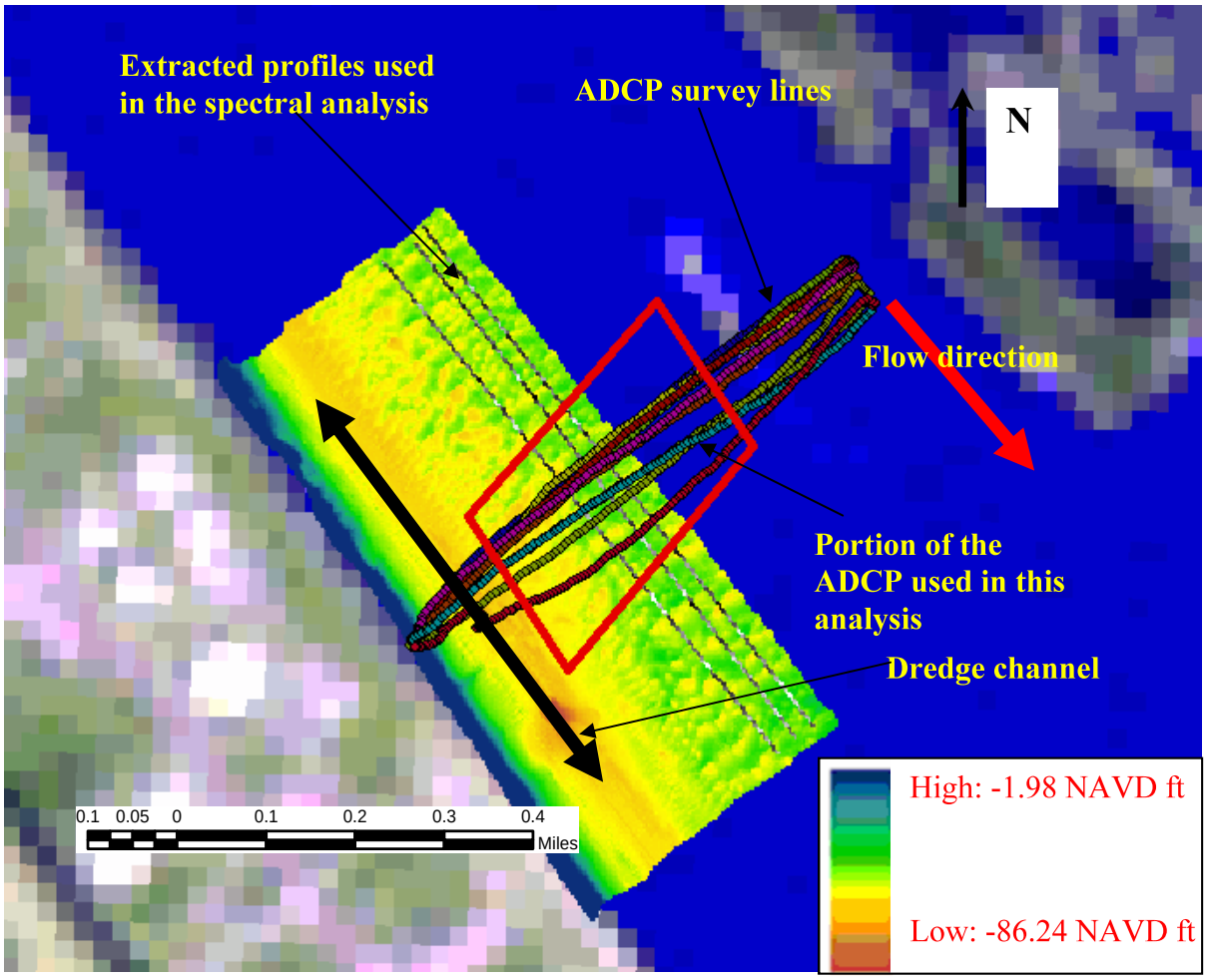

Figure 3.24 ADCP and bathymetry surveys at RM 11.55 near Venice, LA

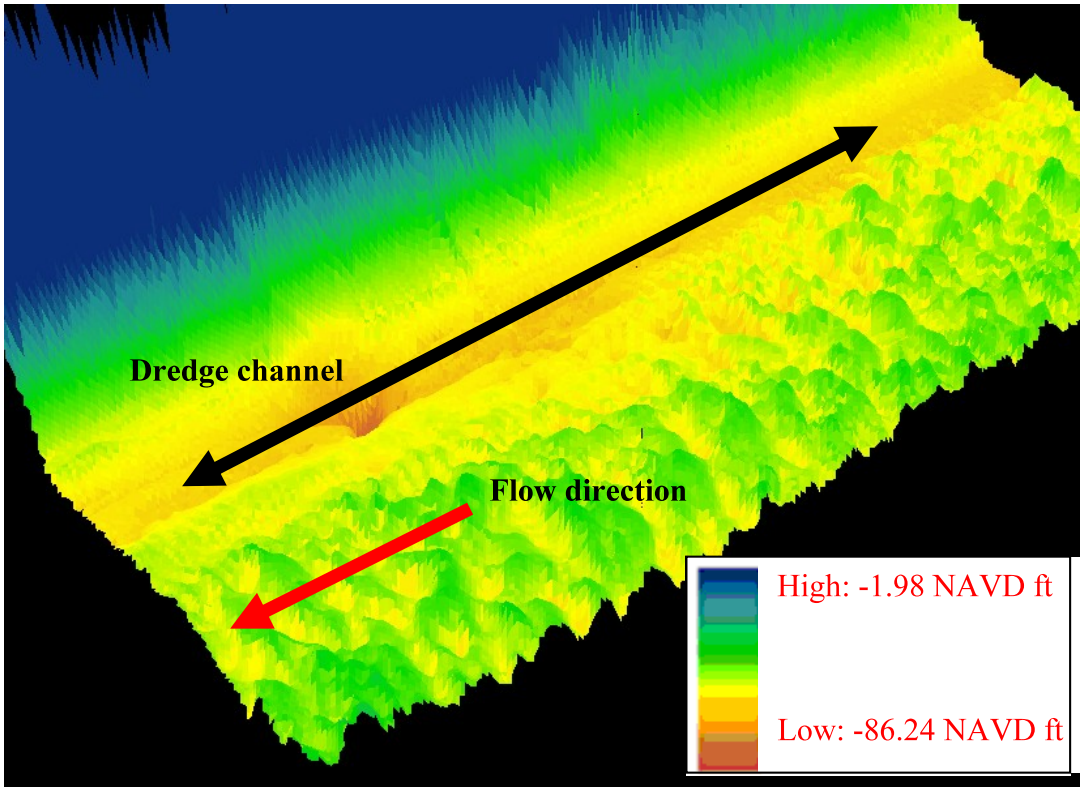

Figure 3.25 3D view of bathymetry surveys at RM 11.55 near Venice, LA

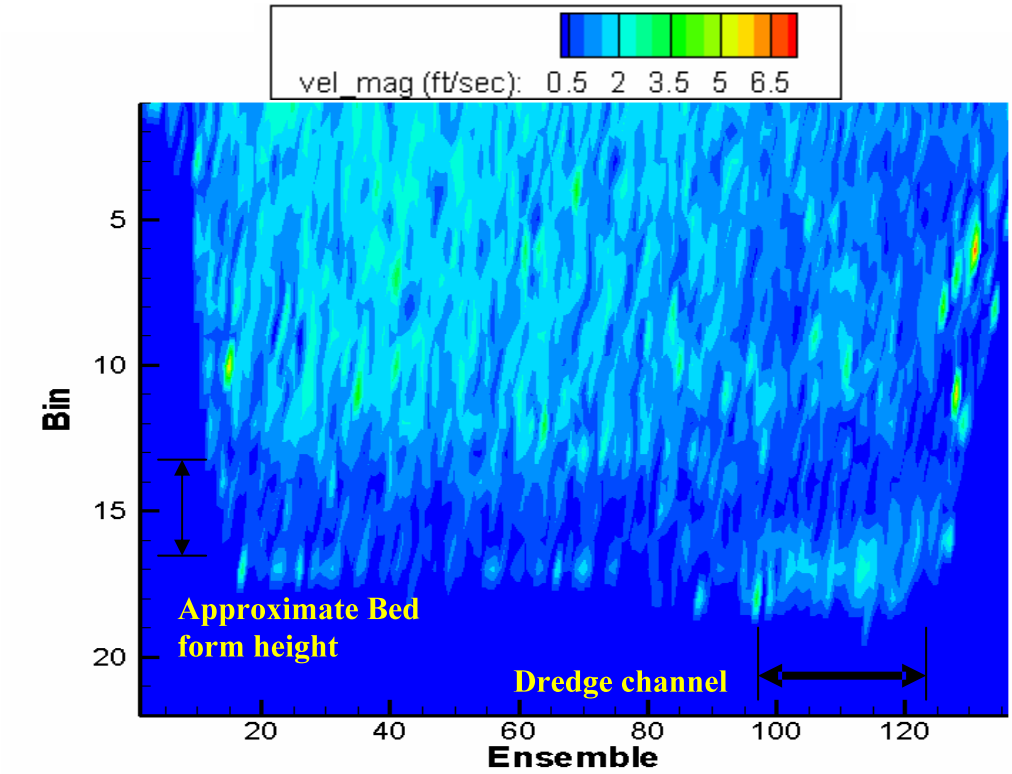

Figure 3.26 ADCP surveys at RM 11.55 near Venice, LA

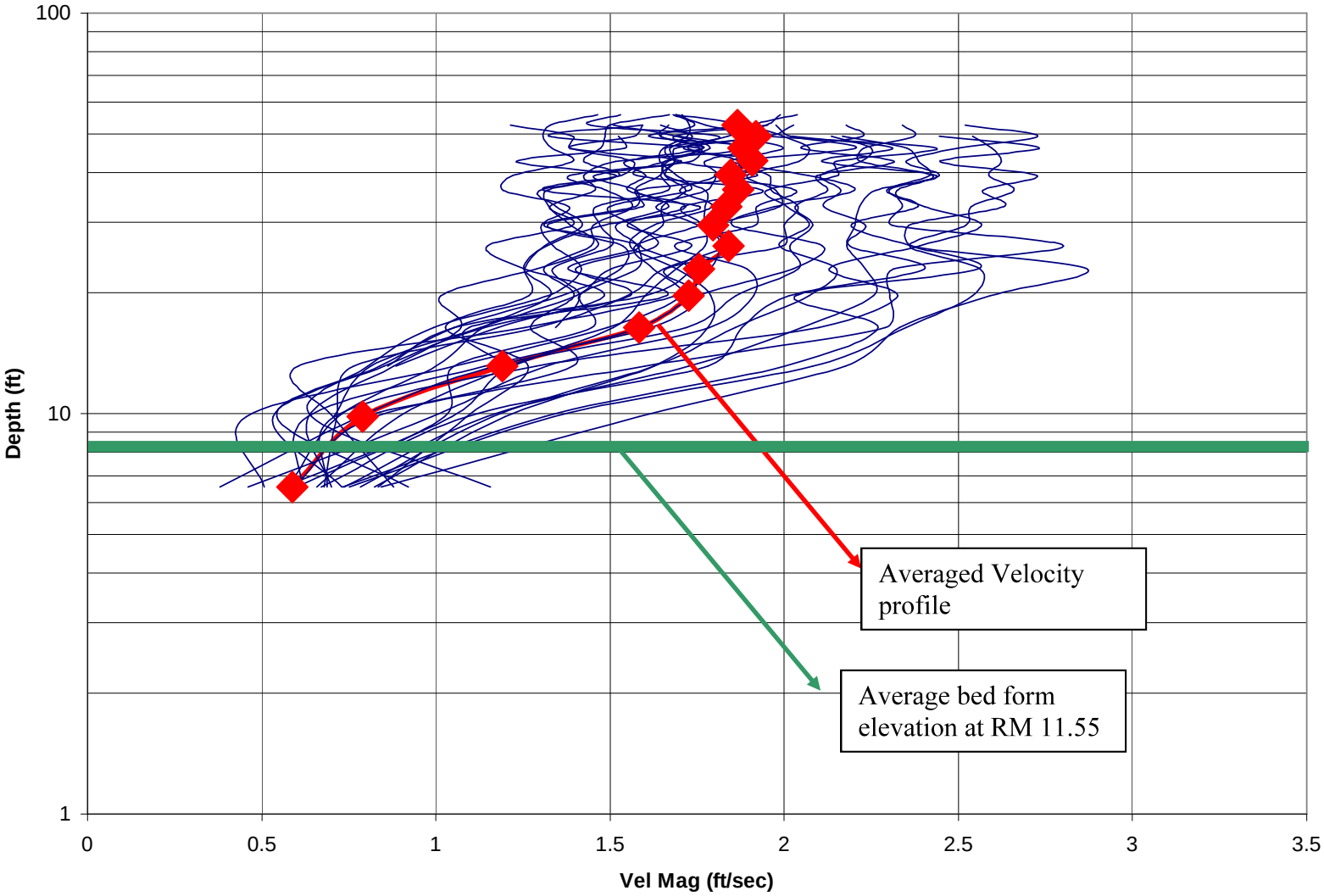

Figure 3.27 Velocity vertical profile at RM 11.55 near Venice, LA (Logarithmic scale)

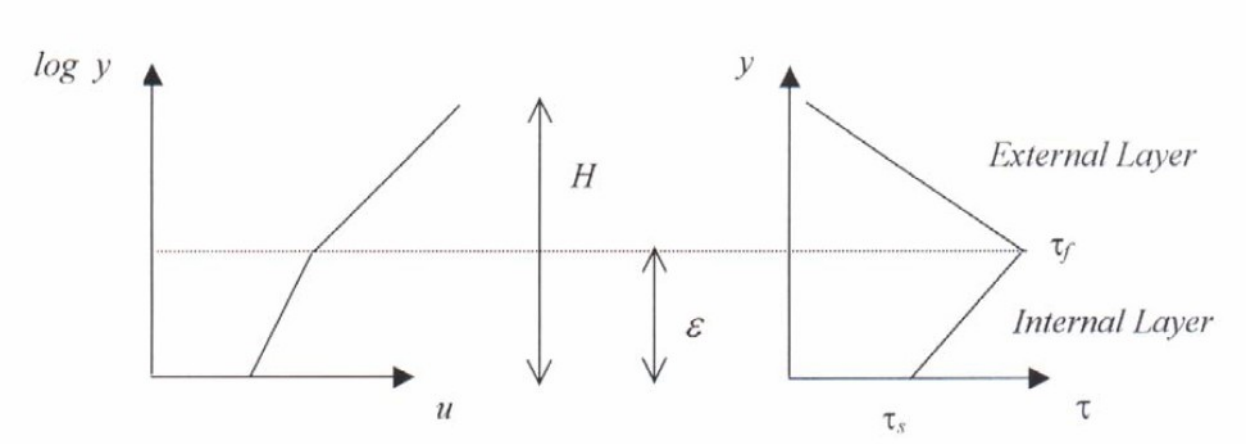

Figure 3.28 Velocity profile and spatially averaged Reynolds stress profile (Fedele and Garcia, 2001)

The slope of the observed velocity profile (Figure 3.27) followed Fedele (2001) slope at the lower section of the river; however near the surface the profile appeared to have a different slope.

3.3. FLOW RESISTANCE RELATION

The one dimensional model results were utilized to calculate the bed form shear stress according to Smith and McLean (1977) as follows:

$$\tau''_0 = \frac{1}{2}\rho C_d \frac{H_d}{\lambda} U^2 \qquad [3.2]$$

where τ_0" is the bed form shear stress; ρ is the density of water; C_d is the drag coefficient; H_d is the bed form height; λ is the bed form wave length; U is the average cross sectional velocity.

Different values for C_d for different flow conditions have been obtained from the literature ranging from 0.21 (Smith and McLean, 1977) to 0.23 (Wilberg and Nelson, 1992) to 0.25

(Nelson et al., 1993). The effect of changing the C_d on the shear computations is shown in Figure 3.29 and 3.30. The bed form shear velocity (u_*") was then calculated as follows:

$$u_*" = \sqrt{\frac{\tau_0"}{\rho}} \quad [3.3]$$

The flow parameter ψ_{35} was then calculated as follows:

$$\psi_{35} = \frac{\rho_s - \rho}{\rho} x \frac{d_{35}}{R'_h S} \quad [3.4]$$

where R'_h is the grain friction hydraulic radius, S is the energy slope, ρ_s is the bed material density; d35 is the sieve size in the bed material of which 35 percent is finer (ranged from 0.2 to 0.3 mm in the studied reach with a trend towards smaller values in downstream direction, Corps of Engineers, US Army (1935)) and plotted versus U/ u_*". The effect of changing the d_{35} value is shown in Figure 3.31. According to Figure 3.30, the increase in the value of C_d caused a decrease in $\frac{U/u*"}{\psi_{35}}$ according to the following equation:

$$y = 0.0694^{x-0.5} \quad [3.5]$$

where y is $\frac{U/u*"}{\psi_{35}}$, and x is C_d., in other words, a 0.1 increase in C_d. results in around 18 % decrease of U/ u_*". According to Figure 3.32; the increase in the value of d_{35} caused an increase in $\frac{\psi_{35}}{U/u*"}$ according to the following equation:

$$y = 26.312x + 0.0002 \quad [3.6]$$

where y is $\frac{\psi_{35}}{U/u*"}$, and x is $d_{35,}$ in other words, a 0.1 increase in d_{35} results in around 25 % increase of $\psi_{35.}$

The plot where d_{35} = 0.3 (U.S. ARMY 1935) and C_d = 0.25 (Nelson et al 1993)is shown in Figure 3.33.

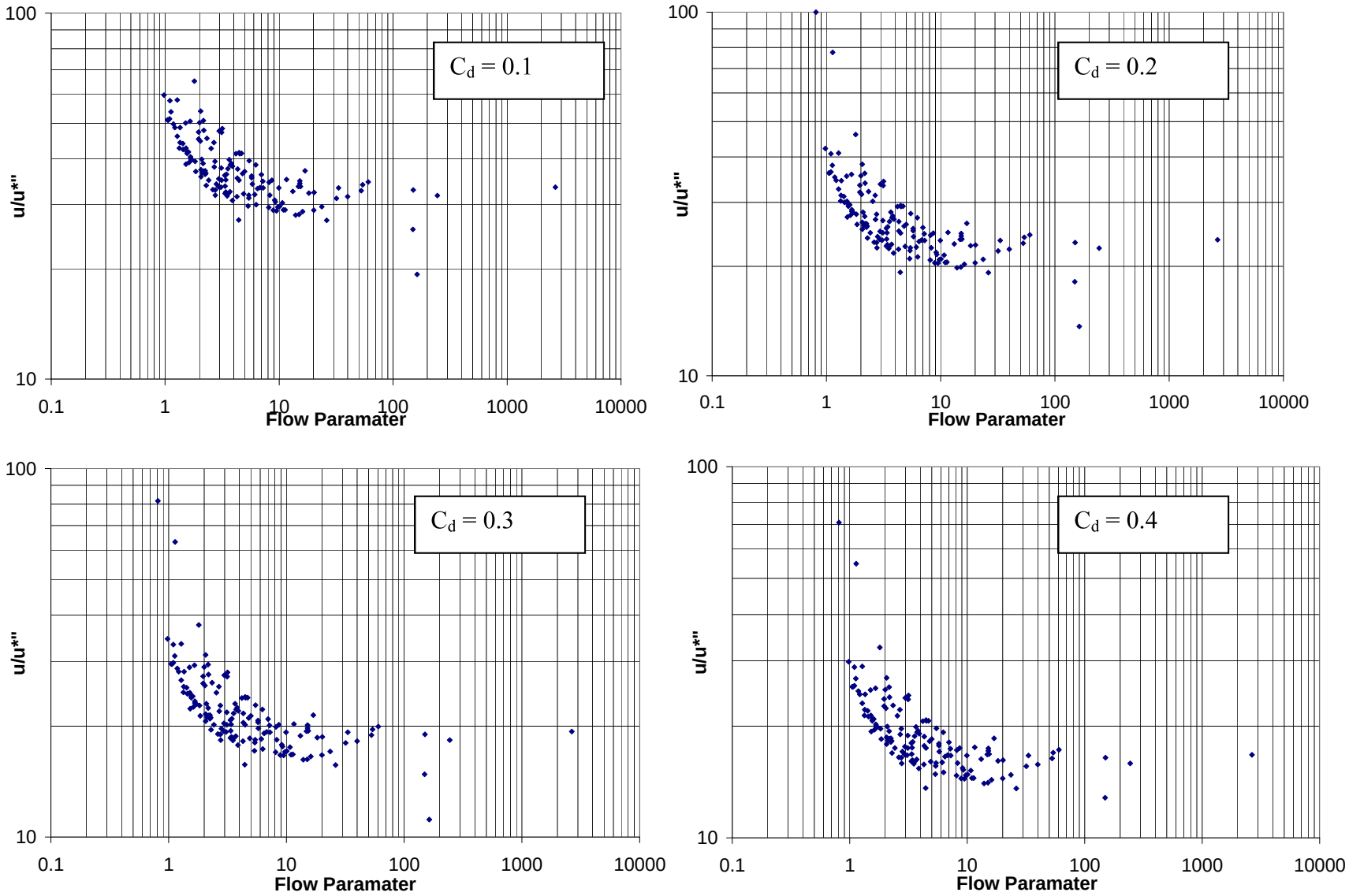

Figure 3.29 Effect of changing C_d on the flow-resistance plot with d_{35} = 0.3 (Downward shift with increase of C_d)

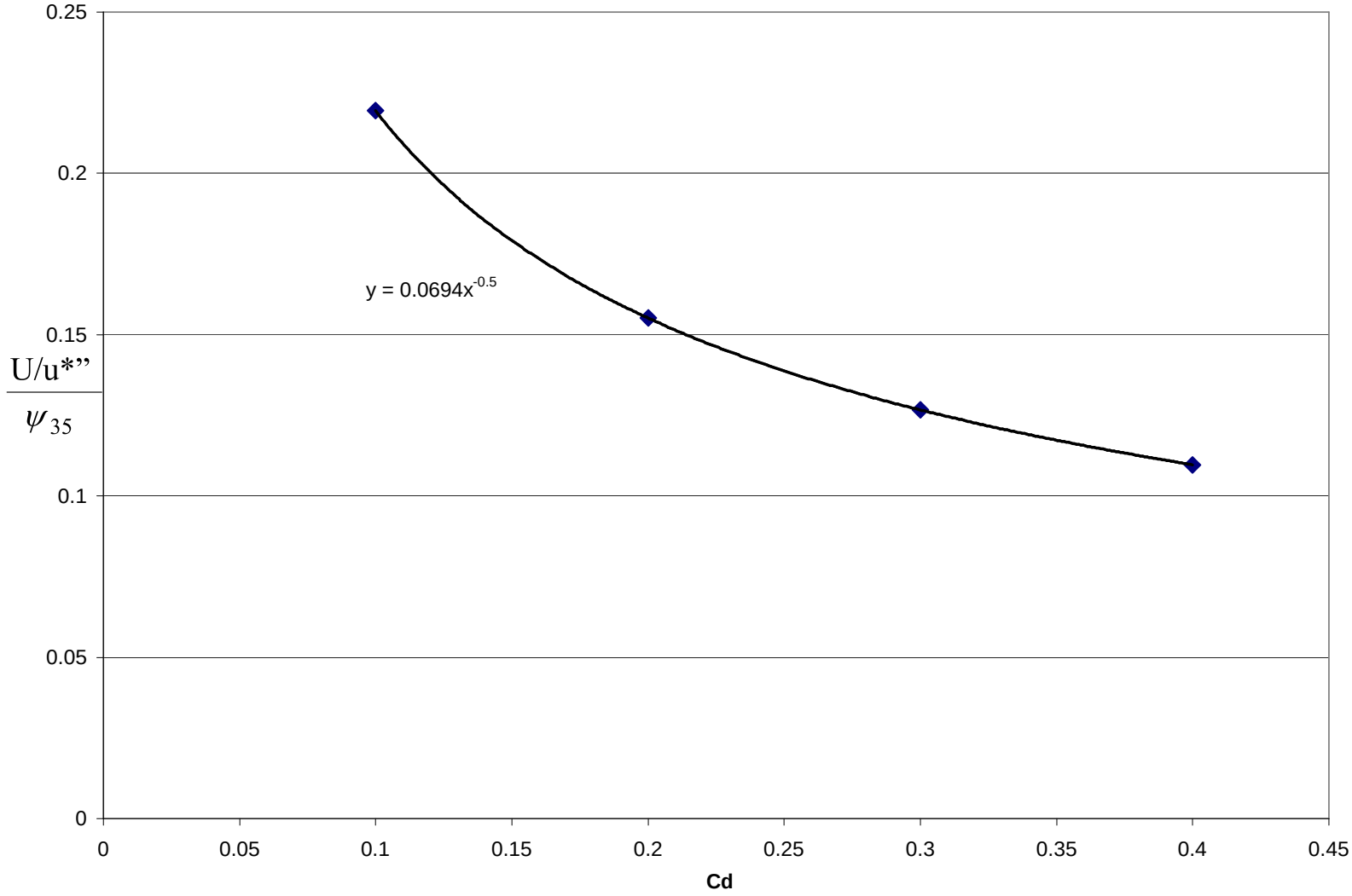

Figure 3.30 Relationship between $\frac{U/u^{*”}}{\psi_{35}}$ and C_d

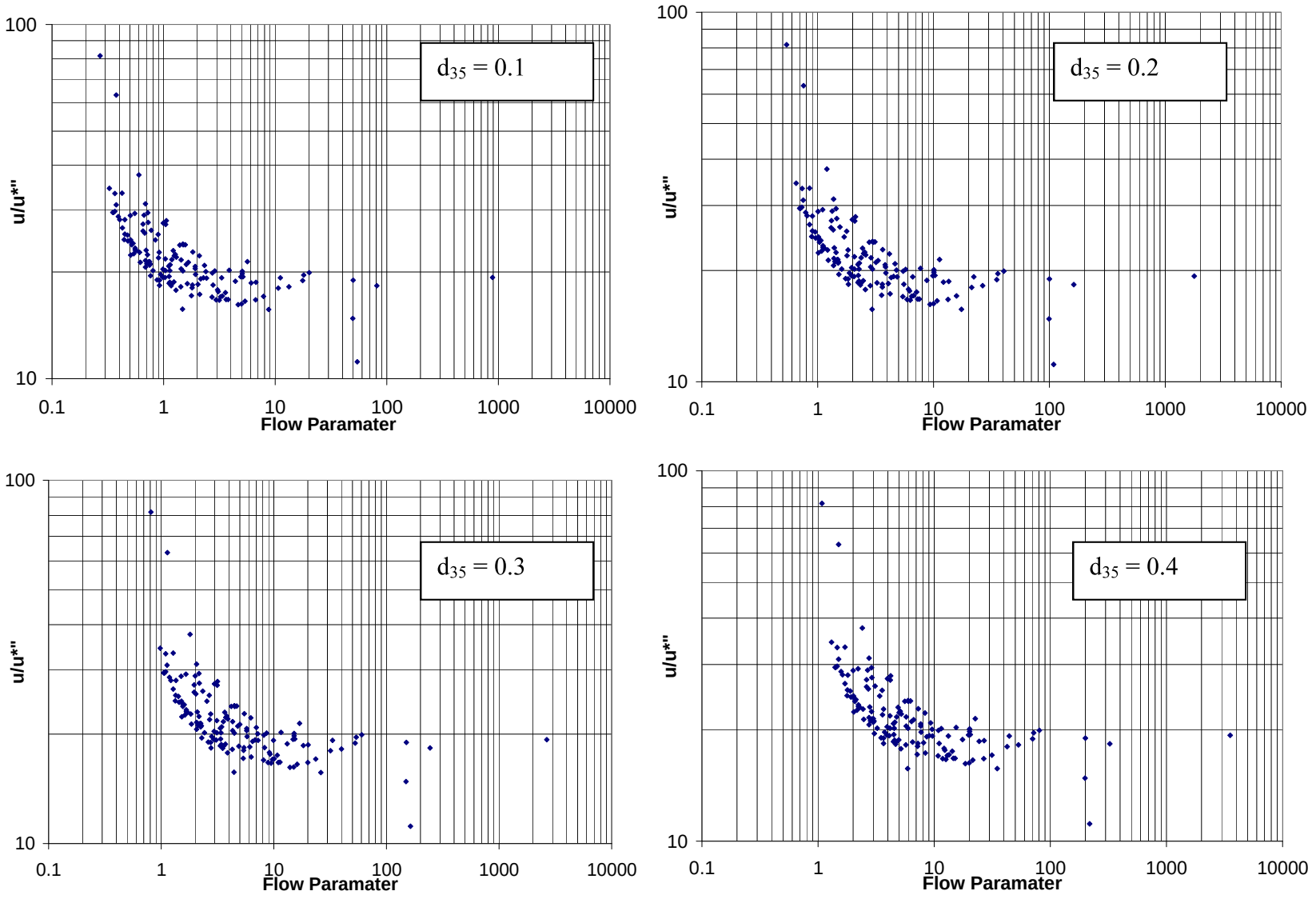

Figure 3.31 Effect of changing d_{35} on the flow-resistance plot with $C_d = 0.25$ (rightward shift with the increase of d_{35})

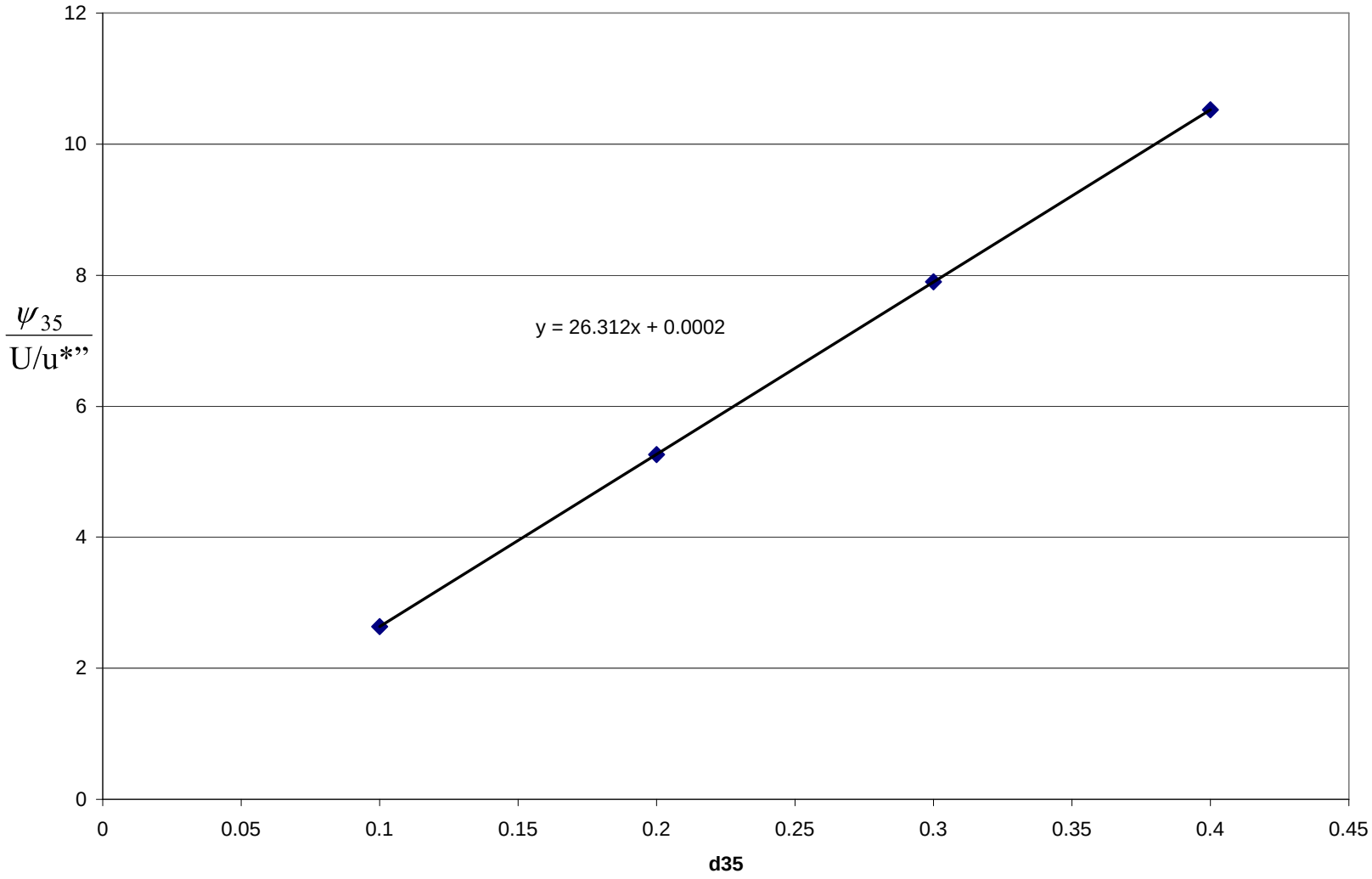

Figure 3.32 Relationship between $\frac{\psi_{35}}{U/u^{*}”}$ and d_{35}

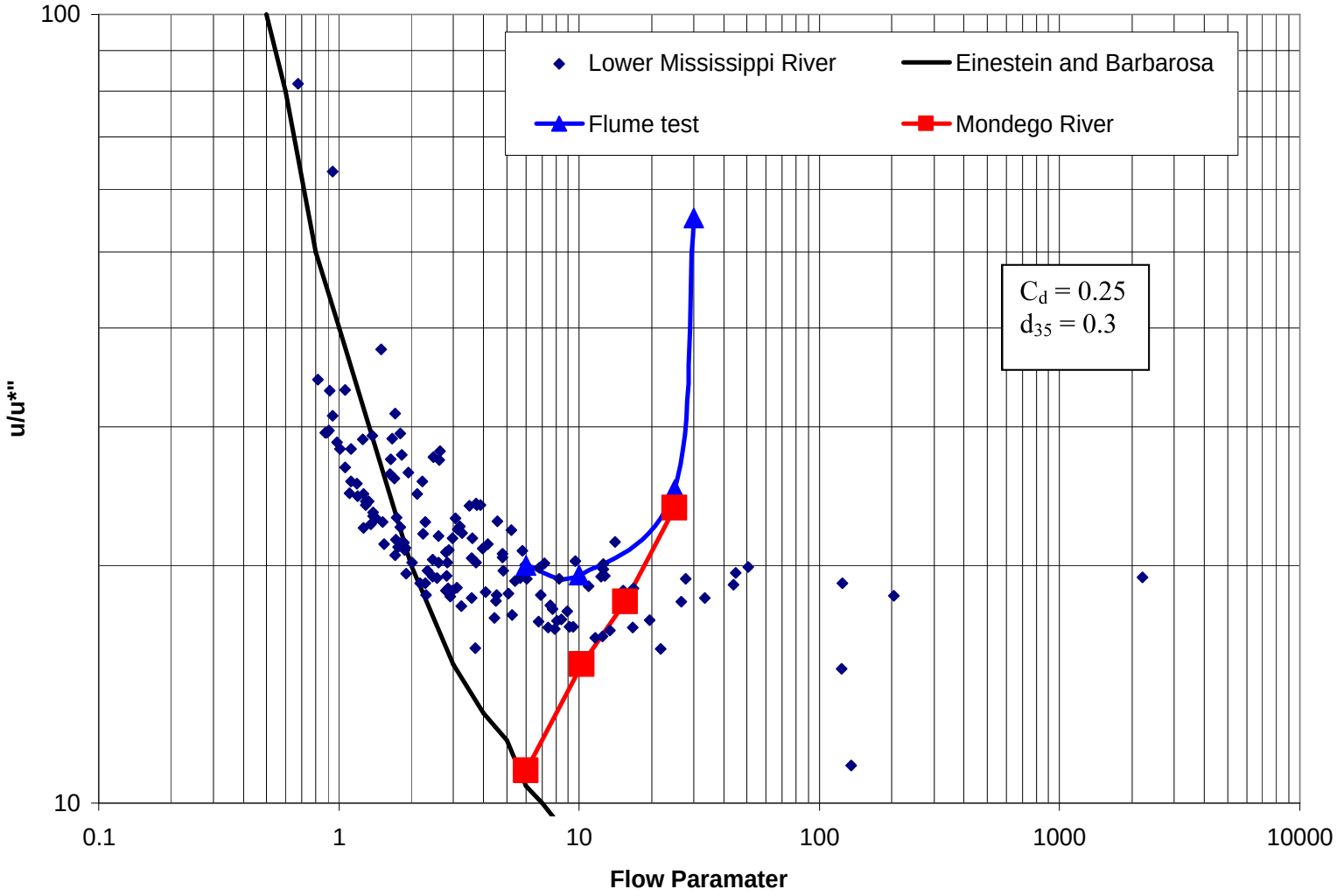

Figure 3.33 Bed form resistance versus flow parameter for the Lower Mississippi River (June 2003-September 2003) in addition to Einstein (1952) and Cunha (1967) laboratory and field experiments.

Einstein and Barbarosa (1952) utilized data from 10 rivers in the United States to establish a relationship for the bed form resistance. They were the first to introduce the flow parameter which has been used by several investigators. Among the 10 rivers analyzed by Einstein and Barbarosa, eight rivers had d_{35} less than 0.5 mm, and the other two d_{35} had values of 0.7 and 1.0 mm. In later experiments with coarser bed material, the results departed from the mean curve of the 10 U.S. rivers and they concluded that the bed form resistance for coarse sand was shown to be smaller than for medium and fine sand. In 1967, Cunha provided data for the Mondego River in Portugal d_{35} = 1.7 mm, his results followed Einstein's flume experiments but was positioned lower.

The results shown in Figure 3.33 follow the general trend established by Einstein and Barbarossa (1952) for the U.S. rivers; however the data in the lower section of the plot are in better agreement with the curve based on later flume tests by Einstein (1952) and another curve for the Mondego River in Portugal by Cunha (1967). However, as mentioned above, both of these experiments included coarser sand (coarser than 0.6 mm) than that in this study (0.2 to 0.3 mm).

Previous research on bed forms was primarily laboratory studies or small scale field investigations. This study extends the range of bed form dimensions beyond those that have been considered in the current literature. Future analysis and ongoing acquisition of more detailed sediment size distribution of the Lower Mississippi River is needed to validate the plot in Figure 3.33.

CHAPTER 4
NUMERICAL MODELING OF FLOW AND TRANSPORT OVER BED FORMS

This portion of the study discusses ***Hypothesis Two*** which assumes that three-dimensional hydrostatic numerical models are capable of simulating the flow and transport environments over the surface of bed forms.

4.1. THREE DIMENSIONAL MODELING

The approach in this portion of the study was to setup 3-D computer models for hypothetical triangular dunes surfaces with dimensions obtained from statistical analysis of multibeam survey data of the Lower Mississippi River presented in Chapter Three utilizing three different modeling systems: ECOMSED (HydroQual, Inc., 2002), , MIKE 3 (DHI 2005) and H3D (Stronach 1993).

These models were used to assess the effect of applying different vertical descritization schemes (sigma level, vs. constant and variable z-level) and the effect of incorporating either the hydrostatic or the non-hydrostatic pressure approximation when simulating the flow separation phenomenon on the surface of bed forms.

4.1.1. GOVERNING EQUATIONS AND APPROXIMATIONS

The governing three dimensional primitive variable equations describing the free surface flows can be derived from the Navier-Stokes equations after Reynolds averaging. These equations represent the principle of conservation of mass and momentum.

Pedlosky (1979) presented the following form for the momentum equation for incompressible fluid:

$$\rho\left(\frac{\partial u}{\partial t}+u\frac{\partial u}{\partial x}+v\frac{\partial u}{\partial y}+w\frac{\partial u}{\partial z}\right)=-\frac{\partial p}{\partial x}+\mu^h\left(\frac{\partial^2 u}{\partial x^2}+\frac{\partial^2 u}{\partial y^2}\right)+\frac{\partial}{\partial z}\left(\mu^v\frac{\partial u}{\partial z}\right)+\rho fv \qquad [4.1]$$

$$\rho\left(\frac{\partial v}{\partial t}+u\frac{\partial v}{\partial x}+v\frac{\partial v}{\partial y}+w\frac{\partial v}{\partial z}\right)=-\frac{\partial p}{\partial y}+\mu^h\left(\frac{\partial^2 v}{\partial x^2}+\frac{\partial^2 v}{\partial y^2}\right)+\frac{\partial}{\partial z}\left(\mu^v\frac{\partial v}{\partial z}\right)-\rho fu \qquad [4.2]$$

$$\rho\left(\frac{\partial w}{\partial t}+u\frac{\partial w}{\partial x}+v\frac{\partial w}{\partial y}+w\frac{\partial w}{\partial z}\right)=-\frac{\partial p}{\partial z}+\mu^h\left(\frac{\partial^2 w}{\partial x^2}+\frac{\partial^2 w}{\partial y^2}\right)+\frac{\partial}{\partial z}\left(\mu^v\frac{\partial w}{\partial z}\right)-\rho g \qquad [4.3]$$

where, *u(x, y, z, t), v(x, y, z, t)* and *w(x, y, z, t)* are the velocity components in the horizontal x, y and the vertical z, *t* is time; *p(x, y, z, t)* is pressure and *g* is the gravitational acceleration; ρ is fluid density; μ^h is the horizontal eddy viscosity parameter and μ^v is the vertical eddy viscosity parameter; the incompressibility equation (continuity) has the following form:

$$\frac{\partial u}{\partial x}+\frac{\partial v}{\partial y}+\frac{\partial w}{\partial z}=0 \qquad [4.4]$$

Recent advances in computing power have eased the restrictions of utilizing three dimensional models in modeling flow applications. Several of these applications were developed using the hydrostatic pressure approximation where the vertical momentum equation is omitted and the vertical velocity is solely calculated from the continuity equation. In general, the pressure is given by,

$$p = \rho\, g\, (h-z) + q \qquad [4.5]$$

where *q(x, y, z, t)* is the non hydrostatic pressure.

The hydrostatic assumption that q = 0 becomes increasingly inaccurate as the ratio of the vertical to horizontal flow motion increases as the case in the flow over bed forms. In recent years, several numerical models have been developed that solve for the non-hydrostatic pressure either by correcting the pressure term by solving a Poisson equation for the pressure (Casulli 1998) or by utilizing the artificial compressibility approach where the time derivative of the density in the mass conservation equation is replaced with the pressure term in the equation of state (Chorin 1967).

4.2. METHODOLOGY

1- Hydrostatic ECOMSED, 2- Hydrostatic and non-Hydrostatic MIKE 3 and 3- Hydrostatic and non-Hydrostatic H3D were utilized to simulate the flow over the surface of bed forms. These models were selected due to their record of successful 3D flow modeling applications in coastal, riverine and estuarine environments.

ECOMSED:

ECOMSED (HydroQual, Inc., 2002), is a public domain finite volume hydrostatic and sediment transport model which computes water circulation, temperature, salinity, mixing and transport, deposition and resuspension of cohesive and non-cohesive sediments. The hydrostatic module incorporates the Mellor-Yamada turbulence closure model (Mellor and Yamada, 1982) to provide parameterization of the vertical mixing processes and the Samogorinsky formulation (Samagorinsky 1963) for the horizontal. It is based on the Princeton Ocean Model by Blumberg and Mellor (1987). ECOMSED utilizes a horizontal, orthogonal curvilinear coordinates system and sigma coordinates in the vertical which enables it to simulate different bed topography configurations.

MIKE 3 Flow Model:

MIKE 3 flow model (DHI 2005). is a proprietary three dimensional, baroclinic hydrostatic and non-hydrostatic modeling system that simulates unsteady 3D flows taking into account density variations, bathymetry and other external forcings (tidal elevations, current...etc).

MIKE 3 solves for the time dependent non-linear equations of continuity and conservation of momentum in three dimensions using finite difference techniques on x, y Cartesian grid and bottom fitted constant z-spacing vertical grid. MIKE 3 incorporates several turbulence models to characterize the eddy viscosity (Smagorinsky model, k model, k-ε model, mixed Smagorinsky / k-ε model and a constant eddy viscosity model). MIKE 3 non-hydrostatic version utilizes the artificial compressibility approach.

H3D:

H3D (Stronach 1993), is a proprietary finite difference hydrostatic and non hydrostatic numerical model that solves the three-dimensional Reynolds averaged Navier-Stokes equation on either a Cartesian or an orthogonal curvilinear grid with a variable z-level discretization in the vertical. The Volume of Flow (VOF) method is used to fit the free surface ant eh bathymetry. H3D is based on models described in Backhaus (1985) and Stronach et al., (1993). H3D uses a shear-dependent turbulence formulation in the horizontal, (Smagorinsky, 1963) and a shear- and stratification-dependent formulation in the vertical for momentum transfer, a procedure referred to as the Mellor-Yamada Level 2 scheme (Mellor and Yamada, 1982). H3D non-hydrostatic version utilizes the pressure correction method (Poisson equation for the pressure term).

4.3. MODEL SETUP

4.3.1. MODEL HORIZONTAL AND VERTICAL GRID

The bathymetry for the horizontal grid was created using information obtained from the spectral analysis results presented in Chapter Three. Bed form wave length (λ_d = 30 m) and height (H_d = 3 m) were obtained to create a one dimensional profile of bed forms. The profile was then interpolated to create a two dimensional bed form using a FORTRAN code. The bathymetry file contains five bed forms (5 X 30m = 150 m) and width = 10 m as shown in Figures 1 and 2. Table 1 summarizes the horizontal and vertical grid information used in the three models.

	ECOMSED	**MIKE 3**	**H3D**
Depth	10 m	10 m	10 m
Horizontal Grid	0.5 m X 0.5 m	0.5 m X 0.5 m	0.5 m X 0.5 m
Vertical Grid	20 sigma layers distributed along the whole length	40 levels with constant spacing of 0.25 m	40 levels with constant spacing of 0.25 m
Time Step	0.005 sec	0.005 sec	0.01 sec
Horizontal Turbulence model	Smagorinsky formulation	Smagorinsky formulation	Smagorinsky formulation
Vertical Turbulence model	Mellor-Yamada level 2.5 scheme	k-ε turbulence model	Mellor-Yamada level 2 scheme

Table 4.1: Three dimensional models comparisons

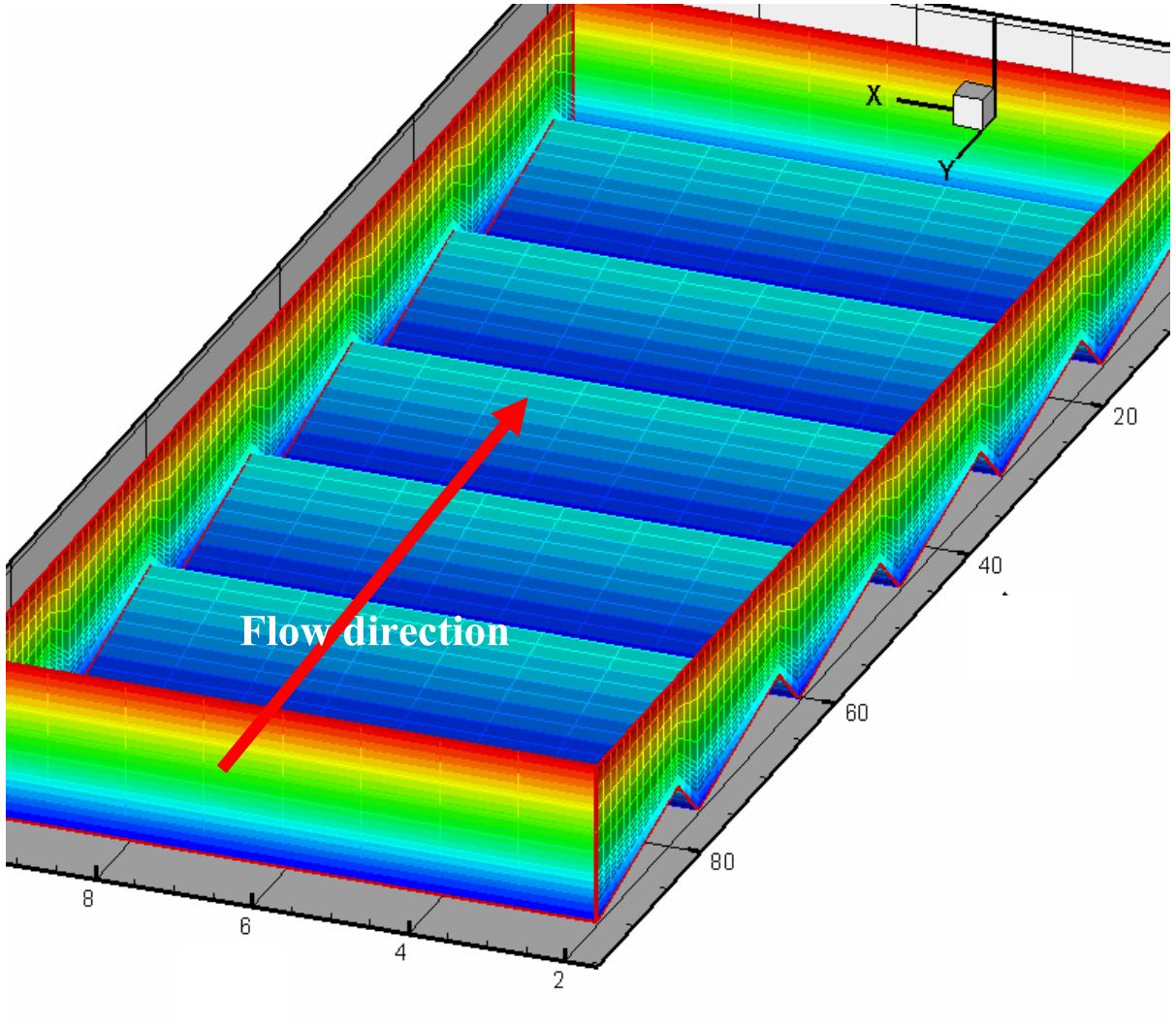

Figure 4.1: Three dimensional view of the models bathymetry

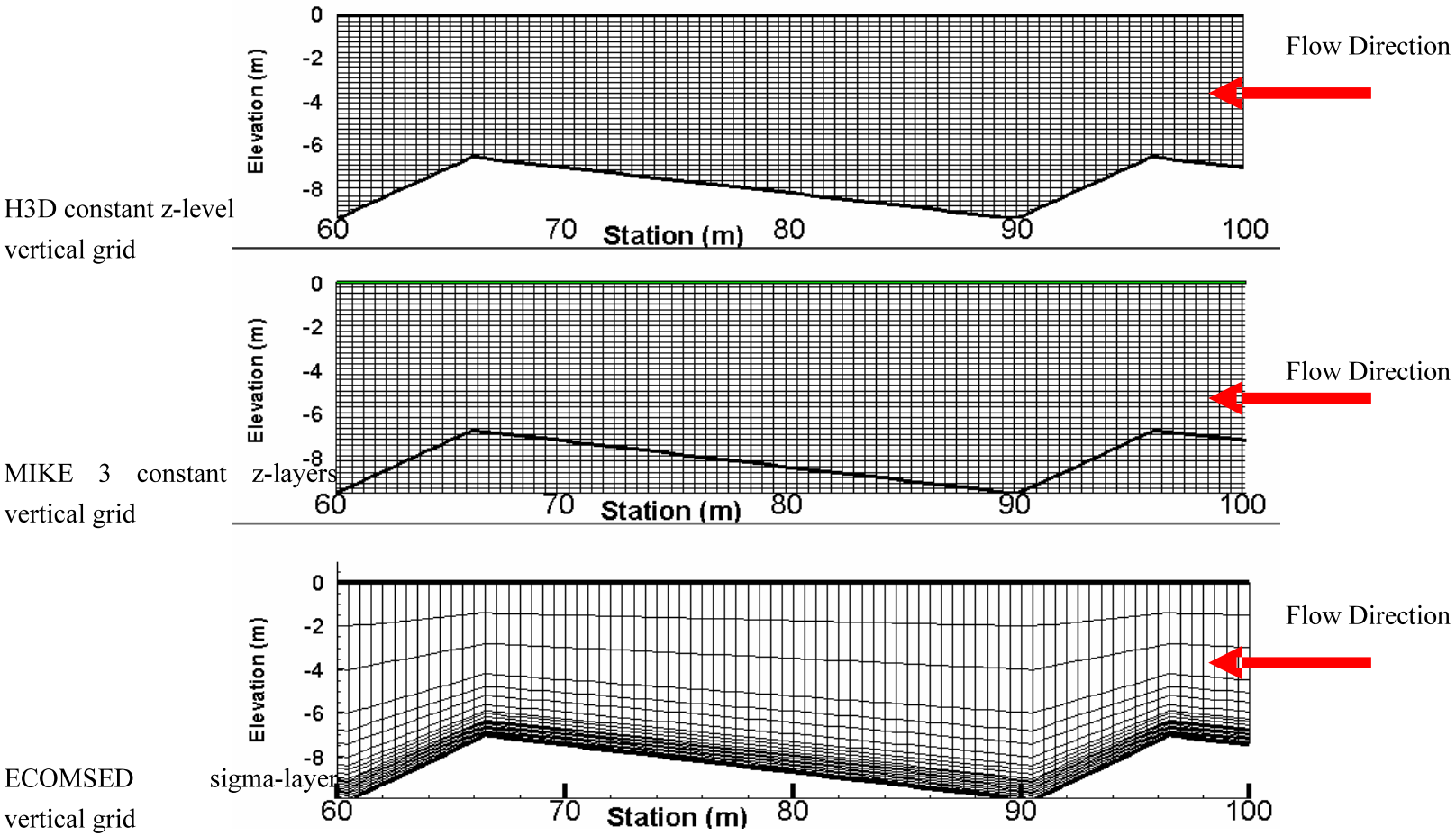

Figure 4.2: Models vertical grid discretization

4.3.2. HYDRODYNAMICS BOUNDARY CONDITIONS

An average logarithmic velocity profile based on ensemble averaged Acoustic Doppler Current Profiler (ADCP) measurements from the river (collected around the same time period where the multibeam data were collected, June 2003 to September 2003) was applied at the upstream side. A constant water level was imposed at the downstream side for all the models for consistency. Full slip assumption was applied at the side walls when the option was available (MIKE3).

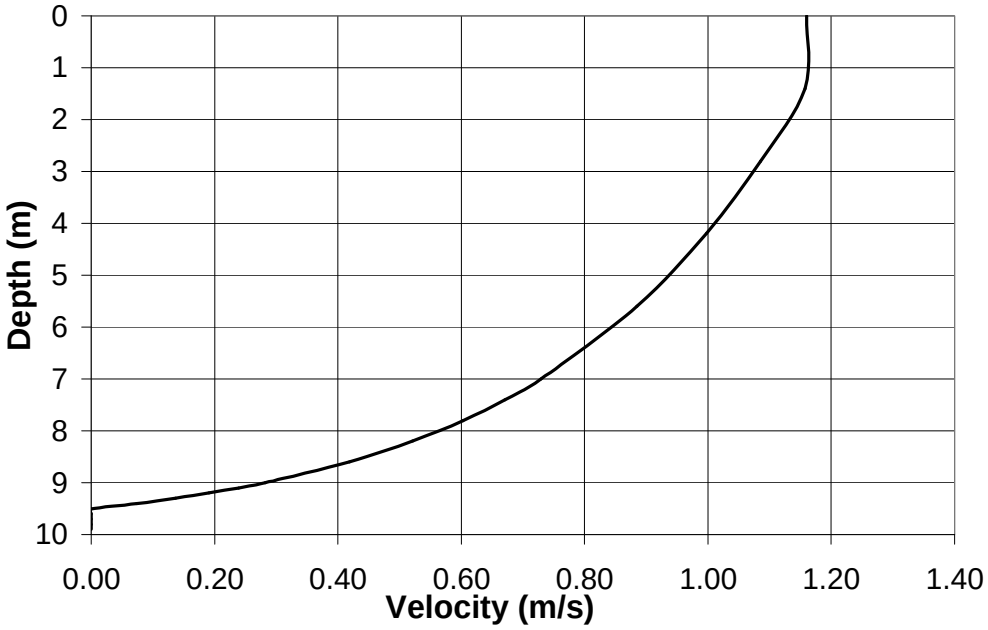

Figure 4.3: Velocity profile upstream boundary condition

The MIKE 3 model used the velocity profile directly as a boundary condition, while the corresponding grid-cell discharge was computed for ECOMSED and subsequently used as a boundary condition. H3D used a constant discharge as its boundary condition. Thus H3D had a different upstream boundary condition which may account for a different initial shear stress as will be explained later. Care was taken to ensure that the simulated velocity fields resulting from the different boundary conditions gave the same discharge.

4.4. MODEL CALIBRATION AND VERIFICATION

Model calibration and verification were done in two steps. The first step was setting up a set of flat bed bathymetry models with the same configuration as the bed forms models described in Table 4.1 to assess the responses of the numerical models to flat bed bathymetries before testing bed form bathymetries.

The second step included setting up another set computer models for laboratory scale bed forms. The small scale computer models were built with the same horizontal and vertical dimensions as the physical model presented in Nelson et al (1993).

4.4.1. FLAT MODEL CASE

Flat bed bathymetries were created with the same configuration (Figure 4.4) (width, length, horizontal grid dimensions and vertical grid) as the bed form models presented in Table 4.1. The models were then simulated using ECOMSED, MIKE 3 Flow model and H3D to assess the individual model's ability to correctly simulate the flow over flat bed before testing the models in the bed forms case. The flat bed models input skin friction as represented by bed roughness is shown in Table 4.2.

	ECOMSED	**MIKE 3**	**H3D**
Model Friction	1-Bottom Friction coefficient = 0.003 (non-dimensional), 2-Bottom roughness coefficient : 0.003 m	Bottom roughness: 0.003 m	Bottom Friction coefficient = 0.003 (non-dimensional)

Table 4.2: Models bed friction

Model input bed (skin) friction was intentionally assumed small in magnitude to represent a smooth surface. The same calibrated minimum skin friction values will be then applied in the bed form case models so that the simulated resistance of the bed form can be separated from the smooth surface resistance.

Results of the computer models are presented as a series of water surface profiles, contours overlaid with stream traces and vertical velocity profiles as shown in Figure 4.5 through 4.7 respectively.

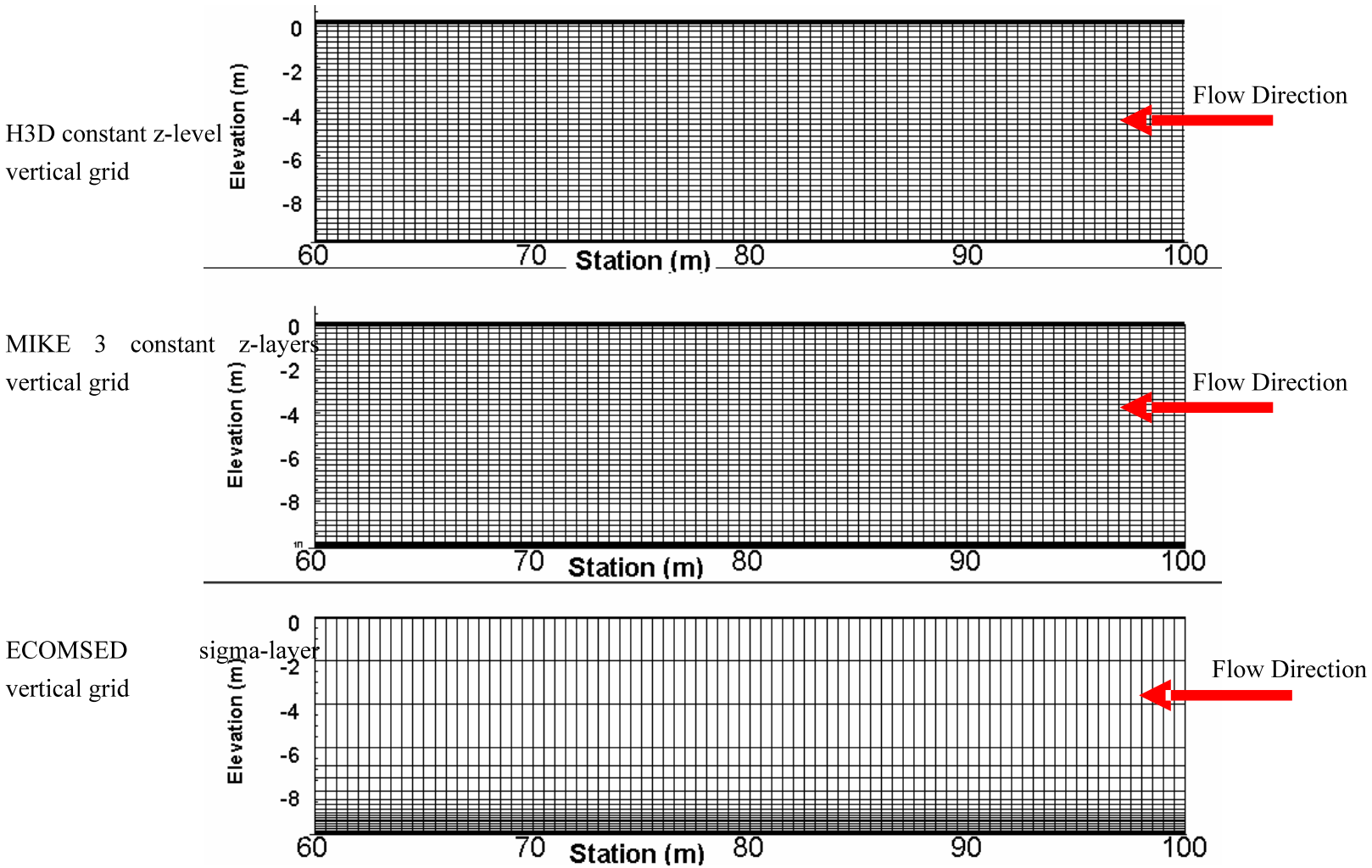

Figure 4.4: Flat models vertical grid discretization

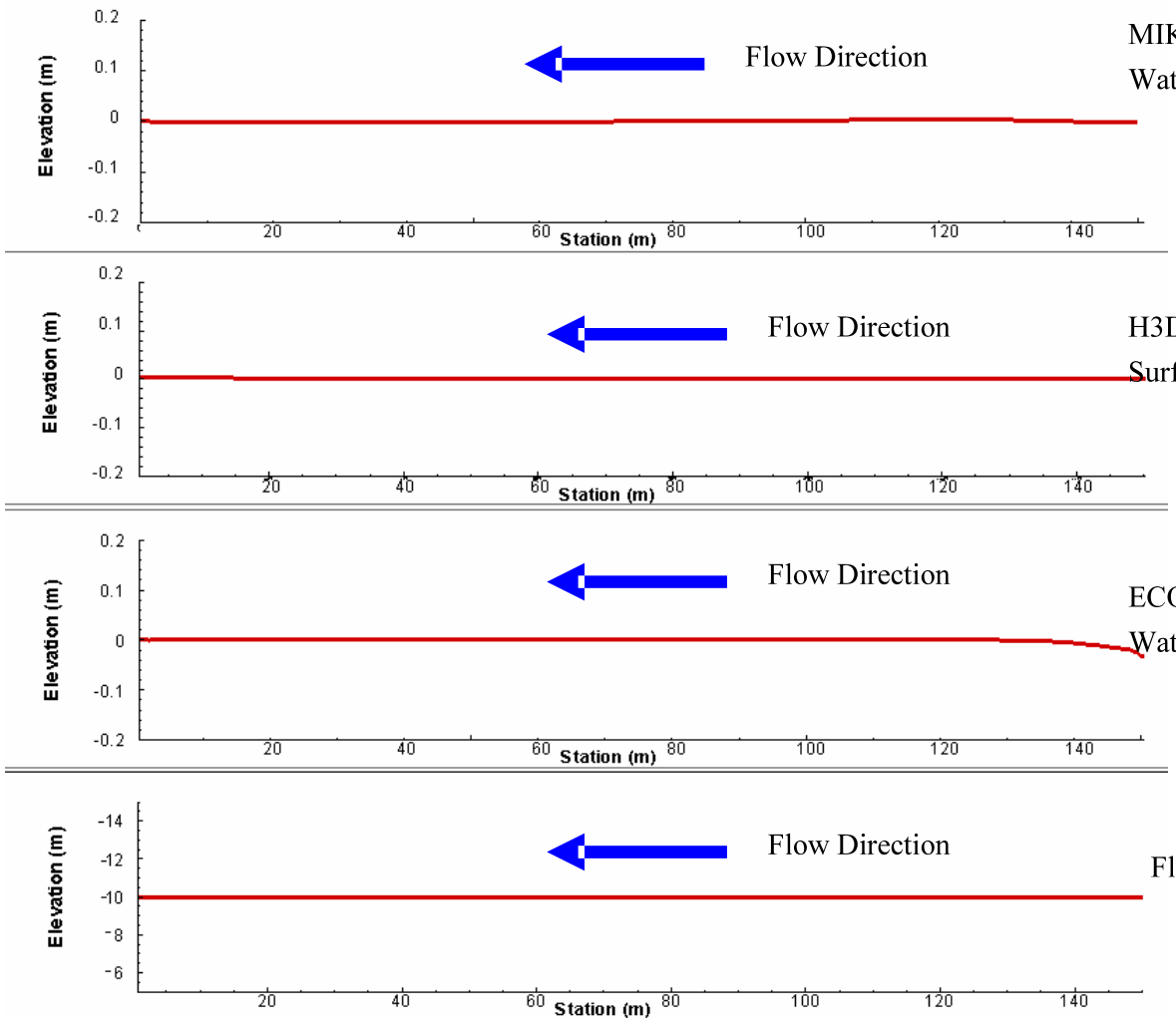

Figure 4.5: Water surface profiles on top of bed forms

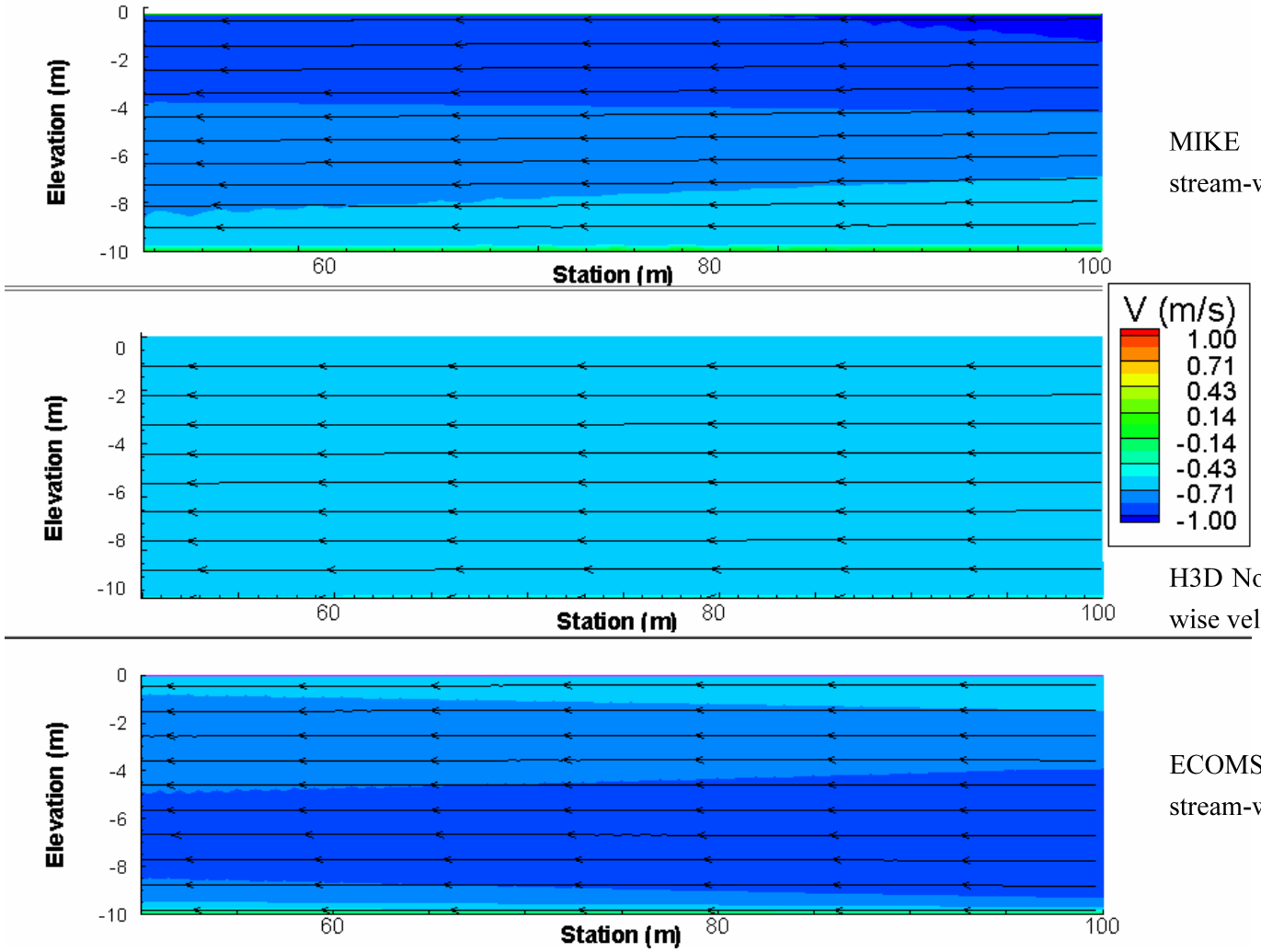

MIKE 3 Non Hydrostatic stream-wise velocity contours

H3D Non Hydrostatic stream-wise velocity contours

ECOMSED Hydrostatic stream-wise velocity contours

Figure 4.6: Flat model stream-wise velocity contours overlaid with stream-traces

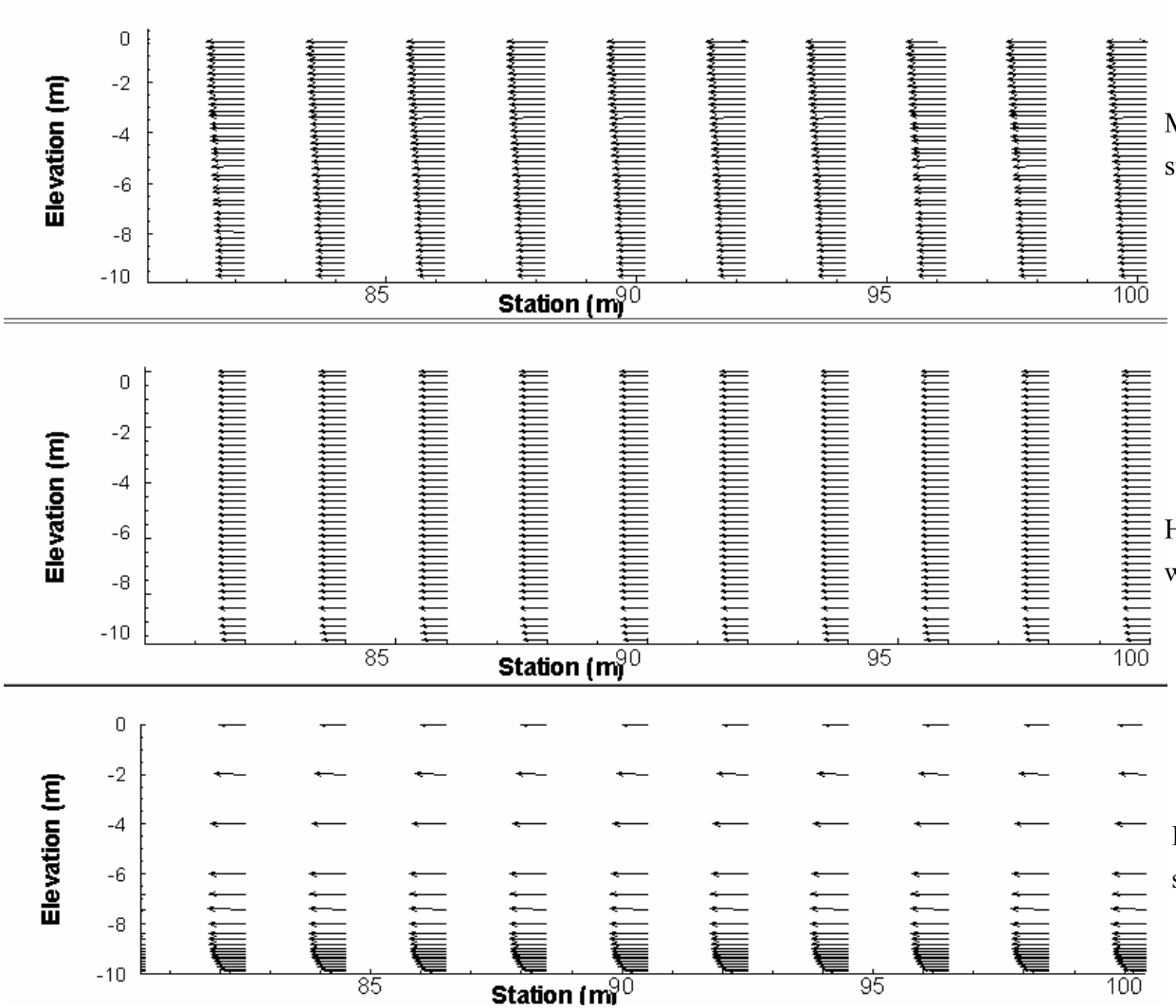

MIKE 3 Non Hydrostatic stream-wise velocity vectors

H3D Non Hydrostatic stream-wise velocity vectors

ECOMSED Hydrostatic stream-wise velocity vectors

Figure 4.7: Flat model stream-wise velocity vectors

The three models reproduced relatively similar water surface profiles and as a result very similar values of Manning's n. ECOMSED water level profile showed a kink in the upstream side of the model resulting from some inconsistencies in the model in transferring the upstream boundary conditions (cell input discharges) to the inner cells. The equivalent Manning's n shown in Table 4.3 was small in magnitude as a result of using relatively small bed roughness heights in the models input. This was done intentionally to be able to provide representative skin friction for the cases of bed form simulation, form resistance as will be explained in Section 4.5. H3D and MIKE 3 predicted a nearly constant velocity vertical distribution of the longitudinal velocity, while ECOMSED predicted lower magnitude velocities near the bed. The reason behind this is thought to be that the sigma-layer ECOMSED had better resolution than H3D and MIKE 3 near the bed. However ECOMSED predicted higher velocities in the upper part of the water column than H3D and MIKE as expected due to continuity. A hydraulically smooth bed with fully turbulent flow has a Manning's n in the range 0.007 to 0.009.

	Mean velocity (m/s)	**Hydraulic Radius ~ depth (m)**	**Average Slope**	**Simulated Manning n**
ECOMSED	0.75	10	0.0000026	0.009
MIKE 3	0.75	10	0.0000010	0.006
H3D	0.75	10	0.0000013	0.007

Table 4.3: Models simulated equivalent Manning's n

Although H3D had the option of using variable spacing vertical level discretization, the vertical grid in H3D was retained to match the grid used in MIKE3. However, as mentioned above, H3D and MIKE3 models did not predict the expected logarithmic velocity profiles. Another test run was performed using H3D with the same vertical discretization as ECOMSED to assess the ability of H3D to predict the logarithmic velocity profile. The model grid, along with the model results are shown in Figure 4.8.

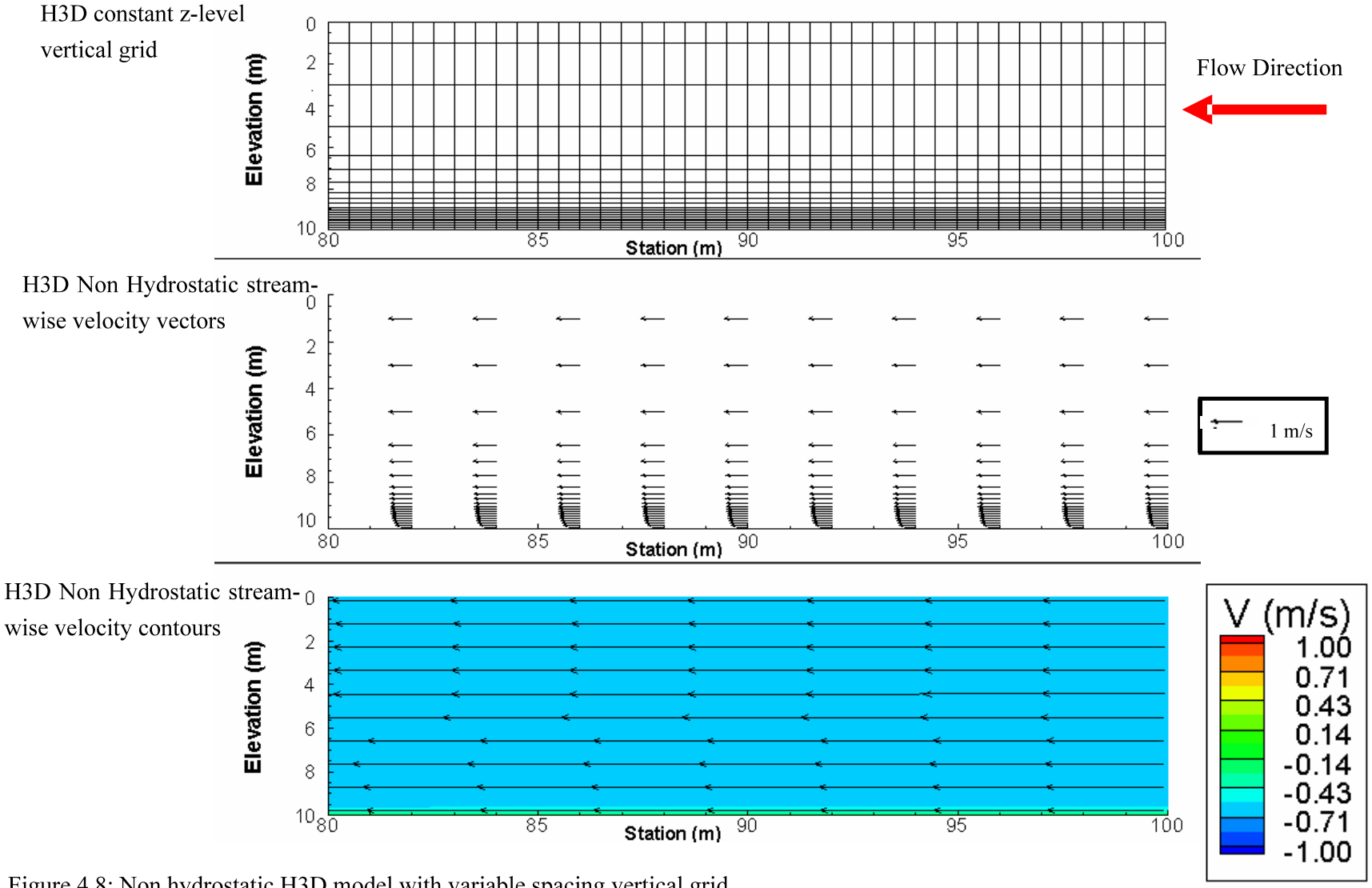

Figure 4.8: Non hydrostatic H3D model with variable spacing vertical grid

Figure 4.8 shows that H3D model was able to correctly predict the logarithmic velocity profile unlike the case where the H3D vertical discretization was kept the same as MIKE 3. This test run was performed to make sure that H3D's inability to reproduce the logarithmic velocity profile (case of H3D grid = MIKE 3 grid) was due to not having enough layers. For the case of the bed forms models (Section 4.5), the H3D grid was kept constant and the same as MIKE 3 for consistency.

4.4.2. PHYSICAL MODEL CASE

The second step in the model calibration and verification was performed by setting up another set of two dimensional small scale computer models. The computer models were built using the same horizontal and vertical dimensions of the physical model presented in Nelson et al (1993) shown in Figure 4.9. H3D and ECOMSED were used in this step. Input skin roughness in Table 4.2 was used for these runs.

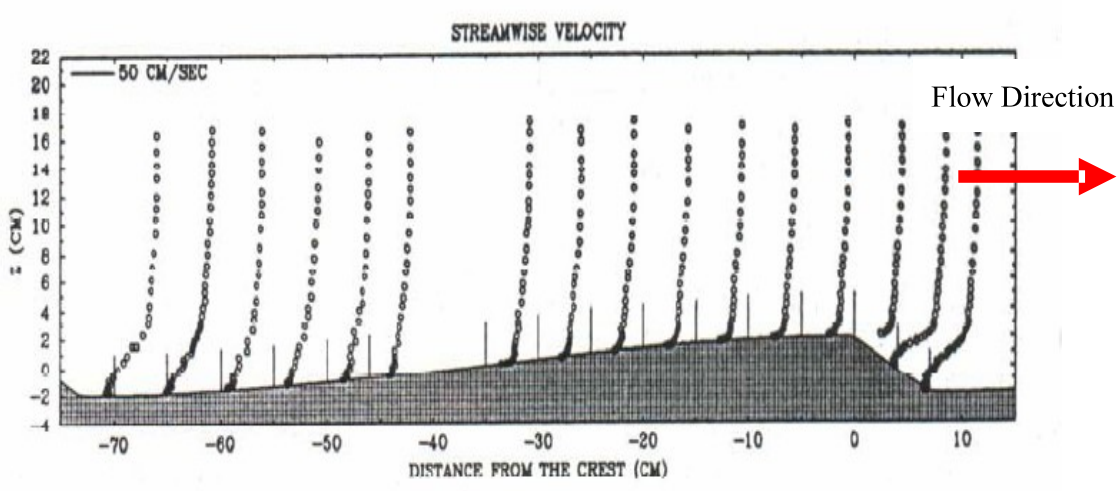

Figure 4.9 Physical model used in Nelson 1993 [After Nelson (1993)]

A comparison of model grids is shown in Table 4.4 and Figure 4.10.

	ECOMSED	H3D
Depth	0.20 m	0.20 m
Horizontal Grid	0.01 m X 0.01 m	0.01 m X 0.01 m
Vertical Grid	20 sigma layers distributed along the whole length	24 levels distributed along the whole length
Time Step	0.0001 sec	0.0001 sec
Horizontal Turbulence model	Smagorinsky formulation	Smagorinsky formulation
Vertical Turbulence model	Mellor-Yamada level 2.5 scheme	Mellor-Yamada level 2 scheme

Table 4.4: Small scale models grids comparisons

Model results are presented as a series of water surface profiles, velocity contours overlaid with stream-wise velocity traces and velocity vertical profiles as shown in Figure 4.11 through 4.13. Figure 4.14 and 4.15 show a comparison for the velocity vertical profiles model results versus Nelson et al (1993) physical model results. Profiles are shown at the crest, lee and the developing zone of the bed form. These figures also show the effect of increasing the resolution of the vertical layers in H3D on the predicted velocity profile.

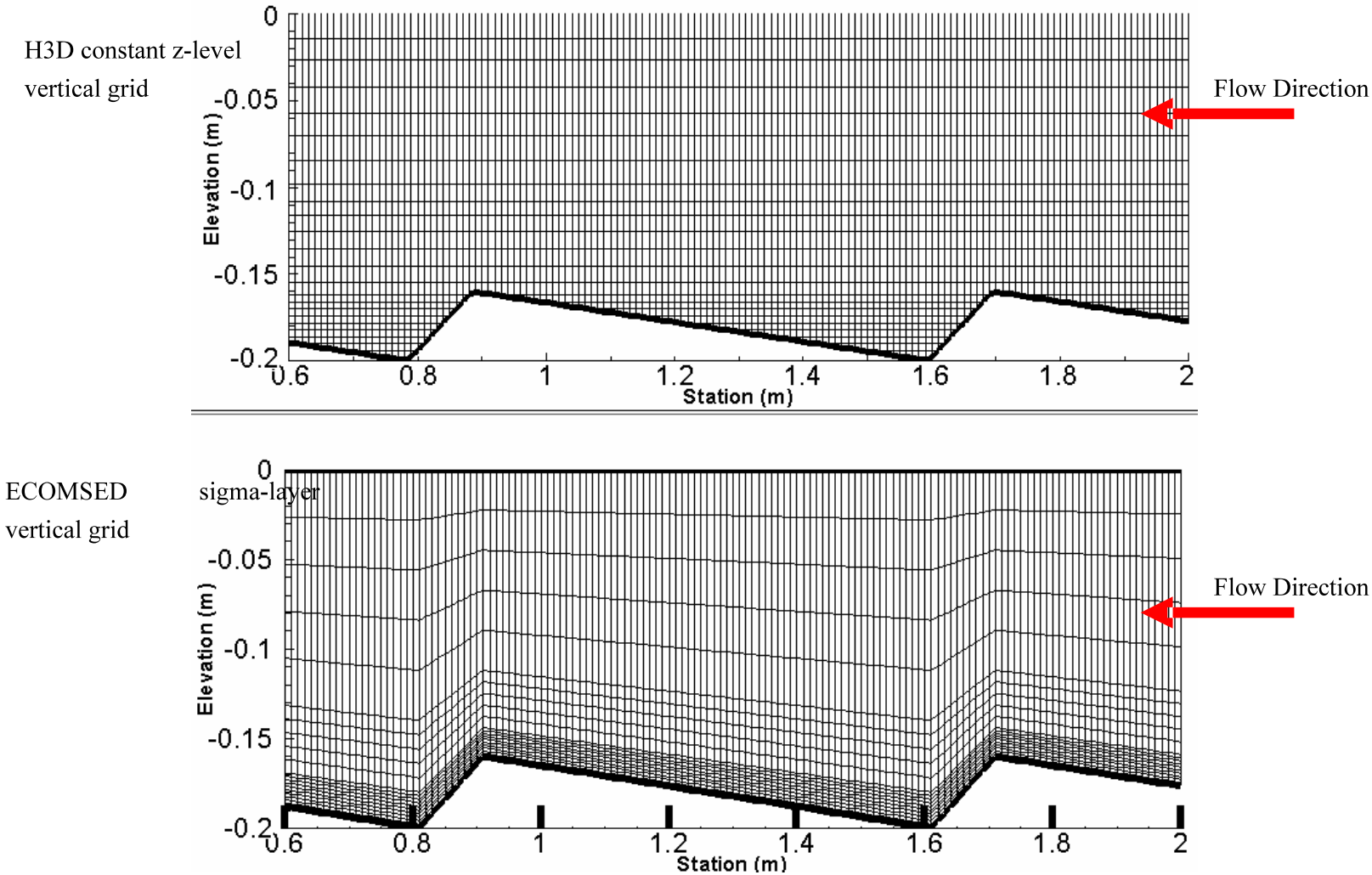

Figure 4.10: Small scale model vertical grid discretization

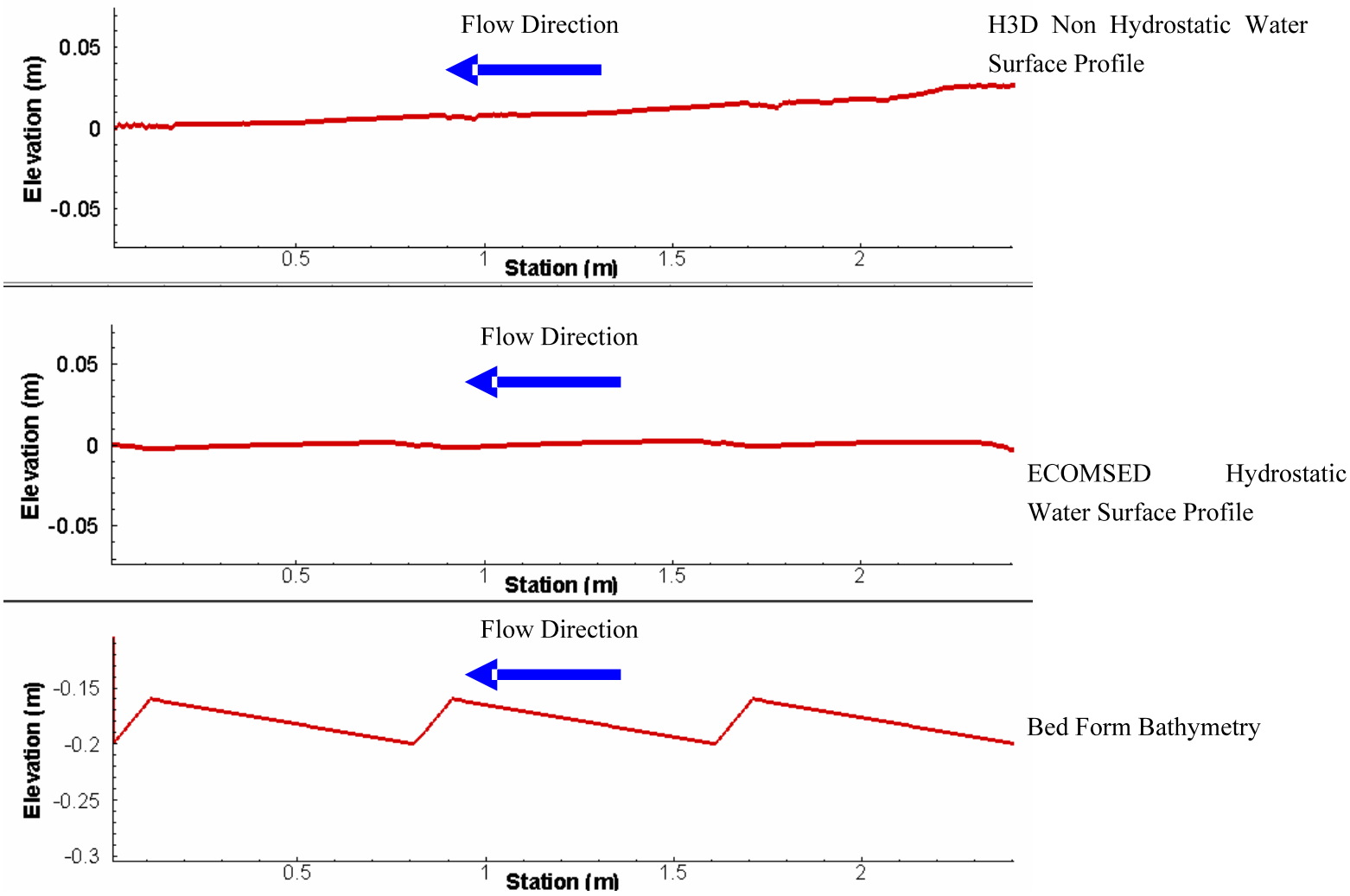

Figure 4.11: Small scale water surface profiles on top of bed forms (Flow direction)

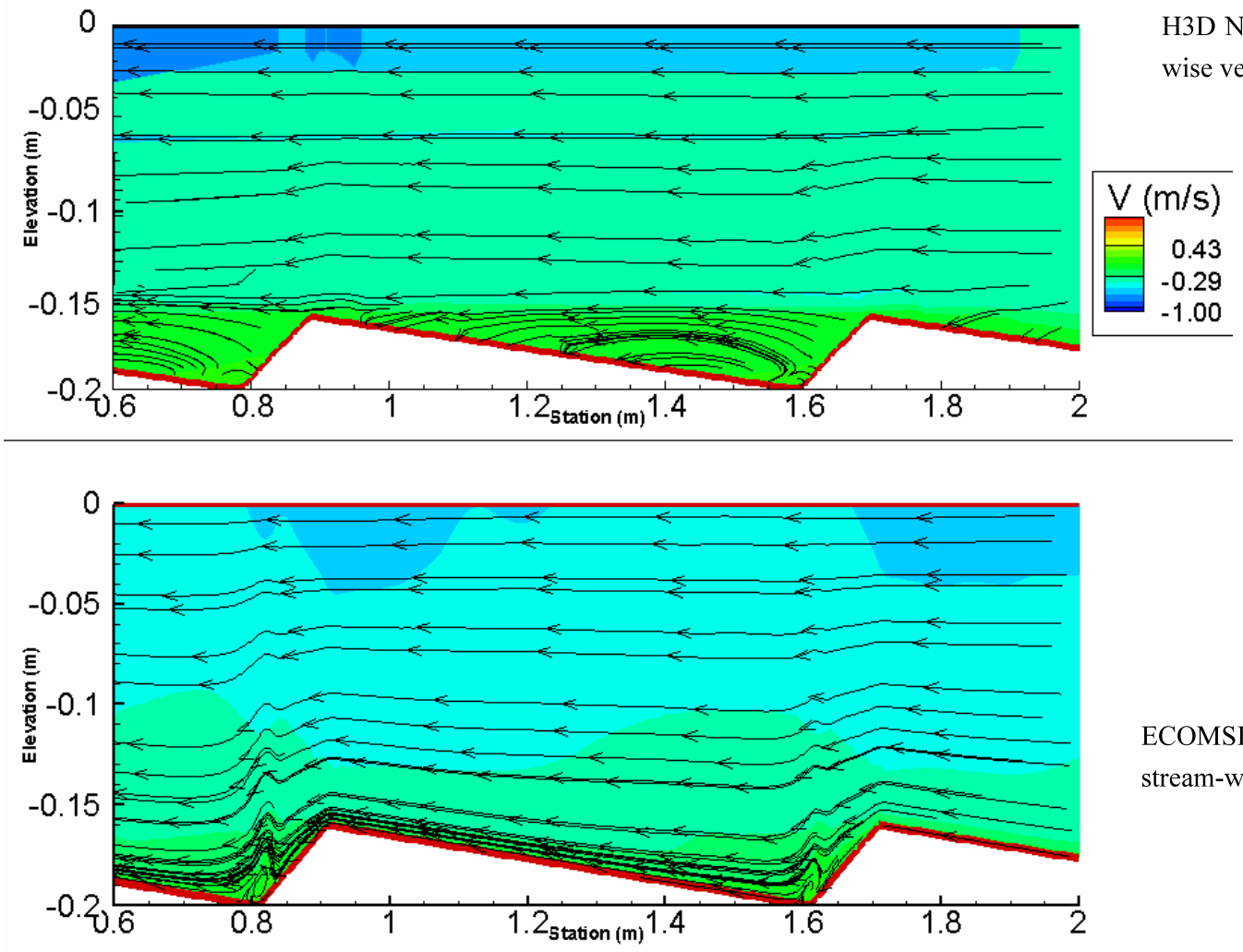

Figure 4.12: Small scale model stream-wise velocity contours overlaid with stream-traces

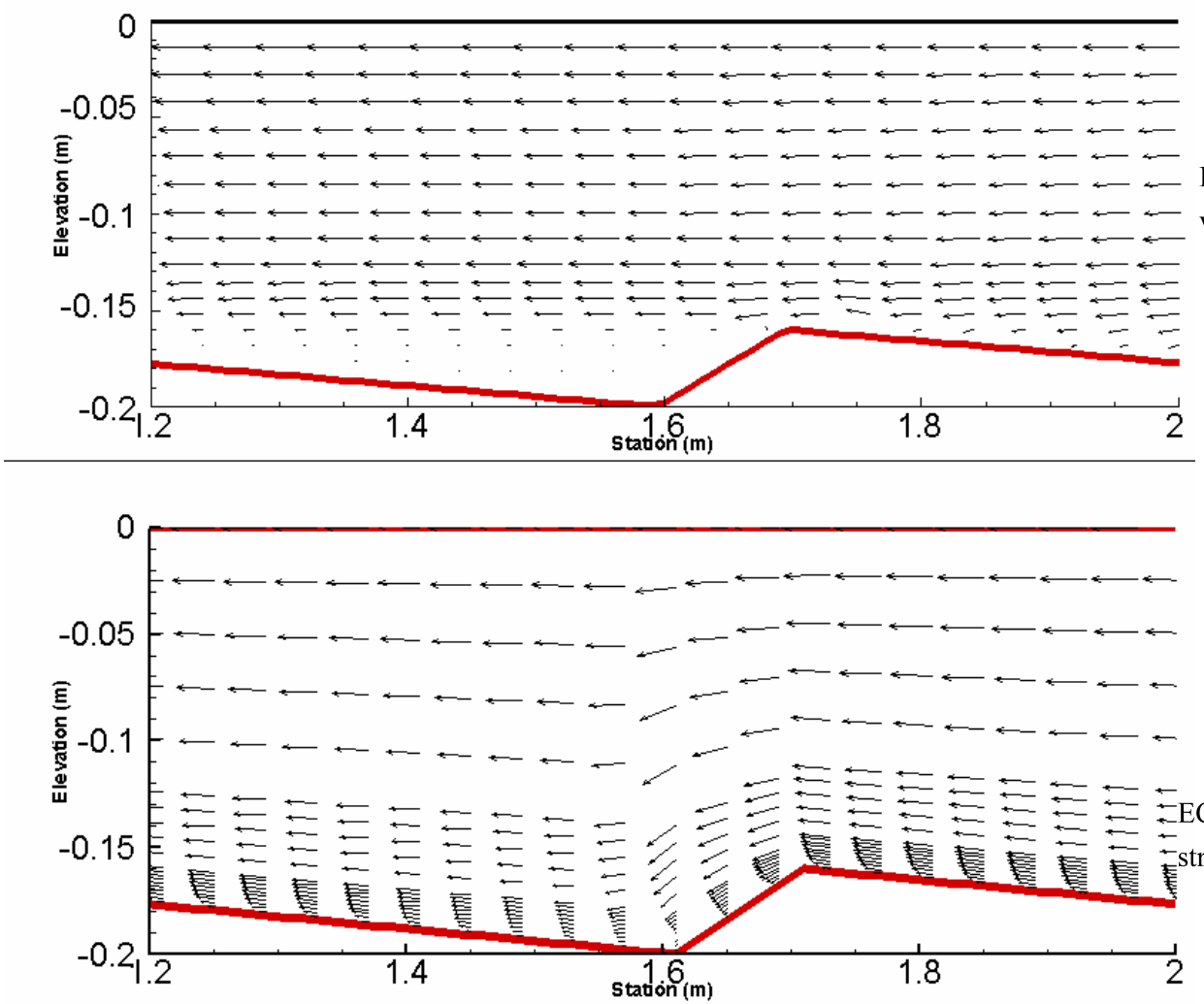

H3D Non Hydrostatic stream-wise velocity vectors

ECOMSED Hydrostatic stream-wise velocity vectors

Figure 4.13: Small scale model stream-wise velocity vectors

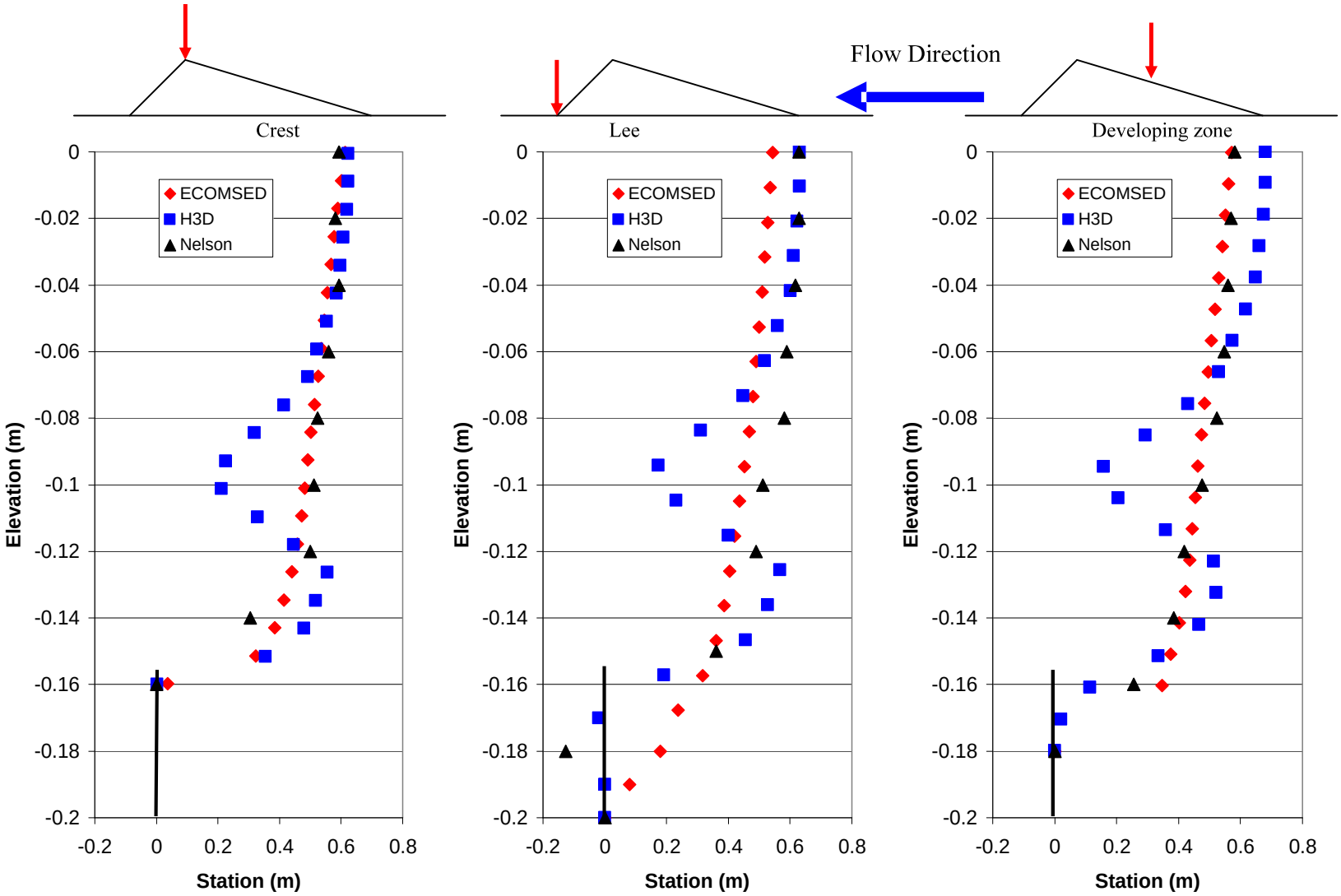

Figure 4.14: Comparisons of velocity vertical profiles for Nelson, H3D (20 vertical layers) and ECOMSED models

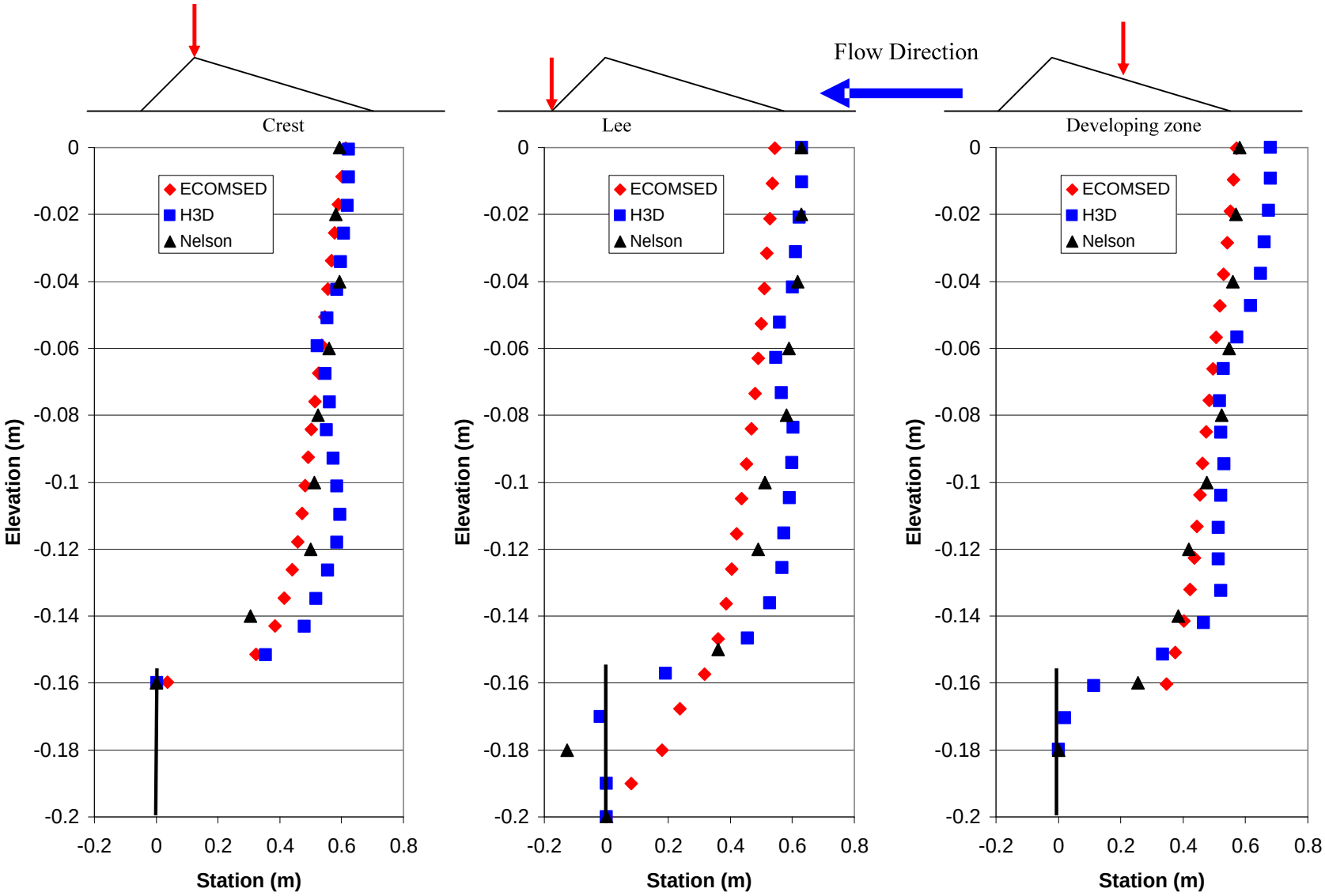

Figure 4.15: Comparisons of velocity vertical profiles for Nelson, H3D (24 vertical layers) and ECOMSED models

The non-hydrostatic H3D and hydrostatic ECOMSED predicted very similar water surface profiles. H3D predicted a higher water surface profile at the upstream boundary. This increase in the water surface slope is attributed to the constant discharge boundary imposed in H3D. ECOMSED was able to correctly predict the out of phase relation between the bed and the water surface profile. H3D on the other hand, predicted rather a small out of phase relationship. The simulation times for the two models were very long due to the small grid size (1 cm) and the small time step (0.0001 sec) and that made it relatively difficult to simulate more than three successive bed forms. Flow separation was observed in both models. ECOMSED model predicted a very weak local separation at the lee side of the bed form. H3D model correctly predicted the separation phenomena on the lee side of the bed form. The velocity vertical distribution in ECOMSED was very close to the distribution observed in Nelson 1993 except in the lee of the dune where the flow separation was under-estimated.

The increase in the resolution of the vertical layers in H3D (20 layers to 24 layers) proved to be essential in correctly predicting the velocity profile. It is also thought that ECOMSED did not produce this erroneous kink in the profile, since it ignores the vertical accelerations (hydrostatic assumption). H3D predicted lower magnitude velocities in the lower section of the model. The increase of the velocity magnitude along the slope of the bed form was evident in ECOMSED and less evident in H3D.

The predicted velocity vertical profiles by ECOMSED followed the same logarithmic profile in Nelson (1993) physical model (Figure 4.15). At the crest side of the bed form, ECOMSED closely matched Nelson results; however it did not predict the full extent of the separation at the lee side observed in Nelson results. On the developing side of the bed form, ECOMSED

predicted slightly higher velocities than Nelson. At the lee side, H3D results were closer to those of Nelson than ECOMSED.

The magnitude of the out of phase relationship $\delta_{energy\text{-}12}$ in the small scale model between the water surface profile and the bed form surface was checked against the energy principle where $\delta_{energy\text{-}12} \sim \frac{V_1^2}{2g} - \frac{V_2^2}{2g}$, where V_1 and V_2 are the average velocities at point 1 and 2 respectively as shown in Figure 4.16 since the energy loss in the contracting flow (1 → 2) is relatively small..

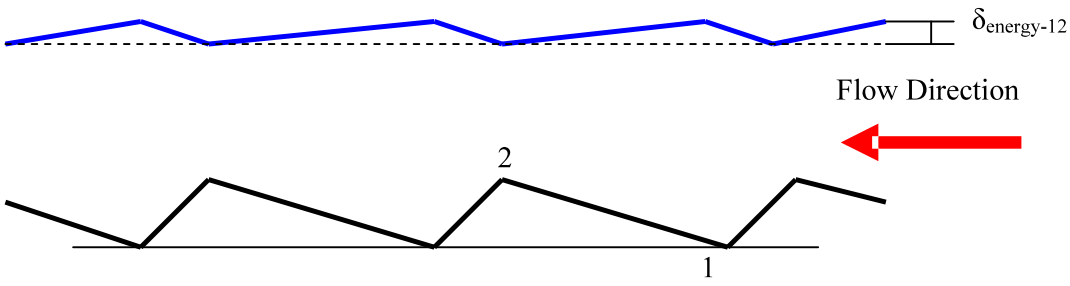

Figure 4.16 Out of phase relationship between the water surface profile and the surface of the bed form

$\delta_{energy\text{-}ECOMSED} \sim \frac{V_1^2}{2g} - \frac{V_2^2}{2g} = 0.00091\text{m} = 0.91\text{ mm},$

$\delta_{simulated\text{-}ECOMSED} = 0.00113\text{m} = 1.13\text{ mm},$

$\delta_{energy\text{-}H3D} \sim \frac{V_1^2}{2g} - \frac{V_2^2}{2g} = 0.0011\text{m} = 1.1\text{ mm},$

$\delta_{simulated\text{-}H3D} = 0.0004\text{m} = 0.4\text{ mm}.$

where $\delta_{simulated\text{-}model}$ is the simulated water level difference between point 1 and 2 and $\delta_{energy\text{-}model}$ is the water level difference resulting from applying the conservation of energy principal at point 1 and 2.

As mentioned earlier, H3D predicted a weaker out of phase relationship than ECOMSED. A possible reason for this is the stair-stepping effect resulting from H3D application of the volume of fluid method at the lower most computational cell and the over-estimation of the leeside wake. This point is discussed more in Chapter Six.

4.5. MODEL RESULTS

H3D and MIKE 3 had the options of selecting a hydrostatic or a non-hydrostatic simulation engine, while ECOMSED can only simulate hydrostatic flow conditions. A hydrostatic simulation was performed with H3D and MIKE 3 flow model to assess the ability of hydrostatic simulation engines to predict the flow separation phenomenon at the crest of the bed forms. H3D hydrostatic results are shown in Figure 4.17, while MIKE3 hydrostatic results are shown in Figure 4.18. In addition, a non-hydrostatic simulation was performed using H3D and MIKE 3 along with a hydrostatic simulation with ECOMSED.

The non-hydrostatic H3D and MIKE 3 and hydrostatic ECOMSED results are presented as a series of water surface profiles, velocity contours overlaid with stream traces and vertical velocity profiles as shown in Figure 4.19 through 4.21. Figure 4.22 shows the velocity vertical profiles along the crest, lee and the developing side of the bed form.

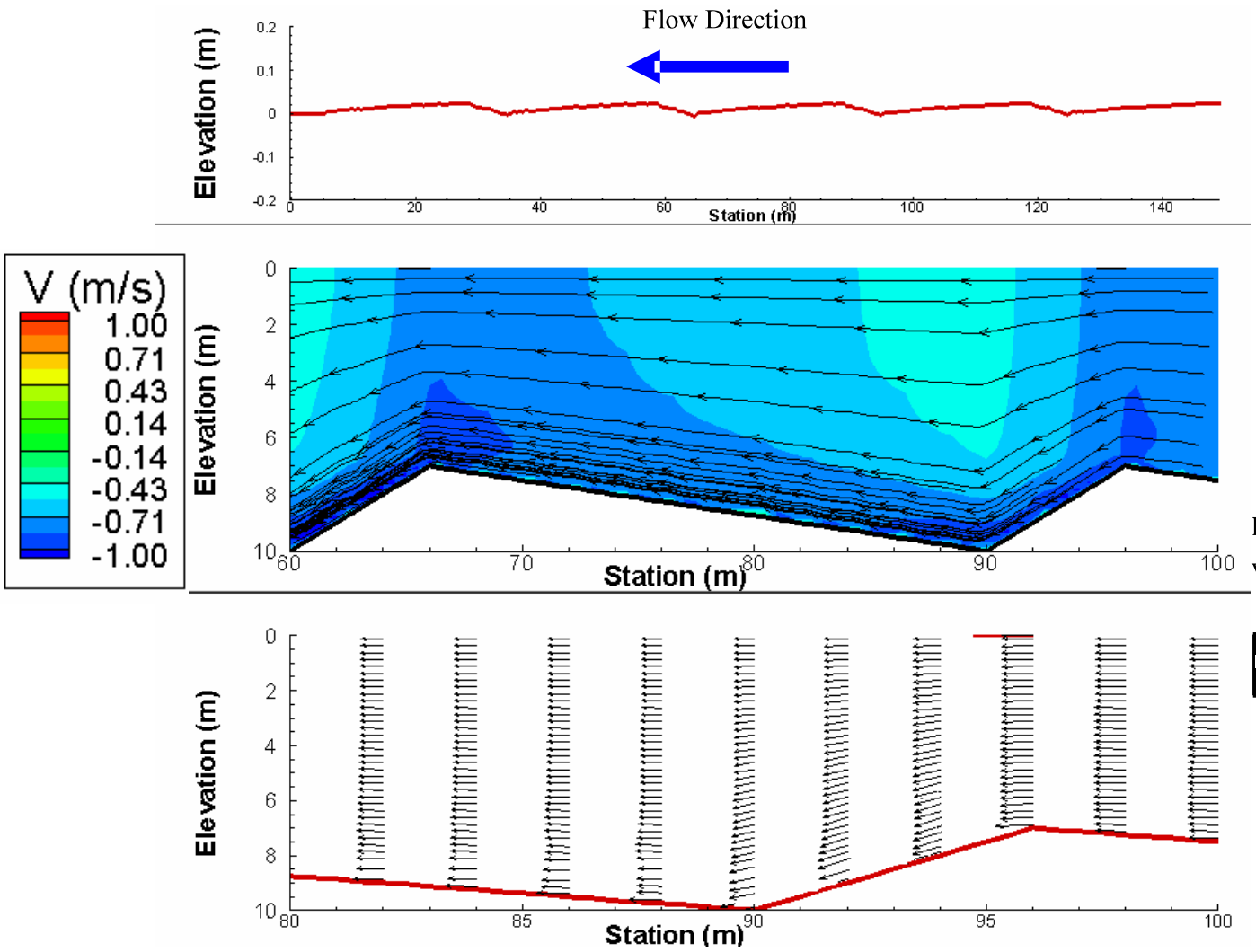

H3D Hydrostatic water surface profile

H3D Hydrostatic stream-wise velocity contours

H3D Hydrostatic stream-wise velocity vectors

Figure 4.17: Hydrostatic H3D model results

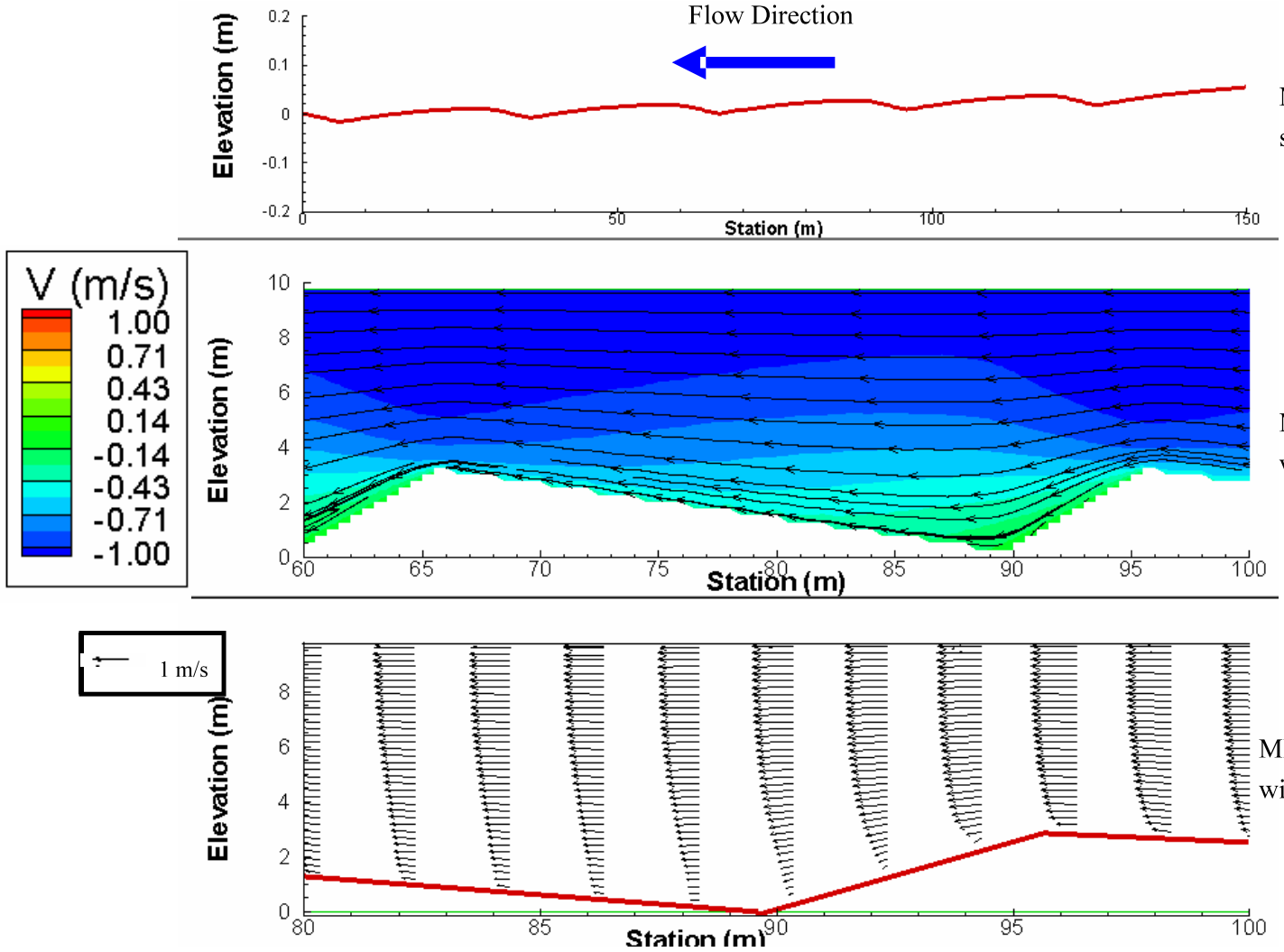

Figure 4.18: Hydrostatic MIKE3 model results

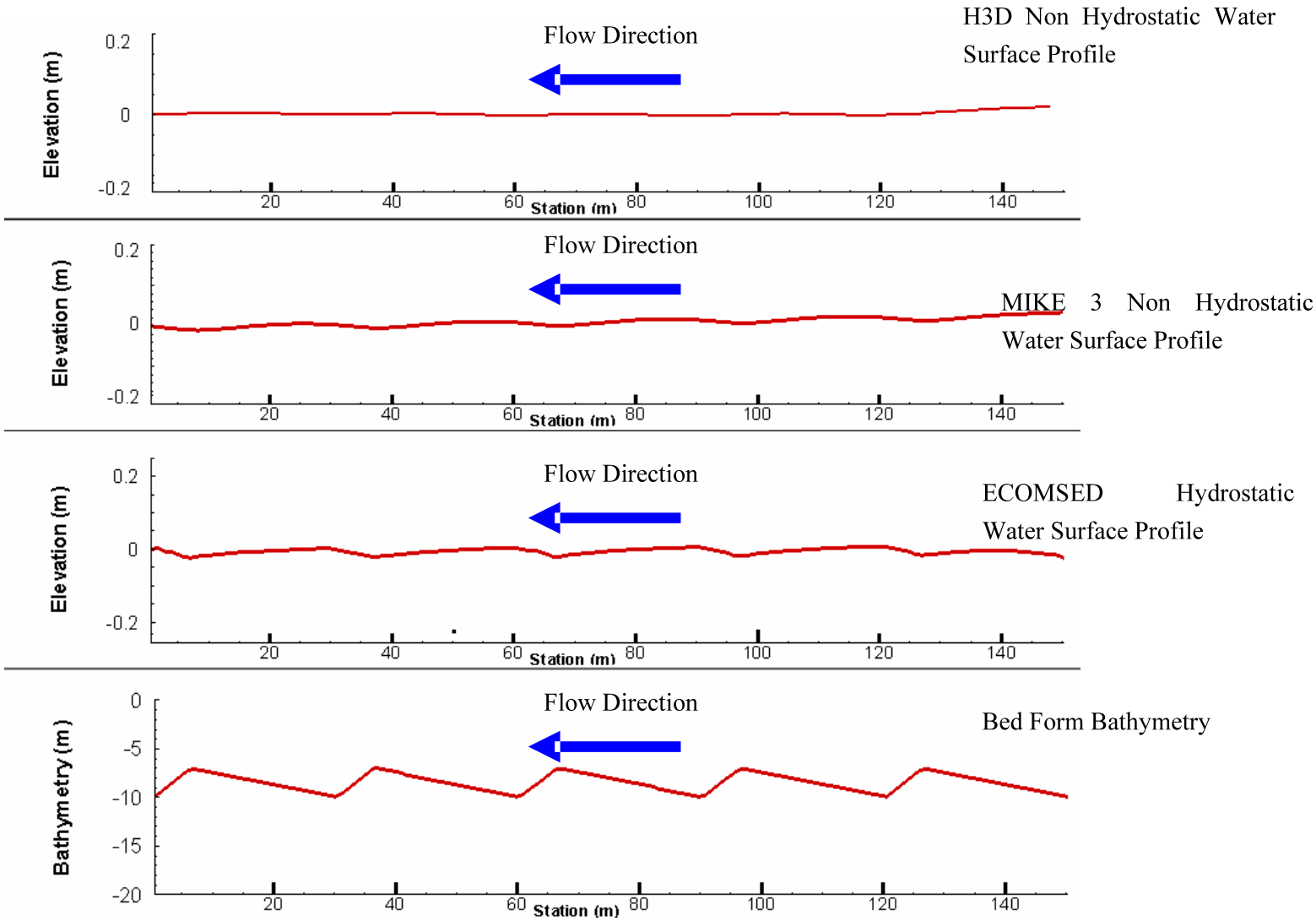

Figure 4.19: Water surface profiles on top of bed forms

H3D Non Hydrostatic stream-wise velocity contours

MIKE 3 Non Hydrostatic stream-wise velocity contours

ECOMSED Hydrostatic stream-wise velocity contours

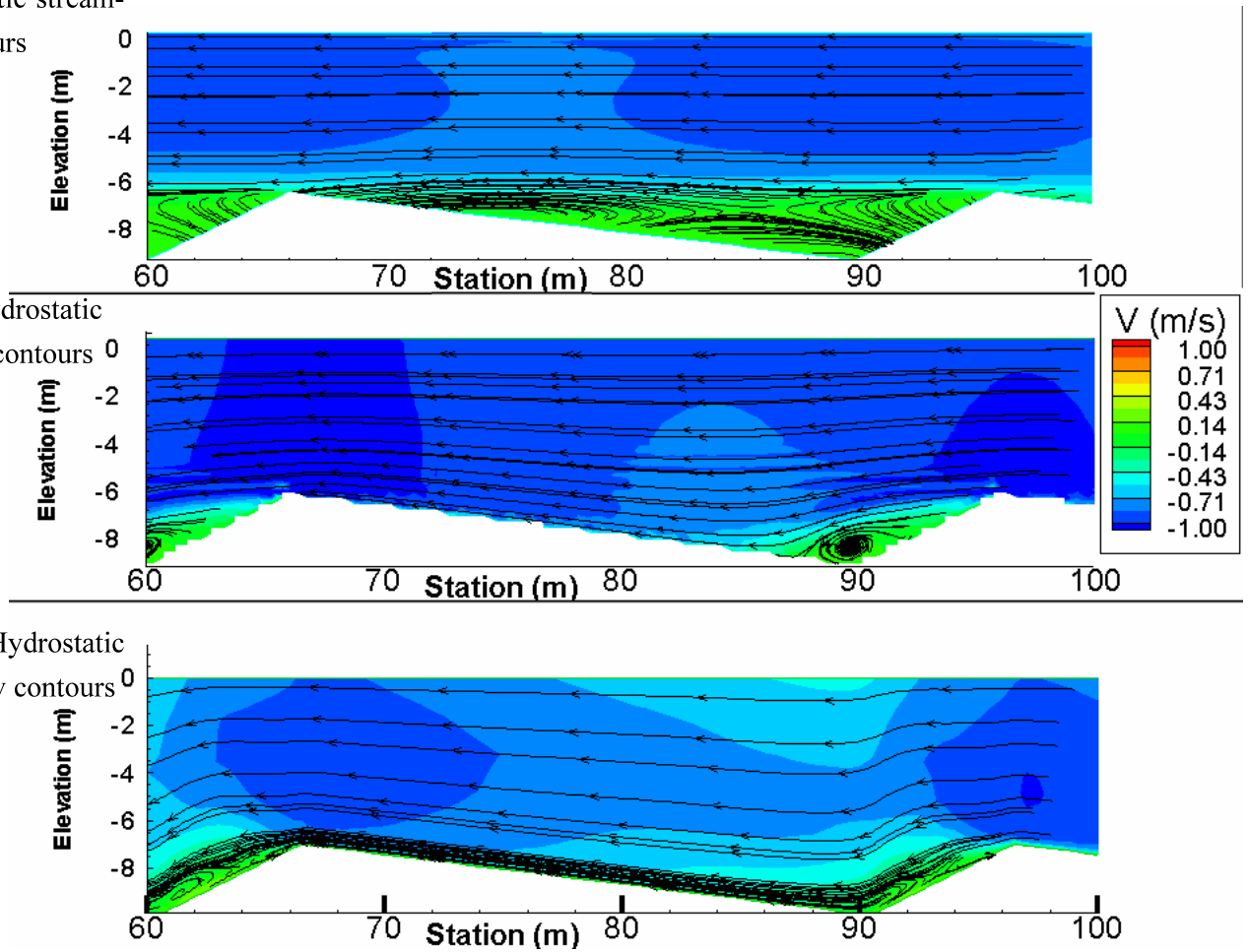

Figure 4.20: Stream-wise velocity contours overlaid with stream-traces

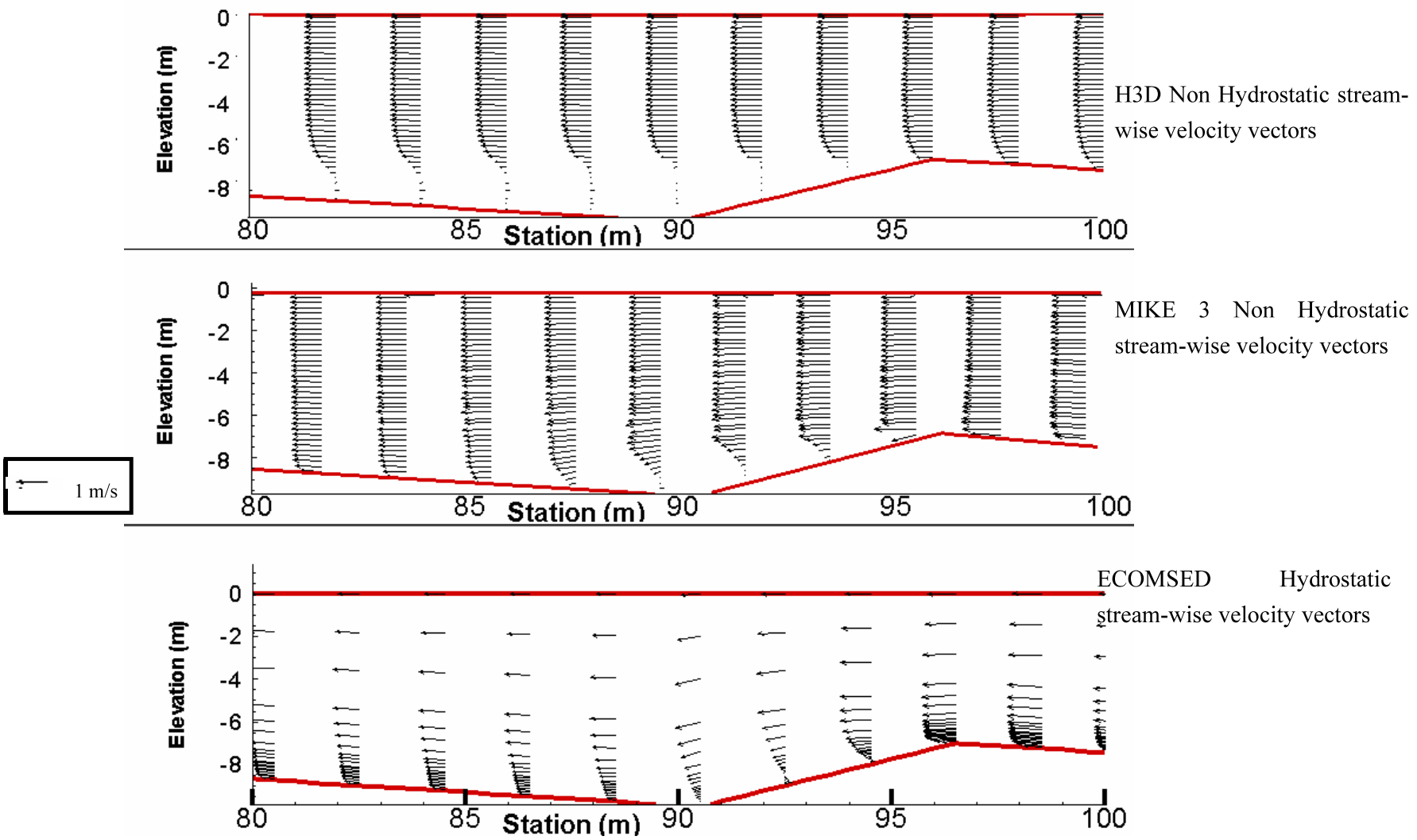

Figure 4.21: Stream-wise velocity vectors

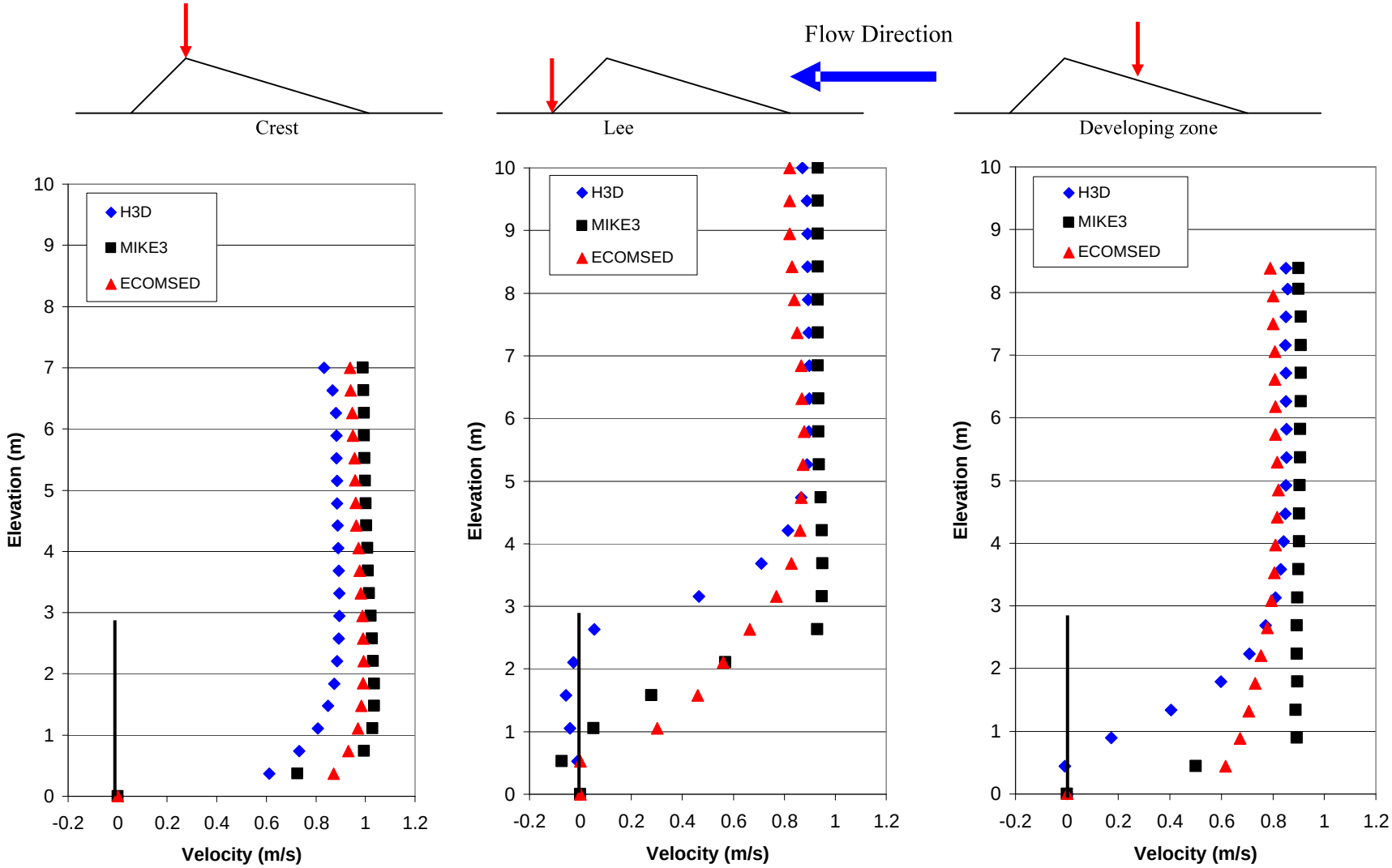

Figure 4.22: Comparisons of velocity vertical profiles for MIKE3, H3D and ECOMSED models

The hydrostatic H3D model correctly predicted the out of phase relation between the water surface profile and the bed bathymetry; however it failed to reproduce the flow separation on the surface of the bed forms as shown in Figure 4.17. The predicted velocity vectors did not show much increase as expected along the slope of the bed form by comparison with the results of Giratella (1977) and Nelson (1993).

The hydrostatic MIKE 3 also correctly predicted the out of phase relationship but failed to predict the flow separation on top of the bed forms. However, the model correctly predicted the increase of the velocity magnitude along the slope of the bed forms as shown in Figure 4.18.

The hydrostatic ECOMSED model did not adequately reproduce the expected flow separation phenomenon at the downstream side of the bed form crest. In relatively shallow flow there was a slight separation but it was weaker than that observed in experiments. The model was able to produce a free water surface profile both with respect to the pattern and the magnitude of the depression that is out of phase with the bed form surface that occurs in natural river systems with bed forms as shown in Figure 4.19. The simulated hydraulic grade line in ECOMSED showed a smaller slope compared to MIKE 3 and closer to H3D and as a result the Manning's n for ECOMSED was smaller as shown in Table 3.

The predicted vertical distribution of the longitudinal velocity for ECOMSED were similar to those observed in laboratory experiments (Nelson et al 1993) where the velocity magnitude increased towards the crest of the bed form as shown in Figure 4.21. The use of only 20 sigma layers in ECOMSED made it the most computationally efficient of the three models.

These results proved as anticipated, the failure of the hydrostatic simulation engines to correctly predict the flow separation phenomena; while on the other hand, the hydrostatic models were able to correctly predict the out of the phase relationship between the bed and surface waves.

The non-hydrostatic MIKE 3 flow model reproduced the flow separation phenomenon more correctly than ECOMSED and H3D at the downstream side of the bed form crest (Figure 4.20). The observed separation was stronger than ECOMSED and more realistic than H3D; however, in MIKE 3, with the constant z-layers discretization, required the use of 40 layers along the vertical which increased significantly the computing time. The model was also able to correctly predict a water surface profile that is out of phase with the bed form surface. The MIKE 3 predicted hydraulic grade line showed an unreasonably high water surface slope and Manning's n as shown in Table 4.5. Different turbulence models were tested in MIKE 3 but the k-ε turbulence model in the vertical and the Smagorinsky in the horizontal direction produced the most stable results and therefore only these results are presented here.

The non-hydrostatic H3D model reproduced the flow separation phenomenon at the downstream side of the bed form crest but the relative turbulence intensity was higher than expected. Two eddy zones occurred in the wake side of the bed form extending the separation zone along the whole lee and the slope side of the bed form. The out of phase relationship between the water surface profile and the bed form surface was not as evident as in the MIKE 3 and ECOMSED simulations.

The slope of the simulated free water surface profile in H3D was close to the slope of ECOMSED and much less than MIKE 3; the resulting Manning's n values are shown in

Table 4.5. The imposition of a constant velocity in H3D is thought to have increased the upstream shear stress relative to ECOMSED and MIKE 3.

As mentioned before, H3D had the option to use a variable vertical grid cells, but 40 levels with constant spacing were used in H3D to be consistent with the vertical grid used in MIKE 3. H3D time step (0.01 sec) was larger than ECOMSED (0.005 sec) and MIKE 3 (0.005 sec).

	Mean velocity (m/s)	**Hydraulic Radius ~ Average depth (m)**	**Average Energy Slope**	**Simulated Manning's n**
Hydrostatic ECOMSED	0.75	8.5	0.00005	0.039
Non-Hydrostatic MIKE 3	0.75	8.5	0.00008	0.049
Non-Hydrostatic H3D	0.75	8.5	0.00003	0.030

Table 4.5: Models' simulated equivalent Manning's n

The magnitude of the out of phase relationship $\delta_{energy\text{-}12}$ in the large scale model between the water surface profile and the bed form surface was checked against the energy principle where $\delta_{12} = \frac{V_2^2}{2g} - \frac{V_1^2}{2g}$, where V_1 and V_2 are the average velocities at point 1 and 2 respectively as shown in Figure 4.16.

$\delta_{energy\text{-}ECOMSED} = \frac{V_2^2}{2g} - \frac{V_1^2}{2g} = 0.0011\text{m} = 1.1 \text{ mm},$

$\delta_{simulated\text{-}ECOMSED} = 0.0024\text{m} = 2.40 \text{ mm},$

$\delta_{energy\text{-}H3D} = \frac{V_2^2}{2g} - \frac{V_1^2}{2g} = 0.00089\text{m} = 0.891 \text{ mm},$

$\delta_{simulated\text{-}H3D} = .0015\text{m} = 1.5 \text{ mm}.$

$\delta_{energy\text{-}MIKE3} = \frac{V_2^2}{2g} - \frac{V_1^2}{2g} = 0.0029\text{m} = 2.95 \text{ mm},$

$\delta_{simulated\text{-}MIKE3} = 0.00358\text{m} = 3.58 \text{ mm}.$

where $\delta_{simulated\text{-}model}$ is the simulated water level difference between point 1 and 2 and $\delta_{energy\text{-}model}$ is the water level difference resulting from applying the energy principal at point 1 and 2. The results above show that $\delta_{simulated\text{-}H3D}$ was the lowest of the three models. The reason for this is attributed to a stair-stepping effect resulting from H3D application of the volume of fluid method at the lower most computational cell and the over-estimation of the leeside wake. This point is discussed more in Chapter Six.

CHAPTER 5
APPLICATIONS AND CORRELATIONS

In this portion of the study, a new procedure is developed to aid in the calibration of numerical riverine models. This process should provide a better representation of flow resistance in hydrodynamic and sediment transport modeling codes. This Chapter addresses ***Hypothesis Three*** which assumes that the hydrodynamic resistance in numerical models is a function of the scale of the observed bed forms relative to the spatial resolution of the model.

5.1. STUDY SITE

RM 223 in the Lower Mississippi River near Baton Rouge, LA was selected as the study site; this location was selected since the bed forms observed through the multibeam bathymetry data were well developed.

Figure 5.1 shows the location of the study site, while Figure 5.2 shows the surveyed bed form.

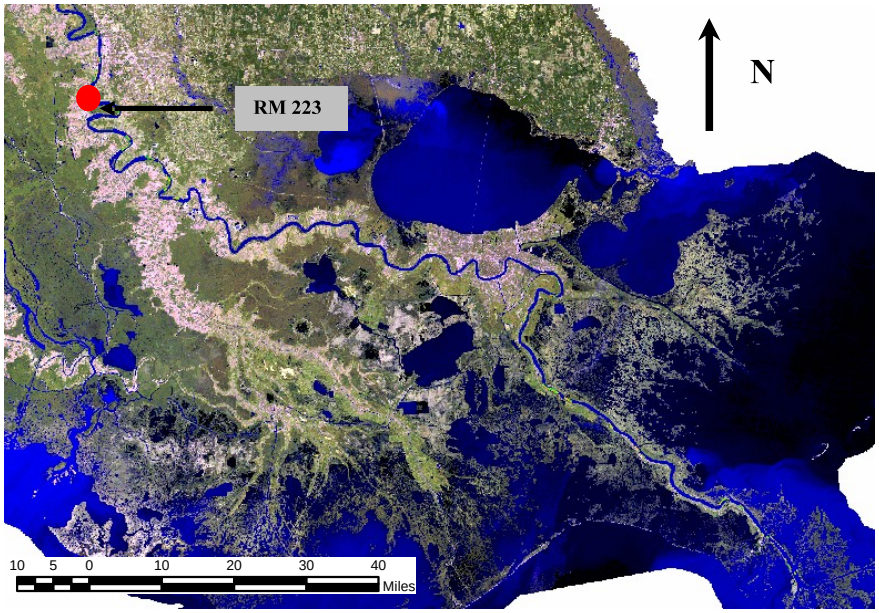

Figure 5.1: Location of RM 223 along the Lower Mississippi River near Baton Rouge, LA

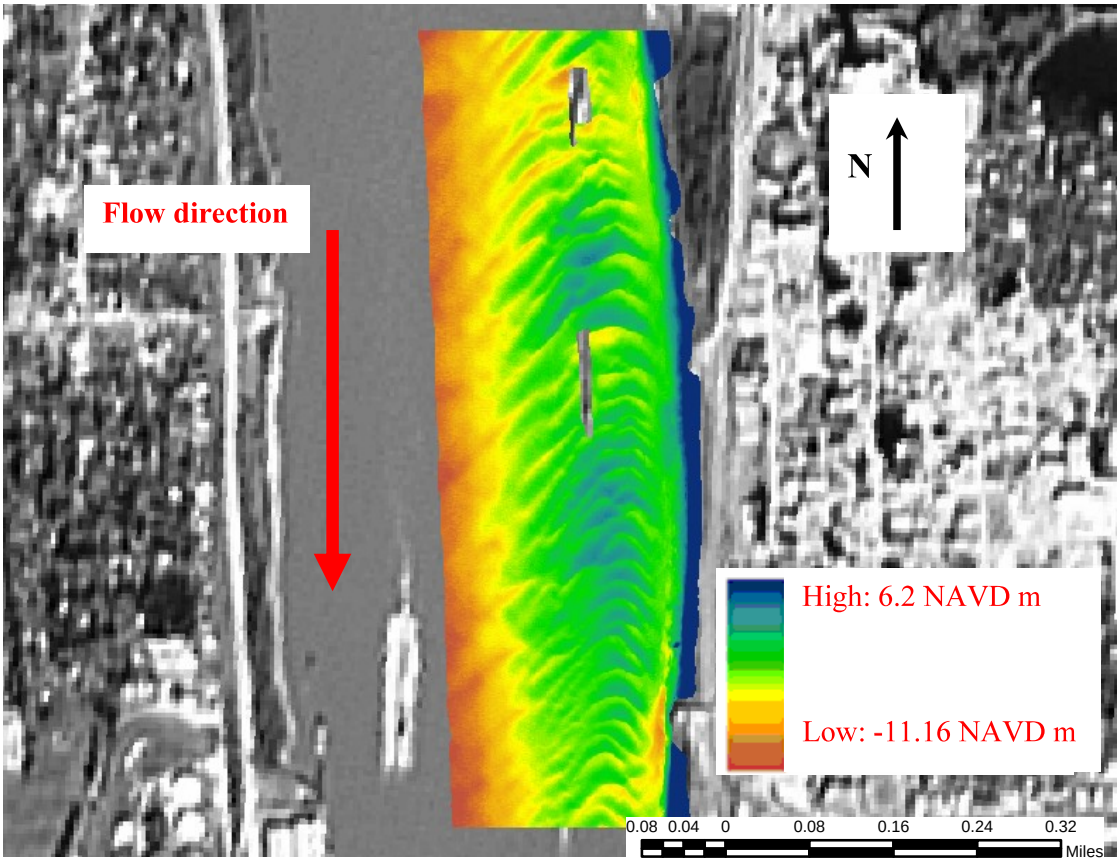

Figure 5.2: Plan view of multibeam dataset at RM 223 along the Lower Mississippi River near Baton Rouge, LA

The original survey data were referenced to the 1988 North American Vertical Datum (NAVD88) in survey feet, while the horizontal coordinate system was the 1983 North American coordinate system (NAD83), Louisiana South State Plan in survey feet. The data had a horizontal resolution of 2 feet and vertical resolution of 0.1 ft.

5.2 METHODOLOGY

The methodology utilized to create the calibration tool can be summarized as follows:

- Conversion of horizontal and vertical multibeam data into SI units (meters).
- Interpolation of the survey data with different sampling intervals (2m, 4m, 8m, 12m, 24m, 36m, 48m, 60m, 72m, 84m & 96m).

- Estimation of the observed bed form dimensions (Length, Height and Steepness) for the different sampling intervals.
- Correlation between the different sampling interval (Grid Spacing) and the observed bed form dimensions.
- Setup of a set of three dimensional simulations for the different grid sizes.
- Estimation of the simulated equivalent Manning's n for each grid size model
- Correlation between the equivalent Manning's n and the bed form dimensions and the grid spacing.

5.2.1. MULTIBEAM BATHYMETRY SURFACES

The horizontal and vertical survey data were converted into meters. These data were then interpolated using different sampling intervals (2m, 4m, 8m, 12m, 24m, 36m, 48m, 60m, 72m, 84m & 96m). Figures 5.3 through 5.13 show three dimensional views of the surfaces for the different grid spacings.

It is clear from Figures 5.3 to 5.13 that increasing the sampling interval greatly affects the observed bed form configurations. Several longitudinal profiles were then extracted from the resulting surfaces to better analyze the data. The extracted profiles are plotted in Figures 5.14 through 5.24.

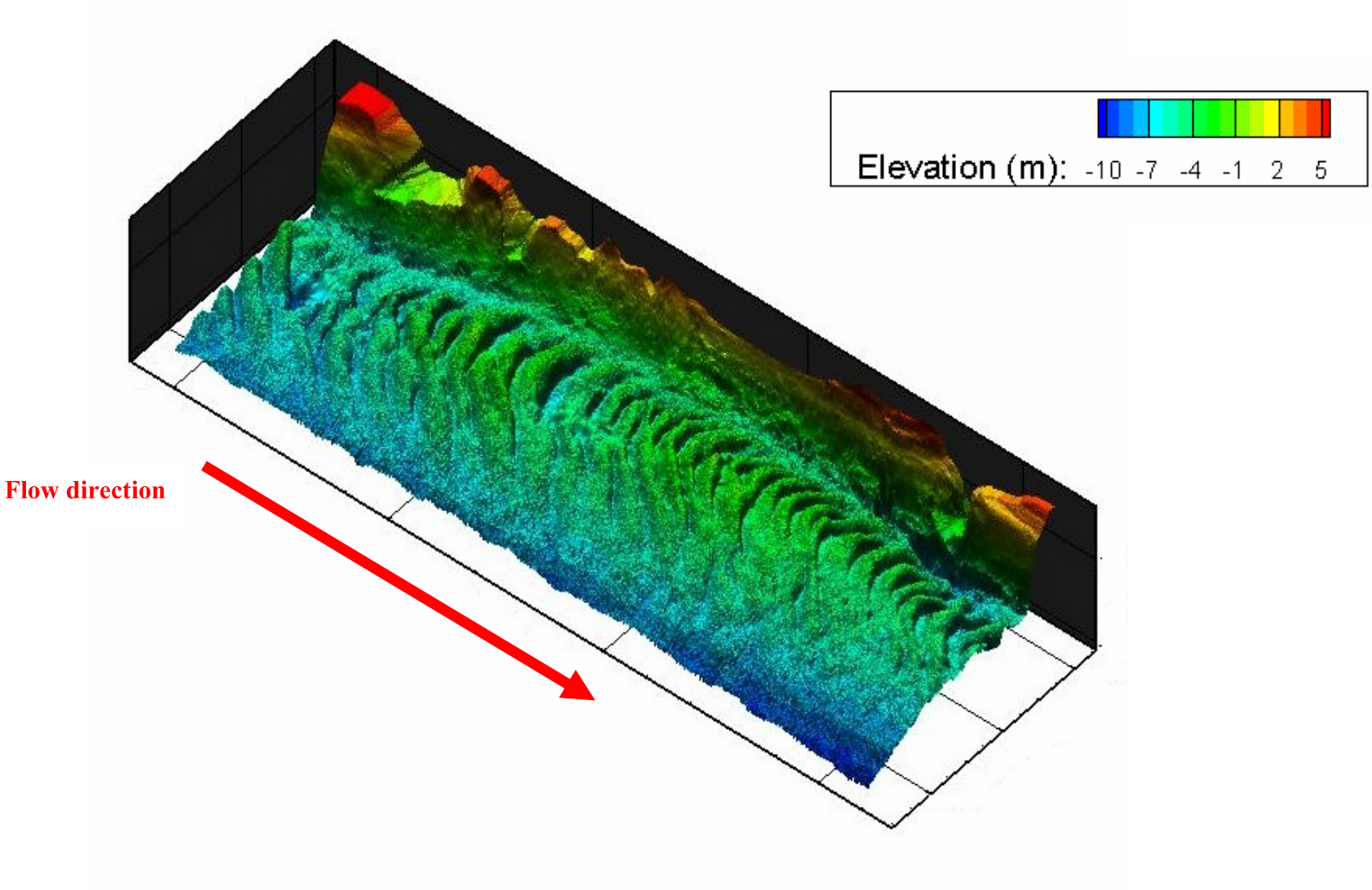

Figure 5.3: 2m sampling of multibeam dataset at RM 223 along the Lower Mississippi River near Baton Rouge, LA

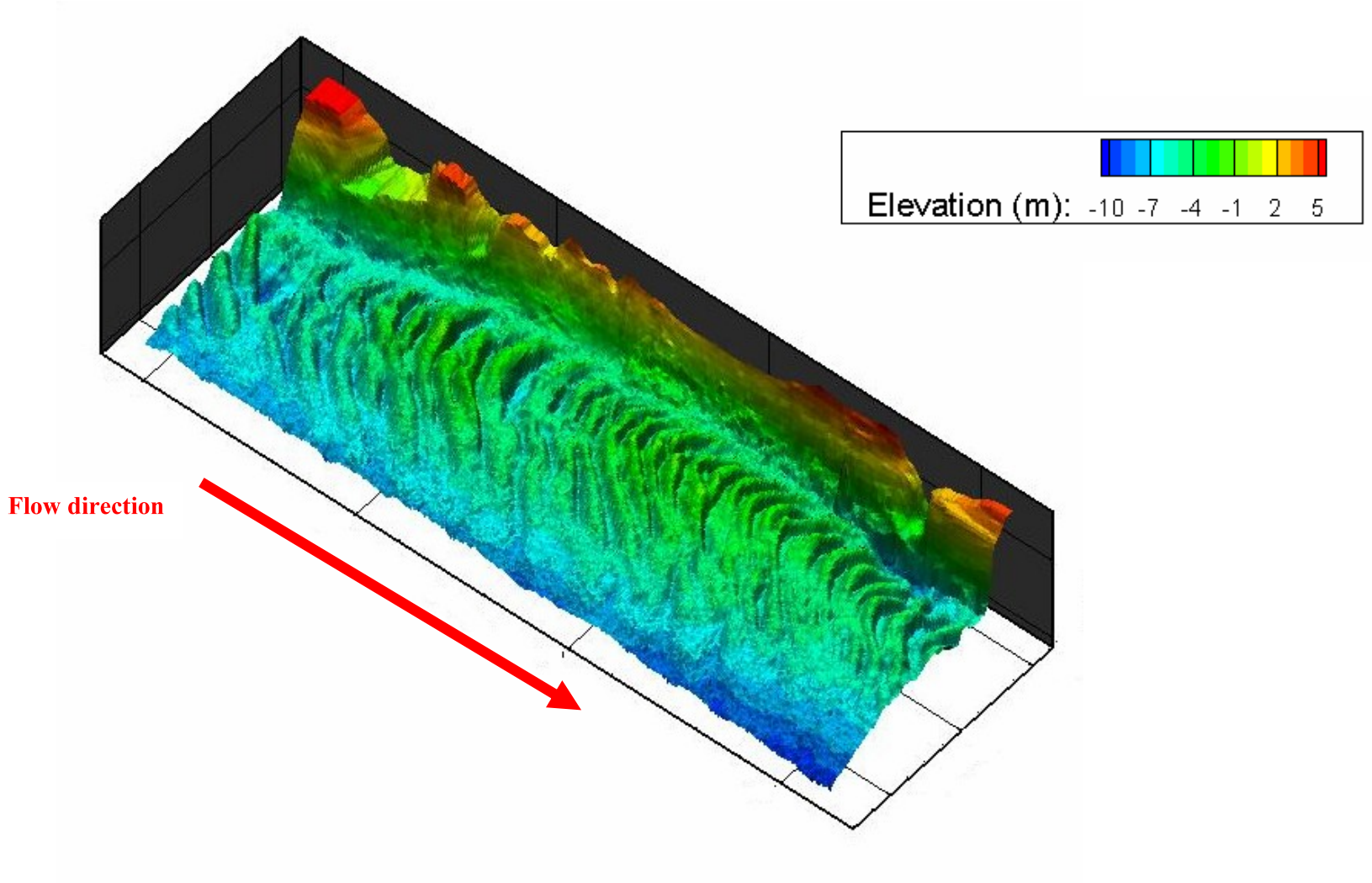

Figure 5.4: 4m sampling of multibeam dataset at RM 223 along the Lower Mississippi River near Baton Rouge, LA

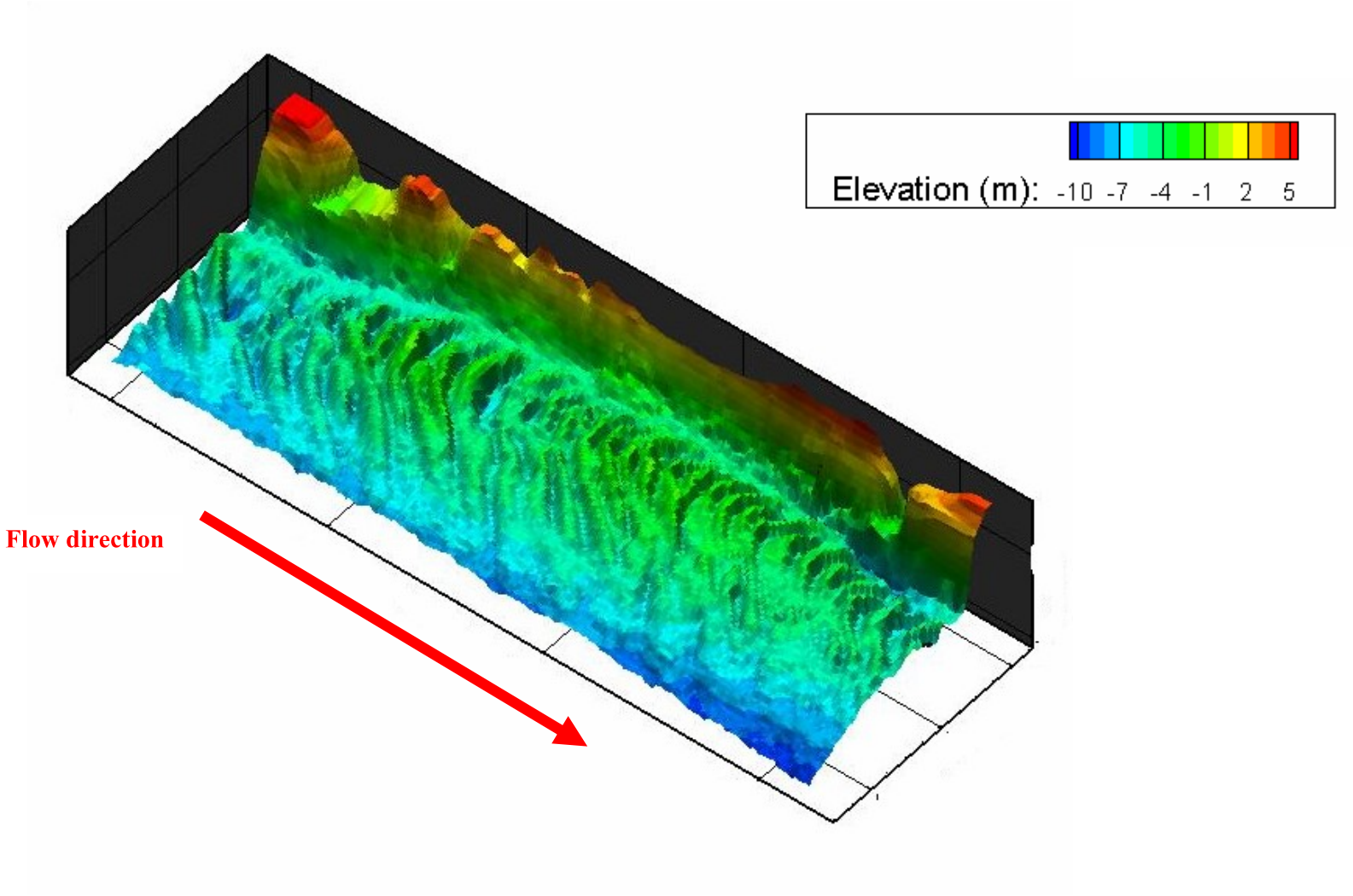

Figure 5.5: 8m sampling of multibeam dataset at RM 223 along the Lower Mississippi River near Baton Rouge, LA

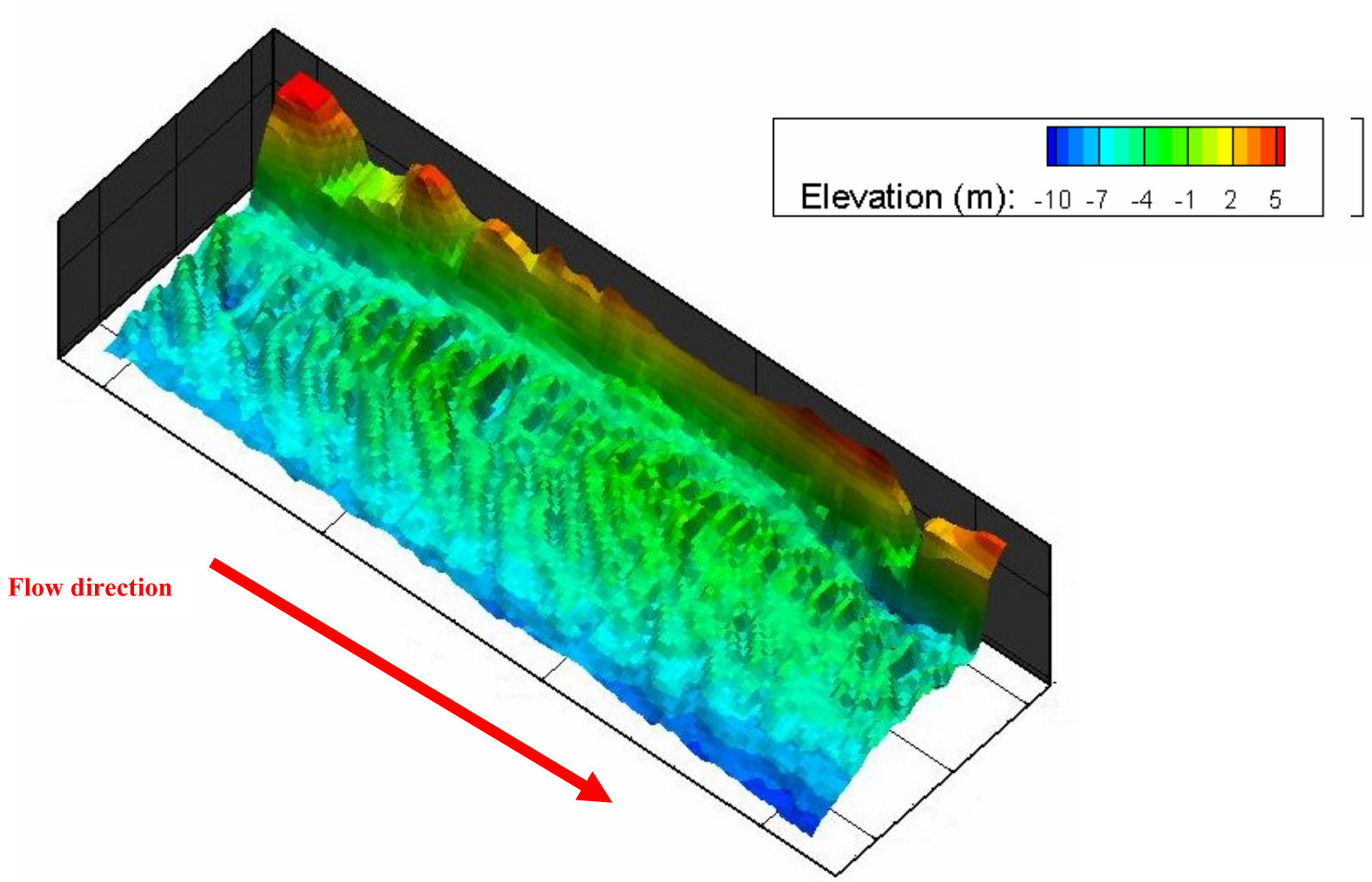

Figure 5.6: 12m sampling of multibeam dataset at RM 223 along the Lower Mississippi River near Baton Rouge, LA

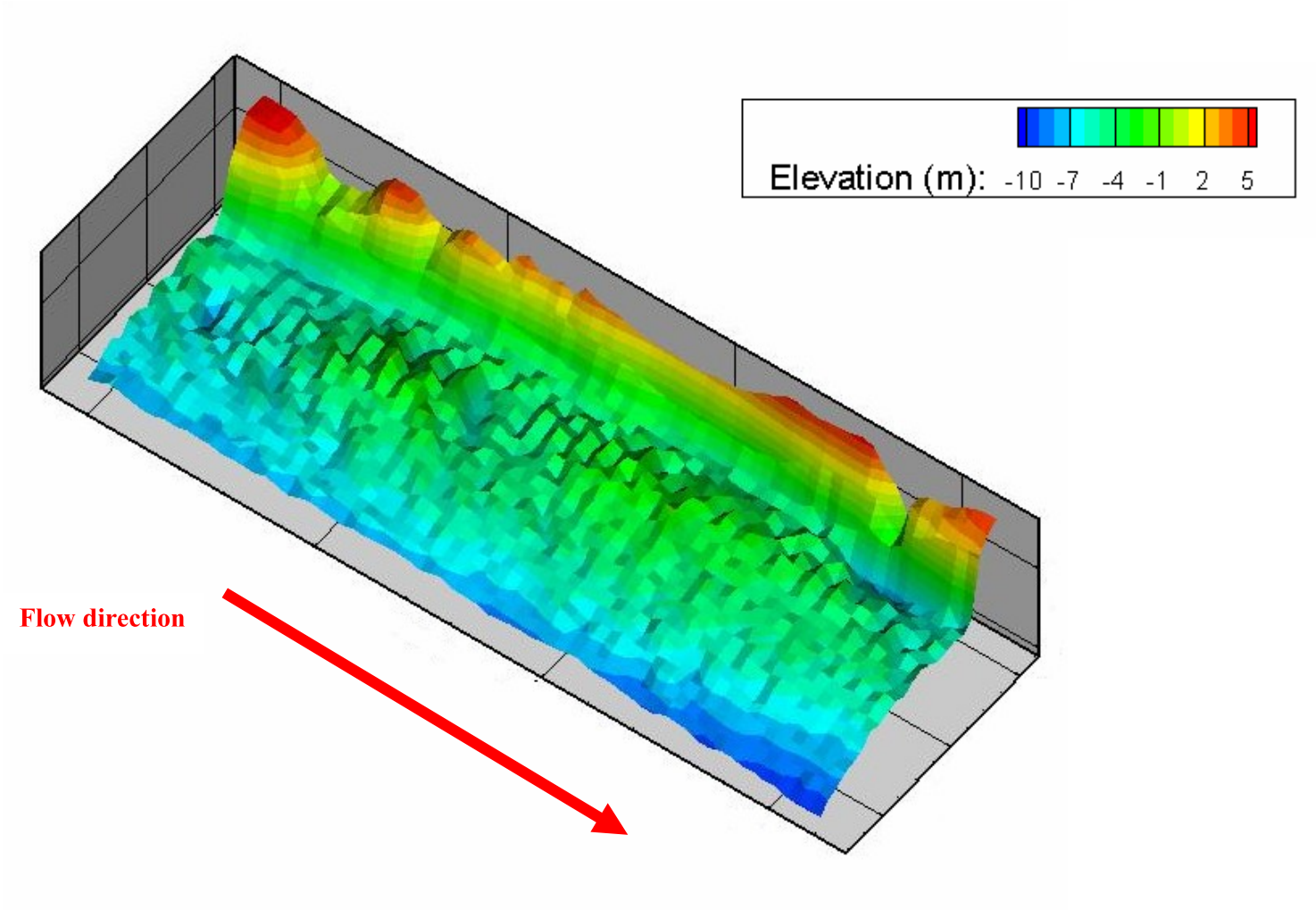

Figure 5.7: 24m sampling of multibeam dataset at RM 223 along the Lower Mississippi River near Baton Rouge, LA

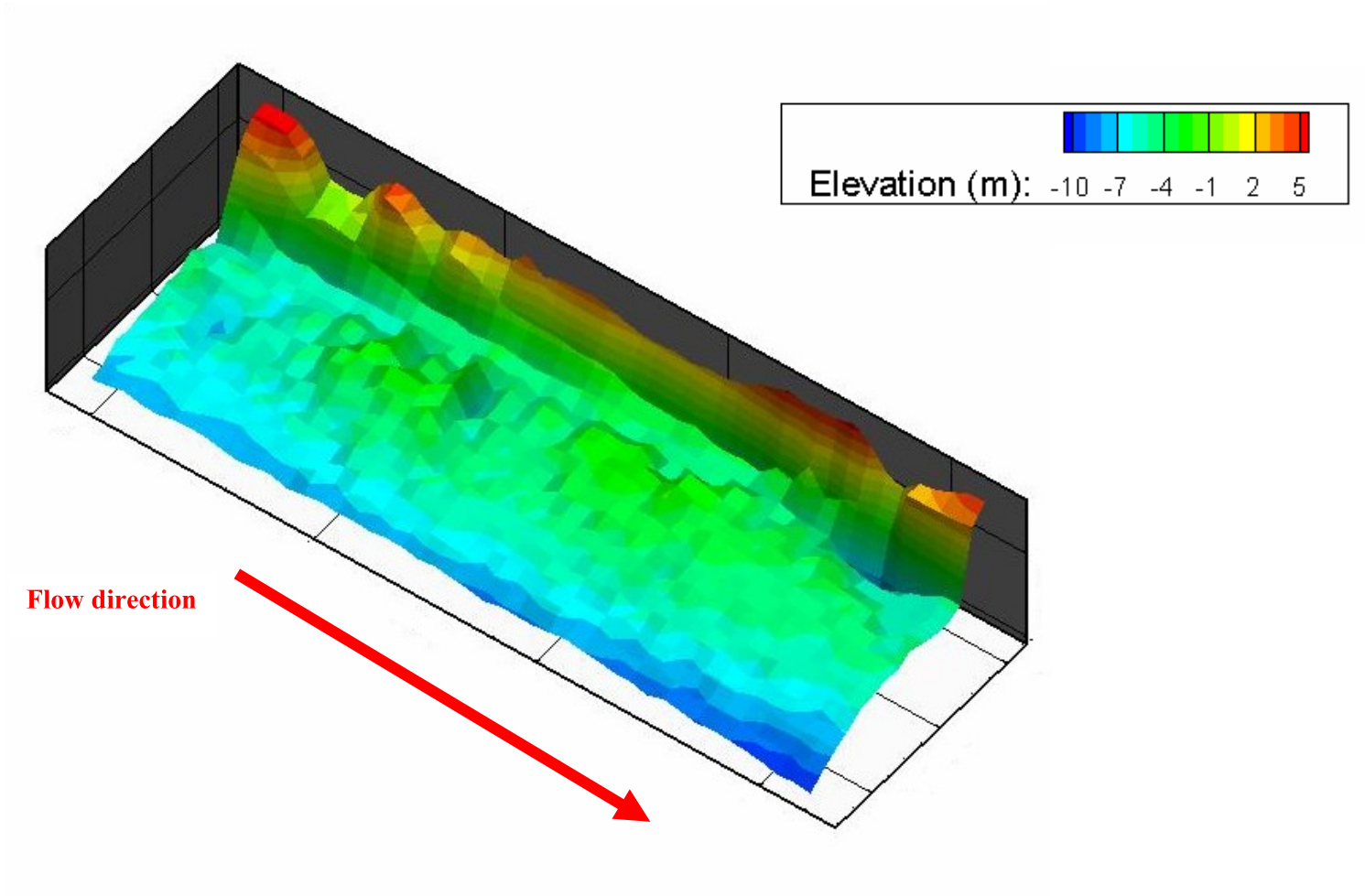

Figure 5.8: 36m sampling of multibeam dataset at RM 223 along the Lower Mississippi River near Baton Rouge, LA

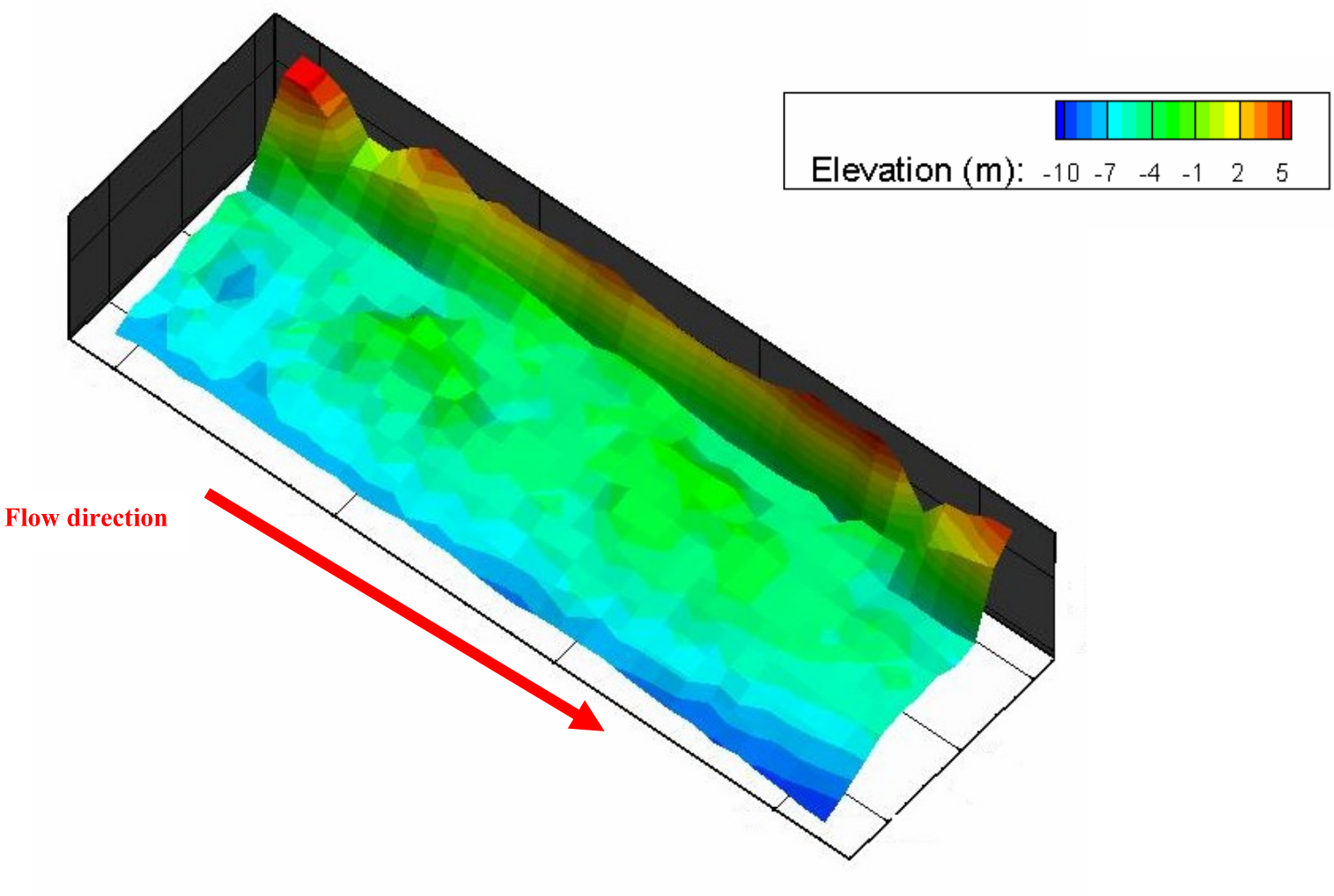

Figure 5.9: 48m sampling of multibeam dataset at RM 223 along the Lower Mississippi River near Baton Rouge, LA

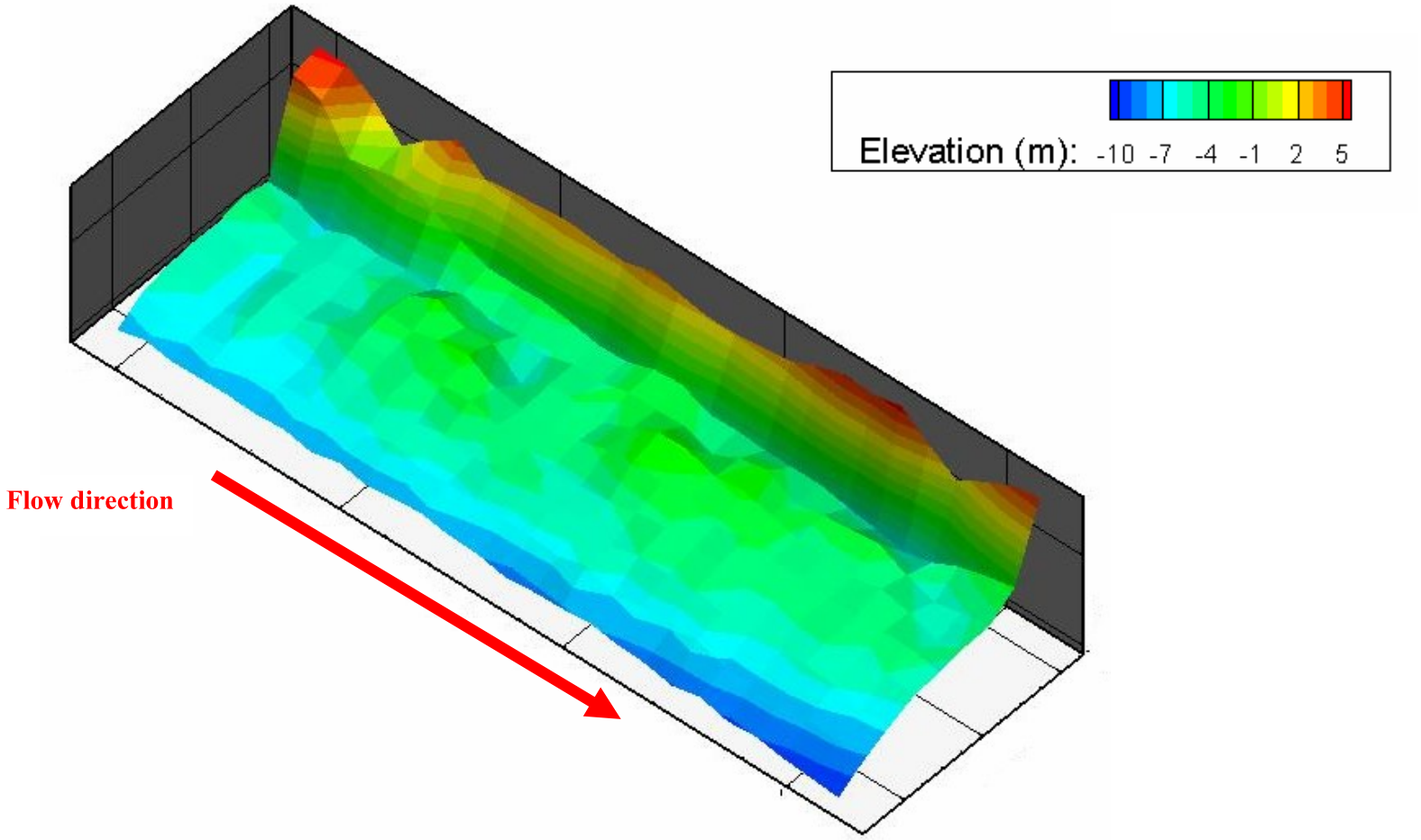

Figure 5.10: 60m sampling of multibeam dataset at RM 223 along the Lower Mississippi River near Baton Rouge, LA

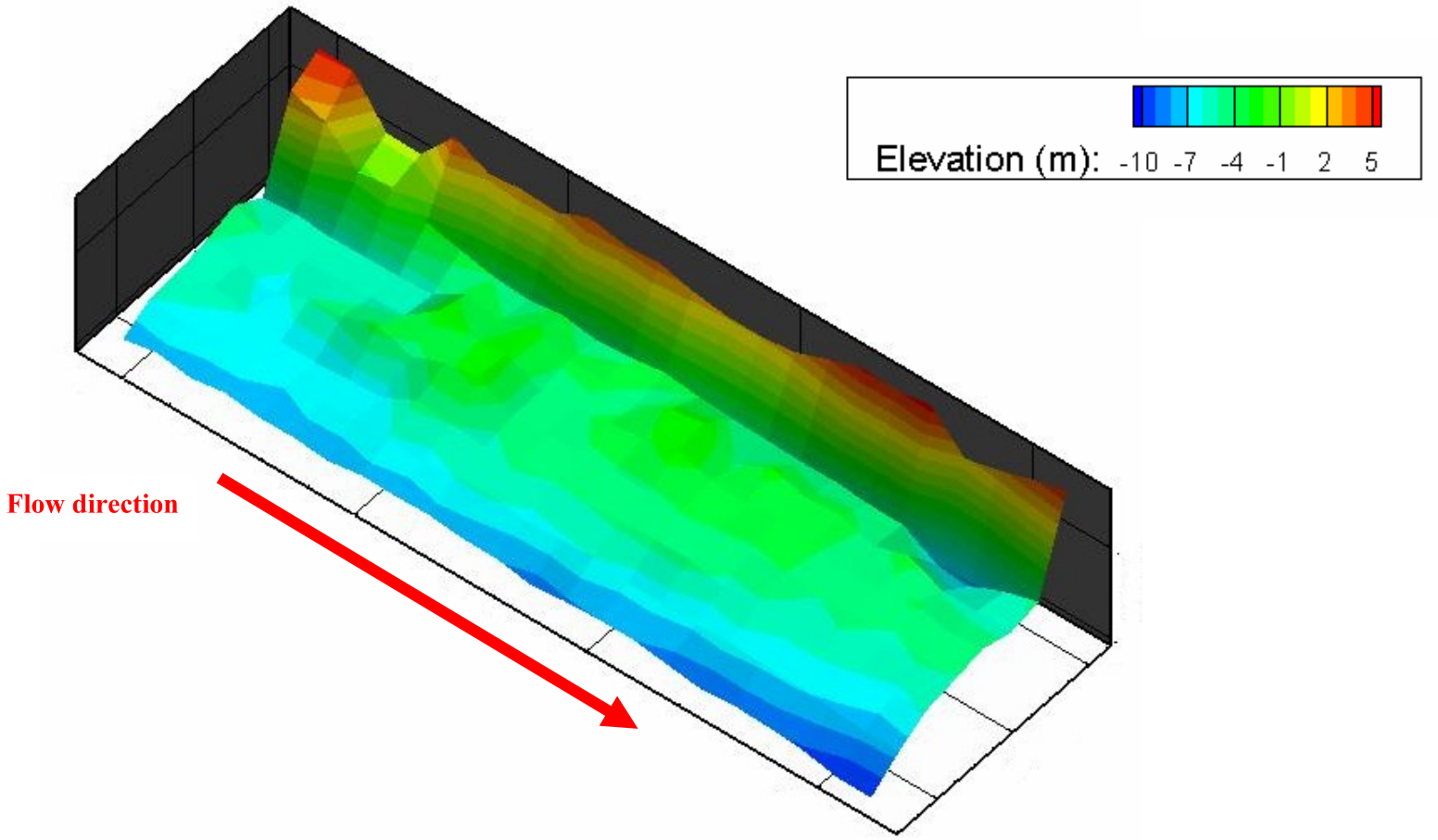

Figure 5.11: 72m sampling of multibeam dataset at RM 223 along the Lower Mississippi River near Baton Rouge, LA

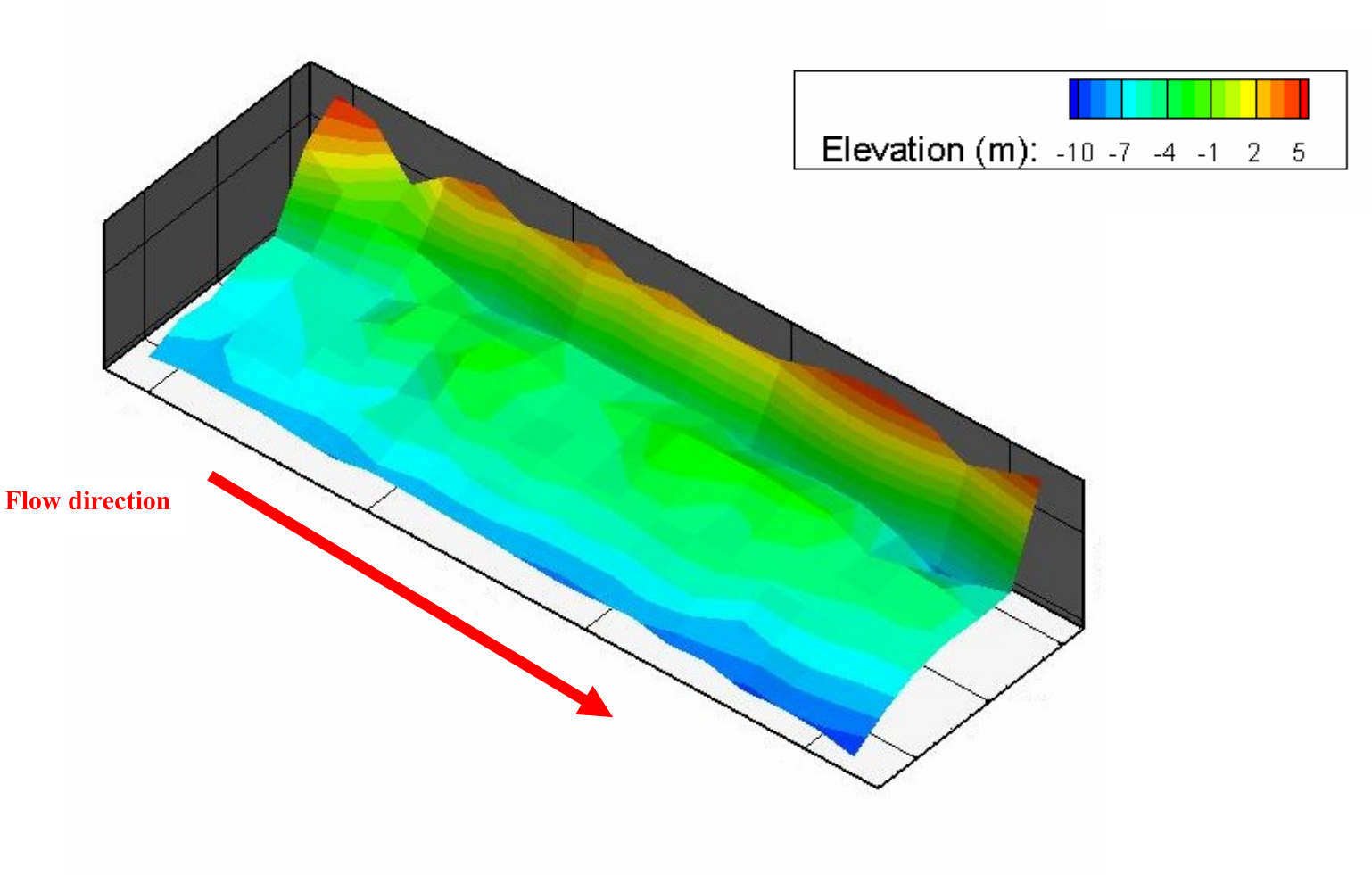

Figure 5.12: 84m sampling of multibeam dataset at RM 223 along the Lower Mississippi River near Baton Rouge, LA

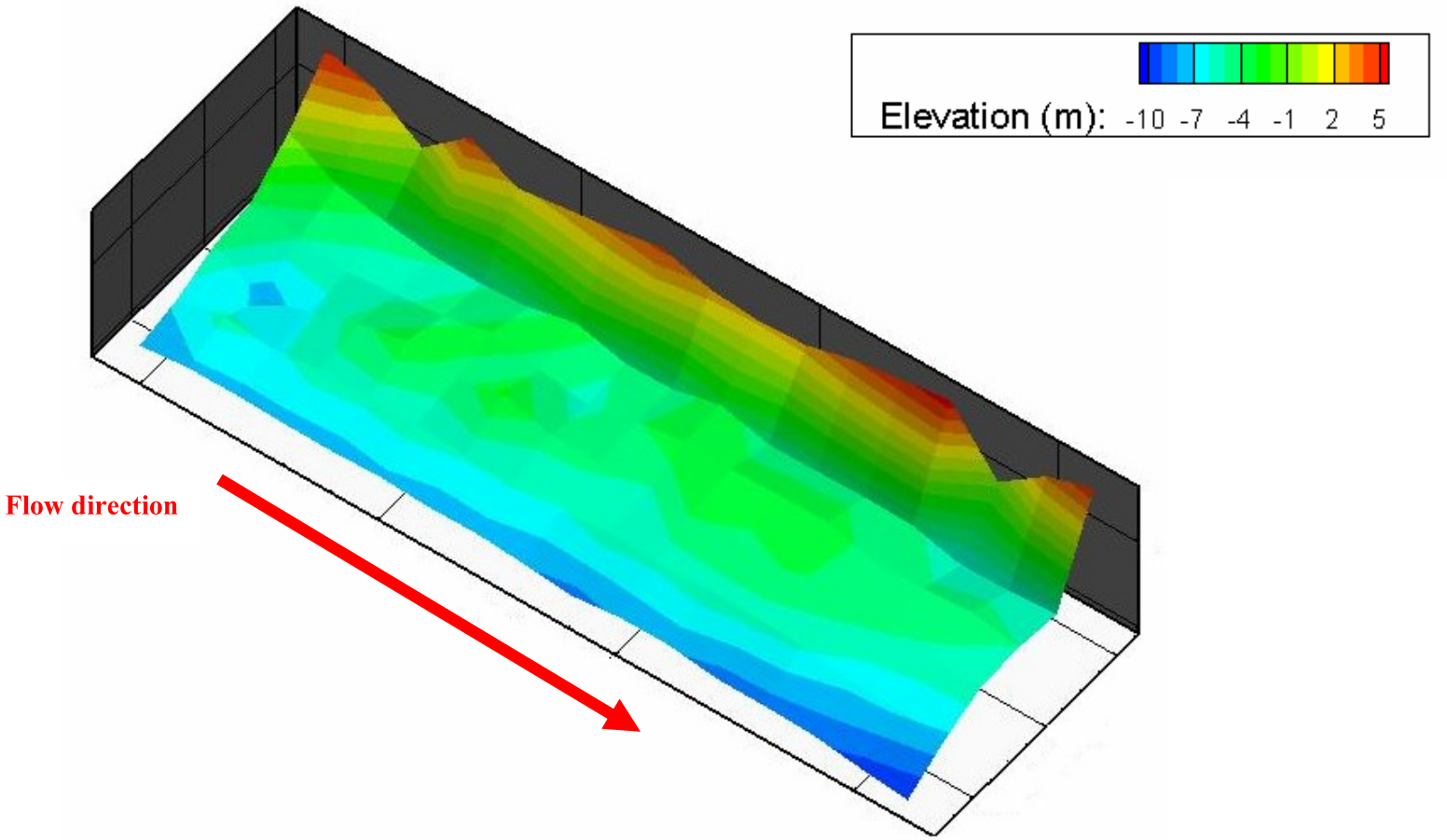

Figure 5.13: 96m sampling of multibeam dataset at RM 223 along the Lower Mississippi River near Baton Rouge, LA

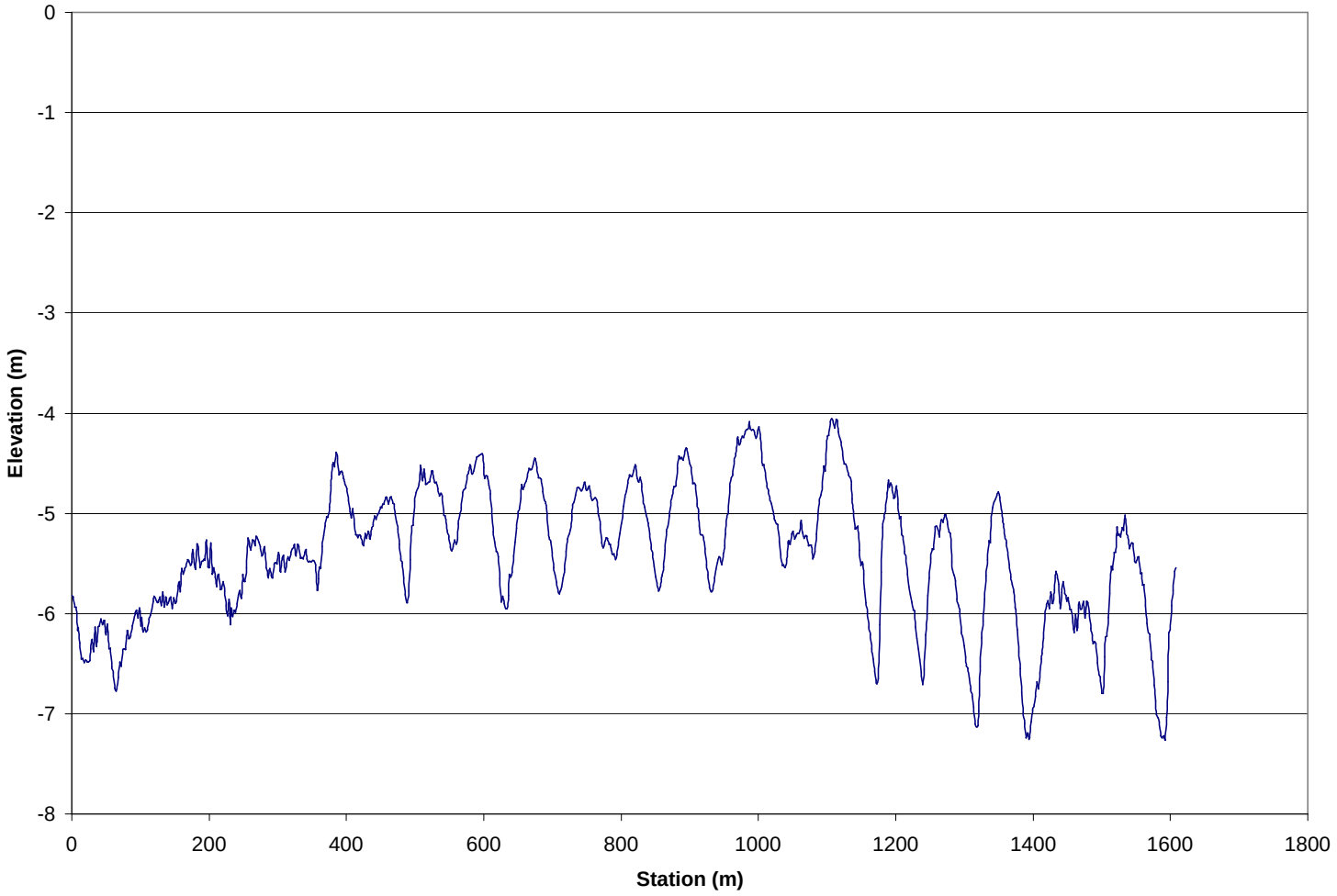

Figure 5.14: Longitudinal profile of the 2 m re-sampling of actual bed forms from the multibeam dataset at RM 223

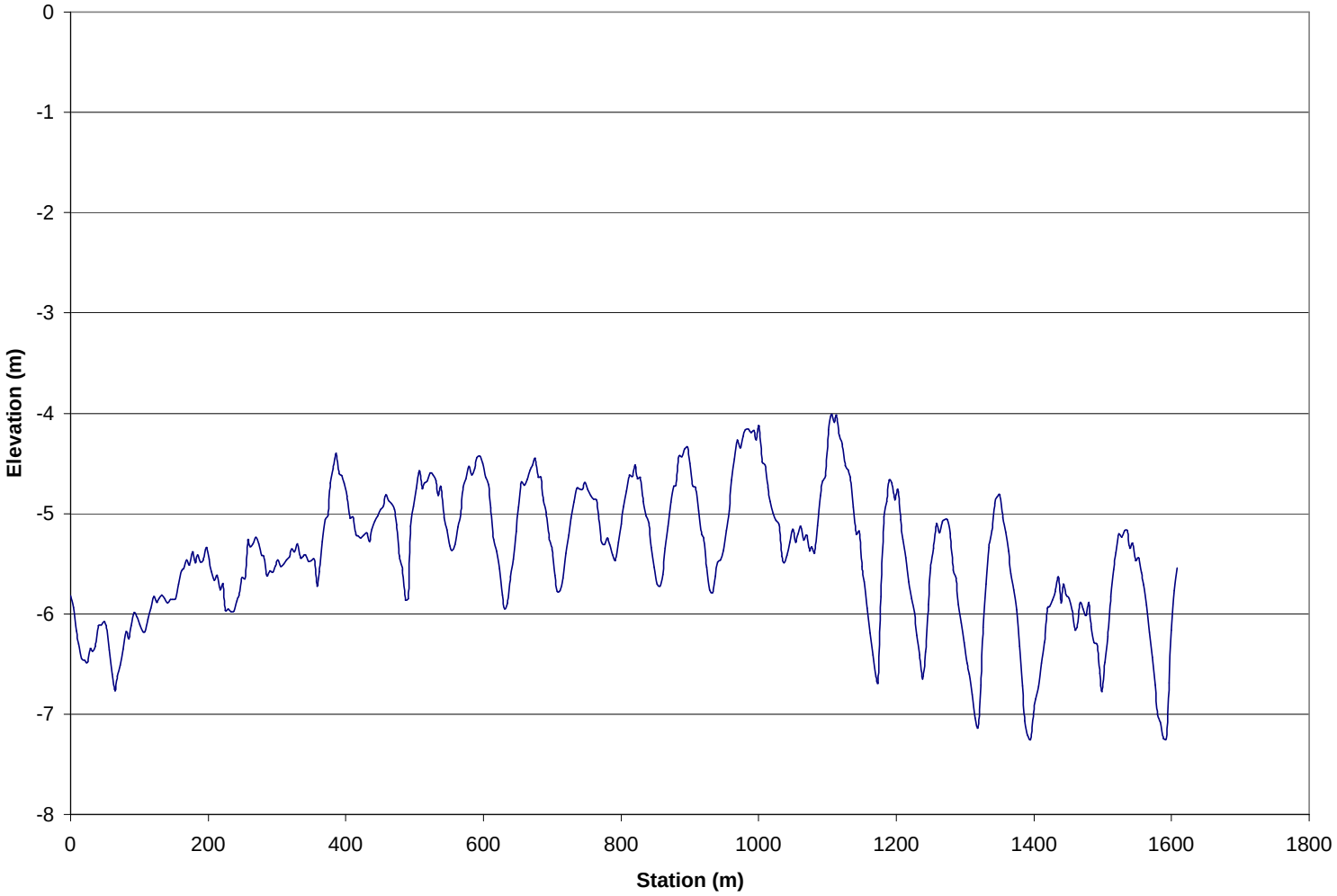

Figure 5.15: Longitudinal profile of the 4 m re-sampling of actual bed forms from the multibeam dataset at RM 223

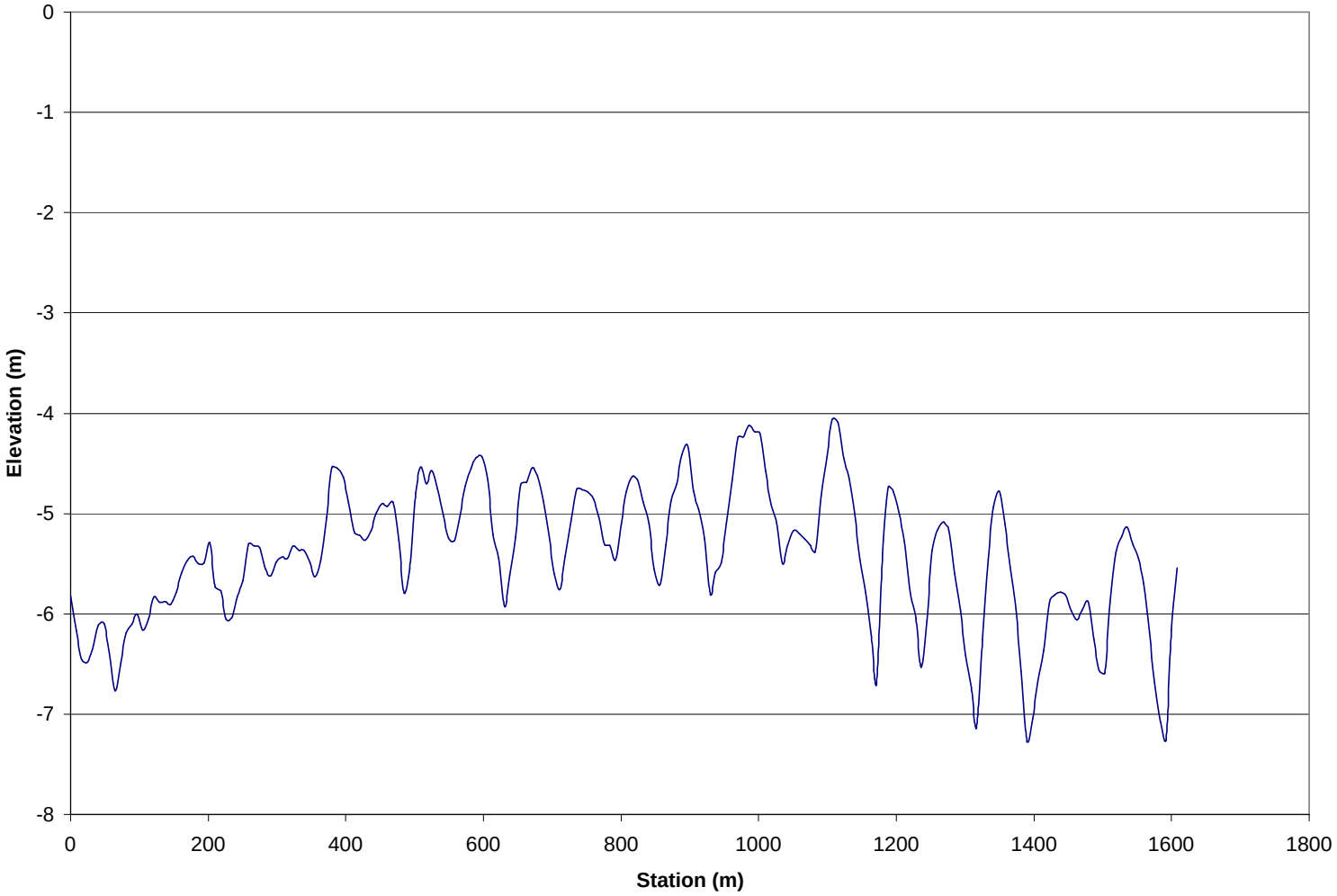

Figure 5.16: Longitudinal profile of the 8 m re-sampling of actual bed forms from the multibeam dataset at RM 223

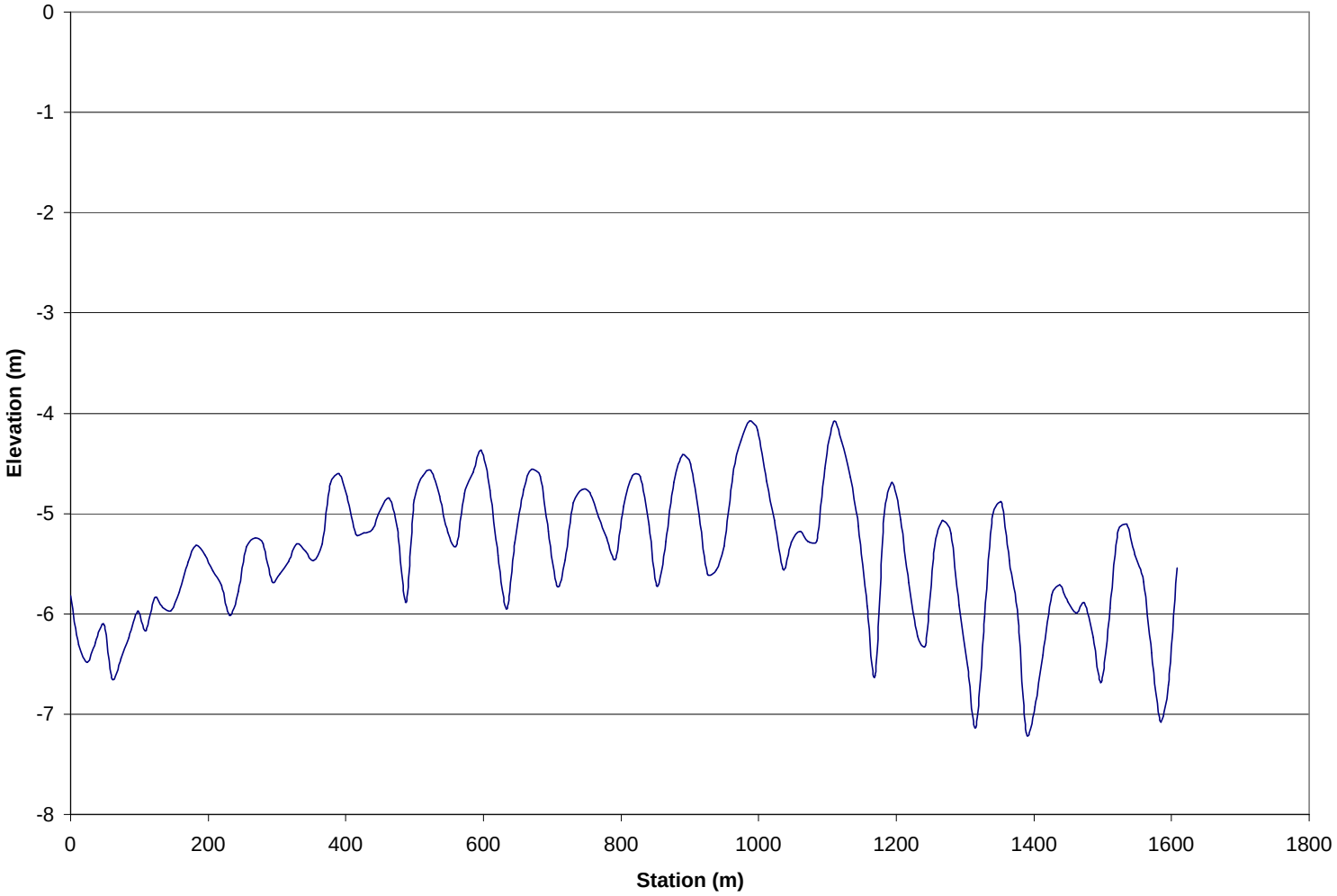

Figure 5.17: Longitudinal profile of the 12 m re-sampling of actual bed forms from the multibeam dataset at RM 223

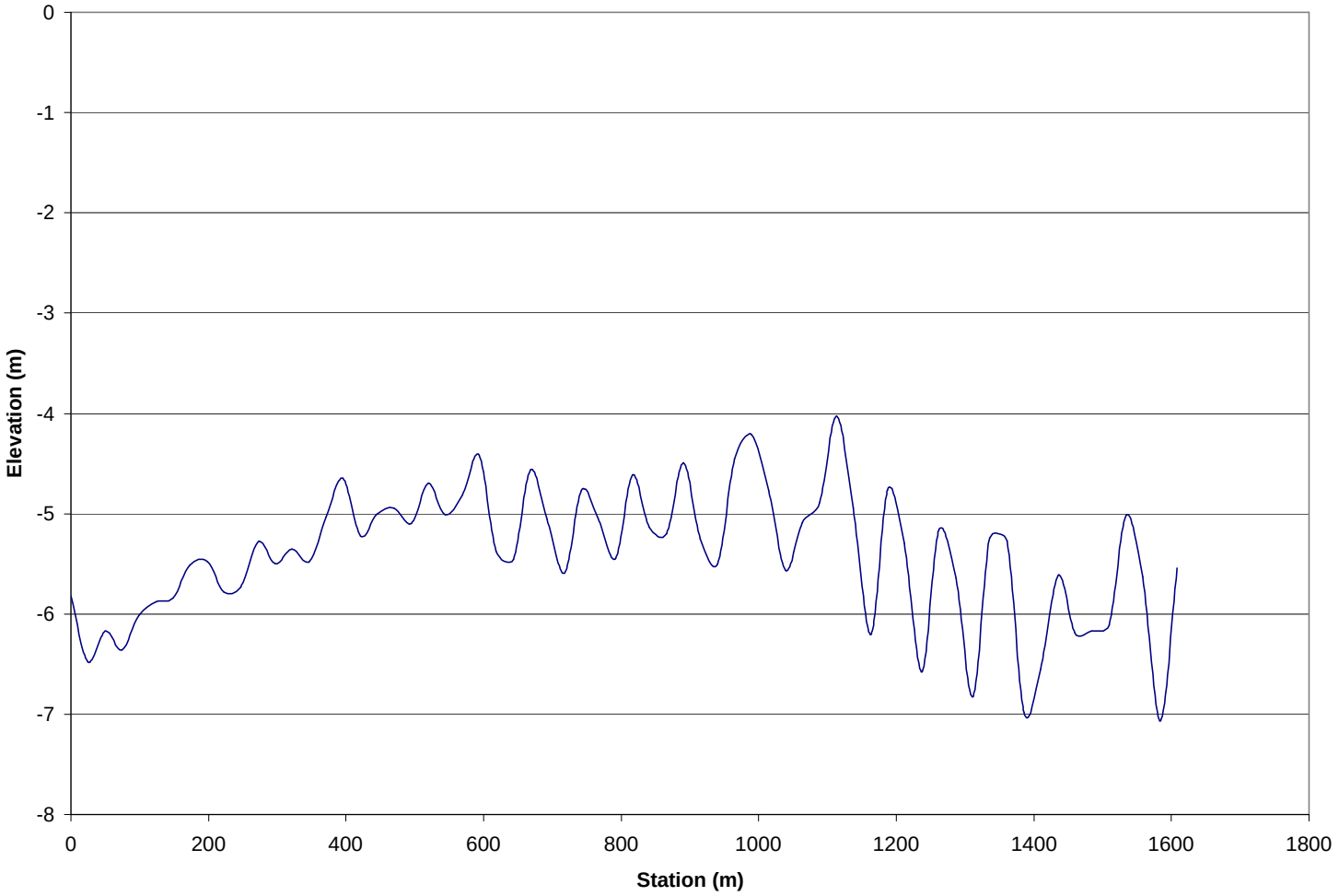

Figure 5.18: Longitudinal profile of the 24 m re-sampling of actual bed forms from the multibeam dataset at RM 223

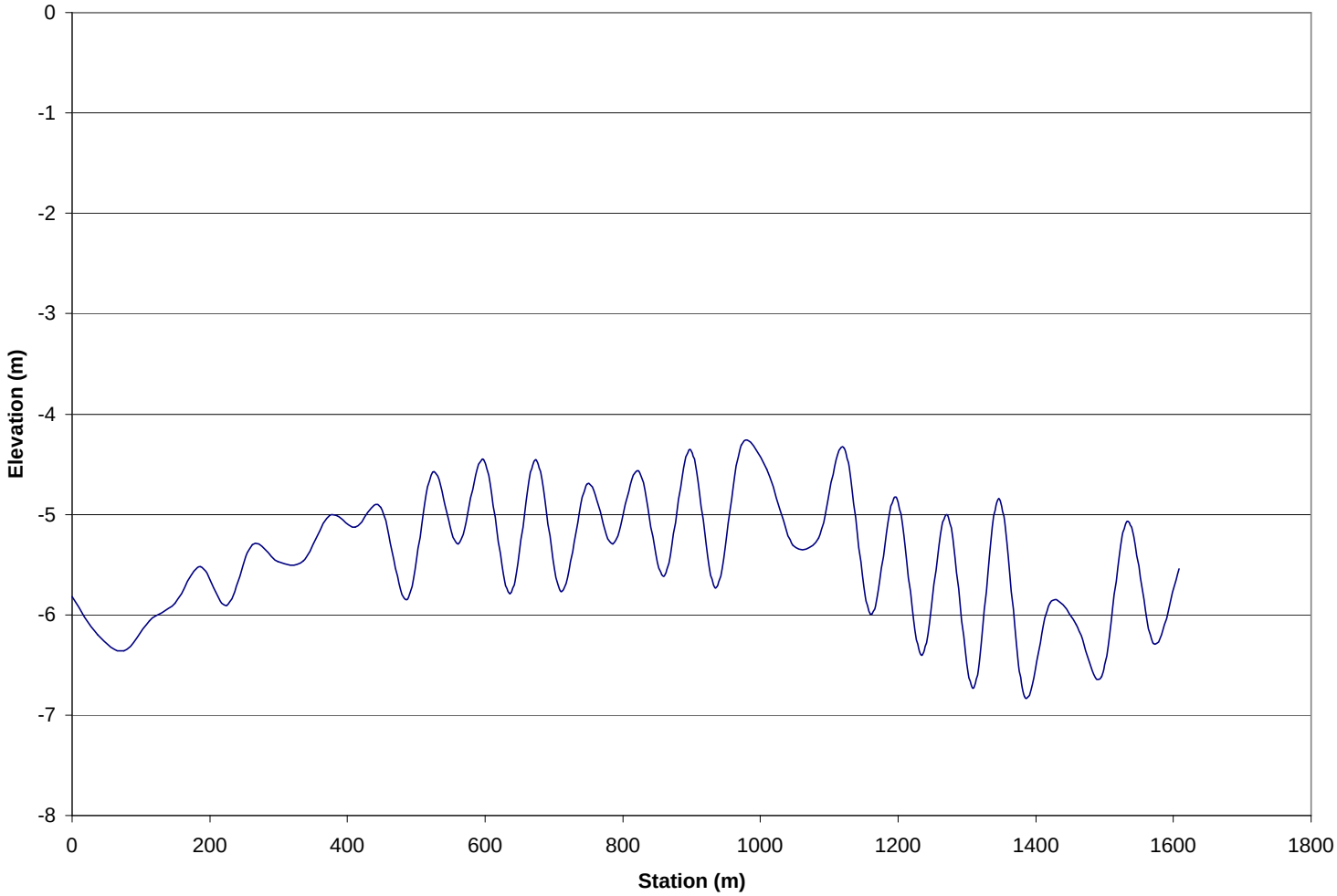

Figure 5.19: Longitudinal profile of the 36 m re-sampling of actual bed forms from the multibeam dataset at RM 223

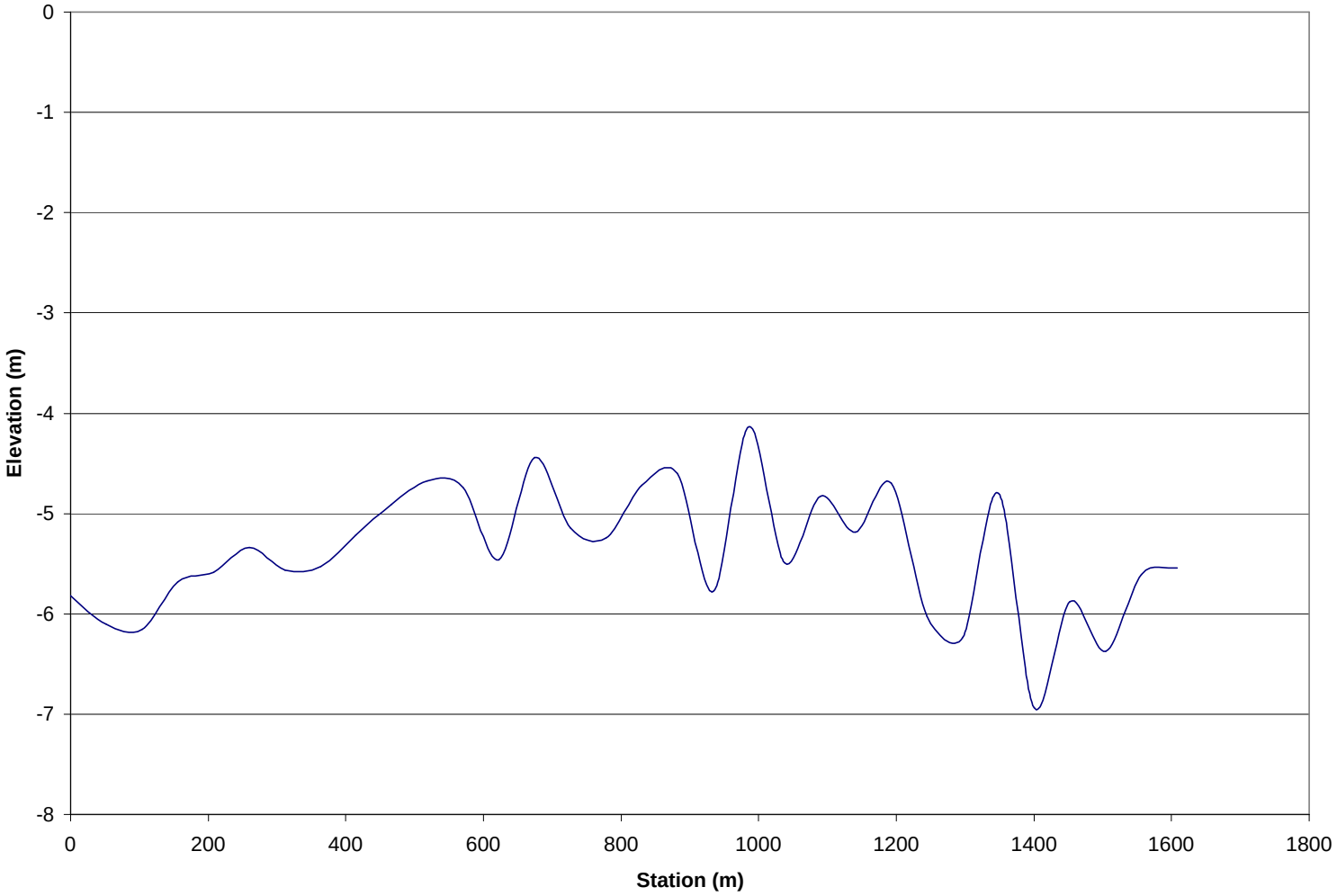

Figure 5.20: Longitudinal profile of the 48 m re-sampling of actual bed forms from the multibeam dataset at RM 223

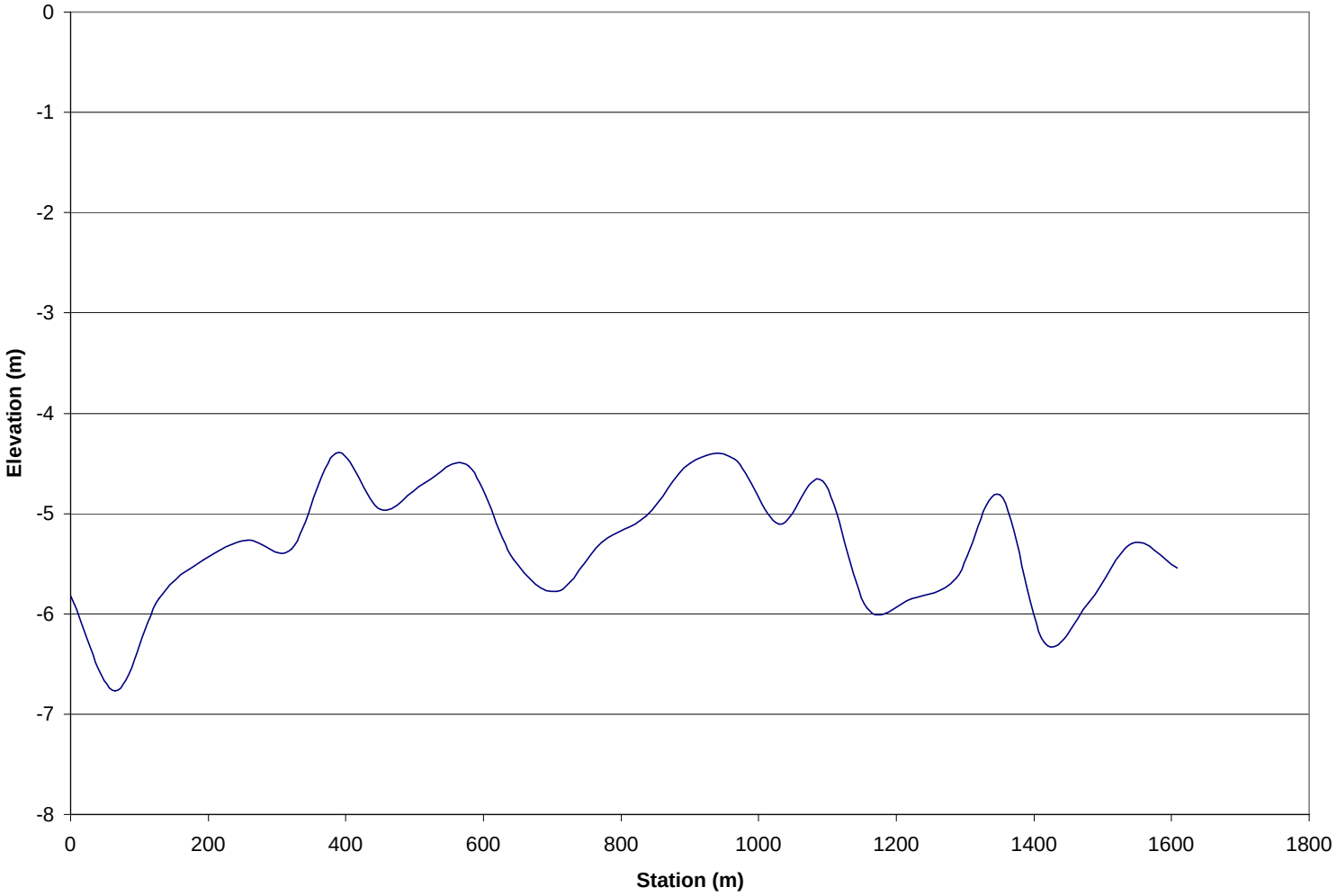

Figure 5.21: Longitudinal profile of the 60 m re-sampling of actual bed forms from the multibeam dataset at RM 223

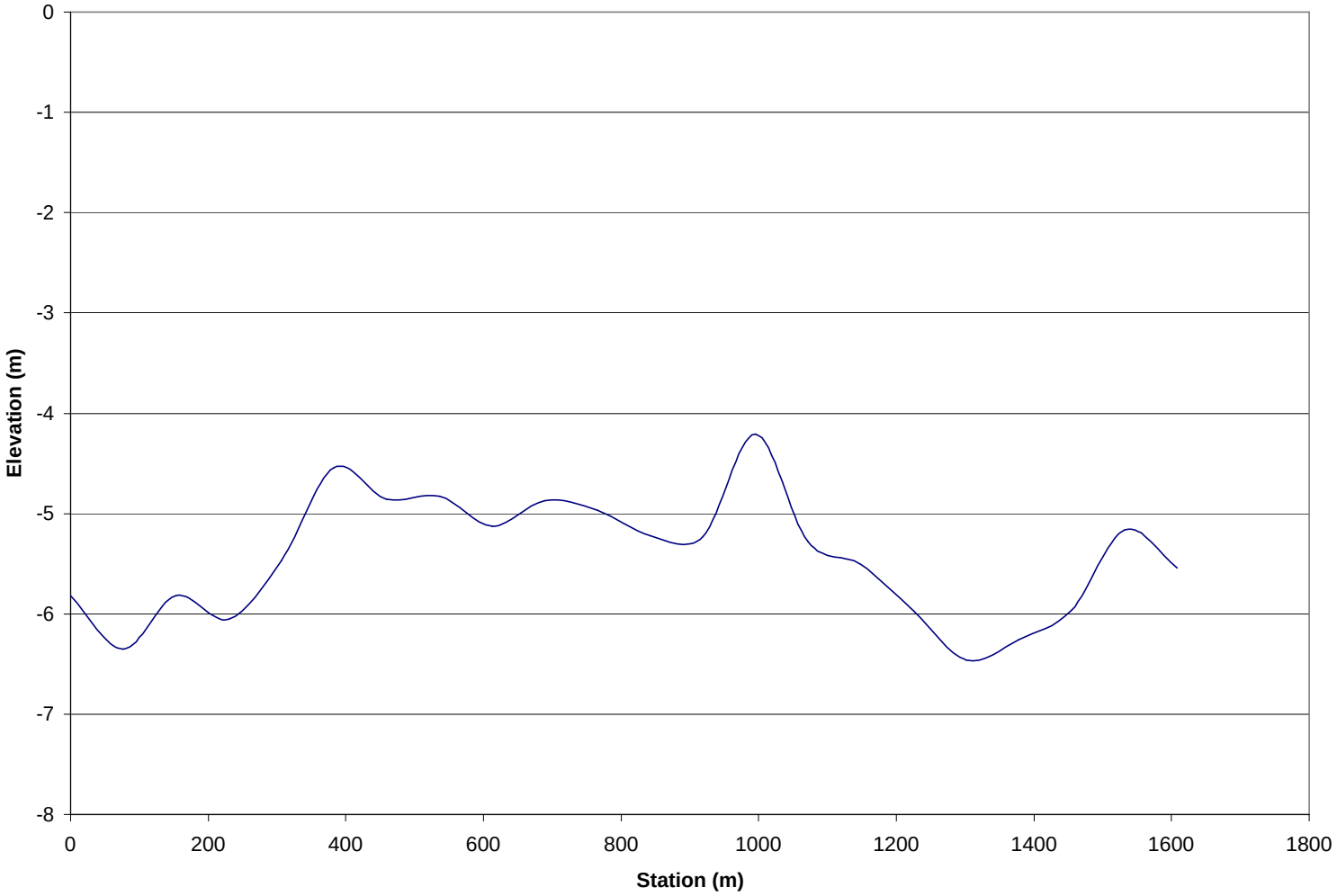

Figure 5.22: Longitudinal profile of the 72 m re-sampling of actual bed forms from the multibeam dataset at RM 223

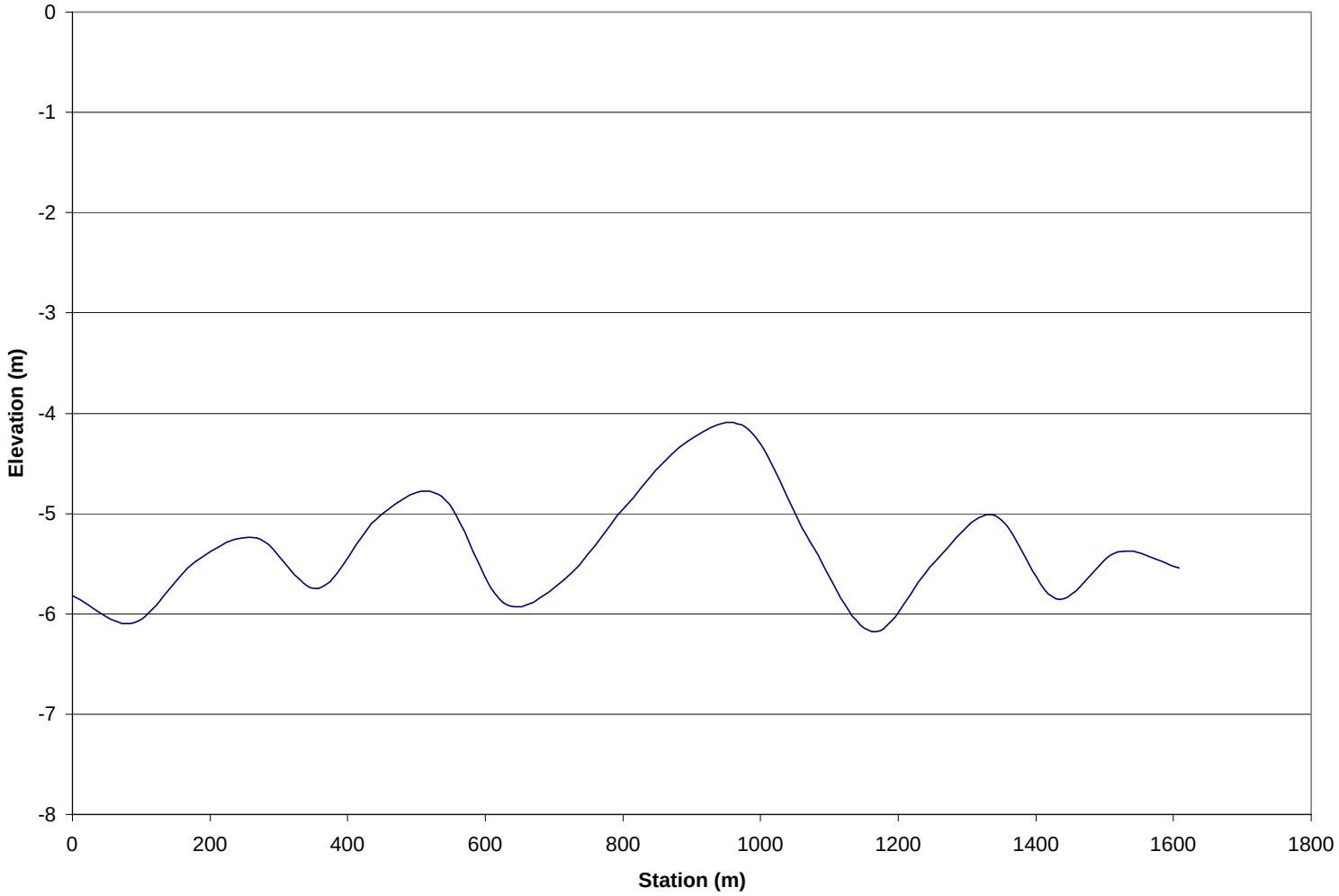

Figure 5.23: Longitudinal profile of the 84 m re-sampling of actual bed forms from the multibeam dataset at RM 223

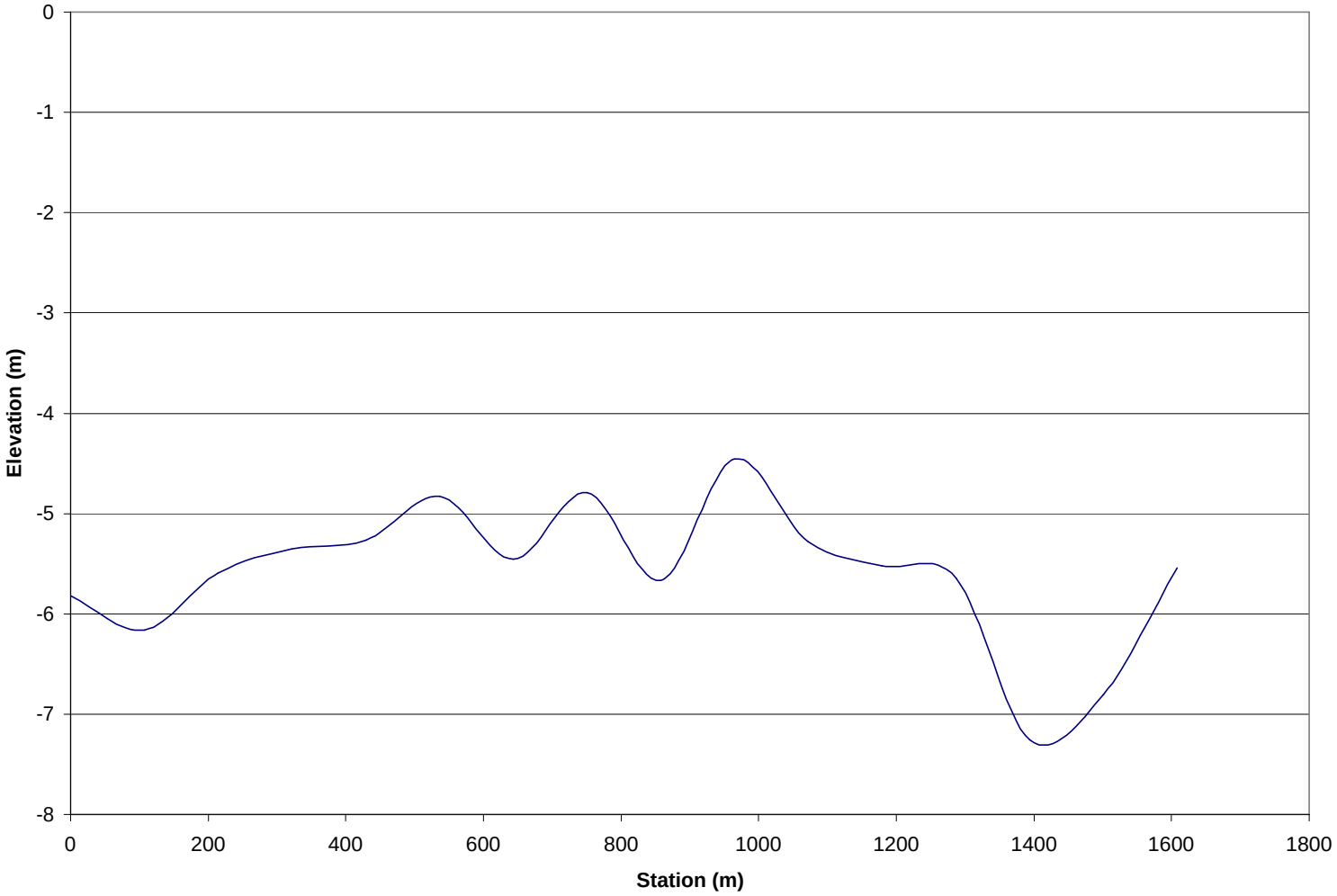

Figure 5.24: Longitudinal profile of the 96 m re-sampling of actual bed forms from the multibeam dataset at RM 223

The extracted profiles clearly show the effect of increasing the grid spacing on the observed bed form configurations. A trend was observed where the bed form length increased by increasing the grid spacing accompanied by a decrease in the bed form height. Also, the extracted profiles showed that not only the bed form dimensions differed by varying the grid spacing, but also the number of observed bed forms decreased by increasing the grid spacing. This resulted in totally different bed form fields (artificial bed forms) for the greater grid spacing dimensions than the one which was originally present. These artificial bed form fields would then contribute to the resistance to the flow to a different extent than the original bed form. Thus different grid resolutions contribute to different flow-resistance environments. The bed form dimensions (height, length and steepness) were estimated for the different grid dimensions as shown in Table 5.1

Grid Spacing (m)	Bed Form Height (m)	Bed Form Length (m)	Steepness
2	1.30	72.00	0.0180556
4	0.80	77.00	0.0103896
8	0.68	81.00	0.0083951
12	0.56	84.00	0.0066667
24	0.96	122.00	0.0078689
36	0.46	73.00	0.0063014
48	0.29	100.00	0.0029000
60	0.90	186.00	0.0048387
72	0.60	219.00	0.0027397
84	0.54	254.00	0.0021260
96	0.30	302.00	0.0009934

Table 5.1 Estimated bed form dimensions for the different grid spacings

Figure 5.29 through 5.31 show correlations between the estimated bed form dimensions and the corresponding grid spacing.

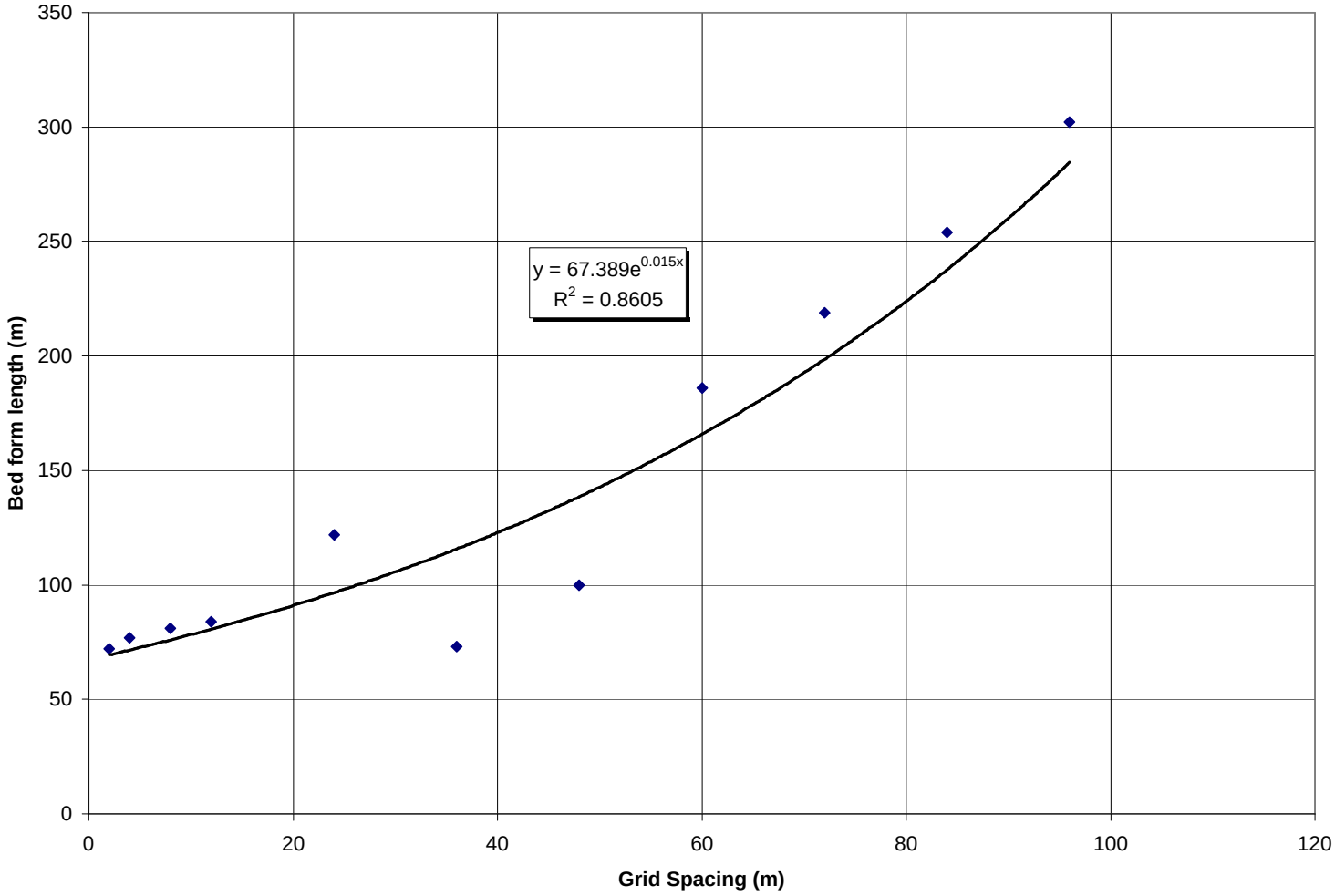

Figure 5.29: Correlation between grid spacing (m) and bed form length (m)

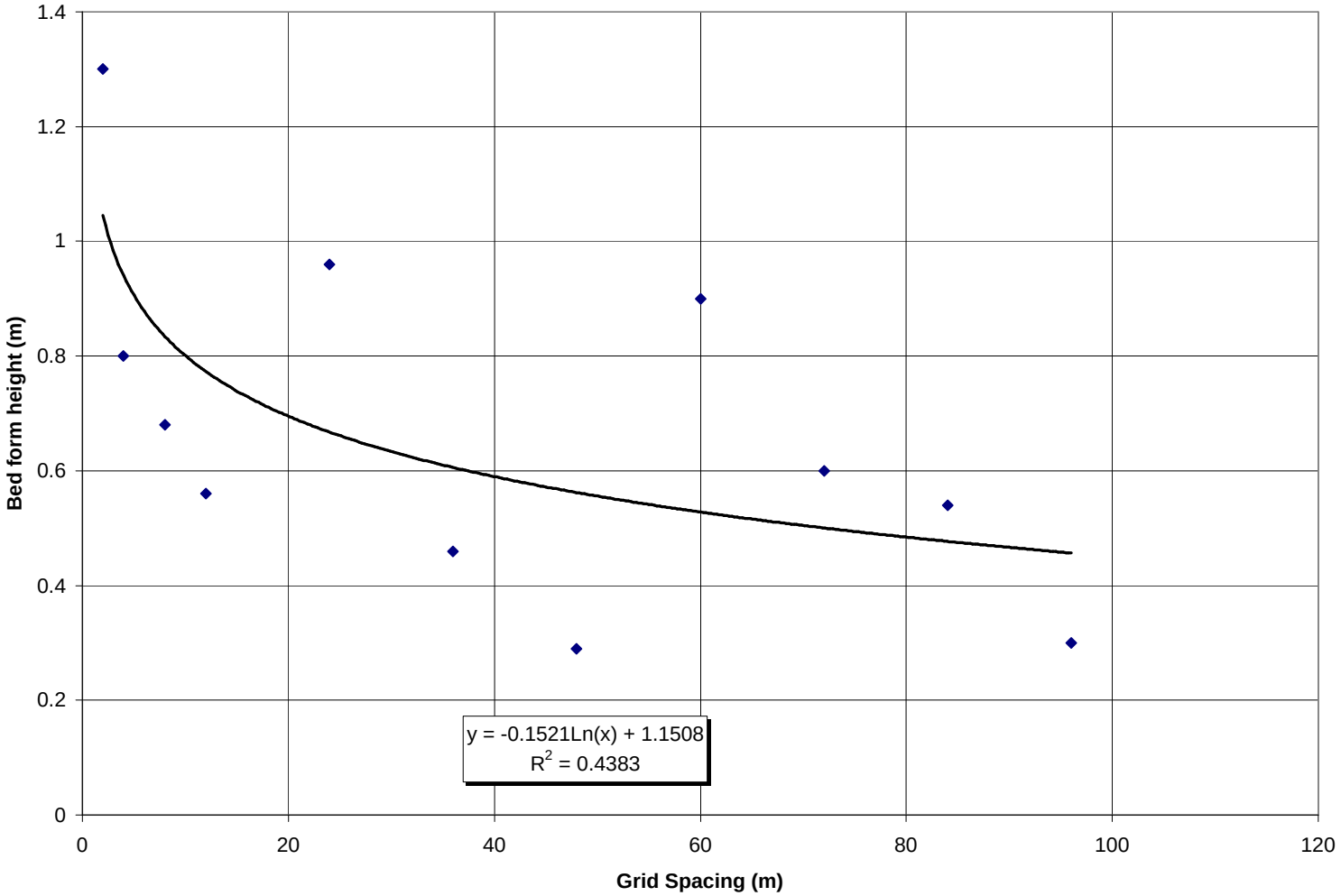

Figure 5.30: Correlation between grid spacing (m) and bed form height (m)

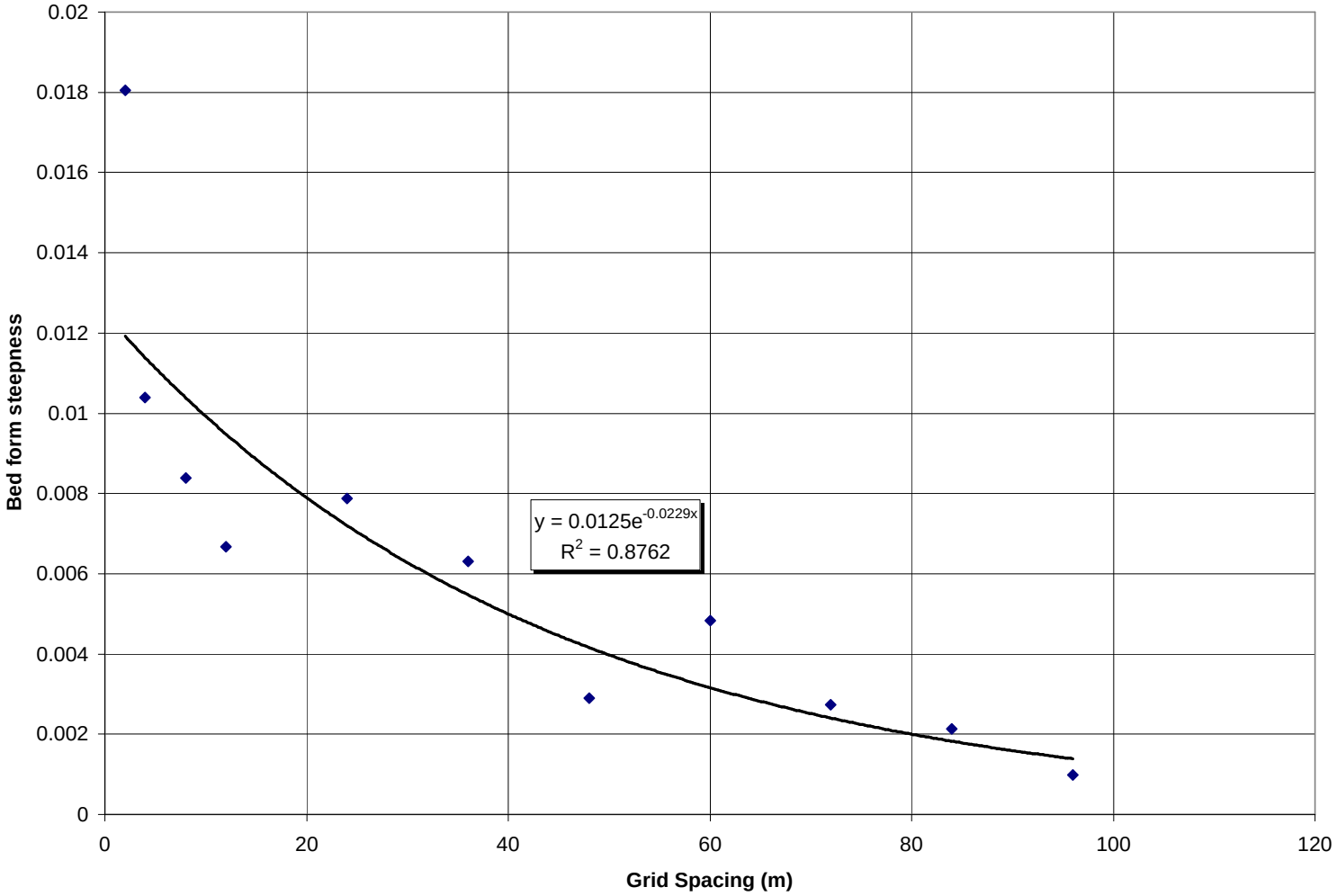

Figure 5.31: Correlation between grid spacing (m) and bed form steepness (m/m)

Based on Figures 5.29 through 5.31, the apparent bed form length appears to have the strongest correlation with the grid spacing. Several equations were fitted for all the plots as follows:

Bed form length and grid spacing

$$\lambda = 67.389\ e^{0.015\Delta x} \qquad [5.1]$$

where λ is the bed form length (m) and Δx is the grid spacing (m)

Bed form height and grid spacing

$$H_d = -0.152\ \ln(x)+1.1508 \qquad [5.2]$$

where H_d is the bed form height (m) and Δx is the grid spacing (m)

Bed form steepness and grid spacing

$$H_d / \lambda = 0.0125\ e^{-0.0229x} \qquad [5.3]$$

where H_d / λ is the bed form steepness and Δx is the grid spacing (m)

A strong correlation was evident in the case of bed form length ($R^2 = 0.8605$) and bed form steepness ($R^2 = 0.8762$), while a weaker correlation was evident for the bed form height ($R^2 = 0.4383$).

5.3. MULTIBEAM THREE DIMENSIONAL MODEL

The different interpolated grids were then used to setup a set of three dimensional hydrodynamic models for the purpose of estimating the effect of varying the grid spacing and the corresponding bed form dimensions on the resistance to the flow. Non-Hydrostatic MIKE 3 flow model was used in this task as its predicted flow separation and vertical velocity profiles were the closest to laboratory experiments (Nelson 1993). However at the same time, MIKE3 over estimated the energy slope for the bed form models presented in Chapter Four and as a result MIKE3 over estimated the resistance on top of the bed forms as explained in Chapter Four.

5.3.1. MODEL SETUP

The calibrated roughness coefficients, turbulence closure model and its coefficients and boundary conditions were migrated from the calibrated models presented in Chapter four. Table 5.2 shows model conditions for the different grid spacing.

	2M Model	**4M Model**
Horizontal Grid	2 m X 2m	4 m X 4 m
Vertical Grid	40 levels with constant spacing of 0.25 m	40 levels with constant spacing of 0.25 m
Time Step	0.005 sec	0.07 sec
Horizontal Turbulence model	Smagorinsky formulation	Smagorinsky formulation
Vertical Turbulence model	k-ε turbulence model	k-ε turbulence model

Table 5.2a MIKE 3 model characteristics for the 2m and 4m grid spacing.

	8M Model	**12M Model**
Horizontal Grid	8 m X 8 m	12 m X 12 m
Vertical Grid	40 levels with constant spacing of 0.25 m	40 levels with constant spacing of 0.25 m
Time Step	0.5 sec	0.5 sec
Horizontal Turbulence model	Smagorinsky formulation	Smagorinsky formulation
Vertical Turbulence model	k-ε turbulence model	k-ε turbulence model

Table 5.2b MIKE 3 model characteristics for the 8m and 12m grid spacing.

	24M Model	36M Model
Horizontal Grid	24 m X 24 m	36 m X 36m
Vertical Grid	40 levels with constant spacing of 0.25 m	40 levels with constant spacing of 0.25 m
Time Step	2 sec	2 sec
Horizontal Turbulence model	Smagorinsky formulation	Smagorinsky formulation
Vertical Turbulence model	k-ε turbulence model	k-ε turbulence model

Table 5.2c MIKE 3 model characteristics for the 24m and 36m grid spacing.

	48M Model	60M Model
Horizontal Grid	48 m X 48 m	60 m X 60 m
Vertical Grid	40 levels with constant spacing of 0.25 m	40 levels with constant spacing of 0.25 m
Time Step	5 sec	10 sec
Horizontal Turbulence model	Smagorinsky formulation	Smagorinsky formulation
Vertical Turbulence model	k-ε turbulence model	k-ε turbulence model

Table 5.2d MIKE 3 model characteristics for the 48m and 60m grid spacing.

	72M Model	84M Model
Horizontal Grid	72 m X 72 m	84 m X 84 m
Vertical Grid	40 levels with constant spacing of 0.25 m	40 levels with constant spacing of 0.25 m
Time Step	15 sec	20 sec
Horizontal Turbulence model	Smagorinsky formulation	Smagorinsky formulation
Vertical Turbulence model	k-ε turbulence model	k-ε turbulence model

Table 5.2e MIKE 3 model characteristics for the 72m and 84m grid spacing.

	96M Model
Horizontal Grid	96 m X 96 m
Vertical Grid	40 levels with constant spacing of 0.25 m
Time Step	30 sec
Horizontal Turbulence model	Smagorinsky formulation
Vertical Turbulence model	k-ε turbulence model

Table 5.2f MIKE 3 model characteristics for the 96 m grid spacing.

5.3.2. MODEL RESULTS

MIKE 3 Model results are presented as a series of water level profiles as shown in Figures 5.25 through 5.8.

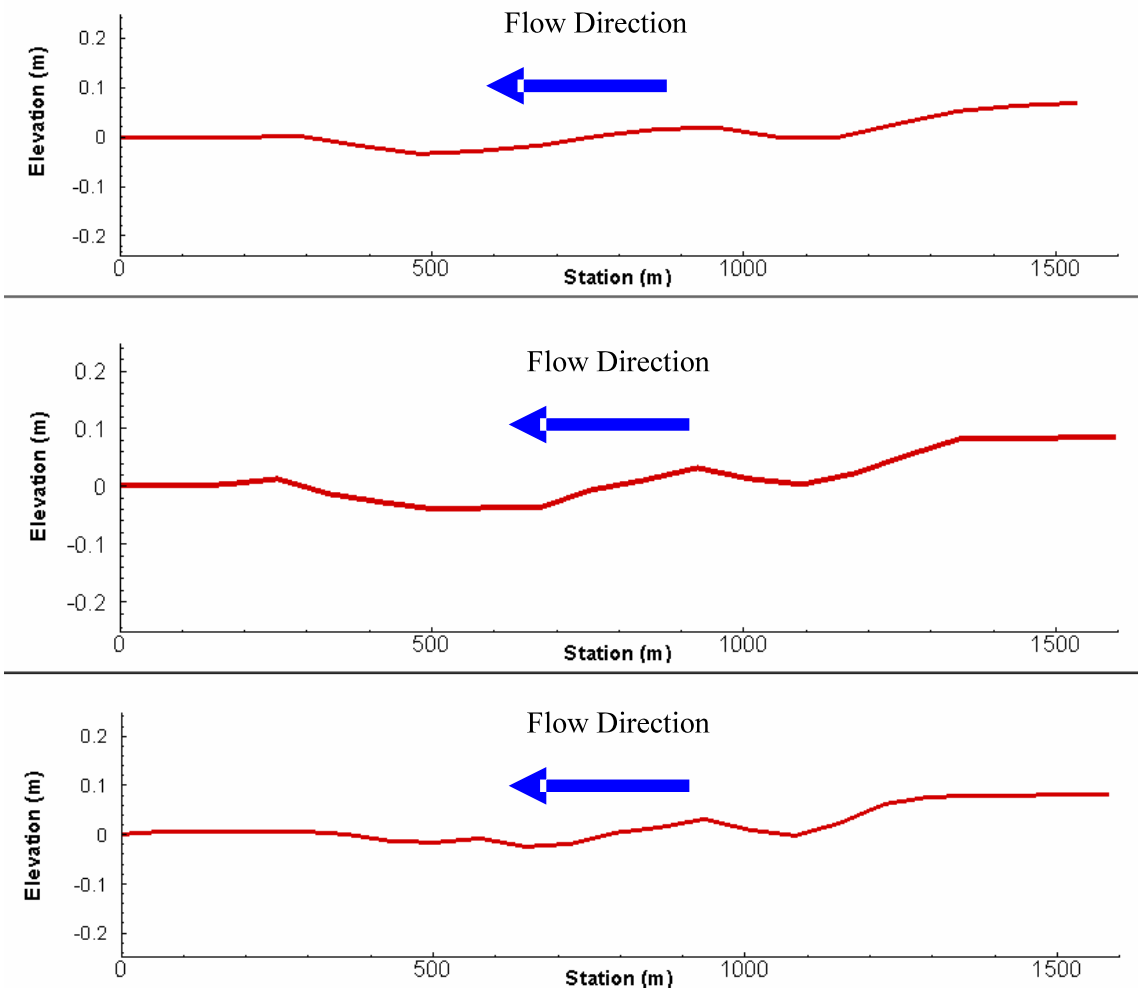

MIKE 3 - 96 m grid water surface profile

MIKE 3 - 84 m grid water surface profile

MIKE 3 - 72 m grid water surface profile

Figure 5.25: Simulated MIKE 3 water level results for 96, 84 & 72 m grids (top to bottom)

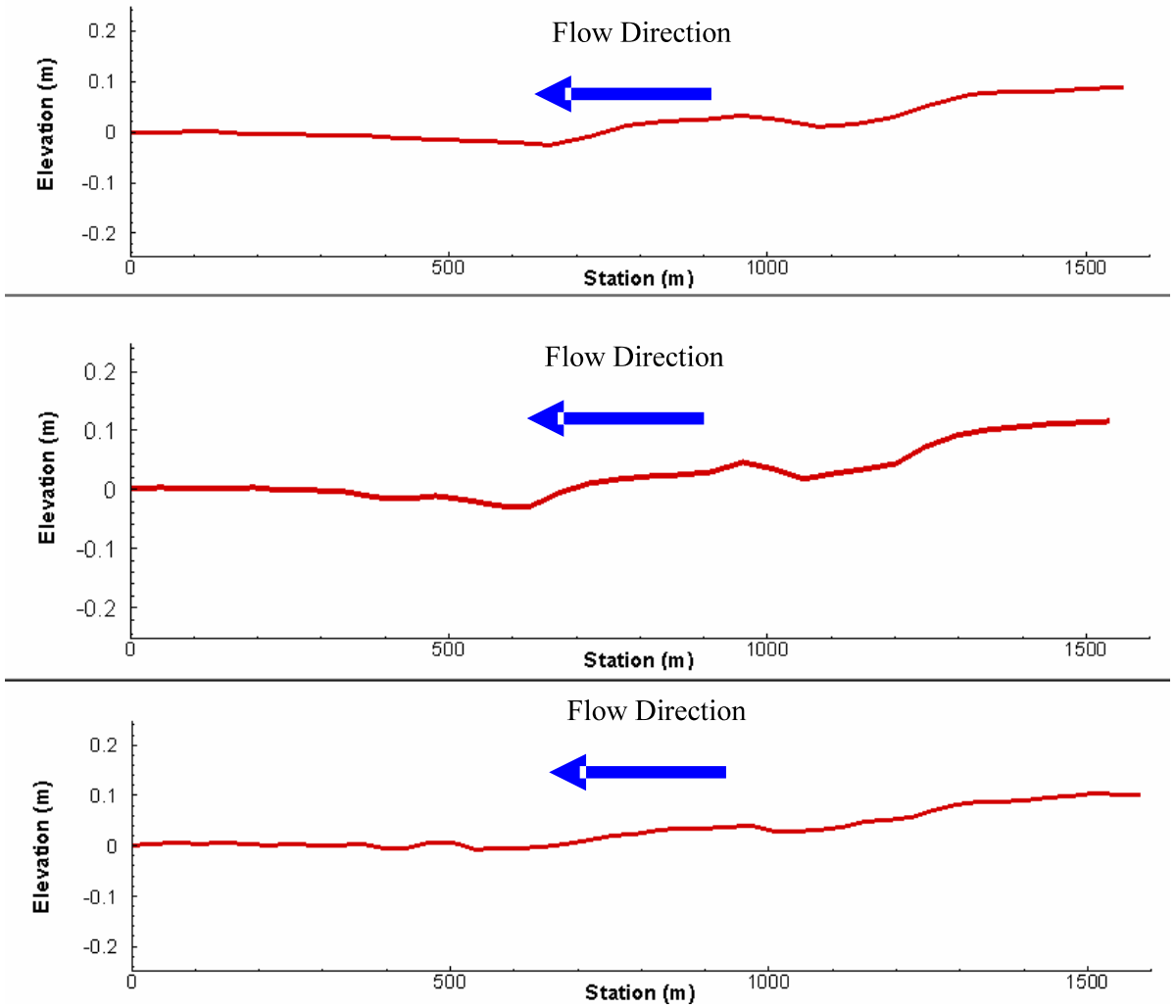

MIKE 3 - 60 m grid water surface profile

MIKE 3 - 48 m grid water surface profile

MIKE 3 - 36 m grid water surface profile

Figure 5.26: Simulated MIKE 3 water level results for 60, 48 & 36 m grids (top to bottom)

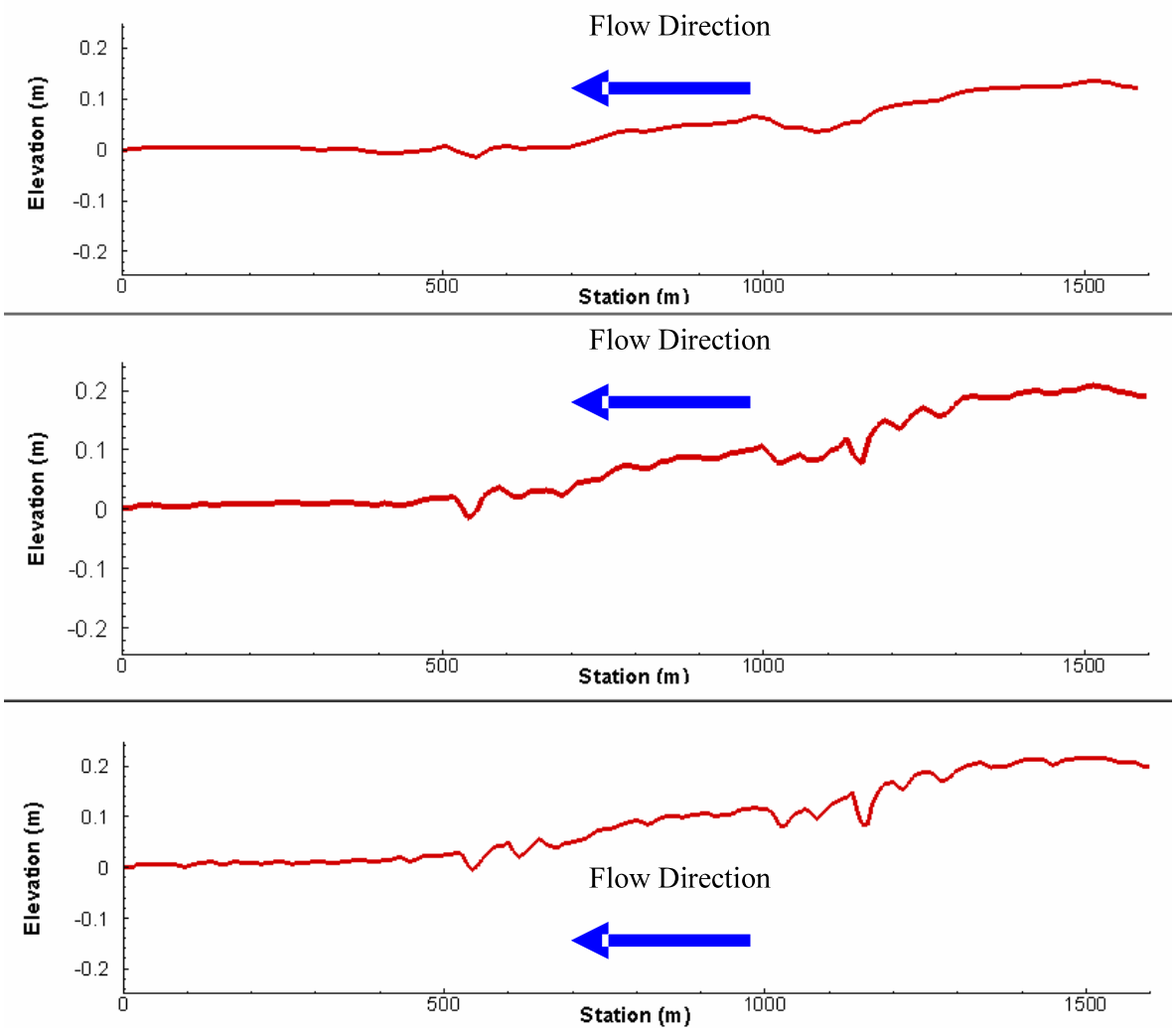

MIKE 3 - 24 m grid water surface profile

MIKE 3 - 12 m grid water surface profile

MIKE 3 - 8 m grid water surface profile

Figure 5.27: Simulated MIKE 3 water level results for 24, 12 & 8 m grids (top to bottom)

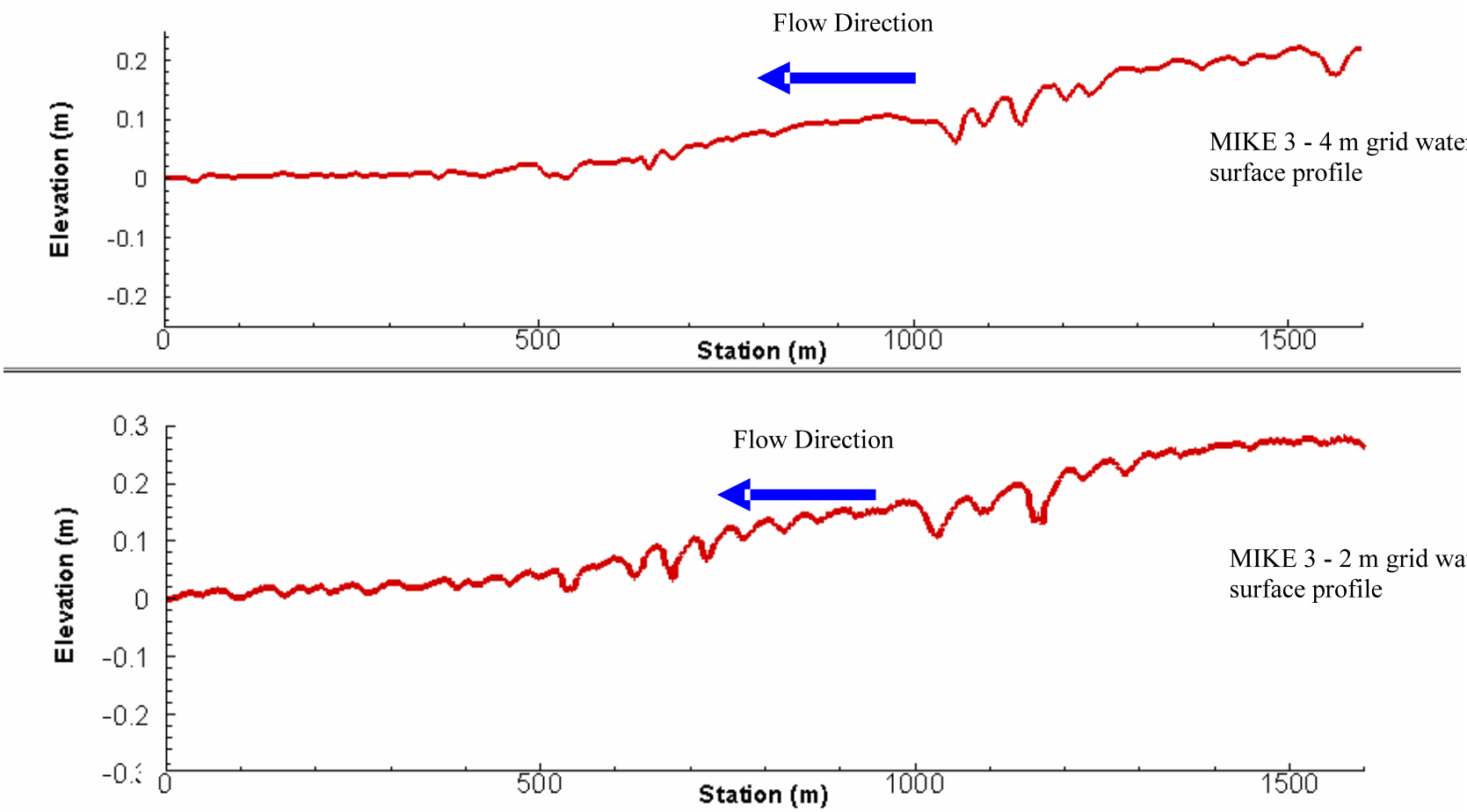

Figure 5.28: Simulated MIKE 3 water level results for 4 & 2 m grids (top to bottom)

The water level profiles for the different models showed an increased water surface slope with the decrease of the grid spacing, where the highest slope was observed in the 2 m grid model and the least slope for the 96 m grid. The corresponding equivalent Manning's n as shown in Table 5.3 was then calculated by using a 6 m average depth (hydraulic radius) and an average velocity of 0.75 m/s.

.

Grid Spacing	Average Energy Slope	Equivalent Manning's n
2	0.0001648	0.0565
4	0.0001366	0.0515
8	0.0001244	0.0491
12	0.0001182	0.0479
24	0.0000769	0.0386
36	0.0000631	0.0350
48	0.0000745	0.0380
60	0.0000562	0.0330
72	0.0000522	0.0318
84	0.0000529	0.0320
96	0.0000445	0.0294

Table 5.3 Models simulated equivalent Manning's n

The equivalent Manning's n decreased by the increase of the grid spacing, where the range was in between (0.056 – 0.0294) which is considered somewhat higher than the typical range for the Lower Mississippi River (0.024 – 0.035).

5.4. CORRELATIONS

The simulated equivalent Manning's n was then correlated with the grid spacing and bed form dimensions as shown in Figures 5.32 to 5.34

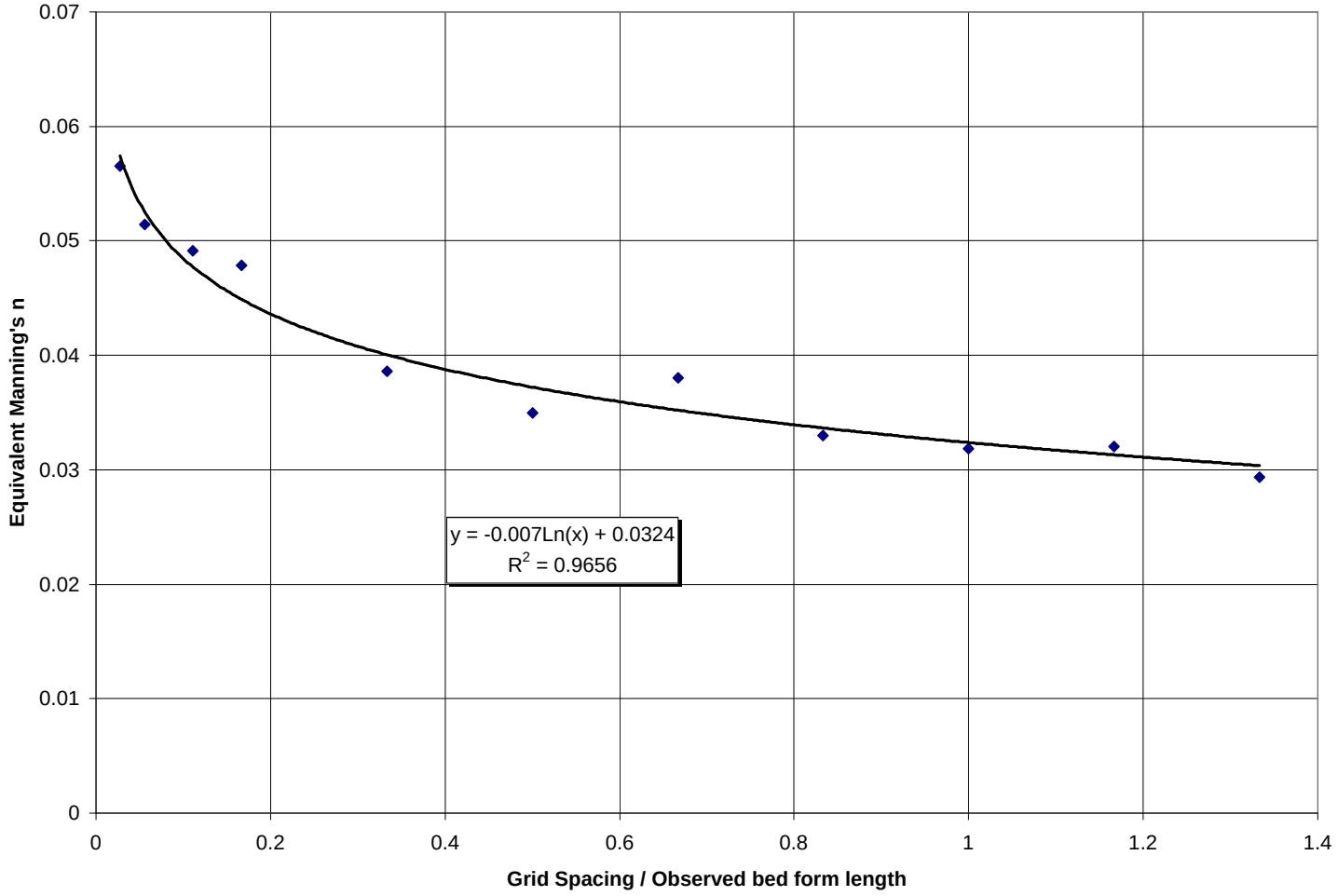

Figure 5.32: Correlation between grid spacing/observed bed form length and equivalent Manning's n

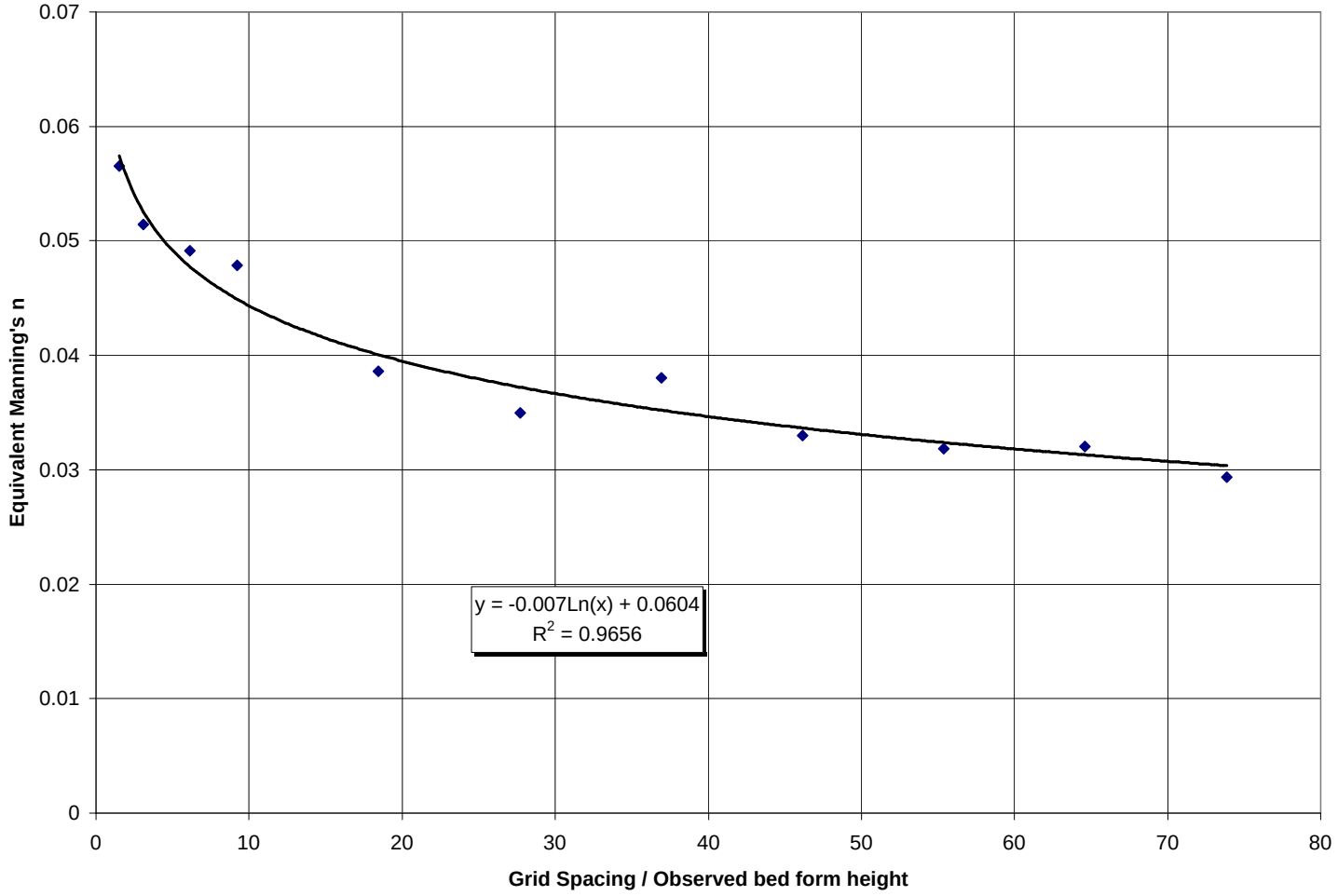

Figure 5.33: Correlation between grid spacing/observed bed form height and equivalent Manning's n

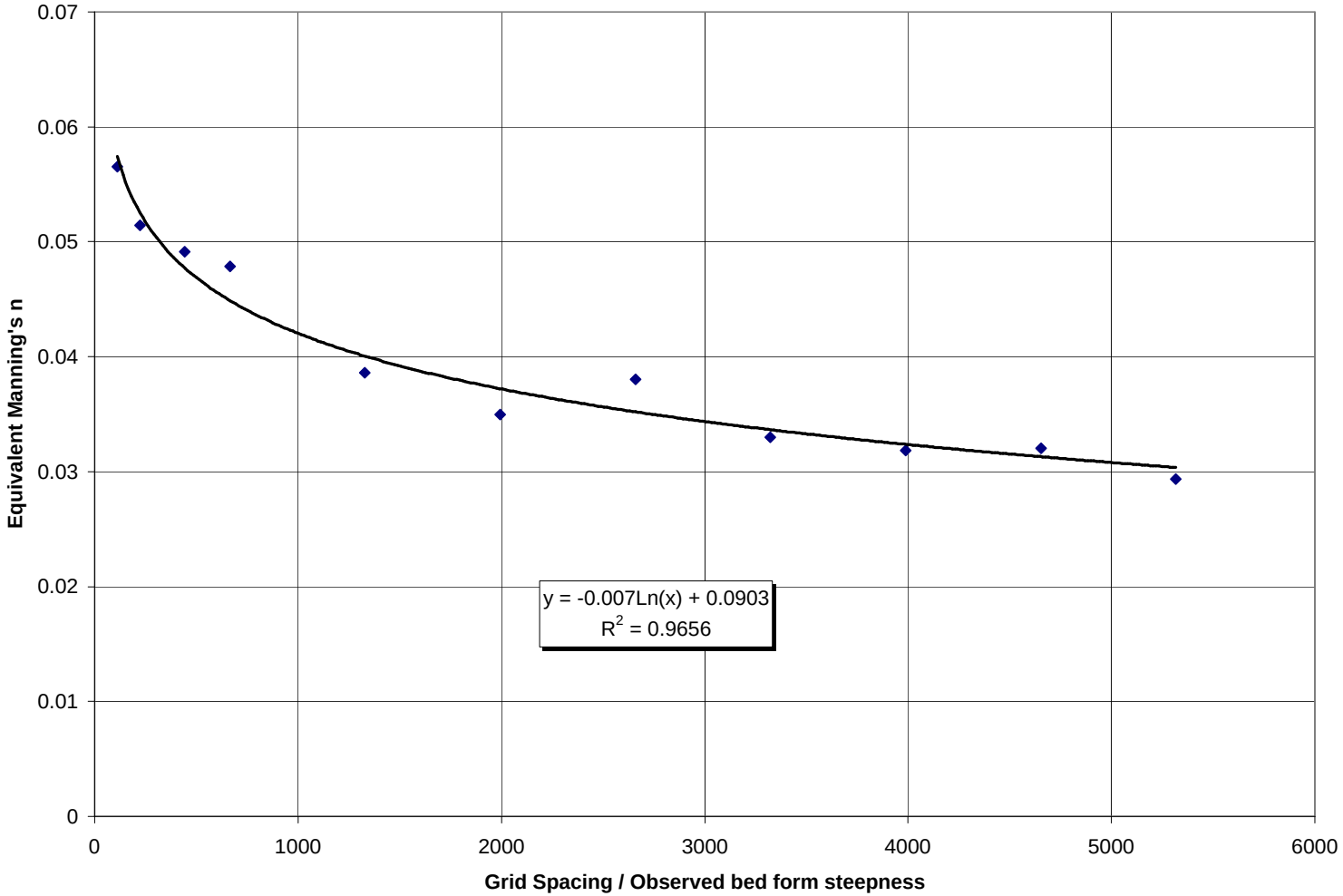

Figure 5.34: Correlation between grid spacing/observed bed form steepness and equivalent Manning's n

As anticipated, a trend was observed in all the plots. Several equations were fitted for various plots as follows:

Equivalent Manning's n and grid spacing/ bed form length

$$n = -0.007\ln(\Delta x/\lambda) + 0.0324 \quad [5.4]$$

where n is the equivalent Manning's n; Δx is the grid spacing and λ is bed form length

Equivalent Manning's n and grid spacing/ bed form height

$$n = -0.007\ln(\Delta x / H_d) + 0.0604 \quad [5.5]$$

where n is the equivalent Manning's n; Δx is the grid spacing and H_d is bed form height

Equivalent Manning's n and grid spacing/ bed form steepness

$$n = -0.007\ln(\Delta x / (H_d / \lambda)) + 0.0903 \quad [5.6]$$

where n is the equivalent Manning's n; Δx is the grid spacing and (H_d / λ) is bed form steepness.

A strong correlation was evident for all the cases ($R^2 = 0.9656$ for grid spacing/bed form length, $R^2 = 0.9656$ for grid spacing/bed form height and $R^2 = 0.9656$ for grid spacing/bed form steepness).

CHAPTER 6
DISCUSSIONS AND RECOMMENDATIONS

6.1. HYPOTHESIS ONE

6.1.1. STATEMENT

The resistance to the flow in alluvial rivers such as the Lower Mississippi River is a function of the bed form geometry and varies by River Mile.

6.1.2. METHODOLOGY

Spectral analysis process was performed to 31 multibeam datasets covering approximately 234 miles of the Lower Mississippi River for the purpose of quantifying the periodicity of bed form geometry in the river.

6.1.2. DISCUSSIONS OF RESULTS

The spectral results indicated that the dominant wave lengths varied from 50 to 500 ft (15m – 152m) at the downstream part of the study reach and 250 to 1000 ft (76m – 305m) in the upper part of the study reach. Similarly the bed forms heights increased in the upstream direction from 1 – 7 ft (0.3m – 2m) to 4 -15 ft (1.2m – 4.5m) (Figures 3.8 to 3.10). However, a clear pattern was not observed for the steepness case. This increase in the bed form geometry caused an increase in the corresponding bed form shear stress and the corresponding bed form shear velocity (Figure 6.1) which was consistent with an increase in the total bed shear stress in the upstream direction as was predicted by the hydrodynamic model results (MIKE11) (Figure 3.23). These results validate Hypothesis One stating that the resistance to the flow is related to the bed form geometry in alluvial rivers and varies by River Mile.

Statistical characterization of the bed form properties was also performed for the purpose of quantifying the variability in the data. Results from histogram plots, box plots and spatial series plots indicated the existence of high variability in the data and the existence of a strong right skewness phenomenon in the data. The results of the histograms and the box plots indicate that the extreme peaks while present in the natural system, they do not represent the majority of the data and can be disregarded from the analysis which in turns makes it feasible to utilize the bed form geometry in estimating relationships with the bed shear stress and eventually the resistance to the flow (Hypothesis One).

Correlations between the bed form geometry and some hydrodynamic features of the river were also performed. The results show a distinct relation between the bed form resistance and the flow characteristics, particularly the bed shear stress. The results showed that the increase of bed form dimensions results in an increase in bed shear stress. However this relation is limited by the depth of the water where the bed form occurs. Figure 3.11 showed that the bed form height is most frequently in the range of 1/10-1/6 of the water depth; however at some areas, the ratio extends to 1/3. It is thought that the ratio of 1/3 corresponds with fully or near fully developed bed form fields (equilibrium with flow regimes); wherever 1/10-1/6 corresponds with undeveloped (non-equilibrium with flow regimes) bed forms fields. This relation matches the ratios presented in Fedele and Garcia (2001) and Nordin (1965) as mentioned in Chapter Three.

Figure 6.2 (reciprocal of Figure 3.33) below relates the reciprocal of the flow parameter ($1/\psi_{35}=\frac{\tau'}{\gamma(S_s-1)d_{35}}$, where τ' is the grain shear stress, S_s is the specific gravity of sand; γ is the specific weight of water = 62.4 lb/ft^3) and the ratio of bed form shear velocity to the average

velocity (u_*”/U). The figure shows that the data points follow two general trends with a break point of $\frac{\tau'}{\gamma(S_s - 1)d_{35}}$ approximately equal to 0.2. The data points on the right of the break point represent points in the Lower Mississippi River where the ratio of bed form height to water depth = 1/10 – 1/6 (Regime one: non-developed bed form fields); while data points on the left of the break point represent points in the Lower Mississippi River where the ratio of bed form height to water depth = 1/3 (Regime 2: nearly fully developed bed form fields).

Figure 6.2 also shows that within the non-developed bed form fields, as the velocity in the river increases (moving upstream in the river), the grain friction increases and the ratio of bed form shear velocity to the average velocity decreases. Figure 6.1 showed that the bed form shear stress in terms of the bed form shear velocity increases from the downstream to the upstream part of the river; however this was also accompanied by a larger increase in the average velocity towards the upstream part of the river (Figure 3.20) and accordingly the ratio u_*”/U decreases towards the upstream part of the river (Figure 6.2).

The discussion of Figure 6.2 indicates the change of resistance of partially-developed bed forms in the Lower Mississippi River with the change in the hydrodynamic properties (flow velocity and grain shear stress) of the river; however this relation differs when the bed form fields enter an equilibrium zone with the flow conditions.

The same phenomenon where the relationship between the bed form resistance and the grain shear stress followed two trends was observed in experiments by Einstein and Barabrosa (1952) and in a study of the Mondego River in Portugal by Cunha (1967). Among 10 rivers analyzed by

Einstein and Barbarosa, eight rivers had d_{35} less than 0.5 mm, and the other two d_{35} had values of 0.7 and 1.0 mm. In later flume experiments with coarser bed material, Einstein found that the results departed from the mean curve of the 10 U.S. rivers and he concluded that the bed form resistance for coarse sand was shown to be smaller than that for medium and fine sand. In 1967, Cunha provided data for the Mondego River in Portugal with $d_{35} = 1.7$ mm, his results followed Einstein's coarser sediment size flume experiments but was positioned lower. The same conclusion was found in this study, but was attributed to the change of bed form dimensions relative to the water depth and not the sediment size as in Einstein (1952) and Cunha (1967).

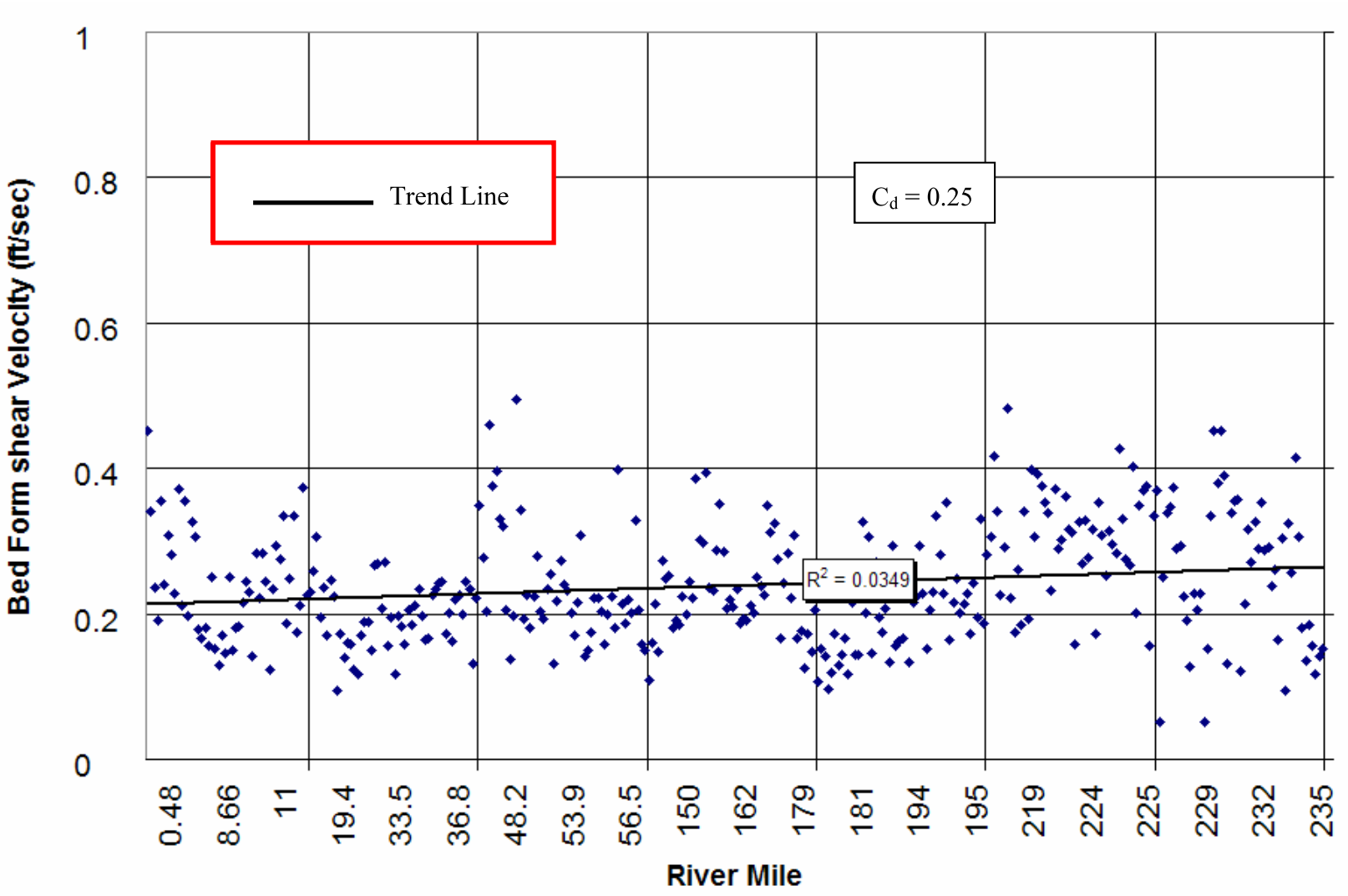

Figure 6.1 Spatial series of calculated bed form shear velocity for Lower Mississippi River between RM 0.00 and RM 234 (349 observations).

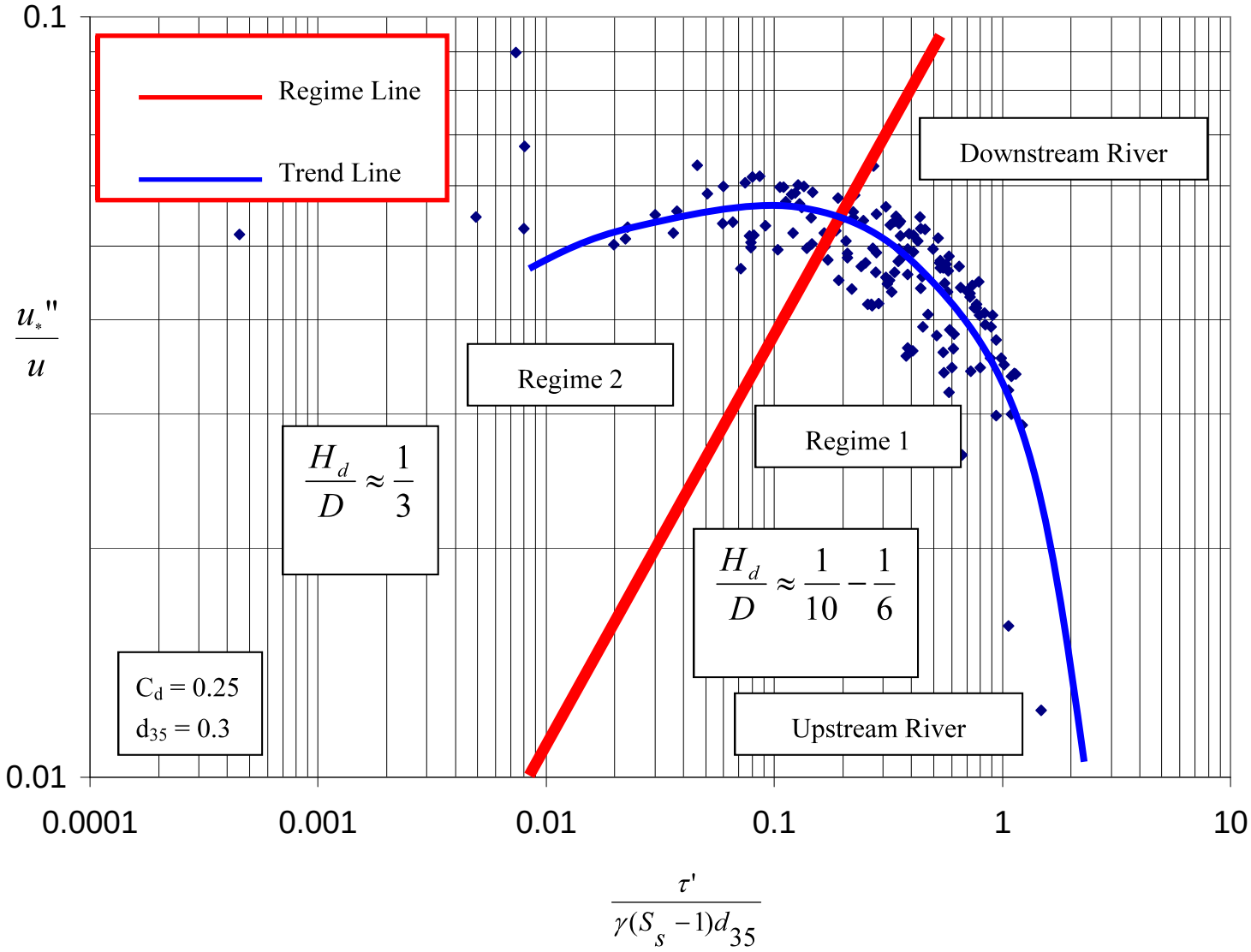

Figure 6.2 Relationship between grain shear stress and bed form shear velocity relative to average velocity in the Lower Mississippi River (June 2003-Septemeber 2003)

The wide range of bed form dimensions presented in this study produced a wider range of bed form resistance than had been previously reported in the published literature. All the bed form geometry that was incorporated into this research was estimated from extracting three profiles on each available multibeam dataset. The profile locations were carefully selected such that they cover the total width of each dataset, one on each side and one in the middle of the dataset in an attempt to cover the three-dimensional nature of the observed bed form without compromising the bathymetric details in the multibeam data. Three highest spectral peaks were then noted for each profile to eliminate some of the uncertainties associated with the spectral analysis and attempt to account for the large variation in the observed bed form geometry. The calculated bed form geometry was then checked against the observed bed form dimensions to eliminate any erroneous bed form dimensions that might have resulted from the spectral analysis.

All the analyses presented in this study were based on data extracted from a large alluvial river (Lower Mississippi River), with a very low energy gradient (less than 0.002 %), covered with a fine sediment bed (0.2 – 0.3 mm) and carrying a wash load in the range of 100-200 mg/L. The results at this time should not be generalized to different natural river systems with higher energy gradients.

All the estimated bed form geometries and the estimated relations between bed form geometry and flow characteristics were based on observations of the bed form geometries and hydrodynamic model results over a 3 months period in the Lower Mississippi River (June 2003 to September 2003). The rate of bed form migration, and how the bed form geometry will change over time might affect the estimated dimensions; however no data were available to the author to

study their effect.

The hydrodynamic results utilized in estimating the total bed shear stress were based on a 1-D numerical model. The uncertainties associated with this approximation of flow in the Lower Mississippi River is thought to be significant, however it was the only source of reliable hydrodynamic information available to the author at the time of writing this document. Several deep areas were observed in the river (Figure 3.19); these deep areas have resulted in several dips in the velocity magnitudes observed in Figure 3.20. These deep areas might have contributed to some errors in the calculation of the total bed shear stress from the numerical model results.

6.1.3. RECOMMENDATIONS

There has been much theoretical research and applications on bed forms as primary contributors to resistance in alluvial rivers; their varying dimensions and migration from one regime to another (e.g. flat to dune to antidune) produce continuing change in the energy gradient. The work presented in this study was aimed at developing resistance relationships based on field data and computational procedures. Future analysis and ongoing acquisition of more detailed sediment size distribution, accounting for the change in the bed material density in the Lower Mississippi River, along with more frequent flow (ADCP) and bottom surveys (multibeam) is necessary to help validating the relationship (Figure 3.33) established in this research.

6.2. HYPOTHESIS TWO

6.2.1. STATEMENT

Three dimensional hydrostatic numerical models are capable of simulating the resistance to flow past bed forms

6.2.2. METHODOLOGY

Three different three-dimensional computational fluid dynamics (CFD) modeling systems (ECMOSED, MIKE 3, H3D) were used in this study to simulate the flow over idealized bed forms. The modeled bed forms dimensions were estimated from Kheiashy et al (2007) based on mean bed form geometries in the Lower Mississippi River.

The three models utilized different approaches to solve the three -dimensional flow momentum and continuity equations. ECOMSED used the hydrostatic approximation, while H3D and MIKE 3 solved for the non hydrostatic pressure utilizing different techniques. H3D non-hydrostatic version utilizes the pressure correction method (Poisson equation for the pressure term), while MIKE 3 non-hydrostatic version utilizes the artificial compressibility approach.

6.2.3. DISCUSSIONS OF RESULTS

Non-hydrostatic MIKE 3 and hydrostatic ECOMSED captured the increase in velocity approaching the bed form crest but the non-hydrostatic H3D did not show as much increase. The non-hydrostatic MIKE 3 and hydrostatic ECOMSED captured correctly the phase relationship between the free water surface profile and the bed form while non-hydrostatic H3D only predicted a weak out of phase effect. The hydrostatic H3D and MIKE 3 correctly predicted the

out of phase relationship but failed to predict the flow separation phenomenon on the surface of the bed forms with depressions that were in agreement with the application of continuity and energy principles between the point of re-attachment and the crest where energy losses are primarily due to grain roughness. The failure of the hydrostatic simulation engines in MIKE3, H3D and ECOMSED to correctly predict the flow separation showed that the inclusion of the non-hydrostatic pressure component when simulating the flow at the lee of the bed forms is necessary; as the ratio of vertical flows becomes proportional to the horizontal flows and can not be disregarded from the calculations for the local flow pattern. The out of phase relationship between the bed forms and the water surface profile is affected by the ratio of the bed form height to the water depth. The higher the ratio, the more evident the out of phase relationship is. The water surface is usually lower near the bed form peak. This relationship is a result of the continuity of flow and the conservation of energy.

Although the model calibration was performed using a small scale model, care was taken to make sure that the ratio of bed form height to water depth (H_d/D), number of computational points along the bed form length and the lee slope are within the same range for the small scale model and the large scale bed forms models. (H_d/D) were equal to 0.2 and 0.3 for the small scale and the large scale bed form models respectively. The number of computational points along the bed form length was equal to 85 points and 60 points for the small and the large scale bed form models respectively. The lee slope was equal to 0.375 and 0.4 for the small and the large scale bed form respectively. This step was done to ensure that the two models are consistent in their horizontal and vertical parameterization and make it feasible to compare the results of the two models.

The models differed in reproducing the flow separation phenomenon at the 'wake' side of the bed forms. Hydrostatic ECOMSED showed less separation than laboratory results (Giratalla 1977 and Nelson et al 1993) indicated; while the non-hydrostatic H3D showed more separation with lower flow intensity than expected and the non-hydrostatic MIKE 3 results were close to observations in natural rivers and laboratory experiments (Giratalla 1977 and Nelson et al 1993).

Numerical models that solve for the non-hydrostatic pressure (non-hydrostatic MIKE3 and non-hydrostatic H3D) component proved to be necessary when solving the three-dimensional Reynolds averaged equations of motion at the lee of the bed forms. Hydrostatic models (ECOMSED, hydrostatic MIKE3 and hydrostatic H3D) that ignore the non-hydrostatic pressure where the vertical momentum equation is omitted and the vertical velocity is solely calculated from the continuity equation showed that it can not adequately predict the flow separation at the crest of the bed form where the ratio of vertical flows (turbulent eddies resulting from the flow separation at the lee side of the bed form) to the horizontal flows is significant.

Capturing the flow separation phenomenon may affect estimating the bed form resistance as the bed form resistance results from the net pressure distribution between the crest and the lee side of the bed form resulting from the slow separation. However, hydrostatic ECOMSED adequately predicted the bed form resistance even though it failed to correctly predict the flow separation. This was attributed to its successful prediction of the eddy loss due to the change of momentum along the bed form.

The predicted equivalent Manning's n (estimated from the energy gradient of each model) varied

from model to the other (0.039, 0.03 and 0.049) for hydrostatic ECOMSED, non-hydrostatic H3D and non-hydrostatic MIKE3 respectively. Although the typical values of Manning's n in the Lower Mississippi River are between 0.024 and 0.035, it was expected that the simulated Manning's n would be higher than those values as the modeled reach was fully covered with equilibrium bed forms which is not the case in the whole route of the Lower Mississippi River.

The difference in predicting the flow separation between the non-hydrostatic H3D and MIKE 3 was attributed to several factors, one being the procedures that each model applies to solve for the non-hydrostatic pressure, and second being the difference turbulence models utilized in each model. MIKE3 uses the artificial compressibility method (Chorin 1967) where the time derivative of the density in the mass conservation equation is replaced with the pressure term in the equation of state to solve for the non-hydrostatic pressure, while H3D uses the pressure correction method by solving a Poisson equation for the pressure (Casulli 1998). Both H3D and MIKE 3 applied the Smagorinsky formulation (Smagorinsky 1963) for the horizontal turbulence while they differed in their vertical turbulence models. H3D applied the Mellor-Yamada Level 2 scheme (Mellor and Yamada, 1982), while MIKE 3 applied the k-ε model whose results appeared to be superior over the Mellor-Yamada scheme in this study. In this research, a combination of the artificial compressibility method for solving for the non-hydrostatic pressure accompanied by a k-ε model for the vertical turbulence (MIKE 3) appeared to produce better results than a combination of pressure correction method to solve for the non-hydrostatic pressure accompanied by Mellor-Yamada scheme for the vertical turbulence (H3D). These conclusions however, should be generalized to conclude that this will always be the case in other three-dimensional modeling applications but should only be regarded in the context of the

variables (geometry and flow conditions) of this study.

A stair stepping effect was also apparent in H3D model results, this stair-stepping effect was attributed to its application of the volume of fluid method when solving the three dimensional equation in the lowermost computational node. MIKE 3 models did not produce this error in its applications, nor did the sigma-layer coordinate ECOMSED.

The increase of the number of vertical layers near the bed assisted in correctly predicting the logarithmic velocity vertical profile. A coarse uniform vertical grid for MIKE 3 and H3D resulted in a nearly constant velocity profile. However, the sigma-layer ECOMSED and variable vertical grid H3D correctly predicted the logarithmic vertical profile. The increase of vertical layers resolution proved to be essential in correctly capturing the logarithmic velocity profile. (Figure 4.14 and 4.15).

The results of the numerical models presented in this study should be regarded as numerical modeling of idealized bed forms in the Lower Mississippi River. The simulated bathymetry information (two dimensional bed forms) in the models differed from the three dimensional bed forms present in the river. However, at the same time, the results showed that with using the appropriate modeling systems, the alluvial bed form resistance can be adequately estimated. This conclusion supports Hypothesis two that states that three dimensional numerical models are capable of simulating the resistance to flow past bed forms.

6.2.4. RECOMMENDATIONS

Obtaining more detailed ADCP flow surveys in the Lower Mississippi River will help in calibrating the model results presented herein. Field observations that show the flow separation on top of the bed form will assist in better calibrating the flow separation predicted from the numerical models. Modeling of sediment transport on the surface of bed forms will assist in better estimating the erosion and deposition rates and eventually permit the computation of the bed form migration rate. Acquisition of more detailed sediment particle size distributions in the Lower Mississippi River along with discrete measurements of vertical sediment profiles will assist in sediment transport models calibration. Future hydrodynamic and sediment transport models should consider the interaction of the suspended solids with the turbulence closure model. The k-ε and k-*l* models currently being used do not allow for this feed-back.

6.3. HYPOTHESIS THREE

6.3.1. STATEMENT

The scale of bed forms relative to the spatial resolution in a numerical model affects the hydrodynamic resistance in the model.

6.3.2. METHODOLOGY

The multibeam survey data at RM 223 for the Lower Mississippi River was obtained and interpolated with different sampling intervals (2m, 4m, 8m, 12m, 24m, 36m, 48m, 60m, 72m, 84m & 96m) to estimate the bed form dimensions (Length, Height and Steepness) for the different sampling intervals. A correlation between the different sampling interval (Grid Spacing) and the observed bed form dimensions was then performed followed by a setup of a set

of three dimensional simulations for the different grid sizes. The results of the computer models were used to estimate the simulated equivalent Manning's n for each model grid size which was then correlated to the bed form dimensions and the grid spacing.

6.3.3. DISCUSSIONS OF RESULTS

The experiments using re-sampling of the multibeam data showed that increasing the grid spacing had an effect on the interpretation of the bed form configurations. A trend was observed where the apparent bed form length increased by increasing the grid spacing accompanied by a decrease in the apparent bed form height. Also, the extracted profiles showed that not only the indicated apparent bed form dimensions changed by varying the grid spacing, but also the number of apparent forms decreased by increasing the grid spacing. This resulted in totally different bed form fields (artificial bed forms) for the greater grid spacing dimensions than the one which was originally present. These artificial bed form fields then contributed to the resistance to the flow at a lower intensity compared to the original bed form. This resulted in grid dependant resistance that is a function of the bed form periodicity and the grid design.

The correlations between the grid spacing and the bed form dimensions revealed that the bed form length appeared to have the strongest correlation with the grid spacing. A strong correlation was evident in the case of bed form length ($R^2 = 0.8605$) and bed form steepness ($R^2 = 0.8762$), while a weak correlation was evident for the bed form height ($R^2 = 0.4383$). The weak correlation is possibly because the shorter wave lengths are eliminated more rapidly than the higher wave heights as the higher wave heights are more often associated with longer waves.

The correlation effort between the equivalent Manning's n and the grid spacing/observed bed form dimensions showed that a strong correlation was evident for all the bed form geometry dimensions (R^2 = 0. 9656 for bed form length, R^2 = 0. 9656 for bed form height and R^2 = 0. 9656 for bed form steepness). These findings validate Hypothesis Three which states that the scale of bed forms relative to the spatial resolution in a numerical model affects the hydrodynamic resistance in the model.

As mentioned in the discussions of Hypothesis Two, it is necessary to mention that the results of modeling effort in this portion of the study should not be regarded as numerical modeling of flow over bed forms in the whole length of Lower Mississippi River. The simulated portion of the study was only in the length of 1600m, where an observed fully developed field of bed forms was present with an observed range of flow (10,000 – 30,000 cfs between June and September 2003). Assuming that the whole route of the Lower Mississippi River bed is covered by the same field of bed forms will not be a correct assumption. It is thought that due to that reason, the equivalent Manning's n estimated by MIKE 3 (0.029 – 0.056) were higher than those obtained from observations in the lower Mississippi River (0.024 – 0.035). Also, it was assumed that the whole width of the simulated river was covered by bed forms, which is not always the case in the Lower Mississippi River, the observed multibeam data showed that the location of bed forms varied from one place to the other. Also, some of the multibeam surveys did not cover the whole width of the river, thus not giving enough information about the whole bottom of the river.

The effect the flow has on the bed form field, e.g. bed form erosion, deposition and migration and the effect of the suspended sediment concentration on the turbulence structure on the surface

of the bed form, was not included in this research. This later effect could not be studied with out setting up sediment transport simulations accompanied by detailed laboratory and field scale investigation to calibrate and validate the numerical model results.

The hydrodynamic boundary conditions (logarithmic velocity profile) for the 3-D models were made equal to the boundary used in Chapter Four for consistency. This assumption is thought to have introduced some uncertainties in the models. However it was used as a boundary condition due to the lack of detailed ADCP velocities profiles at RM 223 of the river at the time of performing the surveys.

6.3.4. RECOMMENDATIONS

Inclusion of the estimated relationships between the bed form geometry, grid spacing and equivalent alluvial resistance (expressed in terms of Manning's) in hydrodynamic and sediment transport numerical codes will assist in better estimating the form drag resistance in the models and could be used as an aid in the calibration of riverine models. By obtaining observations of bed form geometry in a specific river, the modeler will be able to utilize equations like Equations 5.4, 5.5 and 5.6 to choose the adequate grid spacing used to discretize the riverine environment and will also allow the modeler to better estimate an equivalent bed form resistance that is based on the bed form dimensions.

The selection of the appropriate grid for a numerical model of the Lower Mississippi River is a compromise between the resolution needed to define all of the channel features and the consequent execution time required for a certain grid resolution. The execution time is

approximately proportional to the cube of the inverse of the grid spacing for an unsteady 2-D free surface model. The following procedure is proposed for selecting the appropriate grid spacing and equivalent resistance in numerical model setup and calibration:

1. Obtain information about the bed form geometry (bed form length and height) in the studied stream. This step could be accomplished using detailed multibeam surveys, or by using longitudinal surveys of the stream.
2. Utilize Equations 5.1, 5.2 and 5.3 or Figures 5.29, 5.30 and 5.31 to estimate the appropriate grid spacing for discretizing the studied stream.
3. Discretize the stream with the selected grid spacing.
4. Remove the remnants of any bed forms resulted from discretizing the stream with the selected grid spacing; i.e. reduce the bed to a smooth boundary.
5. Utilize Equations 5.4, 5.5 and 5.6 or Figures 5.32, 5.33 and 5.34 to estimate the appropriate equivalent Manning's n to represent the bed form resistance in the model at different locations in the model.
6. Obtain a spatially variable equivalent Manning's n map representing the bed form resistance.
7. Obtain information about the bed material of the studied reach.
8. Estimate skin friction for the stream bed based on the bed material decomposition.
9. Add the skin friction to the bed form friction resulted from step 6 to obtain a final resistance map representing the resistance to the flow in the stream.
10. Utilize Figure 3.33 in addition to hydrodynamics output (average velocity and flow parameter) from the numerical model to update bed form shear stress information by time.

11. Apply available field data to fine tune the bed form resistance to reproduce the observed energy gradient (Calibration).
12. Check the output of the numerical model on different flow conditions to ensure that the model is correctly matching the observed data. (Validation).

Care must be taken into account before attempting to utilize the relationships and dependencies estimated in Chapter Five between bed form geometry, grid spacing and equivalent Manning's n (Equations 5.1 through 5.6) in other locations in the Lower Mississippi River. All the relationships were estimated using observed bed form geometry in River Mile 223 in the Lower Mississippi River. The procedure summarized above does not take into account the effect of the hydrodynamics of the river on the bed form fields in the river, e.g. bed form erosion, deposition and migration and the effect of the suspended sediment concentration on the turbulence structure on the surface of the bed form. As mentioned in Section 6.3.3, future addition of a sediment transport modeling component to the models described in Chapters Four and Five is necessary to accomplish this goal.

The procedures summarized above should only be applied for the Lower Mississippi River as all the data used in this study were obtained from the Lower Mississippi River. However, in other riverine environments, the researcher studying that specific environment can follow the same steps utilized to estimate relationships, e.g. Equations 5.1, 5.2 and 5.3 and consequently the modeling effort described in Chapter Five to estimate the corresponding relationships between bed form geometry, form drag Manning's n and the grid spacing and then follows the procedure listed above.

CHAPTER 7
CONCLUSIONS

Several research investigations have been conducted on the flow and sediment transport over bed forms in alluvial rivers (e.g. mean flow field, turbulence, shear partitioning, bed load transport and bed form geometry). Much of this work was either laboratory studies or small scale field investigations. Recently, advances in technology have improved the way data are collected and analyzed, e.g. flow data, velocity data and detailed bathymetric information that provide greater knowledge about the bed form geometry.

Recent advances in computing power have also reduced the computational restrictions on using three dimensional numerical models in modeling flow applications to predict the temporal and spatial changes of flow and sediment environments.

The work performed in this research quantified the periodic nature of bed forms types and geometries along the Lower Mississippi River. Correlations were performed relating the hydrodynamics of the river to the bed form types and geometries. The research work showed the inability of hydrostatic numerical modeling systems to accurately predict flow separation at the bed form crest but indicated that these models could reasonably predict the out of phase relationship between the bed form and the water surface profile. Furthermore the hydrostatic models predicted the total bed resistance as adequately as the non-hydrostatic models. It was found that non-hydrostatic models are required to properly simulate flow separation at bed form crests. Models such as MIKE 3 with constant z-level vertical discretization failed to capture the observed boundary layers unless very fine grids are used. A new procedure was developed as a part of this research, in which relations and dependencies between the hydrodynamic resistance

and the bed form dimensions relative to the numerical model spatial scale were derived. This procedure can be used to aid in numerical riverine model calibration and to provide a better representation of flow resistance in hydrodynamic modeling codes.

BIBLIOGRAPHY

Ackers, Peter and White, W.R., 1973, Sediment transport: new approach and analysis, Journal of the Hydraulics Division, Vol. 99, No. HY11, pp 2041-2060

Alam, A.M.Z., Cheyer, T.F., and Kennedy, J.F., 1966, Friction factors for flow in sand bed channels , Hydrodynamics Laboratory Report No. 78, Massachusetts Institute of Technology, Cambridge, MA

Alam, A.M.Z. and Kennedy, J.F., 1969, Friction factors for flow in sand bed channels, Journal of the Hydraulics Division, Vol. 95, No. HY6, pp 1973-1992

Allen, J.R.L., 1970, A quantitative model of grain size and sedimentary structures in lateral deposits, Journal of Geology, Vol. 7, No. 9, pp 71-80

Amsler, M.L. and Garcia, M.H., 1997, Discussion of Sand-dune geometry of large rivers during floods, Journal of Hydraulic Engineering, Vol. 125, No. 6, pp 582-584

Anderson, A.G., 1953, The characteristics of sediment waves formed by flow in open channels, 3rd Midwest Conference Fluid Mechanics, University of Minnesota, Minneapolis, MN

Annambhotla, V.A., Sayre, W.W., and Livesay, R.H., 1972, Statistical properties of Missouri River bed forms, Journal of the Waterways, Harbors, and Coastal Engineering Division, Vol. 98, NO. WW4, pp 489-510

Arya, S.P.S., 1975, A drag partition theory for determining the large-scale roughness parameter and wind stress on the Arctic pack ice, Journal of Geophysical Research, Vol. 80, pp3447-3454

ASCE Task Force on Flow and Transport over Dunes, 2002, Flow and Transport over Dunes, Forum paper, Journal of Hydraulic Engineering, Volume 128, No. 8, pp 726-728

ASCE Task Force on Bed Forms in Alluvial Channels, Committee on Sedimentation, 1966, Nomenclature for bed forms in alluvial channels, Journal of the Hydraulics Division, Vol. 92, No. 3, pp 51-64

Bagnold, R.A., 1960, Sediment discharge and streampower, U.S. Geological Survey Circular 421,

Bazin, H.E., 1865, Recherces Hydrauliques: 1re partie. Recherches Experimentales sur l' Ecoulement de l' Eau dans les Canaux Decouverts, 2e partie, Recherches Experimentales Relatives aux Remous et a la Propagation des Ondes, Dunod, Paris

Bennett, J.P., 1995, Algorithm for resistance to flow and transport in sand-bed channels, Journal of Hydraulic Engineering, Vol. 121, No. 8, pp 578-590.

Bennett, S.J. and Best, J.L., 1995, Mean flow and turbulence structure over fixed, two-dimensional dunes: implications for sediment transport and bedform stability, Sedimentology, Vol. 42, pp 491-513

Bhowmik, N.G., Bonini, A.P., Bogner, W.C., and Byrne, R.P., 1980, Hydraulics of flow and sediment transport in the Kankakee River in Illinois, Illinois State Water Survey Report of Investigation 98, 170 p

Blasius, P.R.H., 1913, Das aehnlichkeitsgesetz bei reibungsvorgangen in flussigkeiten, Forschungsheft 131, Vereins Deutscher Ingenieure, pp 1-41, Berlin

Boussinesq, J., 1877, Essai sur la theorie des eaux courantes. Mem. Pres. Academy of Science, Vol. XXIII, Paris

Bradbrook, K.F., Lane, S.N., Richards, K.S., Biron, P.M. and Roy, A.G., 2000, Large Eddy Simulation of Periodic Flow Characteristics at River Channel Confluences, Journal of Hydraulic Research, 38, 3, pages 207-215.

Bray, D.I., 1979, Estimating average velocity in gravel-bed rivers, Journal of the Hydraulics Division, ASCE, Vol. 105, No. HY9, pp 1103-1122

Bridge, J.S. and Best, J.L., 1988, Flow, sediment transport and bedform dynamics over the transition from dunes to upper stage plane beds: implications for the formation of planar formation, Sedimentology, Vol. 35, pp 753-763

Brownlie, W.R., 1981, Re-examination of Nikuradse Roughness Data, Journal of the Hydraulics Division, Vol. 107, No. HY1, pp 115-119

Casulli, V., 1998. Numerical simulation of 3D quasi-hydrostatic free-surface flows, J. Hyd. Eng., 24, 678-586.

Carey, W.C. and Keller, M.D., 1957, Systematic changes in the beds of alluvial rivers, Journal of the Hydraulics Division, Vol. 83, No. HY4,

Carter, R.W., Einstein, H.A., Hinds, Julian, Powell, R.W., and Silberman, E., 1963, Friction Factors in open channels, progress report of the task force on friction factors in open channels of the Committee on Hydromechanics of the Hydraulics Division: Journal of the Hydraulics Division, American Society of Civil Engineers, v. 89, no. HY2, pt. 1, pp 97-143.

Celik, Ismail and Rodi, Wolfgang, 1988, Modeling suspended sediment transport in nonequilibrium situations, Journal of Hydraulic Engineering, Vol. 114, No. 10, pp 1157-1191.

Celik, Ismail and Rodi, Wolfgang., 1984, A deposition entrainment model for suspended sediment transport, Report SFB 210/T/6, Universitat Karlsruhe, Karlsruhe, West Germany

Chein and Wan, “Mechanics of Sediment Transport, ASCE Press, 1998.

Chen, C.L., 1991, Unified theory on power laws for flow resistance, Journal of Hydraulic Engineering, Vol. 117, No. 3, pp 371-389

Cheng, R.T., Ling, Chi-Hai, and Gartner, J.W., 1999, Estimates of bottom roughness length and bottom shear stress in South San Francisco Bay, California, Journal of Geophysical Research, Vol. 104, No. C4, pp 7715-7728.

Cheng, R.T., Ling, Chi-Hai, and Gartner, J.W., 2000, Direct measurements of turbulence properties by a BB-ADCP in bottom boundary layer, in Interactions between Estuaries, Coastal Seas, and Shelf Seas, Ed. T. Yanagi, Terra Scientific Publishing Company, Tokyo, pp 37-55

Chiu, Chao-Lin, Jin, Weixia, and Chen, Yen-Chang, 2000, Mathematical models of distribution of sediment concentration, Journal of Hydraulic Engineering, Vol. 126, No. 1, pp 16-23

Chow, V.T., 1959, Open-Channel Hydraulics, MaGraw-Hill, New York, 680 p.

Chorin, A.J., 1967. A numerical method for solving incompressible viscous flow problems. J. Comput. Phys. 2, 12– 26.

Clauser, F.H., 1956, The turbulent boundary layer, Advances in Applied Mechanics IV, Academic Press, Inc. New York, pp 2-51

Clemens, Herschel, 1897, On the Origin of the Chezy Formula, Journal Association of Engineering Societies, Volume 18, January-June 1897, pp 363-368, Discussion pp 368-369.

Colby, B.R., 1964, Discharge of sands and mean-velocity relationships in sand-bed streams, U.S. Geological Survey Professional Paper 462-A, 47 p.

Colby, B.R. and Hembree, C.H., 1955, Computations of total sediment discharge, Niobrara River near Cody, Nebraska, U.S. Geological Survey Water Supply Paper 1357, 187 p.

Colby, B.R. and Hubble, D.W., 1961, Simplified methods for computing total sediment discharge with the modified Einstein procedure, U.S. Geological Survey Water Supply Paper 1593, 17 p.

Colby, B.R. and Scott, C.H., 1965, Effect of water temperature on the discharge of bed material, U.S. Geological Survey Professional Paper 462-G, 25 p.

Colebrook, C.F., 1938, Turbulent flow in pipes with particular reference to transition region between the smooth and rough pipe laws, Journal Institution of Civil Engineers (London) Vol. 11, pp 133-156

Colebrook, C.F., and White, C.M., 1937, Experiments with fluid friction in roughened pipes, Proceedings, Royal Society of London, Series A, vol. 161, pp 367-381.

Coleman, N.L., 1981, Velocity profiles with suspended sediment, Journal of Hydraulic Research, IAHR, Vol. 19, No. 3, pp 211-219

Coleman, N.L., 1986, Effects of suspended sediment on the open-channel velocity distribution, Water Resources Research, Vol. 22, No. 10, pp 1377-1384

Coleman, N.L. and Alonso, C.V., 1983, Two-dimensional channel flows over rough surfaces, Journal of Hydraulic Engineering, Vol. 109, pp 175-188

Coleman, S.E. and Fenton, J.D., 1996, Potential flow instability theory and bed forms, Proceedings North America Water and Environment Congress '96, American Society of Civil Engineers, Anaheim, CA, 6 pages

Coleman, S.E. and Melville, B.W., 1996, Initiation of bedforms on a flat sand bed, Journal of Hydraulic Engineering, Vol. 122, No. 6, pp 301-310

Coleman, S.E. and Melville, B.W., 1994, Bed form development, Journal of Hydraulic Engineering, Vol. 120, No. 5, pp 544-560

Coleman, S.E. and Eling, Burkhard, 2000, Sand wavelets in laminar open-channel flows, Journal of Hydraulic Research, Vol. 38, pp 331-338

Coles, Donald, 1956, The law of the wake in the turbulent boundary layer, Journal of Fluid Mechanics, Vol. 1, pp 191-226

Colosimo, C., Copertino, V.A., and Veltri, M., 1986, Average velocity estimation in gravel-bed rivers, Proceedings, 5th IAHR-APD Congress, Seoul, Vol. 2, pp 1-15

Crickmore, M. J., 1970, Effect of flume width on bed form characteristics, Journal of the Hydraulics Division, Vol. 96, No. HY2, pp 473-496

Culbertson, J.K. and Dawdy, D.R., 1964, A study of fluvial characteristics and hydraulic variables, Middle Rio Grande, New Mexico, U.S. Geological Survey Water-Supply Paper 1498-F, 73 p.

Culbertson, J.K, Scott, C.H., and Bennett, J.P., 1972, Summary of alluvial-channel data from Rio Grande Conveyance Channel, New Mexico, 1965-1969, U.S. Geological Survey Professional Paper 562-J, 49 p.

Daigle, D., 2006 Background on Lower Mississippi River Basin, http://www.epa.gov/msbasin/subbasins/lower/index.htm

Danish Hydraulic Institute - DHI (2005). MIKE 3 Flow Model: Hydrodynamic Module Scientific Documentation.

Darcy, H.P.G., 1857, Recherches Experimentales Relatives au Mouvement de l'Eau dans les Tuyaux, Mallet-Bachelier, Paris,

Dietrich, W.E. and Whiting, Peter , 1989, Boundary shear stress and sediment transport in river meanders of sand and gravel, in River Meandering, Ikeda and Parker , eds. American Geophysical Union Monograph 12, pp 1-50

Douglas, J F, Gasiorek J M, Swaffield JA. Fluid Mechanics, Longman Publishers 1994

DuBuat, P, 1786, Principles d'Hydraulique, 2nd Edition, De L'Imprimerie de Monsieur, Paris.

Einstein, H.A., 1942, Formulas for the transportation of bed load, Transactions of American Society of Civil Engineers, Vol. 107, pp 561-573

Einstein, H.A., 1950, The bed load function for sediment transportation in open channels, Technical Bulletin 1026, U.S. Department of Agriculture, Soil Conservation Service, Washington, D.C.

Einstein, H.A., and Barbarossa, N.L., 1952, River channel roughness, Transactions of the American Society of Civil Engineers, vol. 117, pp1121-1146.

Einstein, H.A., and Chien, Ning, 1954, Second approximation to the solution of the suspended load theory: University of California Institute Engineering Research/U.S. Army Corps of Engineers Missouri River Division Sediment Series 8, 75 p.

Einstein, H.A., and Chien, Ning, 1955, Effects of heavy sediment concentration near the bed on velocity and sediment distribution, Report 8, University of California-Berkley and Missouri River Division Corps of Engineers, 96 p.

Elata, C. and Ippen, A.T., 1961, The dynamics of open channel flow with suspensions of neutrally buoyant particles, M.I.T. Department of Civil and Sanitary EngineeringTechnical Report 45, Cambridge, MA, 69 p

Elder, J.W., 1959, The dispersion of marked fluid in turbulent shear flow, Journal of Fluid Mechanics, vol. 5, no. 4

Elliot, W.P., 1958, The growth of the atmospheric internal boundary layer, EOS Transactions American Geophysical Union, Volume 38, p 1048,

Emmett, W.W., 1980, A field calibration of the sediment-trapping characteristics of the Helley-Smith bed-load sampler, U.S. Geological Survey Professional Paper 1139, 44 p.

Engel, Peter, 1981, Length of flow separation over dunes, Journal of Hydraulics Division, ASCE, Vol. 107, No. HY8, pp 1133-1143

Engel, Peter and Lau, Y.L., 1980, Computation of bedload using bathymetric data, Journal of the Hydraulics Division, NO. 106, No. HY3, pp 369-380

Engelund, Frank, 1967, A sediment transport theory based on similarity, Hydraulic Laboratory, Technical University of Denmark, Basic Research Progress Report 13

Engelund, Frank, 1970, Instability of erodible beds, Journal of Fluid Mechanics, Vol. 42, Part 2, pp 225-244

Engelund, Frank, 1977, Hydraulic resistance for flow over dunes, Institute for Hydrodynamics and Hydraulic Engineering, Report 44, Technical University of Denmark, pp 19-20

Engelund, Frank, and Hansen, E., 1967, A monograph on sediment transport in alluvial streams, Danish Technical Press, Copenhagen, Denmark.

Engelund, Frank, and Fredsoe, J., 1976, A sediment transport model for straight alluvial channels, Nordic Hydrology, Volume 7, Number 5, pp 293-306

Engelund, Frank, and Fredsoe, J., 1982, Sediment ripples and dunes, Annual Review of Fluid Mechanics, Vol. 14, pp 13-37

Exner, F.M., 1925, Uber die wechselwirkung zwischen wasser und geschiebe in flussen, Sitzenberichte der Academie der Wissenschaften, Wien, Austria, Sec. IIA, 133:199

Fedele, J.J., 1998, Bed roughness in alluvial streams, Masters Thesis, University of Illinois, 111 p.

Fedele, J.J. and Garcia, M.H., 2001, Alluvial roughness in streams with dunes: a boundary-layer approach, in River, Coastal, and Estuarine Morphodynamics. Giovanni Seminara and Paolo Blondeaux, Editors, Springer-Verlag, Berlin, pp37-60

Forchheimer, P., 1930, Hydraulik, 3rd edition, Teubner, Leipzig/Berlin, pp 139-163

Fredsoe, Jorgen, 1974, On the development of dunes in erodible channels, Journal of Fluid Mechanics, Vol. 64, Part 1, pp 1-16

Fredsoe, Jorgen, 1975, The friction factor and height-length relations in flow over a dune-covered bed, Institute of Hydrodynamic and Hydraulic Engineering (ISVA), Technical University of Denmark, Report No. 269

Fredsoe, Jorgen, 1982, Shape and dimensions of stationary dunes in rivers, Journal of Hydraulics Division, Vol. 108, No. HY8, pp 932-947.

Fromm, K., 1923, Stromungswiderstand in rauhen Rohren, Zeitschrift fur Angewante Mathematik und Mechanik, vol. 3, 1923, pp 339-358

Garde, R.J. and Anderson, M.L., 1959, Sand waves and regimes of flow in alluvial channels, Proceedings of the 8th International Association for Hydraulic Research Congress, Montreal, Canada, Vol. IV, Paper No. 28,

Garcia, M.H., 1999, Sedimentation and erosion hydraulics, in Hydraulic Design Handbook, L.W. Mays, Ed., McGraw-Hill, New York, pp 6.1-6.113,

Garcia, M.H. and Parker, G.S., 1991, Entrainment of bed sediment into suspension, Journal of Hydraulic Engineering, Vol. 117, No. 4, pp. 414-435.

Garcia, M.H., 1989, Depositing and eroding sediment-driven flows: turbidity currents, PhD dissertation University of Minnesota

Gartner, J.W. and Cheng, R.T., 2001, The promises and pitfalls of estimating total suspended solids based on backscatter intensity from acoustic Doppler current profiler, Proceedings of the Seventh Federal Interagency Sedimentation Conference, March 2001, Reno, Nevada, pp 119-126.

Gelfenbaum, G., and Smith, J.D., 1986, Experimental evaluation of a generalized suspended-sediment transport theory, in Shelf Sands and Sandstones, R.J. Knight and J.R. McLean, Eds., Canadian Society of Petroleum Geologists, Calgary

Gessler, D., B. Hall, M. Spasojevic, F. Holly, H. Pourtaheri, and N. Raphelt (1999), Application of 3D mobile bed, hydrodynamic model, J. Hydraul. Eng., 125, 737– 749.

Gilbert, G.K., 1914, The transport of Debris by Running water, Professional Paper 86, U.S. Geological Survey, 263 p.

Gill, M.A., 1971, Height of sand dunes in open channel flows, Journal of the Hydraulics Division, Vol. 97, No. HY12, pp 2067-2074

Giovanni Seminara and Paolo Blondeaux, Editors, Springer-Verlag, Berlin, pp37-60

Gladki, H., 1979, Resistance to flow in alluvial channels with coarse bed materials, Journal of Hydraulic Research, IAHR, Vol. 17, No. 2, pp 121-128

Gonzalez, J.A., Melching, C.S., and Oberg, K.A., 1996, Analysis of open-channel velocity measurements collected with an acoustic Doppler current profiler, Proceedings from the 1st International Conference on New/Emerging Concepts for Rivers, International Water Resources Association, September 22-26, 1996, Chicago, Illinois, pp 838-845

Graf, W.H., 1971, Hydraulics of sediment transport, McGraw-Hill, New York, 513 p.

Granger, C. W. J., 1969, Spatial data and time series analysis, in Scott, A.J., editor, Studies in regional science:London, Pion, 217 p.

Granger, C. W. J., and Hatanaka, M., 1964, Spectral analysis of economic time series: Princeton, New Jersey,

Grishanin, K.V., 1979, Dynamics of alluvial streams, Gidrometeoizdat, Leningrad

Guy, H.P., Simons, D.B., and Richardson, E.V., 1966, Summary of alluvial channel data from flume experiments, 1956-1961, U.S. Geological Survey Professional Paper 462-J

Hammond, F.D., Heathershaw, A.D., and Langhorne, D.N., 1984, A comparison between Shield's threshold criterion and the Henderson movement of loosely packed gravel in a tidal channel, Sedimentology, Vol. 31, pp 51-62

Haque, M.I. and Mahmood, Khalid, 1985, Geometry of ripples and dunes, Journal of Hydraulic Engineering, Vol. 111, No. 1, pp 48-63

Hayashi, T., 1970, Formation of dunes and antidunes in open channels, Journal of the Hydraulics Division, Vol. 96, No. HY2, pp 357-367

Hey, R.D., 1979, Flow resistance in gravel-bed rivers, Journal of the Hydraulics Division, ASCE, Vol. 89, No. HY4, pp 365-379

Hill, H.M., Srinivasan, V.S., and Unny, T.E., 1967, Instability of flat bed in alluvial channels, Proceedings American Society of Civil Engineers Conference on Water Resources Engineering, New Orleans, Louisiana (reference from Raudkivi, 1990)

Hino, M., 1968, Equilibrium range spectre of sand waves formed by running water, Journal of Fluid Mechanics, Vol. 34, Part 3, pp 565-573

Holmes, Jr., R.R., 1997, Suspended-sediment budget for the Kankakee River basin, 1993-1995, U.S. Geological Survey Open-File Report 97-120, 8 p.

Hooke, J. M., 1984, Changes in river meanders: a review of techniques and results of analyses: Progress in Physical Geography, v. 8, p. 473–508.

Hopf, L., 1923, Die Messung der hydraulischen Rauhigkeit, Zeitschrift fur Angewandte Mathmatik und Mechanik, vol. 3, 1923, pp.329-339

Hubbell, D.W. and Matejka, D.Q., 1959, Investigations of sediment transportation, Middle Loup River at Dunning, Nebraska, U.S. Geological Survey Water Supply Paper 1476, 123 p.

Hubbell, D.W. and Al-Shaikh Ali, K.S., 1961, Qualitative effects of temperature on flow phenomena in alluvial channels, U.S. Geological Survey Professional Paper 424-D, pp 21-24

Humphreys and Abbott, 1861, Report upon the physics and hydraulics of the Mississippi River, J.B. Lippincott Company, reproduced as U.S. Army Corps of Engineers Professional Paper 13, 1876

HydroQual, Inc., (2002), "A primer for ECOMSED", Users Manual, Version 1.3, HydroQual, Inc., Mahwah, NJ, USA, 188pp.

Ikeda, S., 1983, Flow and bed topography in channels with alternate bars, River Meandering, Proceedings of Conference River '83, Ed. C.R. Elliot, ASCE, pp 733-746

Ikeda, S., 1984, Prediction of alternate bar wavelength and height, Journal of Hydraulic Engineering, Vol. 110, No. 4, pp 371-386

Irmay, S., 1949, On steady flow formulae in pipes and channels, Proceedings IAHR 3rd Congress, Grenoble, France, Paper III-3

Jaeggi, M.N.R., 1984, Formation and effects of alternate bars, Journal of Hydraulic Engineering, Vol. 110, No. 2, pp 142-156

Jain, S.C. and Kennedy, J.F., 1974, The spectral evolution of sedimentary bed forms, Journal of Fluid Mechanics, Vol. 63, Part 2, pp 301-314

Jonys, C.K., 1973, An experimental study of bedform mechanics, PhD dissertation, University of Alberta, at Edmonton, Canada

Jordan, P.R., 1965, Fluvial sediment of the Mississippi River at St. Louis, Missouri: U.S. Geological Survey Water Supply Paper 1802, 89 p.

Julien, P.Y., 1992, Study of bedform geometry in large rivers, Delft Hydraulics Report Q1386, Emmeloord, The Netherlands

Julien, P.Y., 1995, Erosion and sedimentation, Cambridge University Press, Cambridge, England, 280 p.

Julien, P.Y. and Klaassen, G.J., 1995, Sand-dune geometry of large rivers during floods, Journal of Hydraulic Engineering, Vol. 121, No. 9, pp657-663

Kamphuis, J.W., 1974, Determination of sand roughness for fixed beds, Journal of Hydraulic Research, IAHR, Vol. 12, No. 2, pp 193-203

Karim, Fazle, 1995, Bed configuration and hydraulic resistance in alluvial channel flows, Journal of Hydraulic Engineering, Vol. 121, No. 1, pp 15-25

Karim, Fazle, 1999, Bed-form geometry in sand-bed flows, Journal of Hydraulic Engineering, Vol. 125, No. 12, pp 1253-1261.

Karim, Fazle and Kennedy, J.F., 1990, A menu of coupled velocity and sediment-discharge relations for rivers, Journal of Hydraulic Engineering, Vol. 116, pp978-996

Kennedy, J.F., 1963, The mechanics of dunes and antidunes in erodible-bed channels, Journal of Fluid Mechanics, Vol. 16, No. 4, pp 521-544

Kennedy, J.F., 1969, The formation of sediment ripples, dunes, and anti-dunes, Annual Review Fluid Mechanics, Vol. 1, pp 147-168

Kennedy, J.F. and Odgaard, A.J., 1991, Informal monograph on riverine sand dunes, U.S. Army Coastal Engineering Research Center Contract Report CERC-91-2, 192 p.

Keulegan, G.H., 1938, Laws of turbulent flow in open channels: U.S. National Bureau of Standards, Journal of Research, Vol. 21, No. 6, pp 707-741.

Kheiashy, K., McCorquodale, A., Georgiou, I., Meselhe, E. 2007, "Geometric and Statistical Characteristics of Bed Forms in the Lower Mississippi River", Proceedings of the Seventh Coastal Sediment Conference, New Orleans, LA.

Kheiashy, K., McCorquodale, A., Georgiou, I., Meselhe, E. 2007, "Non-hydrostaic versus hydrostatic three dimensional simulation of flow separation over bed forms" Proceedings of the 2007 Environmental and Water Resources Congress, Tampa, FL.

Kondratiev, N.E., Lyapin, A.N., Popov, I. V., Pinikovskii, S.I., Fedorov, N.N., Yakunin, I.I., 1959, Channel Processes, Gidrometeoizdat, Leningrad

Kondraitev, N.E., Lyapin, A.N., Popov, I. V., Pinikovskii, S.I., Fedorov, N.N., Yakunin, I.I., 1962, River flow and river channel formation, from Russian (1959) by Israel Program for Scientific Translations, U.S. Department of the Interior

Kostaschuk, Ray and Villard, Paul, 1996, Flow and sediment transport over large subaqueous dunes: Fraser River, Canada, Sedimentology, Vol. 43, pp 849-863

Lane, E.W. and Eden, E.W., 1940, Sand waves in the lower Mississippi River, Journal Western Society of Civil Engineers, Vol. 45, No. 6

Lane, E.W., and Carlson, E.J., 1953, Some factors affecting the stability of canals constructed in coarse granular materials, Proceedings IAHR 5th Congress, Minneapolis, MN

Lane, S.N., Bradbrook K.F., Richards K.S., Biron P.A. and Roy A.G. 1999. The application of computational fluid dynamics to natural river channels: three-dimensional versus two-dimensional approaches. Geomorphology, 29(1-2), 1-20.

Leliavsky, S., 1955, An introduction to fluvial hydraulics, Constable and Company, Ltd, London

Leopold, L.B., Wolman, M.G., and Miller, J.P., 1964, Fluvial processes in geomorphology, W.H. Freeman and Company, San Francisco, 521 p

Limerinos, J.T., 1970, Determination of the Manning coefficient for measured bed roughness in natural channels, U.S. Geological Survey Water Supply Paper 1898-B, 47 p.

Liu, H.K., 1957, Mechanics of sediment-ripple formation, Journal of Hydraulics Division, Vol. 83, No. HY2, pp 1-23.

Lopez, Fabian and Garcia, M.H., 1999, Wall similarity in turbulent open channel flows, Journal of Engineering Mechanics, Vol. 125, No. 7,

Lopez, Fabian, and Garcia, M.H., 1999, Wall similarity in turbulence open-channel flow, ASCE Journal of Engineering Mechanics, Vol. 125, No. 7, pp 789-796

Lopez, Fabian, and Garcia, M.H., 2001, Risk of sediment erosion and suspension in turbulent flows, Journal of Hydraulic Engineering, Vol. 127, No. 3, pp 231-235

Lohrmann, Atle, Cabrera, Ramon, Gelfenbaum, Guy, and Haines, John, 1995, Direct measurements of Reynolds Stress with an acoustic Doppler Velocimeter, Proceedings IEEE 5th Working Conference on Current Meters, pp 205-210

Lovera, F. and Kennedy, J.F., 1969, Friction factors for flat-bed flows in sand channels, Journal of Hydraulics Division, Vol. 95, No. HY4, pp 1227-1234

Lyn, D.A., 1993, Turbulence measurements in open-channel flows over artificial bed forms, Journal of Hydraulic Engineering, Vol. 119, pp 306-326

M. Spasojevic, F. M. Holly Jr., 1994. Three-Dimensional Numerical Simulation of Mobile-Bed Hydrodynamics. Contract Report HL-94-2, US Army Corps of Engineers, Waterways Experiment Station, August 1994.

Mahmood, K., 1971, Flow in sand-bed channels, Water Management Technical Report 11, Colorado State University, Fort Collins, CO

Manning, R., 1889, On the flow of water in open channels and pipes, Transactions, Institution of Civil Engineers of Ireland, 20, pp 161-207

Matthes, G.H., 1947, Macroturbulence in natural stream flow, Transaction of the American Geophysical Union, Vol. 28, No. 2, pp 255-265

Meselhe E.., Mader C., McCorquodale A., Habib E., Georgiou I. 2005, Hydro-Ecological Modeling of the Lower Mississippi River: Proceedings of the 14th Biennial Coastal Zone Conference, New Orleans, LA.

McQuivey, R.S., 1973A, Principles and measuring techniques of turbulence characteristics in open-channel flows, U.S. Geological Survey Professional Paper 802-A, 82 p.

McQuivey, R.S., 1973B, Summary of turbulence data from rivers, conveyance channels, and laboratory flumes, U.S. Geological Survey Professional Paper 802-B, 66 p.

Menduni, G. and Paris, E., 1986, On the prediction of geometric characteristics of dunes, Proceedings of the 3rd International Symposium on River Sedimentation, Jackson, Mississippi, March 31-April 4, 1986, pp 665-674

Meyer-Peter, E. and Muller, R., 1948, Formulas for bed-load transport, Proceedings 2nd Congress International Association of Hydraulic Research, Stockholm, June 1948

Moody, L.F., 1944, Friction factors for pipe flow, Transactions American Society of Mechanical Engineers, Vol. 66, pp 671-684

Muste, M. and Patel, V.C., 1997, Velocity profiles for particles and liquid in open-channel flow with suspended sediment, Journal of Hydraulic Engineering, Vol. 123, No. 9, pp 742-751

Naden, P. S., 1987, Modelling gravel-bed topography from sediment transport: Earth Surface Processes and Landforms, v. 12, p. 353–367.

Naden, P. S., and Brayshaw, A. C., 1987, Small- and medium-scale bedforms in gravel- ed rivers, in Richards, K., editor, River channels: environment and process: Oxford, United Kingdom, Basil Blackwell, 391 p.

Nelson, J.M. and Smith, J.D., 1989A, Flow in meandering channels with natural topography, in S. Ikeda and G. Parker, eds, River Meandering, Water Resources Monograph No. 12, American Geophysical Union, pp 69-102

Nelson, J.M. and Smith, J.D., 1989B, Mechanics of flow over ripples and dunes, Journal of Geophysical Research, Vol. 94, No. C6, pp 8146-8162

Nelson, J.M., McLean, S.R., and Wolfe, S.R., 1993, Mean flow and turbulence fields over two-dimensional bed forms, Water Resources Research, Vol. 29, No. 12, pp 3935-3953.

Nezu, Iehisa and Rodi, Wolfgang, 1986, Open-channel flow measurements with a laser Doppler anemometer, Journal of Hydraulic Engineering, Vol. 112, No. 5, pp 335-355

Nezu, Iehisa and Nakagawa, Hiroji, 1993, Turbulence in open-channel flows, IAHR Monograph Series, A.A. Balkema Publishers, Rotterdam, Netherlands, 281 p.

Nikuradse, J., 1932, Gesetzmassigkeiten der turbulenten Stomung in glatten Rohren, Forsch. Geb. Ing.-Wes., Heft 356, Berlin (in German)

Nikuradse, J., 1933, Stromungsgesetze in rauhen Rohren, Forschungsheft No. 361, Verein Deutscher Ingenieure, Berlin (translated into English as NACA TM 1292, Nov. 1950), 62 p.

Nino, Yarko and Garcia, M.H., 1996, Experiments on particle-turbulence interactions in the near-wall region of an open channel flow: Implications for sediment transport, Journal of Fluid Mechanics, Vol. 326, pp 285-319

Nordin, Jr., C.F., 1964, Aspects of flow resistance and sediment transport: Rio Grande near Bernalillo, New Mexico, U.S. Geological Survey Water Supply Paper 1498H, 41 p.

Nordin, Jr., C.F., and Dempster, G.R., 1963, Vertical distribution of velocity and suspended sediment, Middle Rio Grande, New Mexico, U.S. Geological Survey Professional Paper 462-B, 20 p.

Nordin, Jr., C.F. and Algert, J.A., 1965, Geometrical properties of sand waves, Discussion, Journal of Hydraulics Division, Vol. 91, No. HY5,

Nordin, Jr., C.F. and Algert, J.A.,1966, Spectral analysis of sand waves, Transactions of the American Society of Civil Engineers, Vol. 92, No. HY5, pp 95-114

Nystrom, E.A., 1999, Applicability of acoustic Doppler profilers to measurement of mean velocity and turbulence parameters, M.S. Thesis, University of Illinois at Urbana-Champaign, 175 p

Nystrom, E.A., Oberg, K.A., and Rehmann, C.R., 2001, Measurement of turbulence with acoustic Doppler current profilers—sources of error and laboratory results, Proceedings Hydraulic Measurements and Experimental Methods Conference sponsored by ASCE and IAHR, Estes Park, Colorado, July 28-August 1, 2002, 10 p.

Nystrom, E.A., Oberg, K.A., and Rehmann, C.R., In Press, Measurement of mean velocity and turbulence with ADCP's, submitted to ASCE Journal of Hydraulic Engineering

Ogink, H.J.M, 1989, Hydraulic roughness of single and compound bed forms, Part XI, Report on Model Investigations, A36, Delft Hydraulics, Emmeloord, The Netherlands

Olsen NRB, Stokseth S. 1995. Three-dimensional numerical modelling of water flow in a river with large bed roughness. Journal of Hydraulic Research 33: 571-581

Orgis, H., 1974, Geschiebebetrieb und Bettbildung, Österreichische Ingenieur-Zeitschrift, 17. Jahrgang, Heft 9, pp 285-292

Owen, P.R., 1964, Saltation of uniform grains in air, Journal of Fluid Mechanics, Vol. 20, No. 2

Parker, G., Garcia, M.H., Fukushima, Y., and Yu, W., 1987, Experiments on turbidity currents over an erodible bed, Journal of Hydraulic Research, 25 (1): pp 123-147

Pedlosky, J .E. (1979). Geophysical Fluid Dynamics. Sringer-Veriag New York, Inc., New York, N.Y.

Perry, A., Schofield, W., and Joubert, P., 1969, Rough wall turbulent boundary layers, Journal of Fluid Mechanics, Vol. 37, Part 2, pp 383-413

Peters, J.J., 1978, Discharge and sand transport in the braided zone of the Zaire Estuary, Netherlands Journal of Sea Research, Vol.. 12 (3/4) pp 273-292

Prandtl, Ludwig, 1904, Ueber Flussigkeitsbewegung bei sehr kleiner Reibung, Proceedings 3rd International Congress of Mathematics, Heidelberg, pp 484-491

Prandtl, Ludwig, 1925, Uber die ausgebildete Turbulenz, ZAMM 5, pp 136-139, also found published in 1926, Proceedings of the 2nd International Congress Applied Mechanics, Zurich pp 62-75

Prony, R. de, 1804, Recherches Physico-Mathematiques sur la Theorie des Eaux Courantes, Paris, 1804

Ranga Raju, K.G. and Soni, J.P., 1976, Geometry of ripples and dunes in alluvial channels, Journal of Hydraulic Research, IAHR, Vol. 14, No. 3,

Raudkivi, A.J., 1990, Loose boundary hydraulics, 3rd Edition, Pergamon Press, Oxford, England, 537 p.

Raudkivi, A.J., 1997, Ripples on stream bed, Journal of Hydraulic Engineering, Vol. 123, No. 1, pp 58-64

Rayner, J. N., 1971, An introduction to spectral analysis: London, Pion, Ltd., 174 p.

Richards, K.J., 1980, The formation of ripples and dunes on an erodible bed, Journal of Fluid Mechanics, Vol. 99, pp 597-618.

Rouse, Hunter, 1943, Evaluation of boundary roughness, Proceedings, 2nd Annual Hydraulics Conference, Iowa City, 1942, Bulletin 27, Iowa Studies in Engineering.

Rouse, Hunter, 1946, Elementary Mechanics of Fluids, John Wiley and Sons, Inc., New York, 376 p.

Rouse, Hunter, 1957, Modern conceptions of the mechanics of turbulence, Transactions of the American Society of Civil Engineers, Volume 102,

Rouse, Huner, 1959, Advanced Mechanics of Fluids, John Wiley and Sons, New York, 444 p.

Rouse, Hunter, 1965, Critical Analysis of Open-Channel Resistance, Journal of Hydraulics Division, American Society of Civil Engineers, v. 91, no. HY4, July 1965, pp.1-25.

Rouse, Hunter and Ince, S, 1963, History of Hydraulics, Dover Publications, New York

Sabersky, R.H., Acosta, A.J., and Hauptmann, E.G., 1989, Fluid Flow, 3rd Edition, McMillan Publishing, New York, 537 p

Sarma, K.V.N., Lakshminarayana, P., and Rao, N.S.L., 1983, Velocity distribution in smooth rectangular channels, Journal of Hydraulic Engineering, Vol. 109, pp 270-289

Schemper, T.J. and Admiraal, D.M., 2002, An examination of the application of acoustic Doppler current profiler measurements in a wide channel of uniform depth for turbulence calculations, Proceedings Hydraulic Measurements and Experimental Methods Conference sponsored by ASCE and IAHR, Estes Park, Colorado, July 28-August 1, 2002, 9 p.

Schlicting, Hermann, 1979, Boundary-layer theory, 7th Edition, McGraw-Hill Books, New York, 817 p.

Scott, C.H. and Stephens, H.D., 1966, Special sediment investigations Mississippi River at St. Louis, Missouri, 1961-1963, U.S. Geological Survey Water-Supply Paper 1819-J, 35 p.

Shen, H.W., 1962, Development of bed roughness in alluvial channels, Journal of the Hydraulics Division, Vol. 88, No. HY3, pp 45-58

Shen, H.W., Mellema, W.J., and Harrison, A.S., 1978, Temperature and Missouri River stages near Omaha, Journal of the Hydraulics Division, Vol. 104, No. HY1, pp 1-20

Shen, H.W., Fehlman, H.M., and Mendoza, Cesar, 1990, Bed form resistances in open channel flows, Journal of Hydraulic Engineering, Vol. 116, No. 6, pp 799-815

Shields, A., 1936, Anwendung der aenlichkeitsmechanik und der turbulenzforschung auf die geschiebebewegung, Mitteilungen der Preussischen Versuchsanstalt fur Wasserbau und Schiffbau, Berlin, Germany, translated to English b W.P. Ott and J.C. van Uchelen, California Institute of Technology, Pasadena, California.

Simons, D.B., Richardson, E.V., and Albertson, M.L., 1961, Flume studies using medium sand (0.45mm), U.S. Geological Survey Water Supply Paper 1498-A, 76 p.

Simons, D.B. and Richardson, E.V., 1961, Forms of Bed Roughness in Alluvial Channels, Transactions of the American Society of Civil Engineers, Vol. 87, No. HY3, pp 87-106

Simons, D.B., Richardson, E.V., and Nordin, C.F., 1965, Bedload equation for ripples and dunes, U.S. Geological Survey Professional Paper 462-H, 9 p.

Simons, D.B., Richardson, E.V., and Nordin,C.F., 1965A, Sedimentary structures generated by flow in alluvial channels, American Association of Petroleum Geologists, Special Publication No. 12

Simons, D.B., and Richardson, E.V., 1966, Resistance to flow in alluvial channels, U.S. Geological Survey Professional Paper 422-J, 61 p.

Simons, D.B. and Senturk, Fuat, 1977, Sediment transport technology, Water Resources Publications, Ft. Collins, Colorado, 897 p.

Sinha, S.K., Sotiropoulos, F., Odgaard, A.J., 1998, Three-Dimensional Numerical Model for Flow through Natural Rivers, J. Hydr. Eng., Vol. 124, No. 1, pp. 13-24.

Smagorinsky, J. 1963 General circulation experiments with the primitive equations: I. The basic experiment. Mon. Weather Rev. 91, 99–164.

Smith, J.D. and McLean, S.R., 1977, Spatially averaged flow over a wavy surface, Journal of Geophysical Research, Volume 82, Number 12, pp 1735-1746.

Song, T. and Graf, W.H., 1996, Velocity and turbulence distribution in unsteady open-channel flows, Journal of Hydraulic Engineering, Vol. 122, No. 3, pp 141-154

Soulsby, R.L. and Dyer, K.R., 1981, The form of the near-bed velocity profile in tidally accelerating flow, Journal of Geophysical Research, Vol. 86, pp 8067-8074.

Speight, J. G., 1965, Meander spectra of the Angabunga River: Journal of Hydrology, v. 3, p. 1–15.

Stacey, M.T. and Monismith, S.G., 1997, Measuring estuarine turbulence with an ADCP, Proceedings Congress of the IAHR, Vol. B, Part 1, pp 155-160

Stacey, M.T., Monismith, S.G., and Burau, J.R., 1999, Measurements of Reynolds stress profiles in unstratified tidal flow, Journal of Geophysical Research, Vol. 104, No. C9, pp 10933-10949

Stapleton, K.R. and Huntley, D.A., 1995, Seabed stress determination using the inertial dissipation method and the turbulent kinetic energy method, Earth Surface Processes and Landforms, Vol. 20, pp 807-815

Straub, L.G., Anderson, A.G., and Flammer, G.H., 1958, Experiments on the influence of temperature on the sediment load, Missouri River Division Sediment Series Number 10, U.S. Army Engineer Division, Missouri River, Omaha, Nebraska

Strickler, A., 1923, Beitrage zur Frage der Geschwindigheits-formel und der Rauhigkeitszahlen fur Strome, Kanale und geschlossene Leitungen, (Some contributions to the problem of the velocity formula and roughness factors for rivers, canals, and closed conduits),

Mitteilungen des eidgenossischen Amtes fur Wasserwirtschaft, Bern, Switzerland, no. 16

Stronach, J.A., Backhaus, J.O., and Murty, T.S. (1993). An update on the numerical simulation of the waters between Vancouver Island and the mainland: the GF8 model. Oceanography and Marine Biology Annual Review. 31, 1-86.

Sutherland, A.J., 1967, Proposed mechanism for sediment entrainment by turbulent flows, Journal of Geophysical Research, Vol. 72, No. 24, pp 6183-6194

Swamee, P.K., 1993, Generalized inner region velocity distribution equation, Journal of Hydraulic Engineering, ASCE. Vol. 119, No. 5, pp 651-656

Thompson, S.M., and Campbell, P.L., 1979, Hydraulics of a large channel paved with boulders, Journal of Hydraulic Research, IAHR, Vol. 17, No. 4, pp 341-354

Toffaleti, F.B., 1968, A procedure for computation of the total river sand discharge and detailed distribution bed to surface, U.S. Army Corps of Engineers, Committee on Channel Stabilization Technical Report 5

Tracy, H.J. and Lester, C.M., 1961, Resistance coefficients and velocity distribution smooth rectangular channel, U.S. Geological Survey Water Supply Paper 1592-A, 18p

Tsai, Chih-Heng and Tsai, Chang-Tai, 2000, Velocity and concentration distributions of sediment-laden open channel flow, Journal of the American Water Resources Association, Vol. 36, No. 5, pp 1075-1086

U.S. Army Corps of Engineers, 1935, Waterways Experiment Station Paper 17 1−161

U.S. Army Corps of Engineers, 1967, Missouri River channel regime studies, Missouri River Division Sediment Series Report No. 13, Omaha, Nebraska

U.S. Army Corps of Engineers, 1968, Missouri River channel regime studies, Missouri River Division Sediment Series Report No. 13A, Omaha, Nebraska

U.S. Army Corps of Engineers, 1969, Missouri River channel regime studies, Missouri River Division Sediment Series Report No. 13B, Omaha, Nebraska

Van Rijn, L.C., 1982A, Equivalent roughness of alluvial bed, Journal of the Hydraulics Division, Vol. 108, No. HY10, pp 1215-1218

Van Rijn, L.C., 1982B, The prediction of bedforms, alluvial roughness, and sediment transport, Research Report, Delft Hydraulics Laboratory, S 484

Van Rijn, L.C., 1984A, Sediment transport, Part I: bed load transport, Journal of Hydraulic Engineering, Volume 110, Number 10, pp 1431-1456.

Van Rijn, L.C., 1984B, Sediment transport, Part II: suspended load transport, Journal of Hydraulic Engineering, Volume 110, Number 11, pp 1613-1641.

Van Rijn, L.C., 1984C, Sediment transport, Part III: bed forms and alluvial roughness, Journal of Hydraulic Engineering, Volume 110, Number 12, pp 1733-1754.

Van Rijn, L.C., 1984D, Sediment pick-up functions, Journal of Hydraulic Engineering, Vol. 110, No. 10, pp 1494-1502.

Vanoni, V.A., 1946, Transportation of suspended sediment by water: American Society of Civil Engineers Transaction Vol. 3, pp 67-133.

Vanoni, V.A., 1974, Factors determining bed forms of alluvial streams, Journal of the Hydraulics Division, Vol. 100, No. HY3, pp 363-377.

Vanoni, V.A., 1975, Sedimentation Engineering, American Society of Civil Engineers Manual 54, New York, 745 p.

Vanoni, V.A. and Brooks, N.H., 1957, Laboratory studies of the roughness and suspended load of alluvial streams, Sedimentation Laboratory Report No. E68, California Institute of Technology, Pasadena, California,

Vanoni, V.A. and Hwang, L.S., 1967, Relation between bed forms and friction in streams, Journal of the Hydraulics Division, Vol. 93, No. HY3, pp 121-144

Velikanov, M.A., 1955, Dynamics of Alluvial Streams, Volume II Sediment and Bed Flow, State Publishing House for Physico-Mathematical Literature, Moscow

Vittal, V.A., Ranga Raju, K.G., and Garde, R.J., 1977, Resistance of two-dimensional triangular roughness, Journal of Hydraulic Research, Vol. 15, No. 1, pp 19-36

Von Karman, Theodore, 1931, Mechanische Ahnlichkeit und Turbulenz, NACA Tech. Memo N0. 611

Voulgaris, G. and Trowbridge, J.H., 1998, Evaluation of the acoustic Doppler velocimeters (ADV) for turbulence measurements, Journal of Atmospheric and Oceanic Technology, Vol. 15, pp 272-289

Wang, 1981, Rivers, three-dimensional phenomena in straight flumes with mobile bed. Effect on resistance to flow and sediment transport, Delft Hydraulics Laboratory, TOW R657-XXVII

Weisbach, J., 1845, Lehrbuch der Ingenieur-und Maschinen-Mechanik, 1st edition, Braunschweig, Germany

Whiting, P.J., and Dietrich, W.E., 1990, Boundary shear stress and roughness over mobile alluvial beds, Journal of Hydraulic Engineering, ASCE, Vol. 116, No. 12, pp 1495-1511

Wiberg, P.L. and Nelson, J.M., 1992, Unidirectional flow over asymmetric and symmetric ripples, Journal of Geophysical Research, Vol. 97, No. C8, pp 12745-12761

Wilcock, P.R., 1996, Estimating local bed shear stress from velocity observations, Water Resources Research, Vol. 32, No. 11, pp 3361-3366

Williams, P.B. and Kemp, P.H., 1971, Initiation of ripples on flat sediment beds, Journal of Hydraulics Division, ASCE, Vol. 92, No. 4, pp 505-522

Willis, J.C. and Kennedy, J.F., 1975, Sediment discharge of alluvial streams calculated from bedform statistics, Iowa Institute of Hydraulic Research Report No. 202, University of Iowa, Iowa City, Iowa,

Yalin, M.S., 1963, An expression for the bed-load transportation, Transactions of the American Society of Civil Engineers, Vol. 89, No. HY3,

Yalin, M.S., 1964, Geometrical properties of sand waves, Journal of Hydraulics Division, Vol. 90, No. 5, pp 105-120

Yalin, M.S., 1977A, Sediment Transport, 2nd Edition, Pergamon Press, Oxford, 298 p.

Yalin, M.S., 1977B, On the determination of ripple length, Journal of Hydraulics Division, Vol. 103, No. HY4, pp 439-442.

Yalin, M.S., 1985, On the determination of ripple geometry, Journal of Hydraulic Engineering, Vol. 111, No. 12??, pp 1148-1155.

Yalin, M.S., 1992, River Mechanics, Pergamon Press, Oxford, 220 p.

Yalin, M.S. and da Silva, A.M.F., 2001, Fluvial Processes, International Association of Hydraulic Engineering and Research Monograph, Delft, The Netherlands, 197 p

Yalin, M.S. and Karahan, E., 1979, Steepness of sedimentary dunes, Journal of Hydraulics Division, Vol. 105, No. HY4, pp 381-392

Yen, B.C., 1992, Hydraulic Resistance in Open Channels, in Channel Flow Resistance: Centennial of Manning's Formula, B.C. Yen, ed. , Water Resources Publications, Littleton, Colorado, pp 1-135

Zippe, H.J. and Graf, W.H., 1983, Turbulent boundary-layer flow over permeable and non-permeable rough surfaces, Journal of Hydraulic Engineering, Vol. 21, pp51-65

Znamenskaya, N.S., 1963, Experimental study of the dune movement of sediment, Transactions State Hydrologic Institute (Trudy GGI), No. 108

Znamenskaya, N.S., 1969, Morphological principle of modeling of river-bed processes, Proceedings 13th Congress International Association of Hydraulic Research, Kyoto, Vol. 5, No. 1 (referenced in Raudkivi, 1990)

Zyserman, J.A. and Fredsoe, J., 1994, Data analysis of bed concentration of suspended sediment, Journal of Hydraulic Engineering, Vol 120, No. 9, pp 10

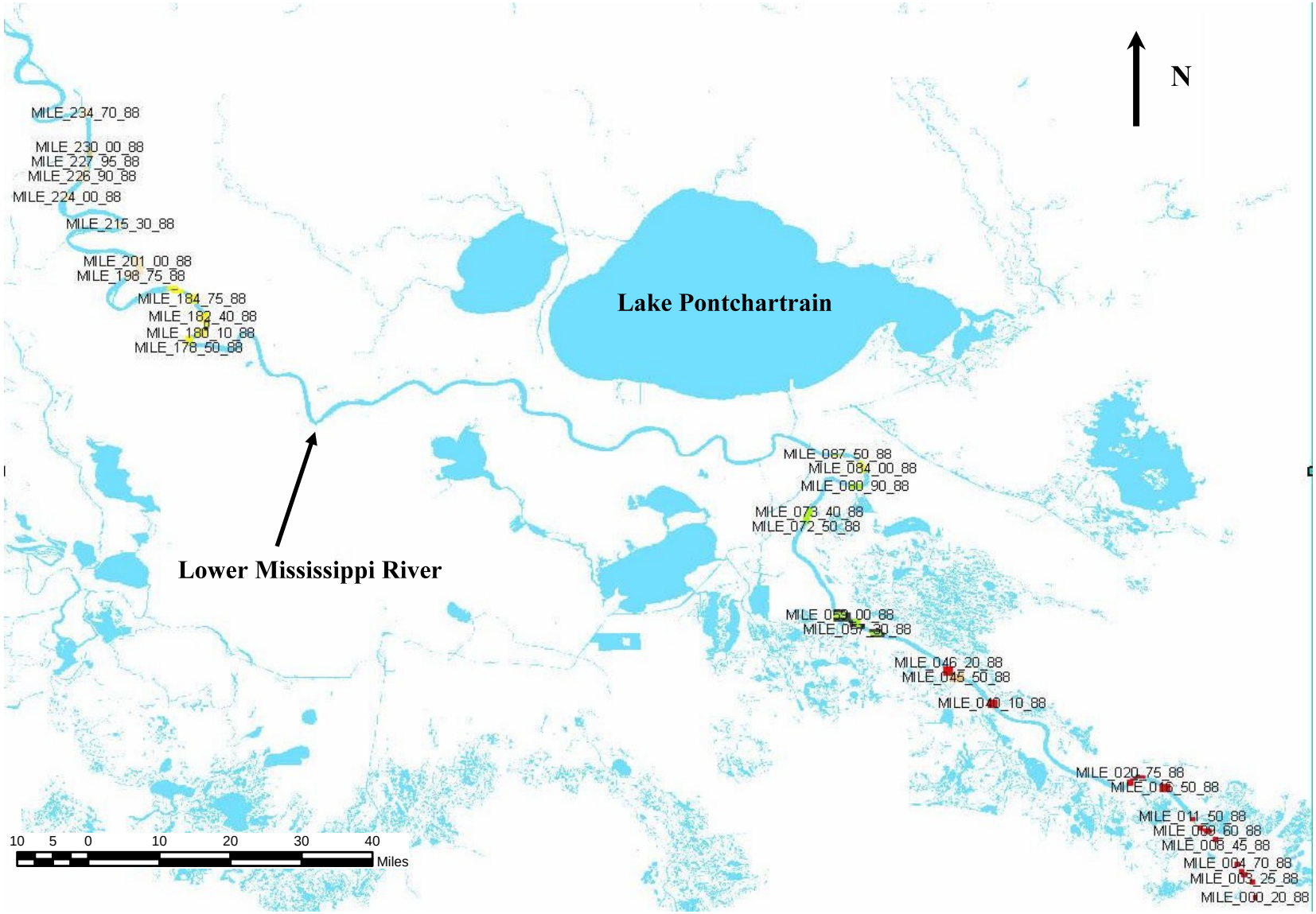

Figure A.1 Multibeam bathymetry data foot print

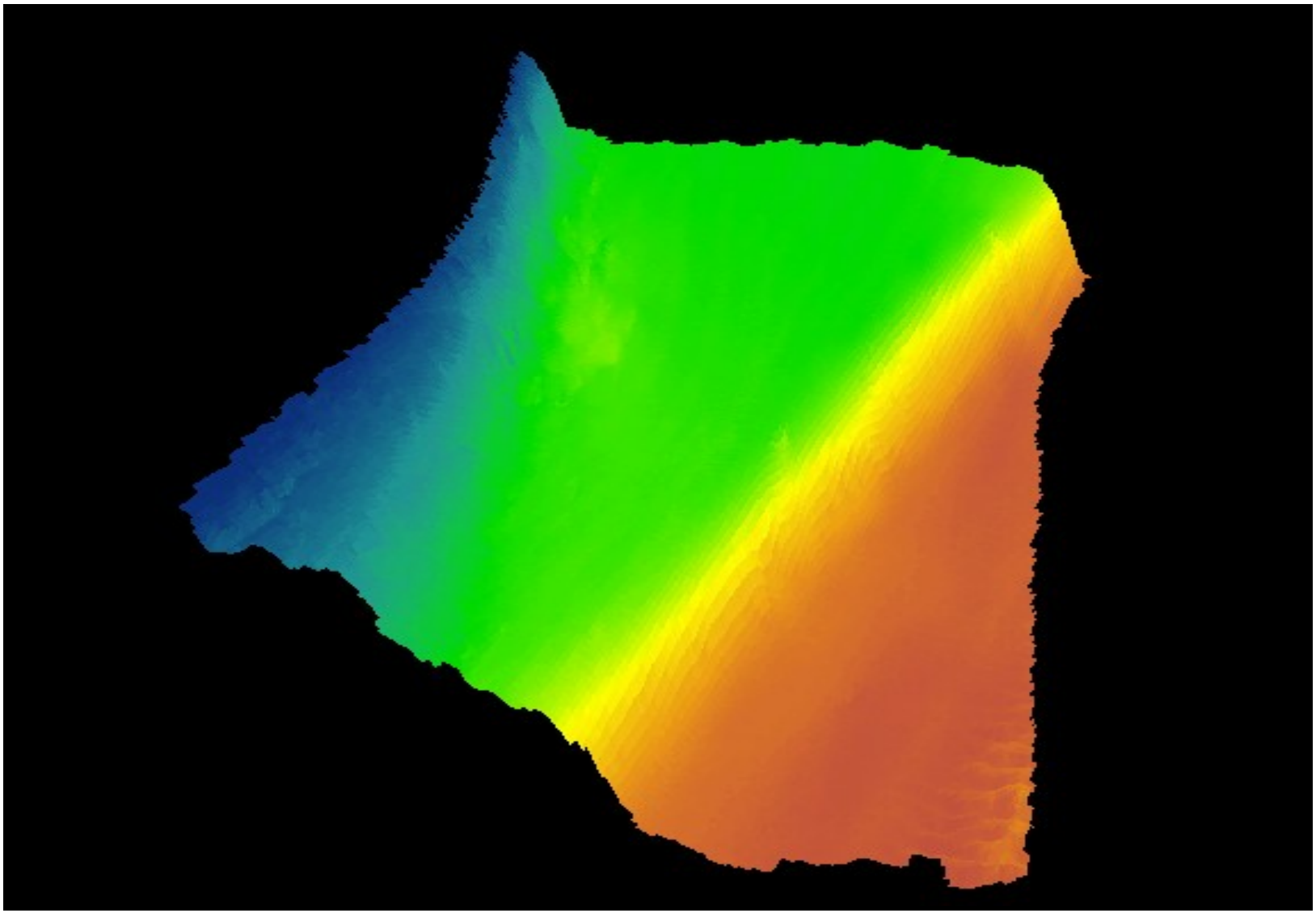

Figure A.2 3D view of multibeam at RM 0.22

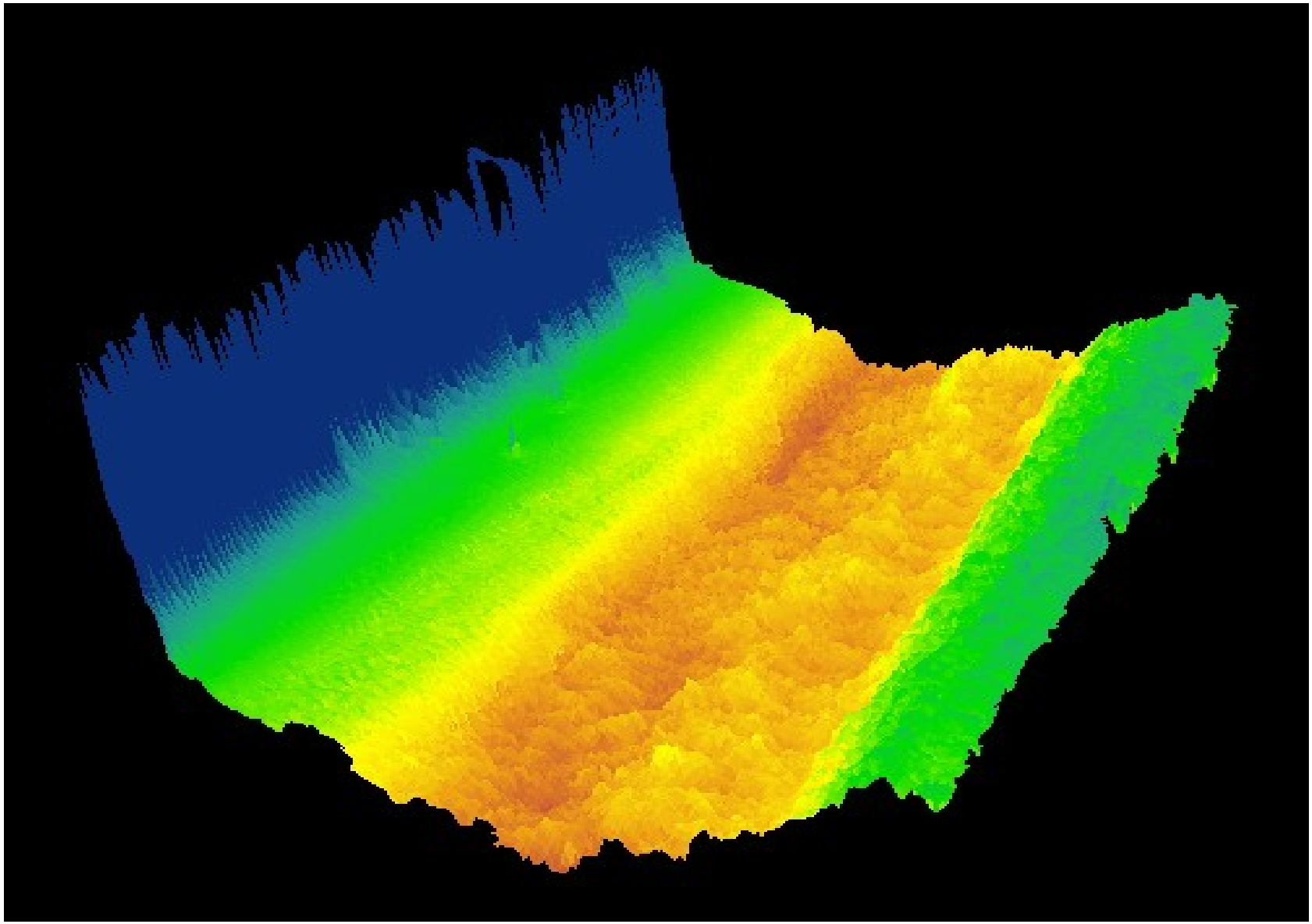

Figure A.3 3D view of multibeam at RM 2.25

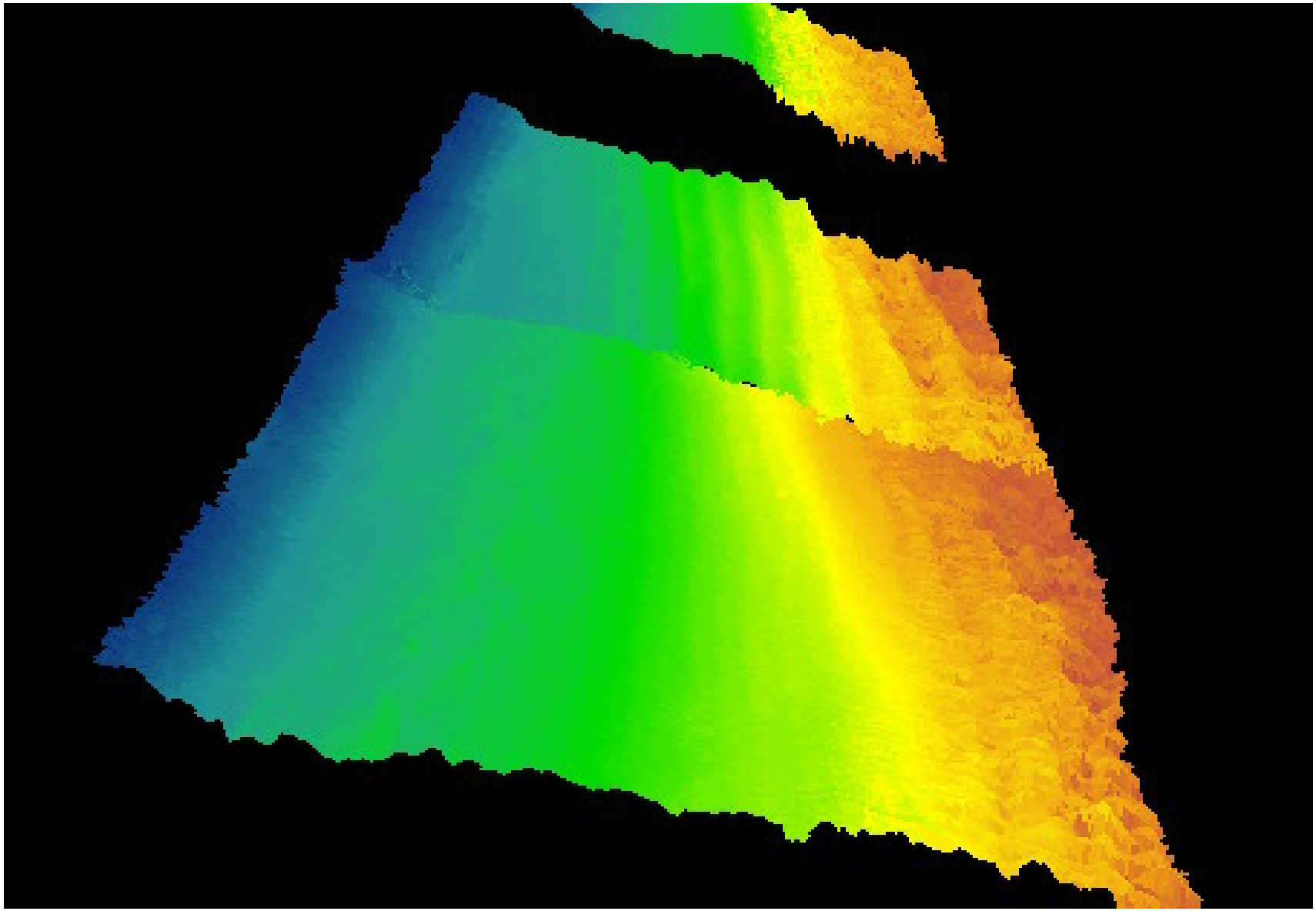

Figure A.4 3D view of multibeam at RM 3.25

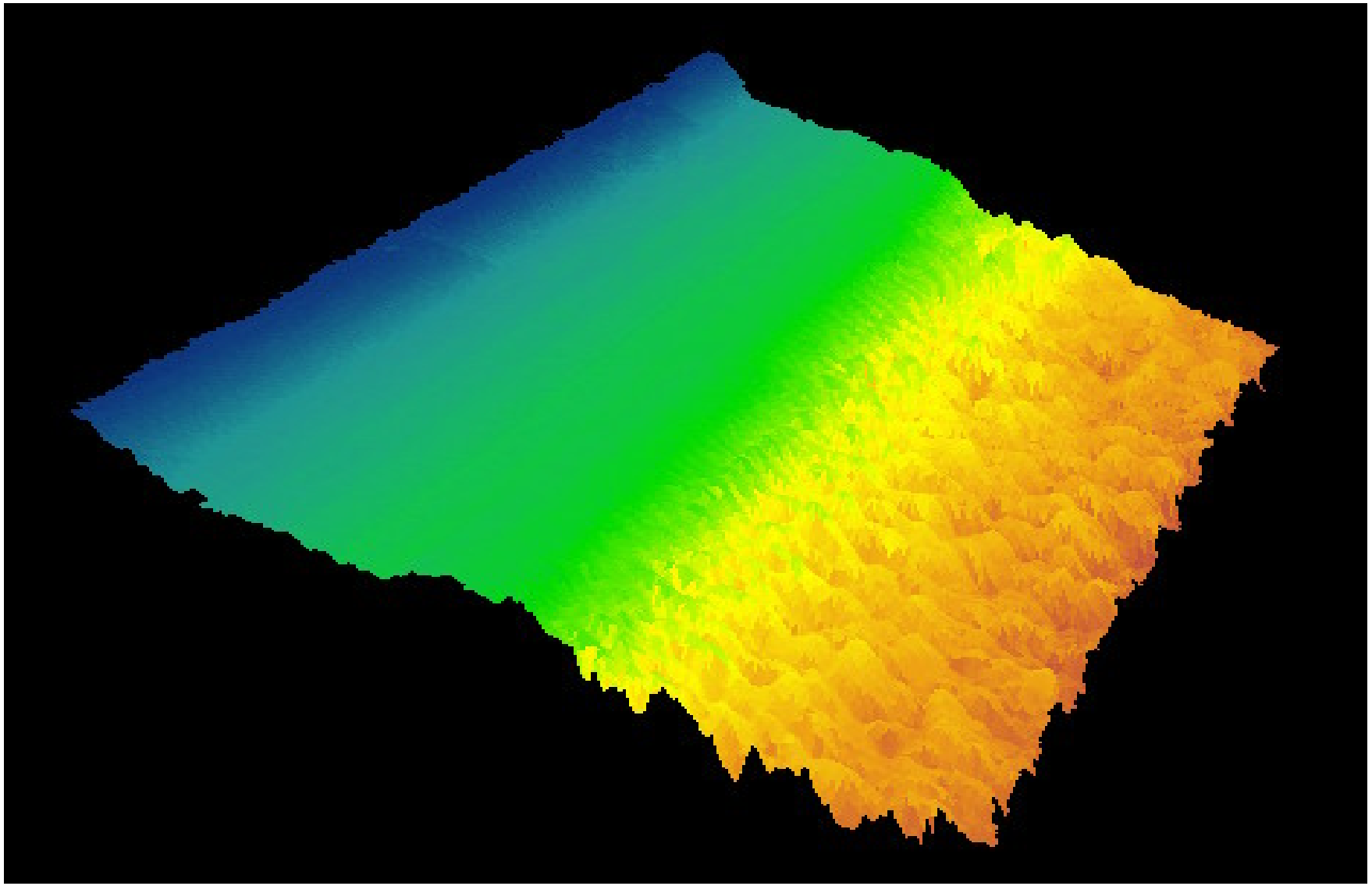

Figure A.5 3D view of multibeam at RM 4.70

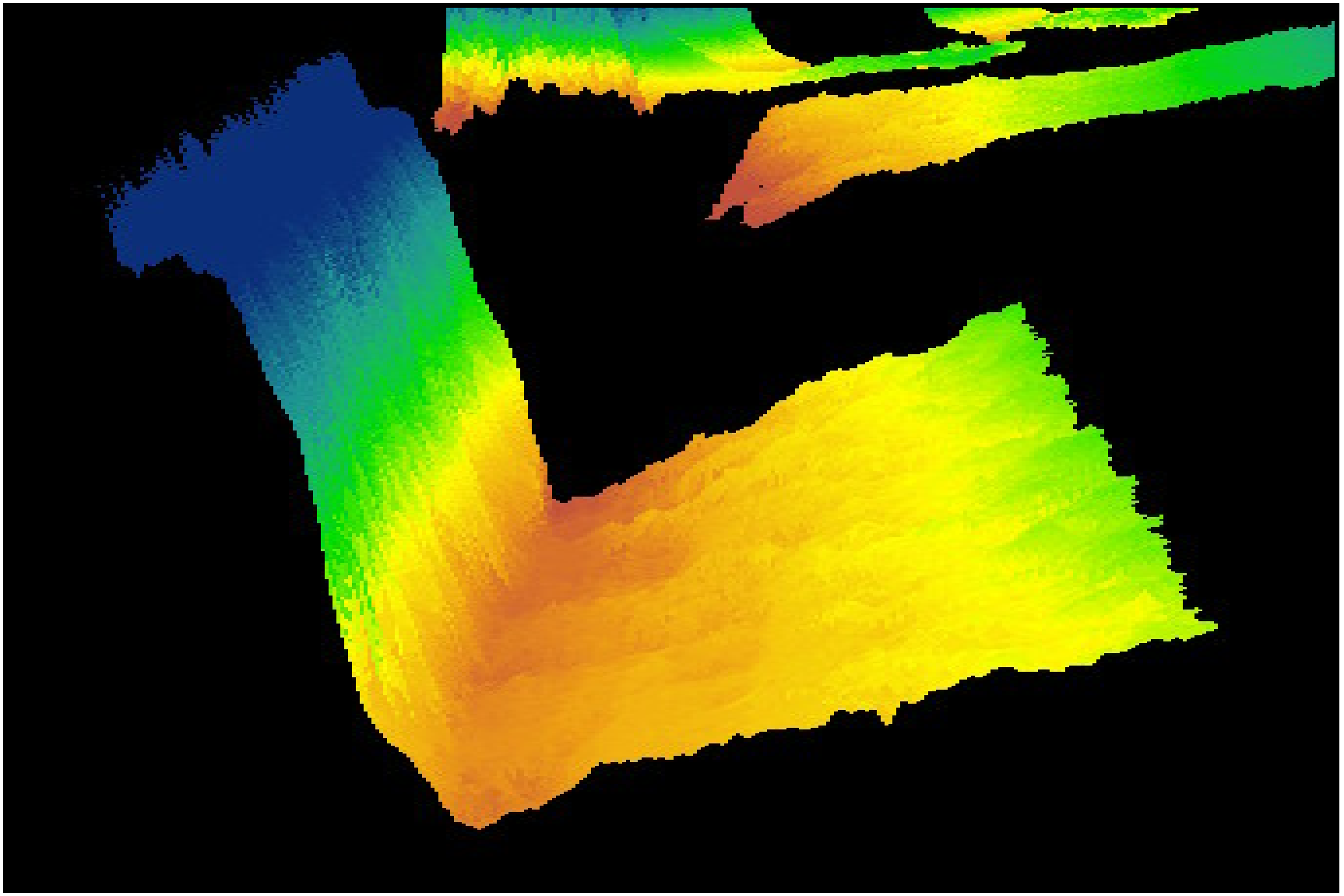

Figure A.6 3D view of multibeam at RM 8.45

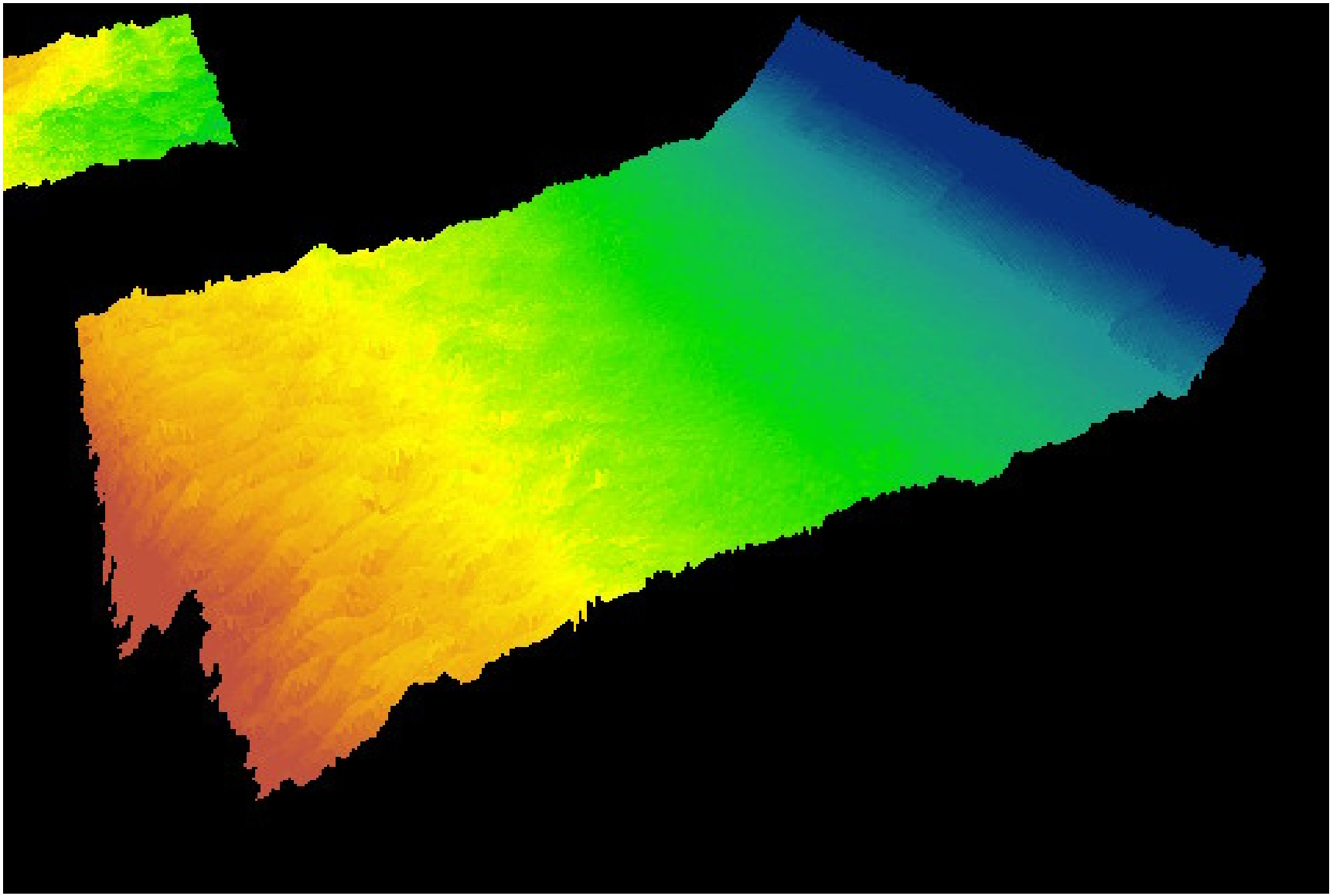

Figure A.7 3D view of multibeam at RM 9.60

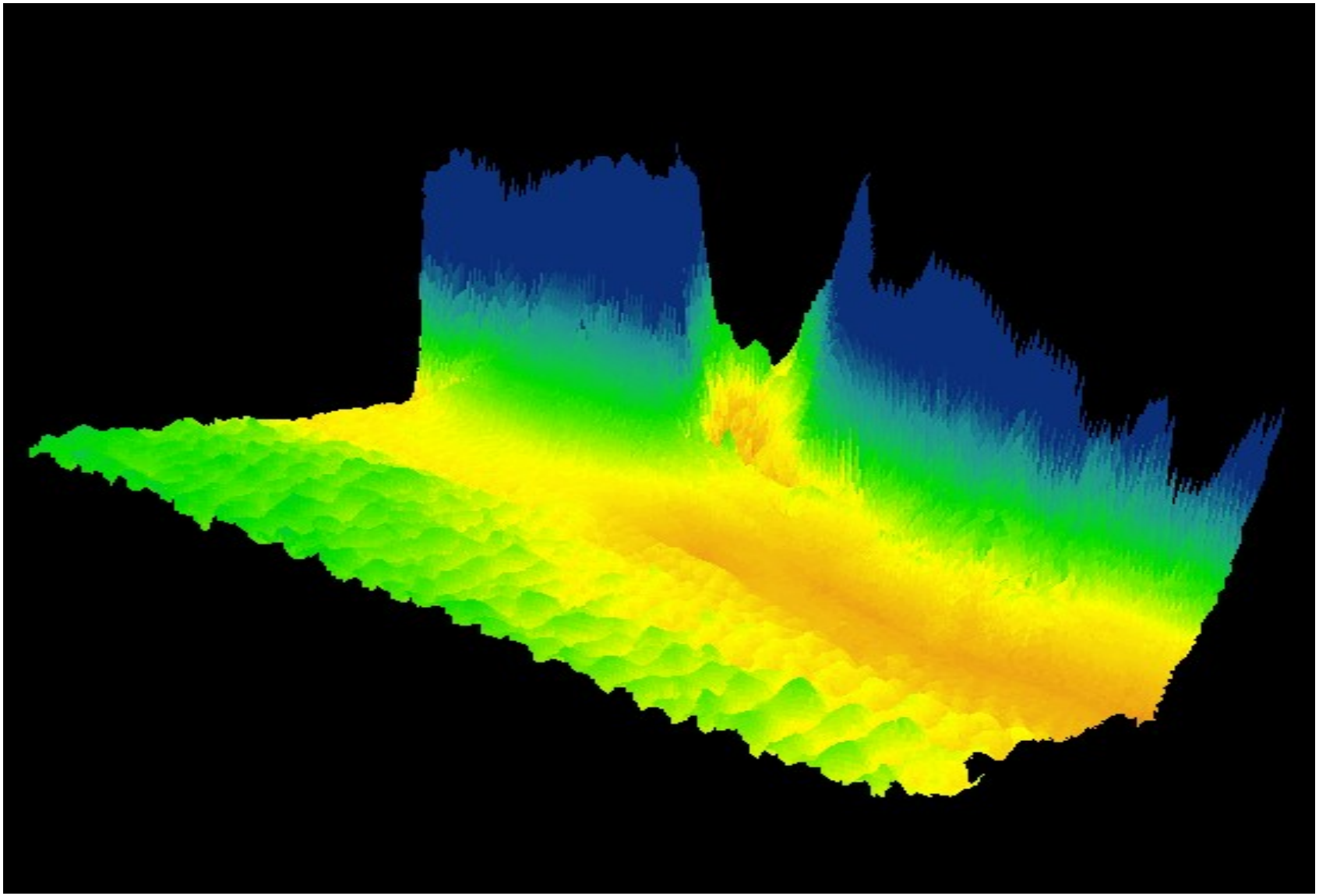

Figure A.8 3D view of multibeam at RM 10.50

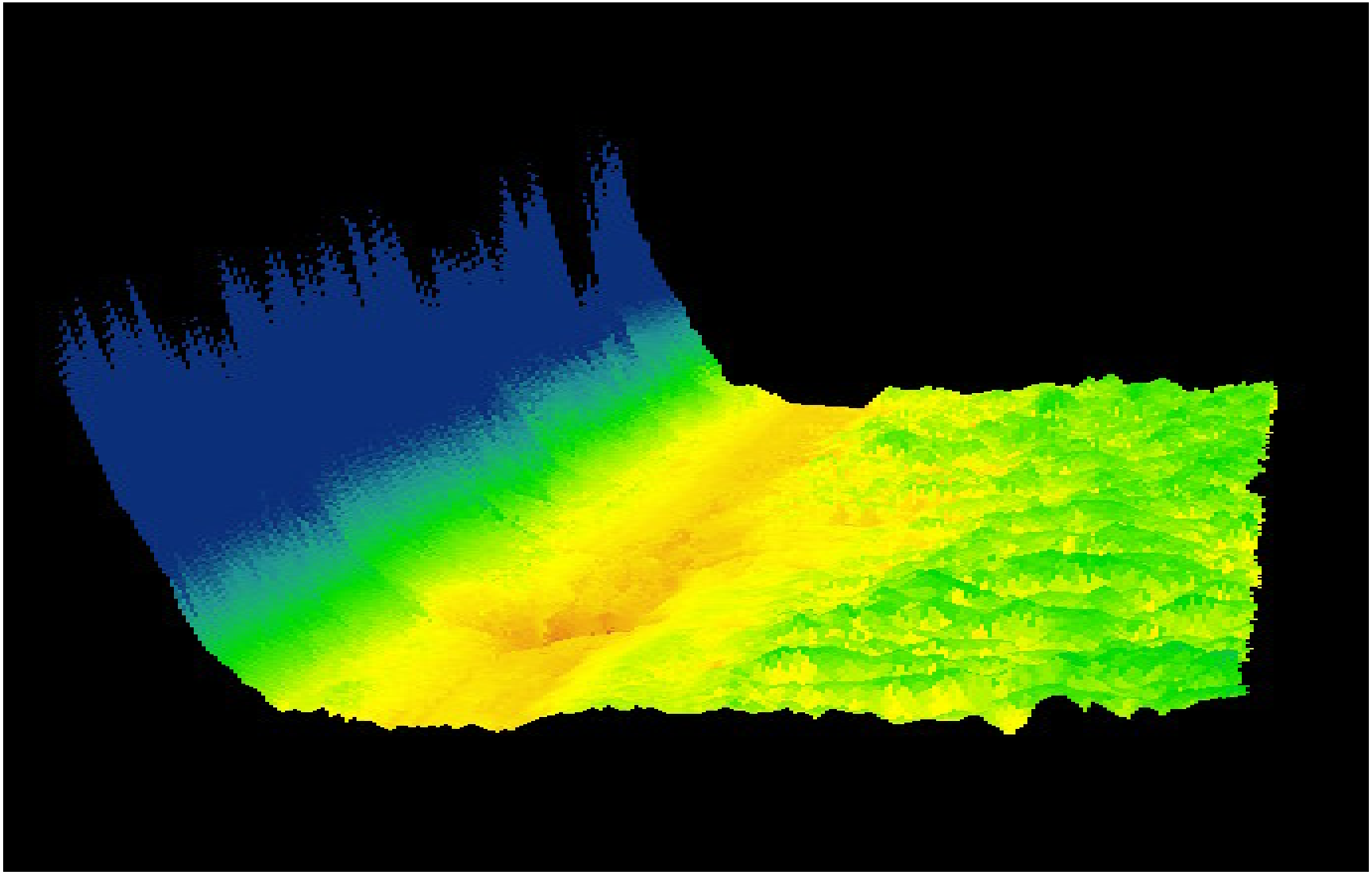

Figure A.9 3D view of multibeam at RM 11.50

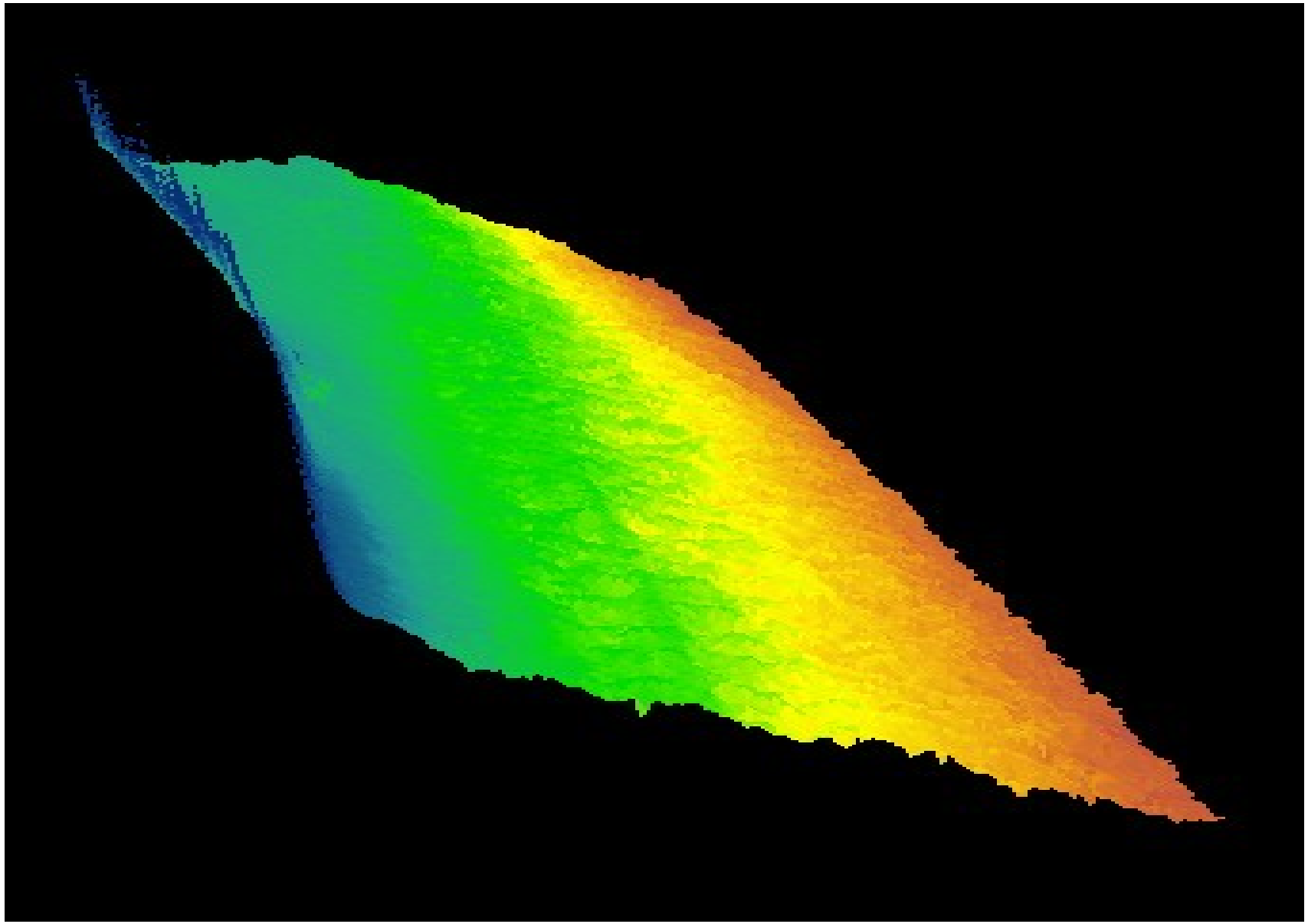

Figure A.10 3D view of multibeam at RM 15.50

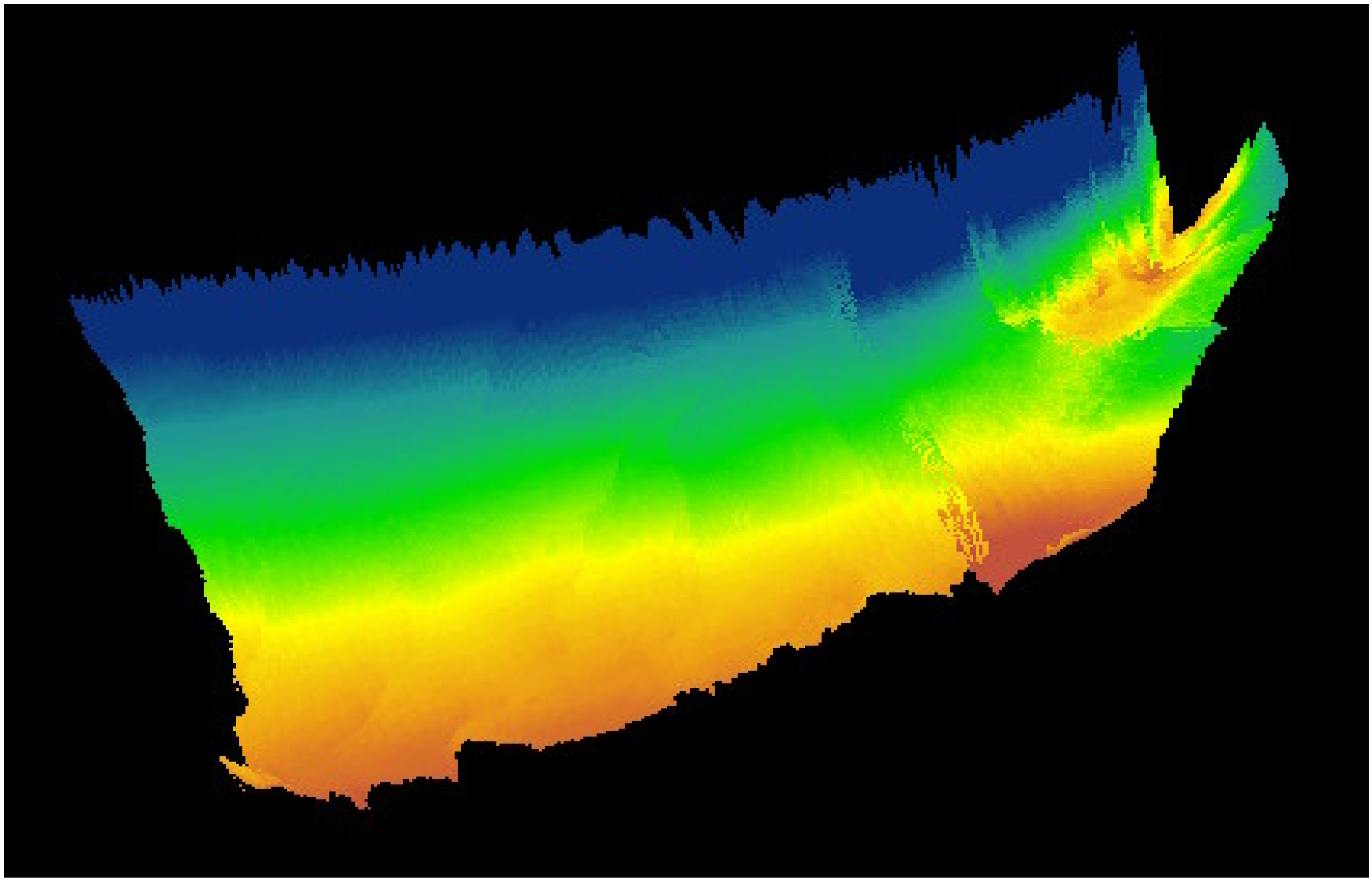

Figure A.11 3D view of multibeam at RM 19.20

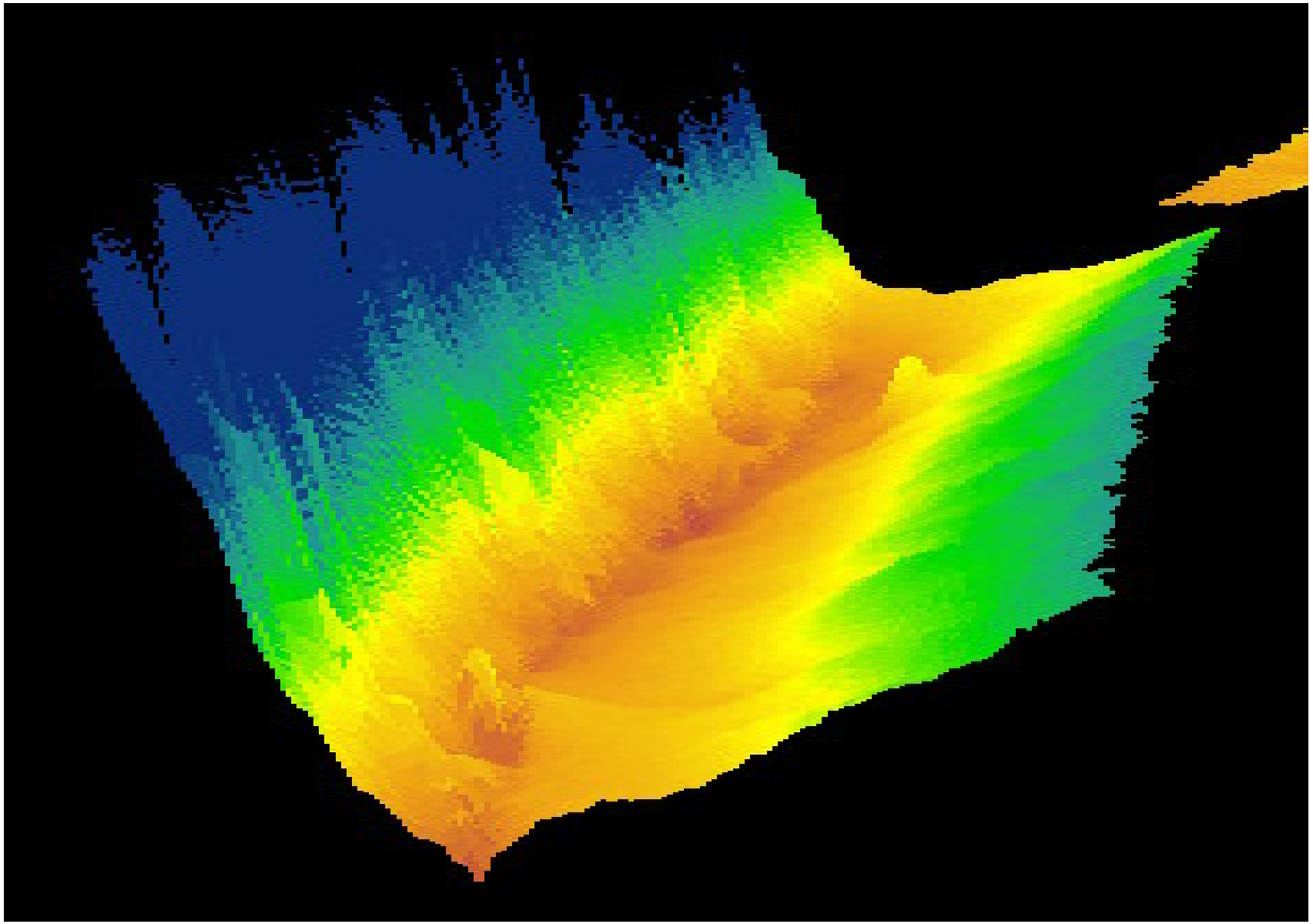

Figure A.12 3D view of multibeam at RM 38.75

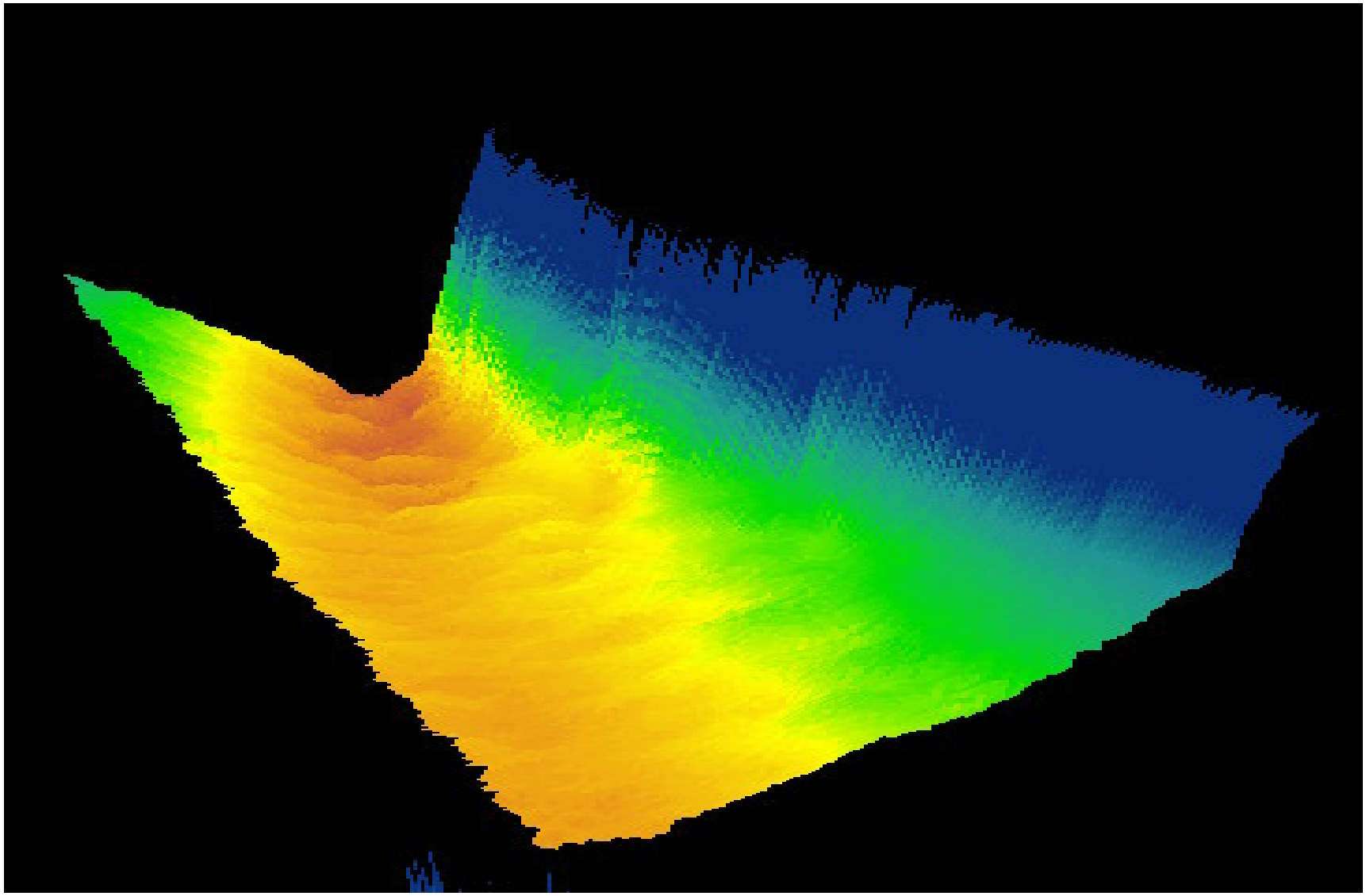

Figure A.13 3D view of multibeam at RM 40.10

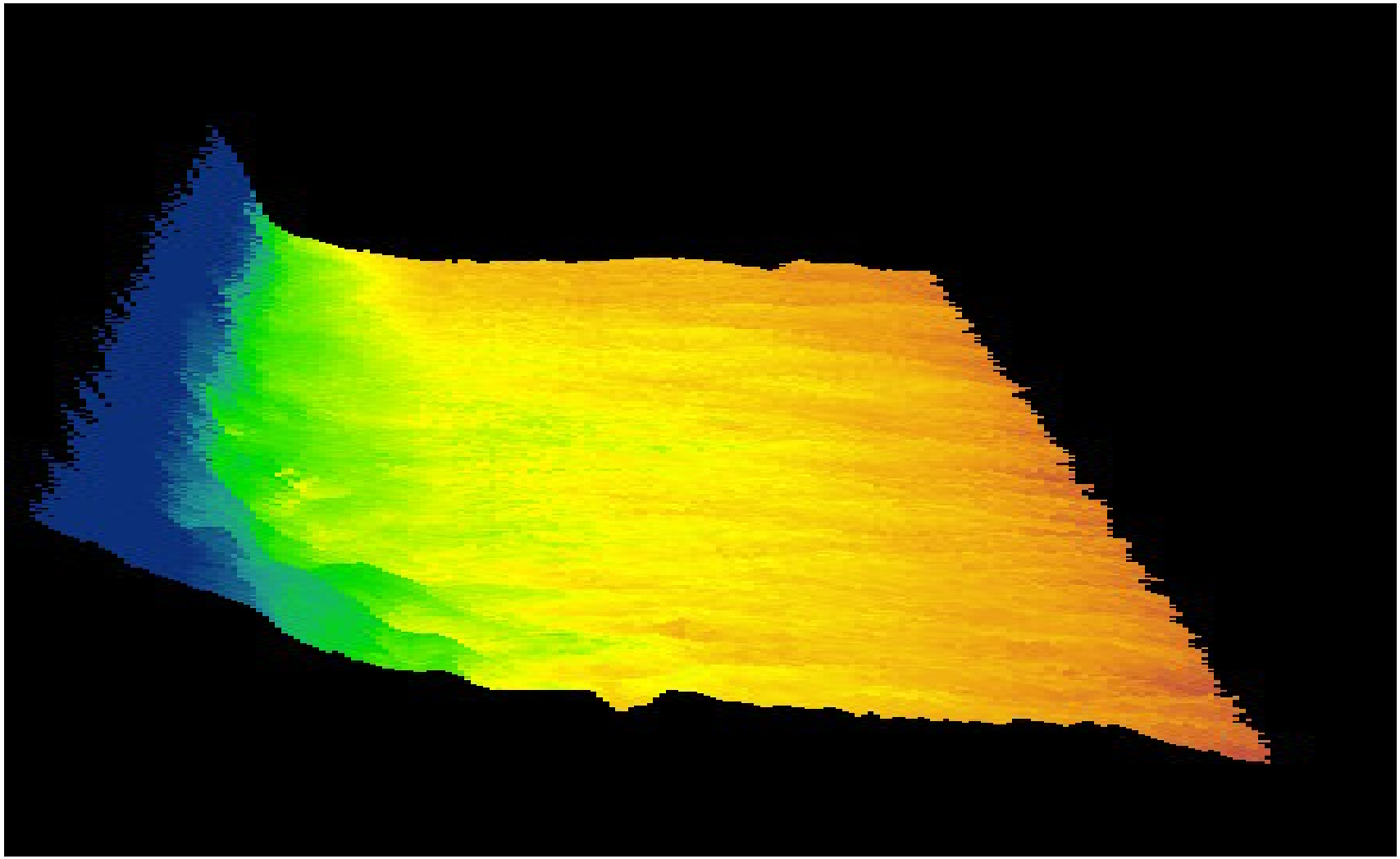

Figure A.14 3D view of multibeam at RM 46.20

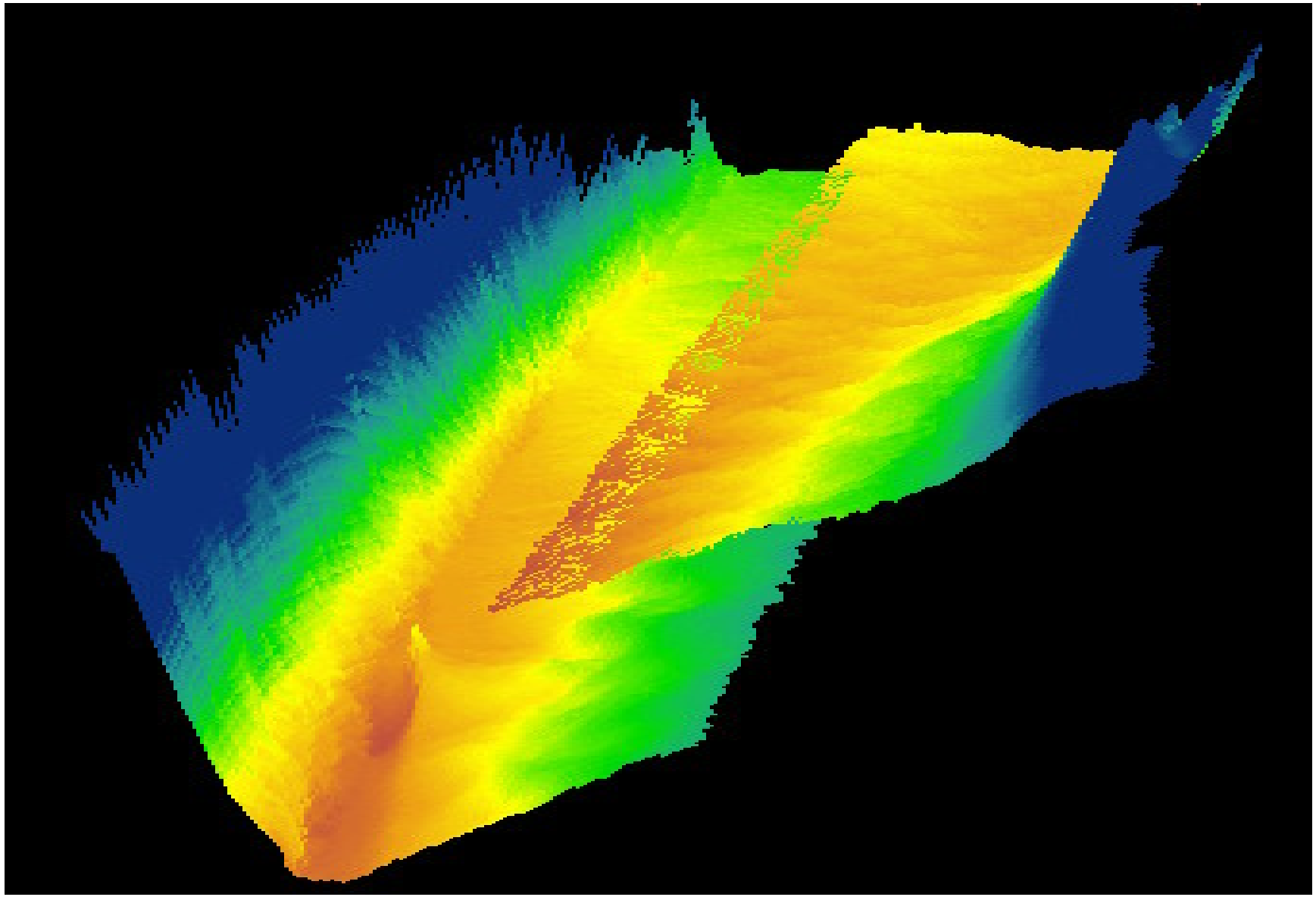

Figure A.15 3D view of multibeam at RM 54.00

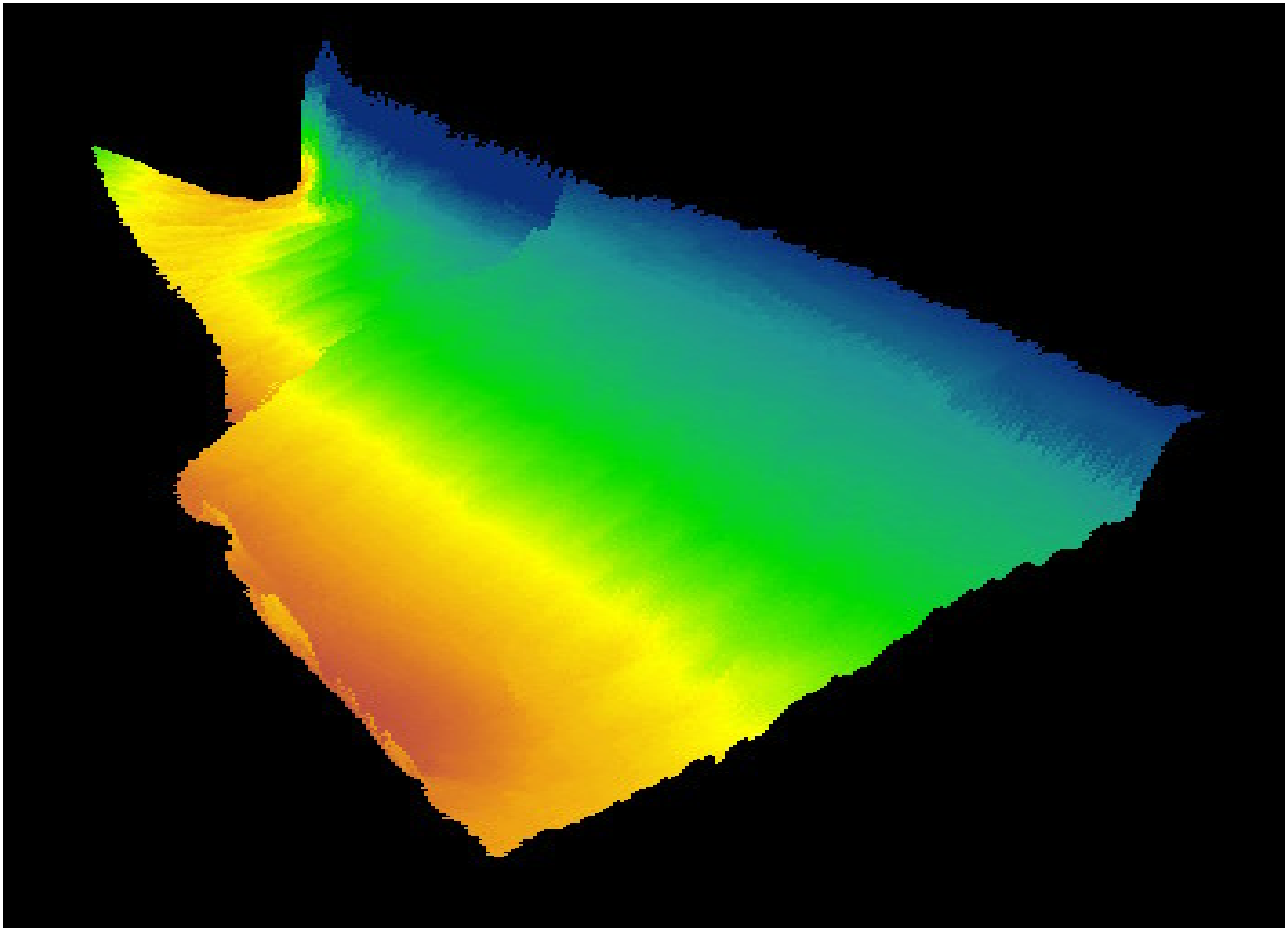

Figure A.16 3D view of multibeam at RM 72.00

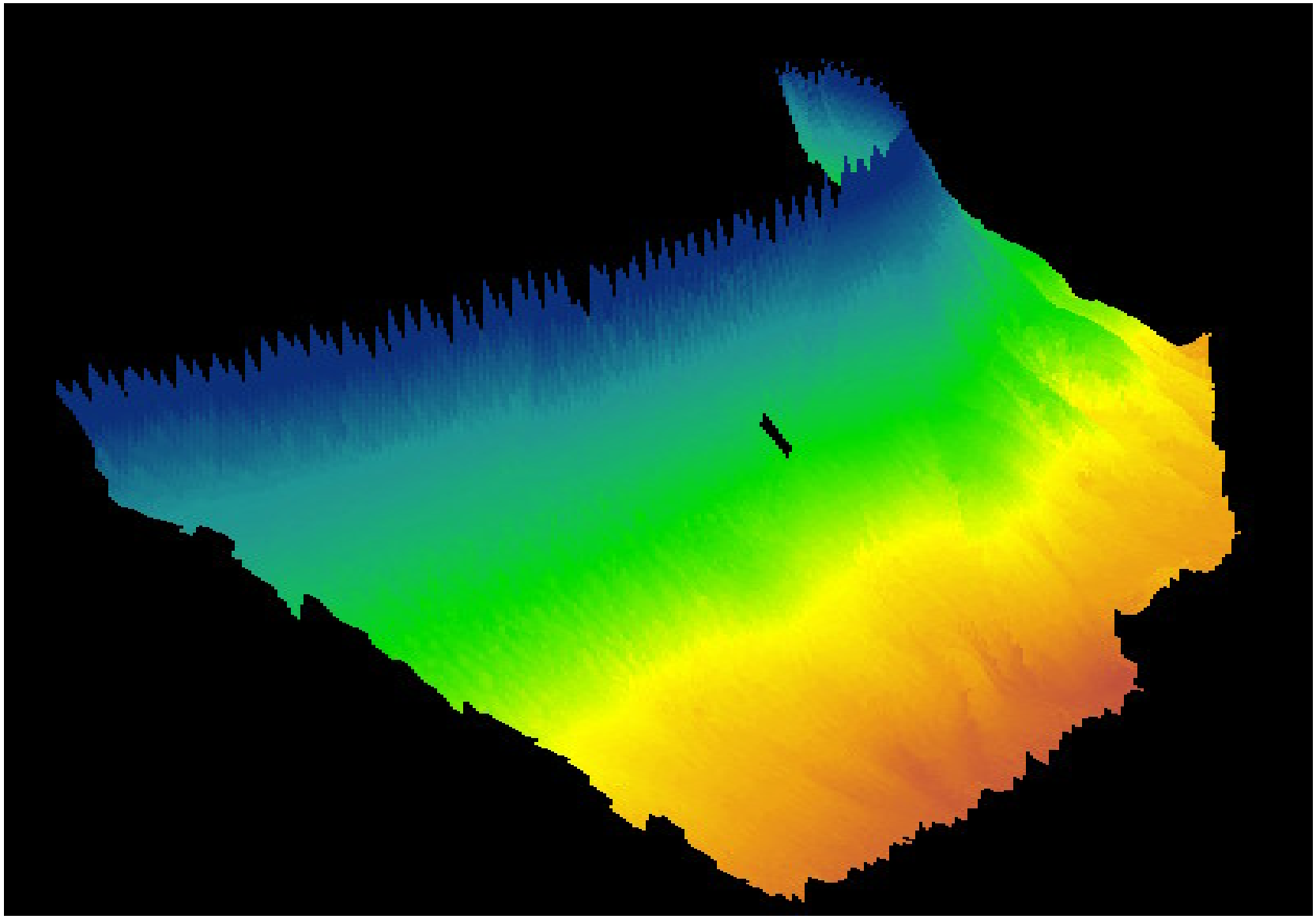

Figure A.17 3D view of multibeam at RM 80.00

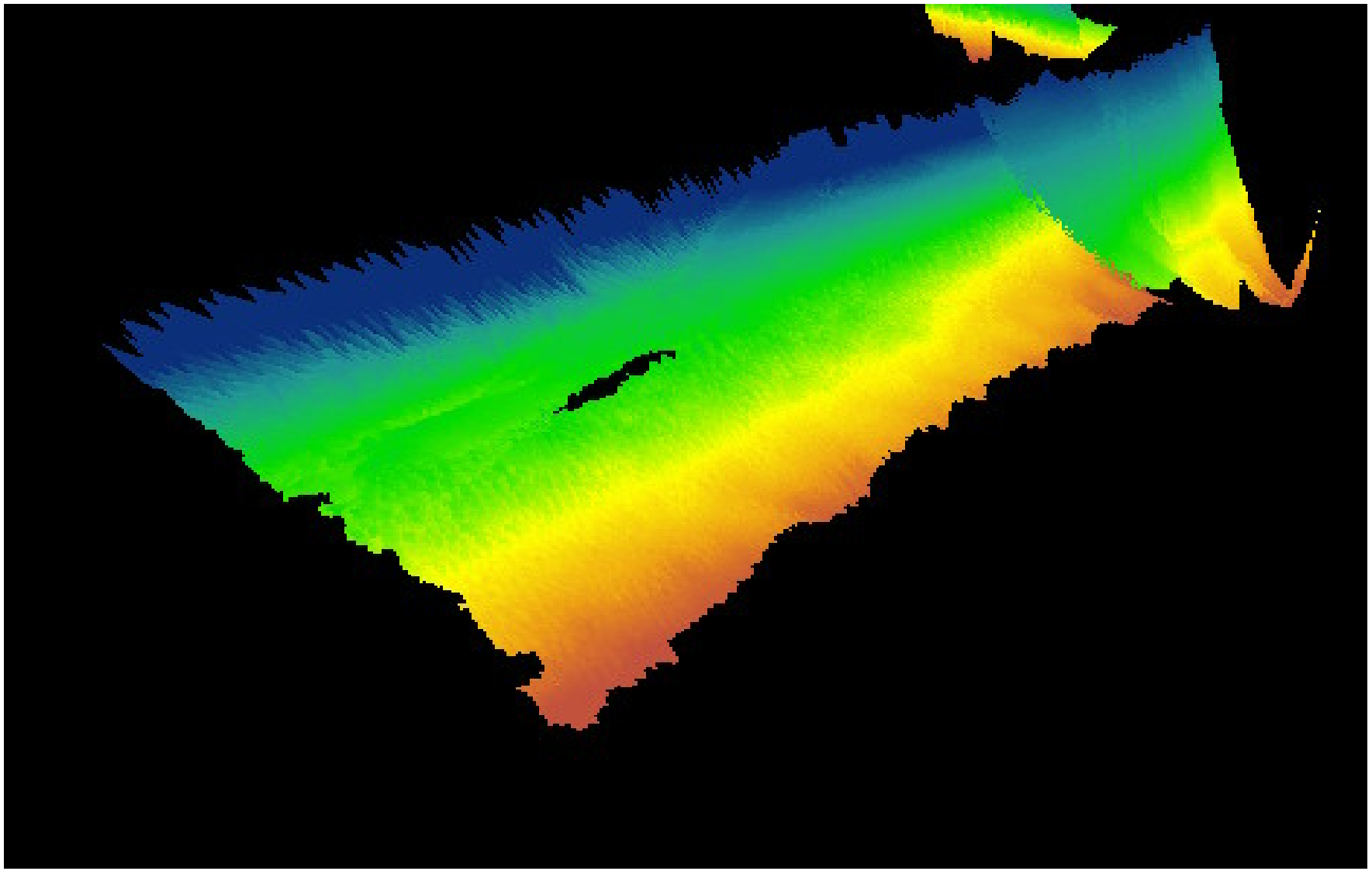

Figure A.18 3D view of multibeam at RM 84.00

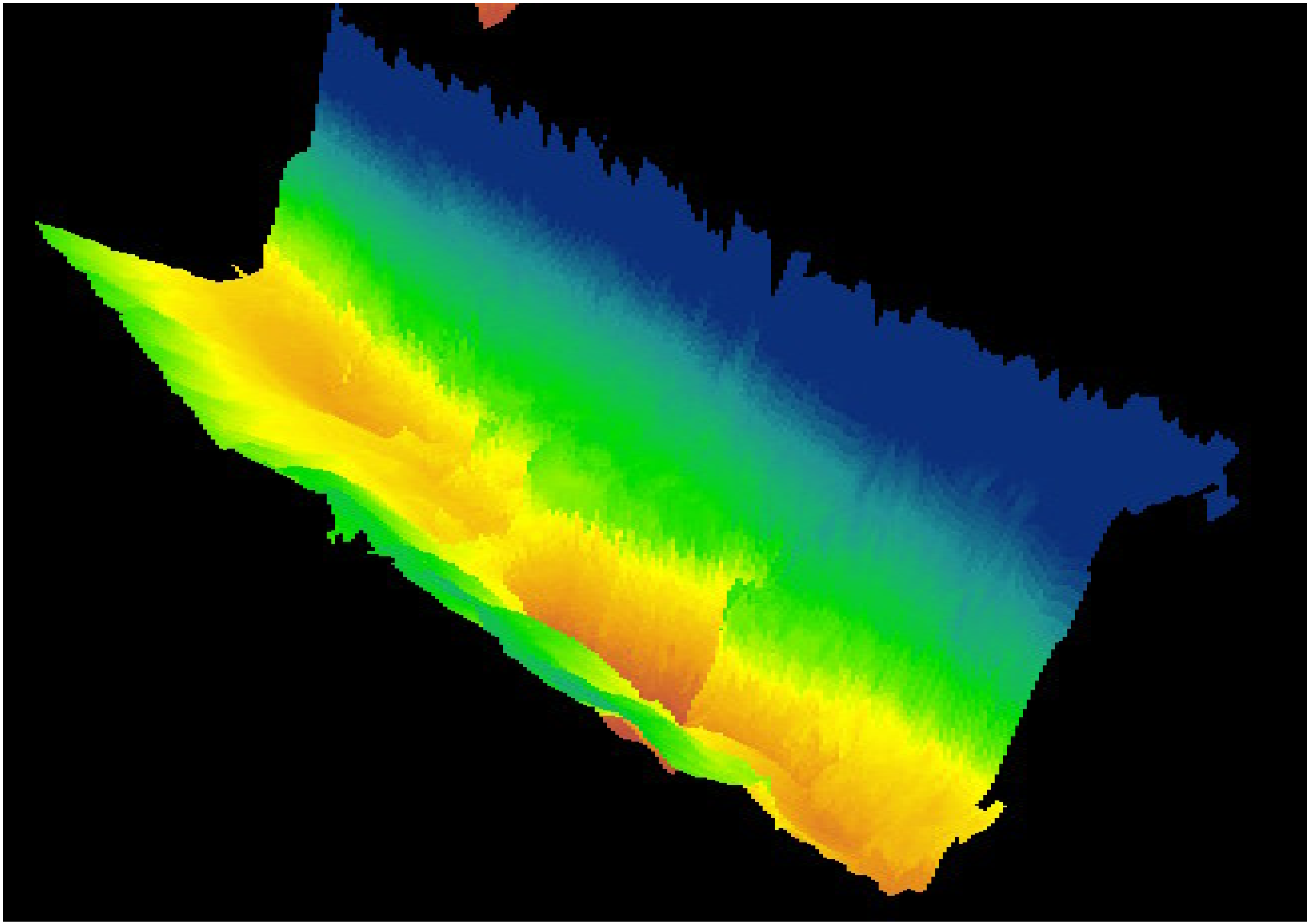

Figure A.19 3D view of multibeam at RM 87.50

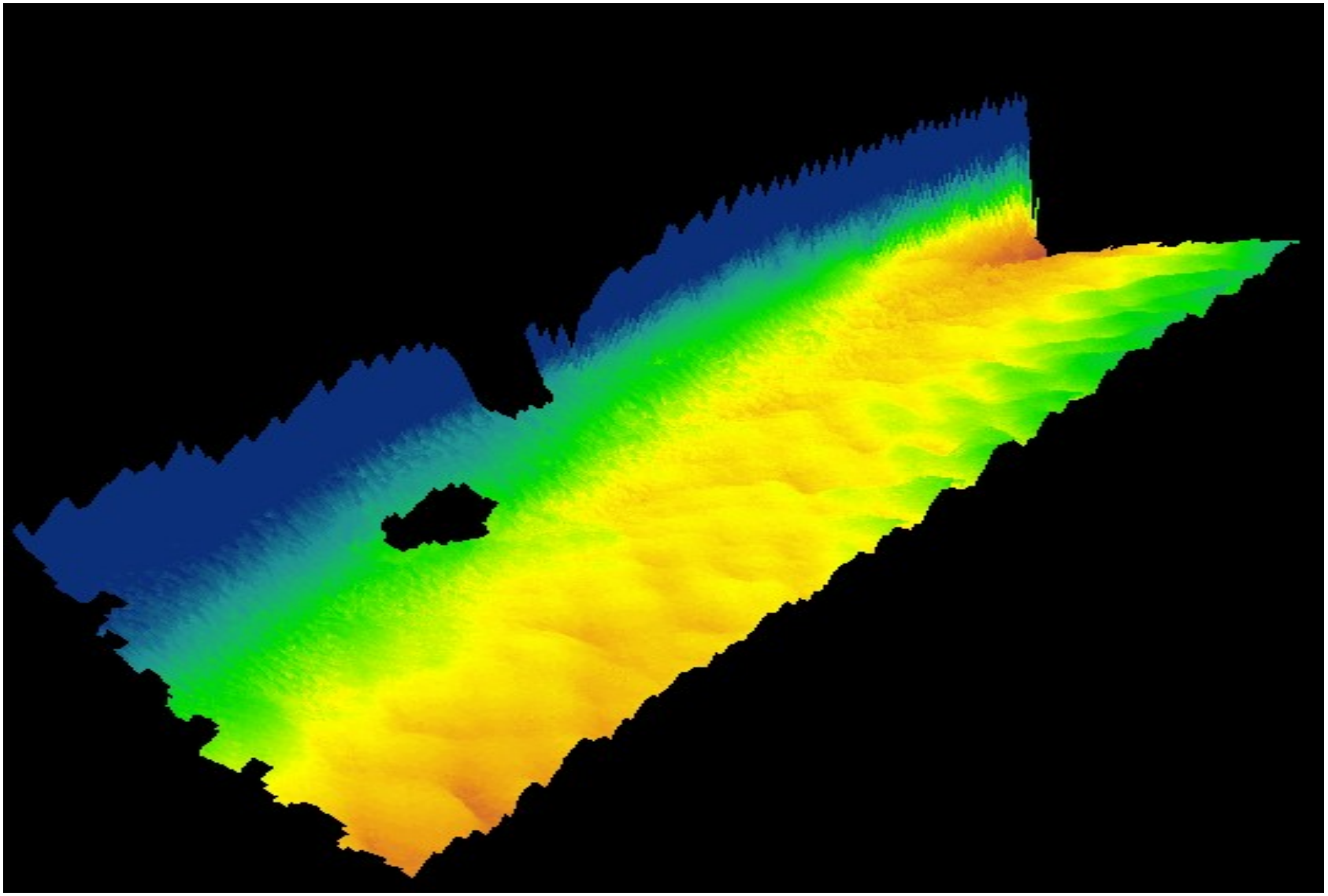

Figure A.20 3D view of multibeam at RM 175.00

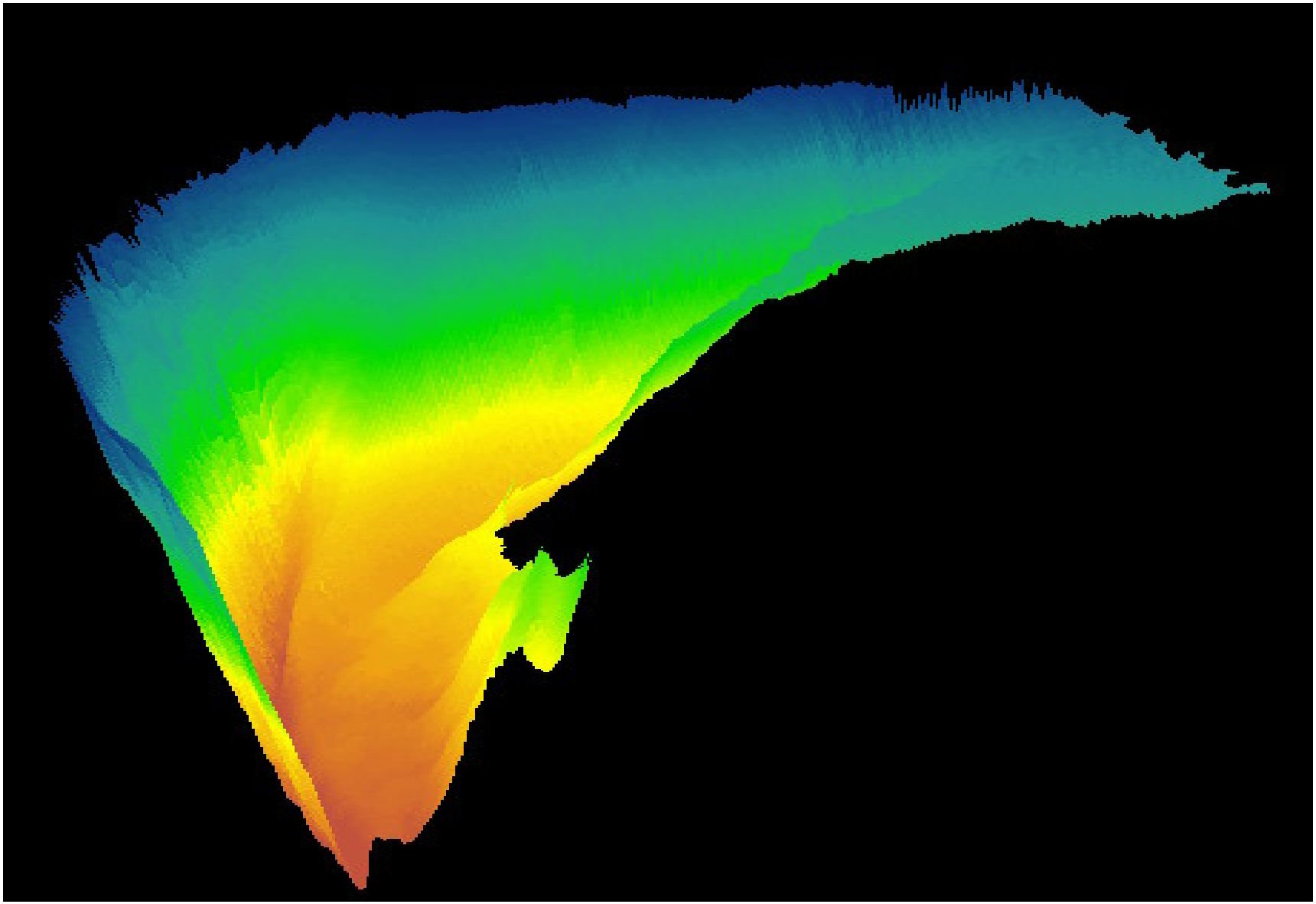

Figure A.21 3D view of multibeam at RM 178.50

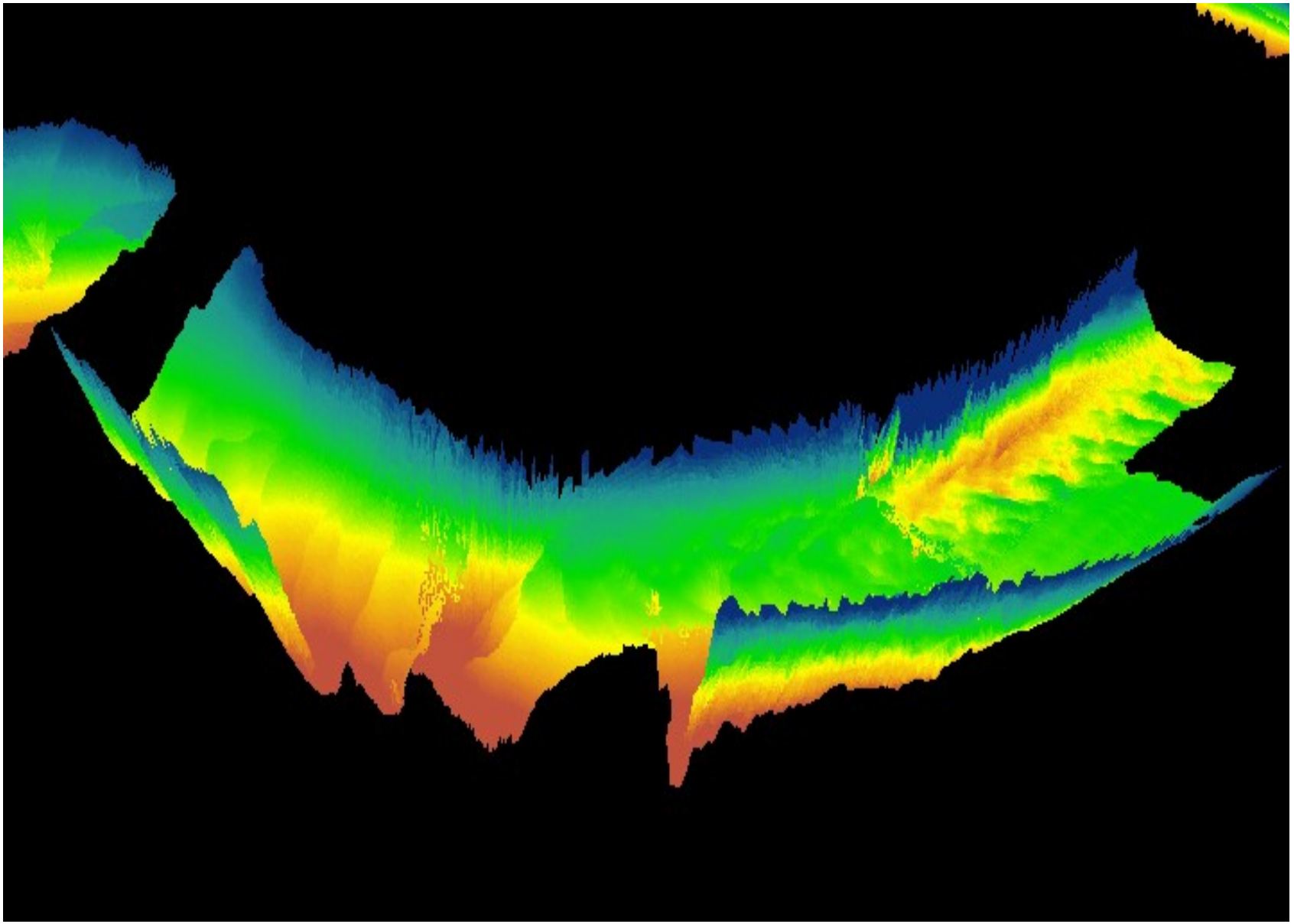

Figure A.22 3D view of multibeam at RM 180.10

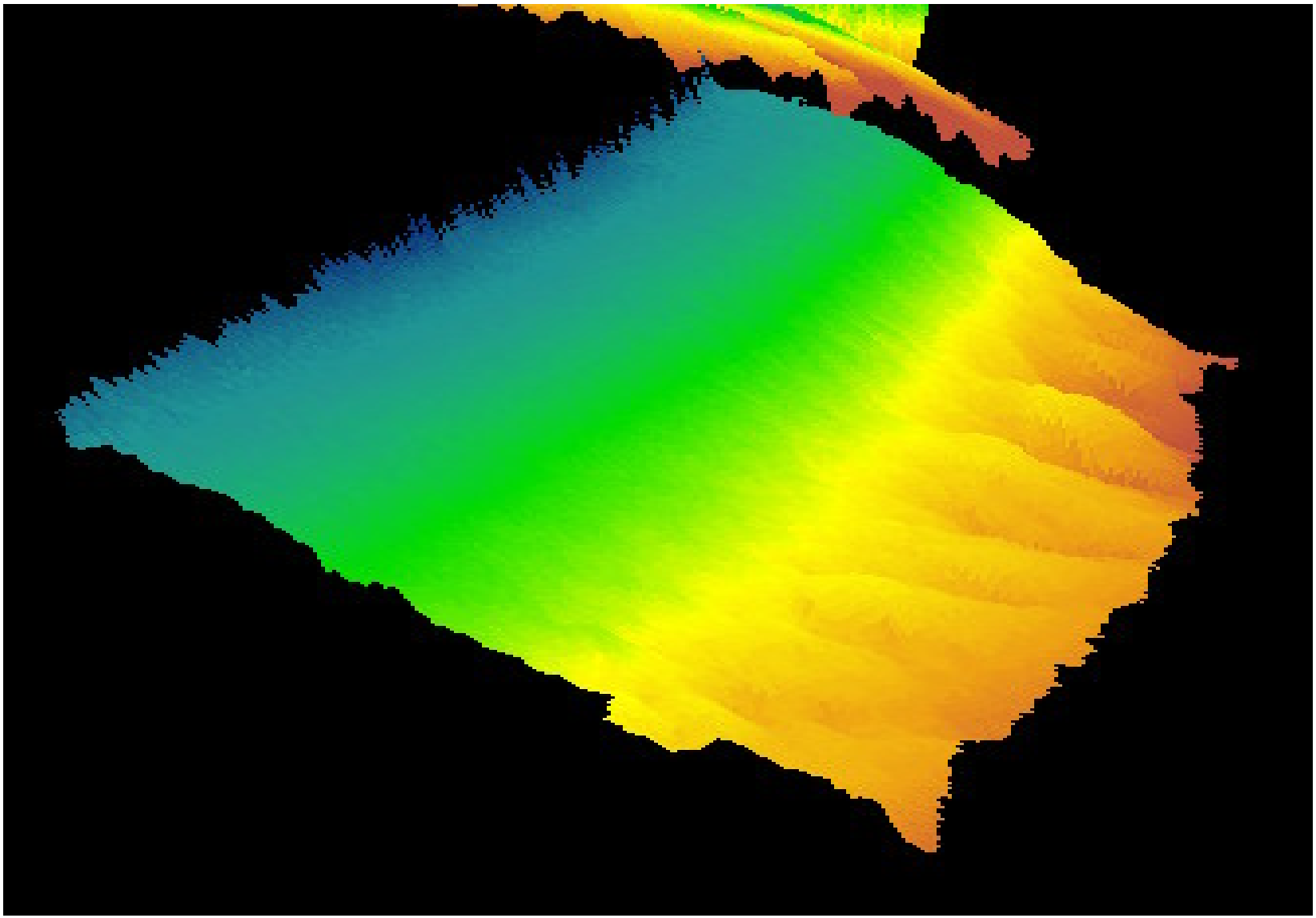

Figure A.23 3D view of multibeam at RM 184.75

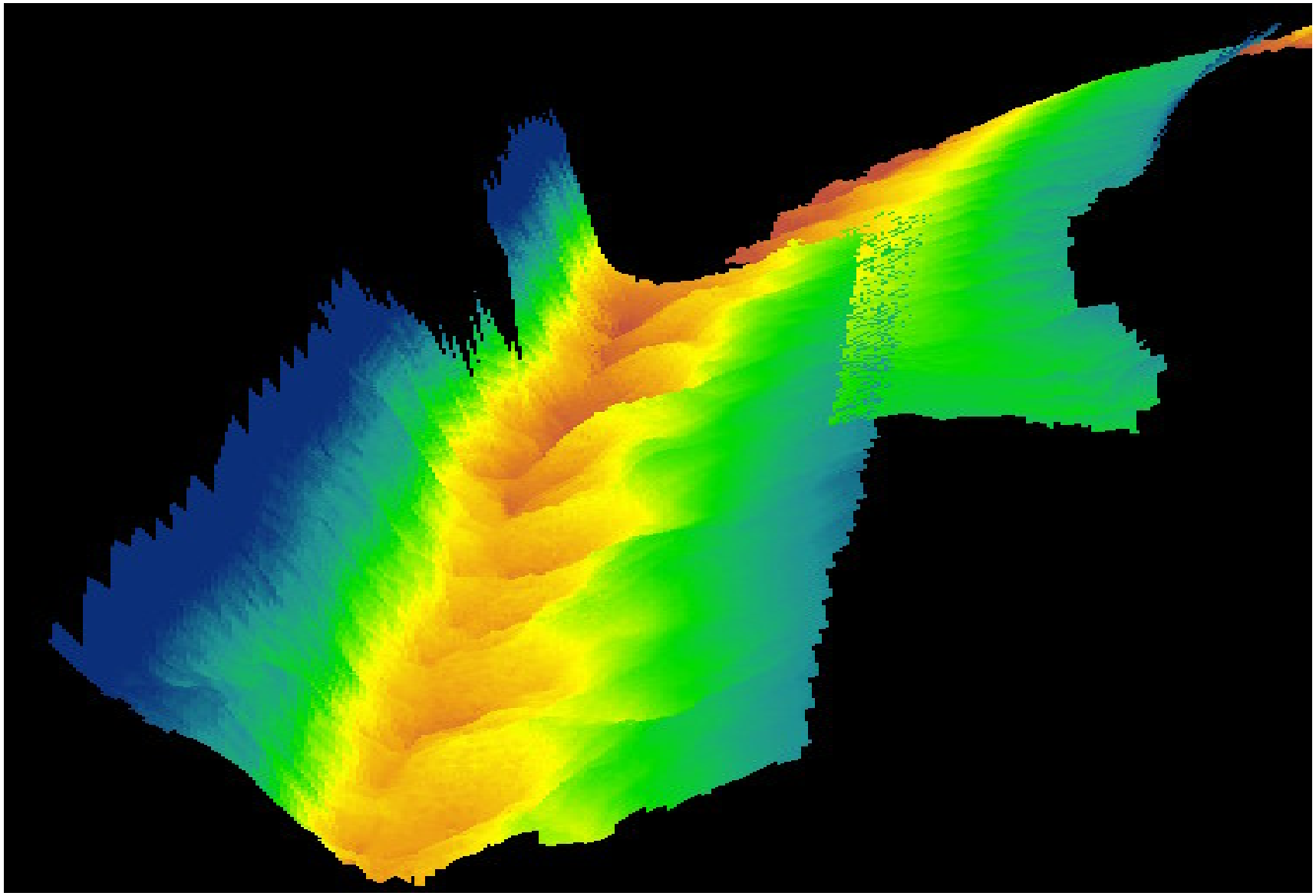

Figure A.24 3D view of multibeam at RM 186.50

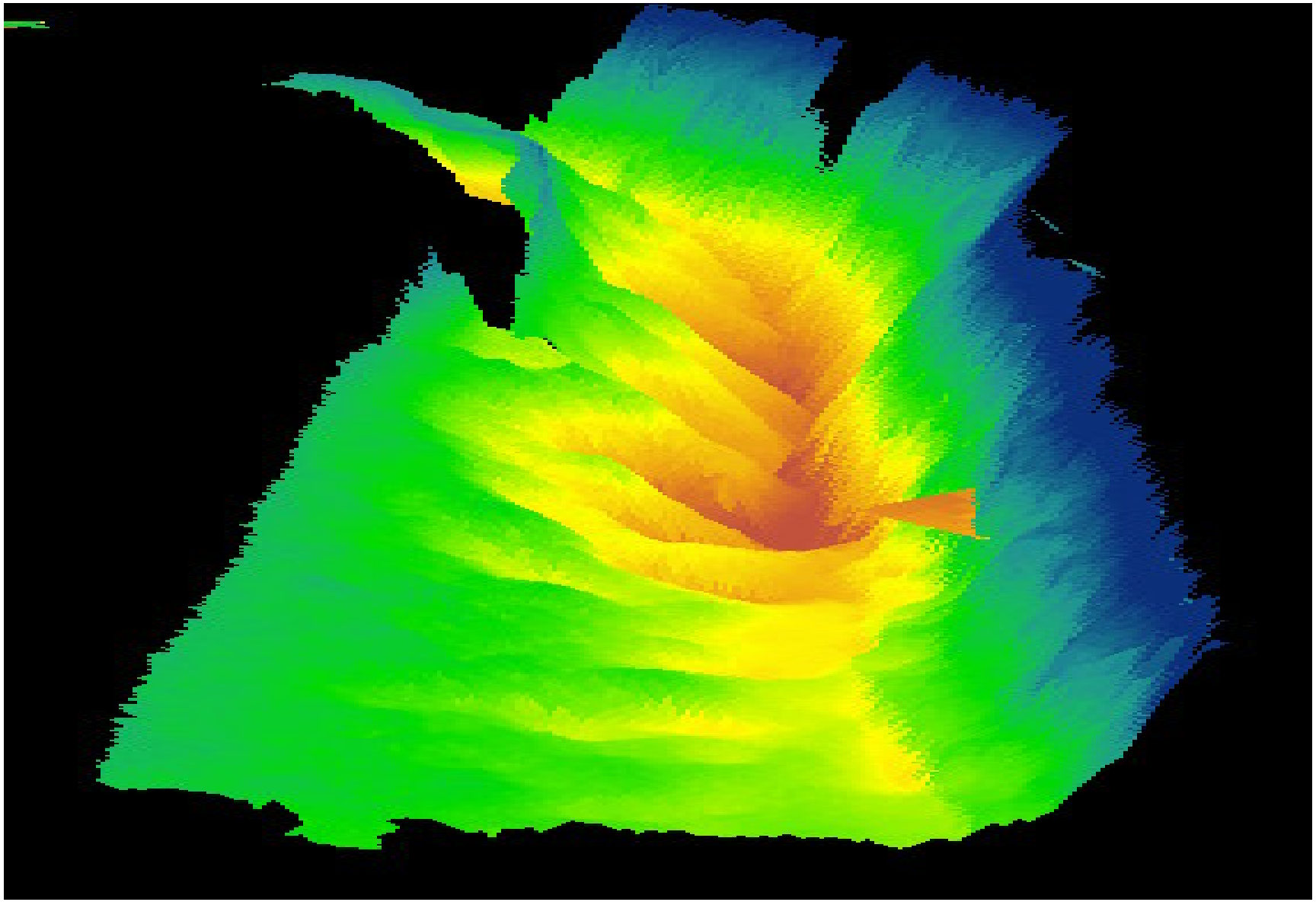

Figure A.25 3D view of multibeam at RM 198.00

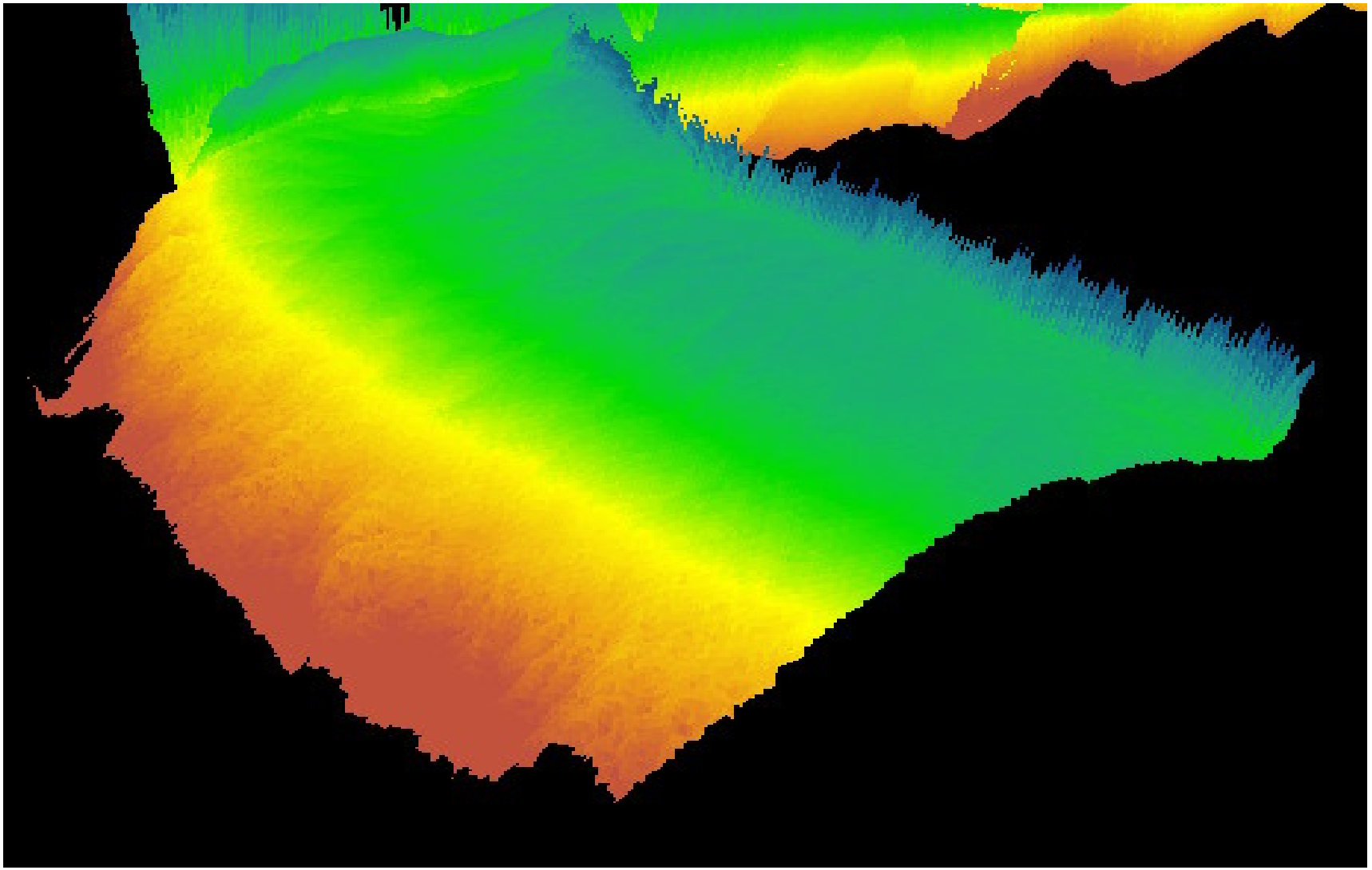

Figure A.26 3D view of multibeam at RM 201.00

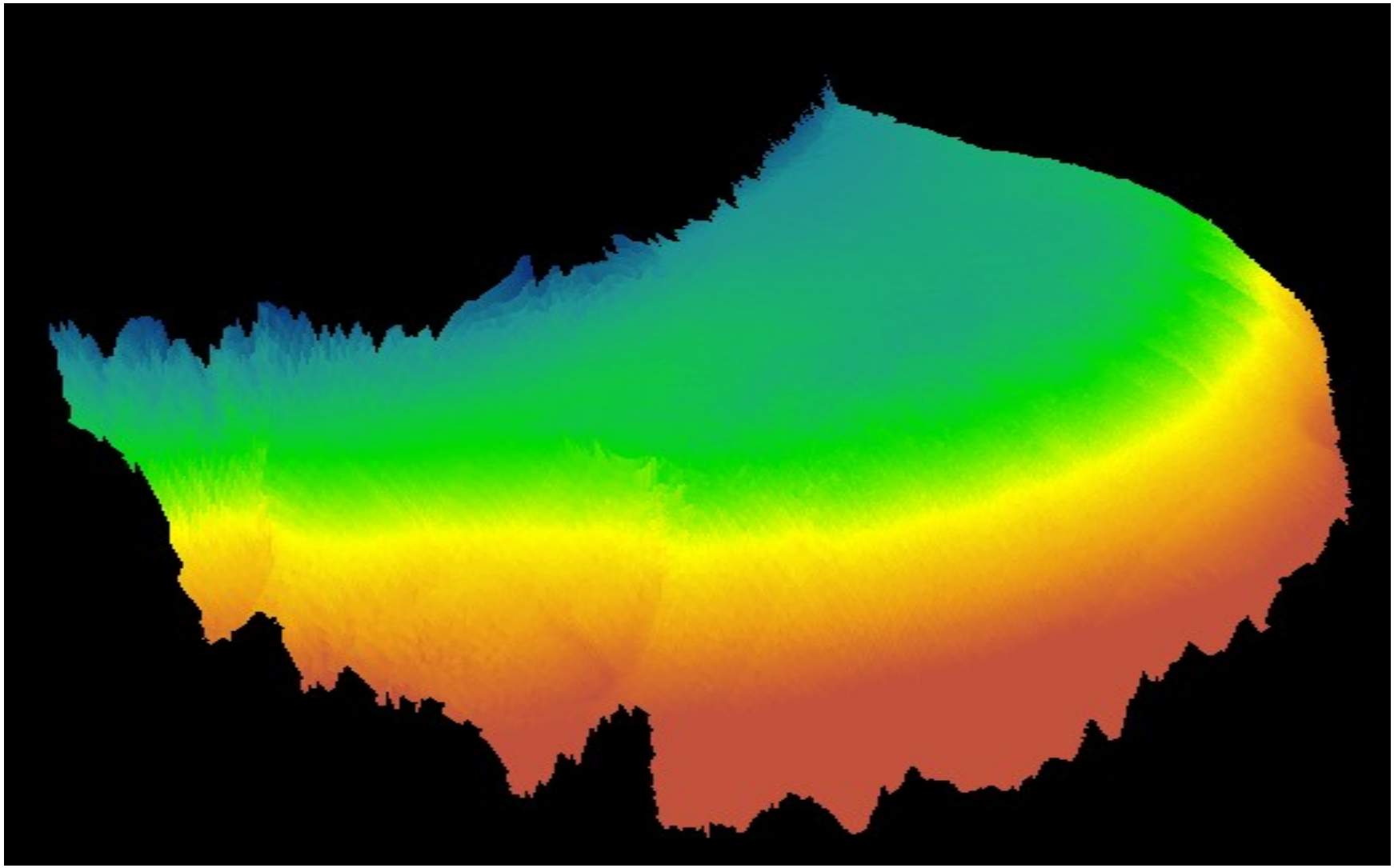

Figure A.27 3D view of multibeam at RM 215.00

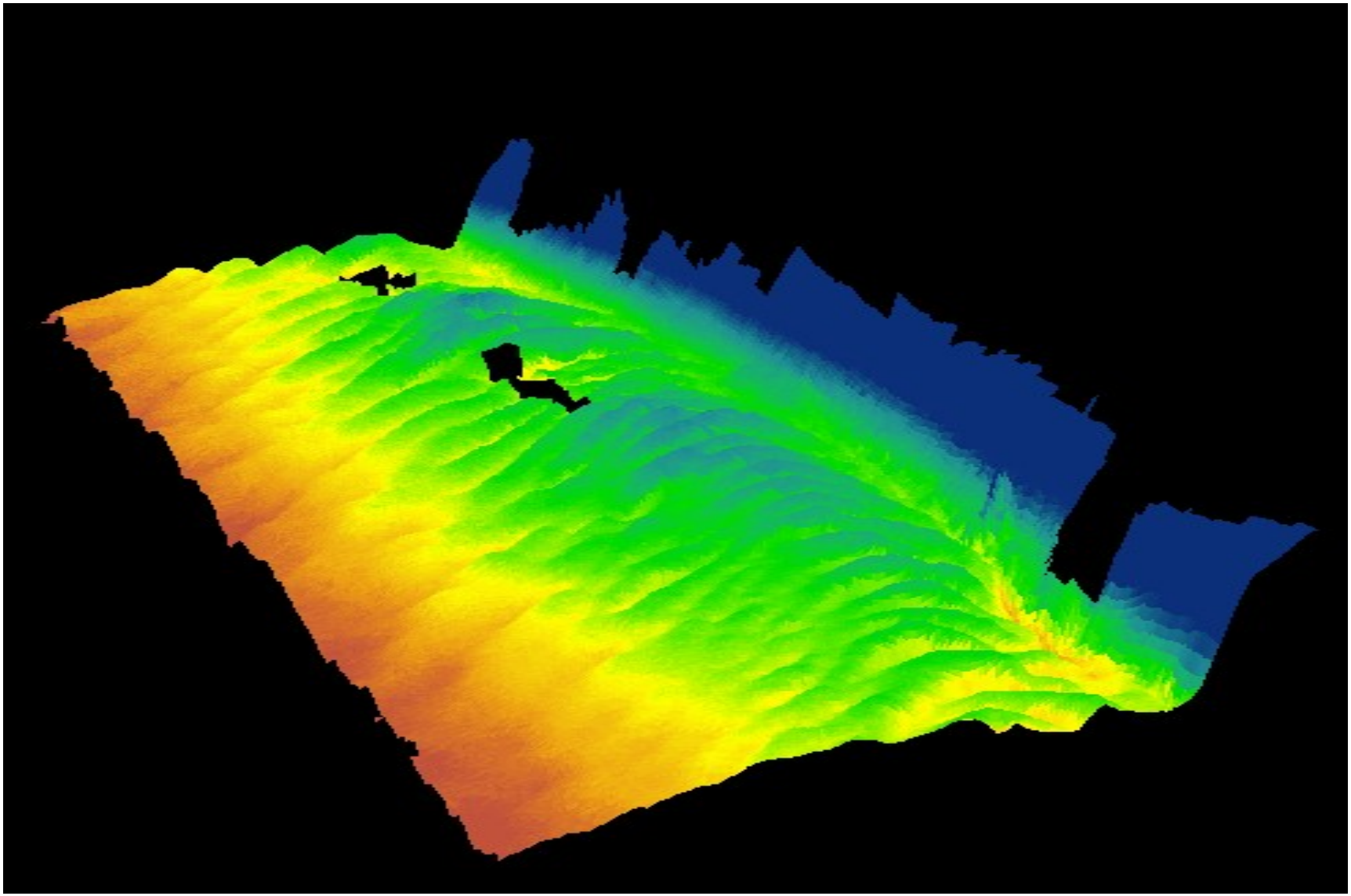

Figure A.28 3D view of multibeam at RM 223.00

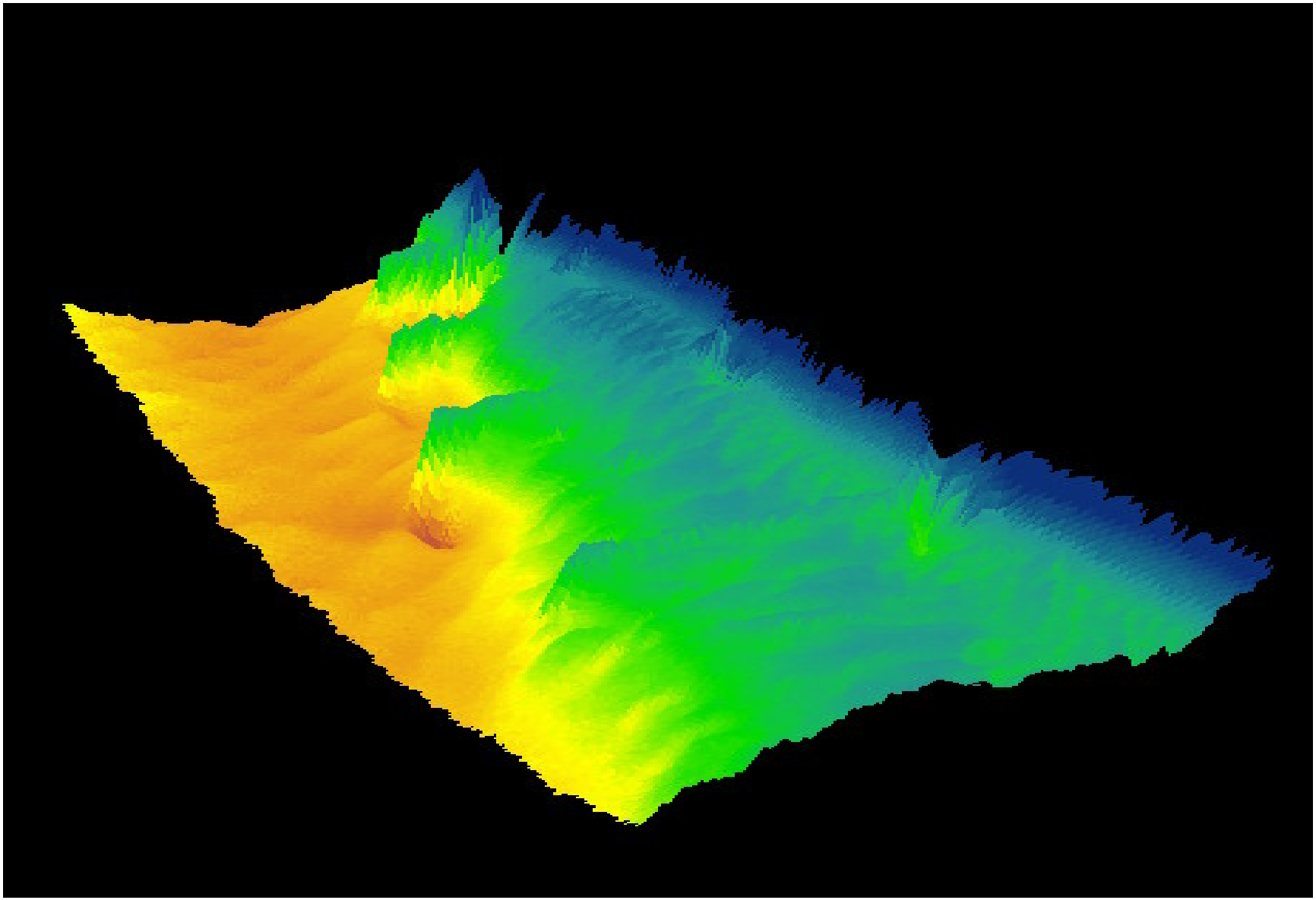

Figure A.29 3D view of multibeam at RM 224.00

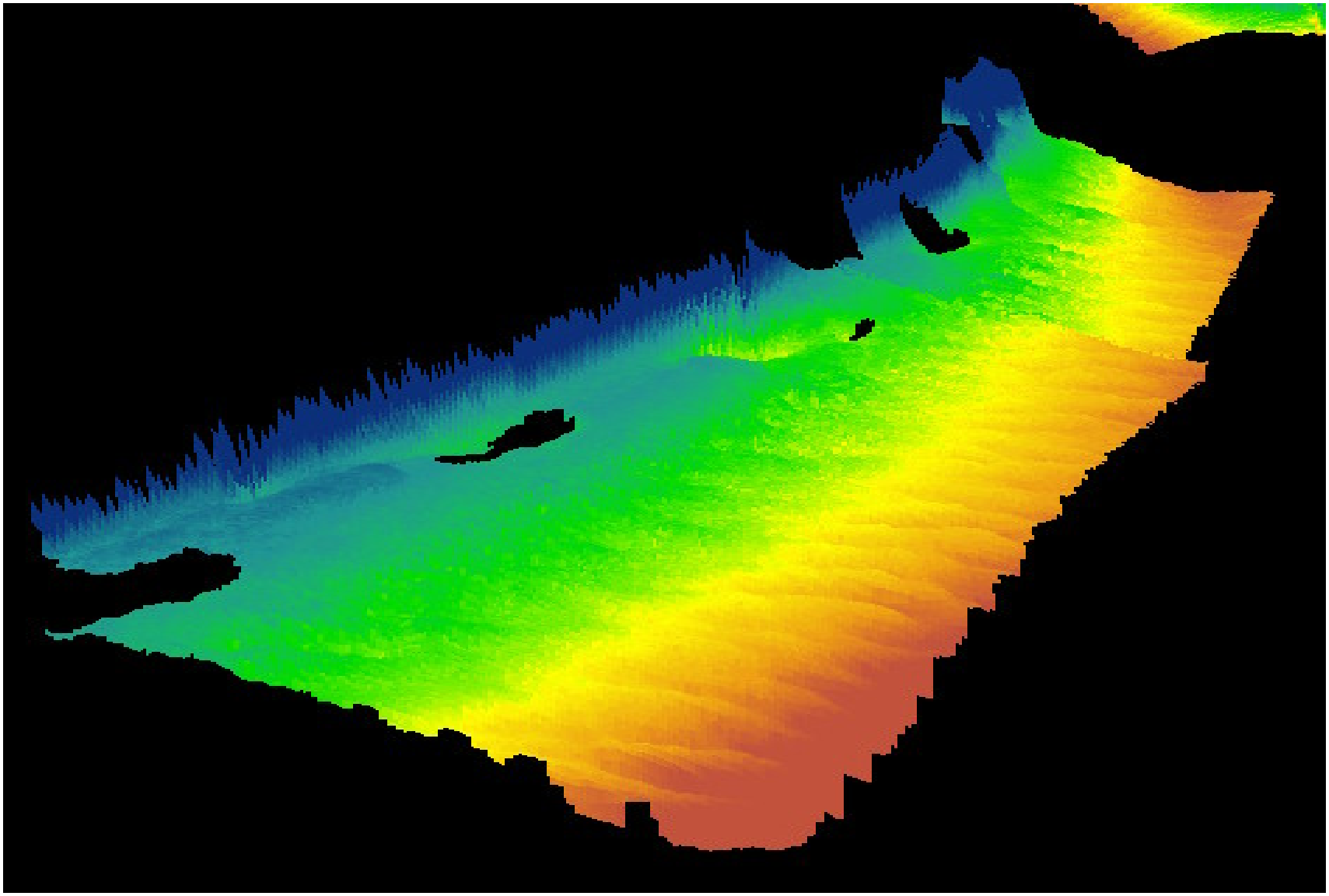

Figure A.30 3D view of multibeam at RM 226.00

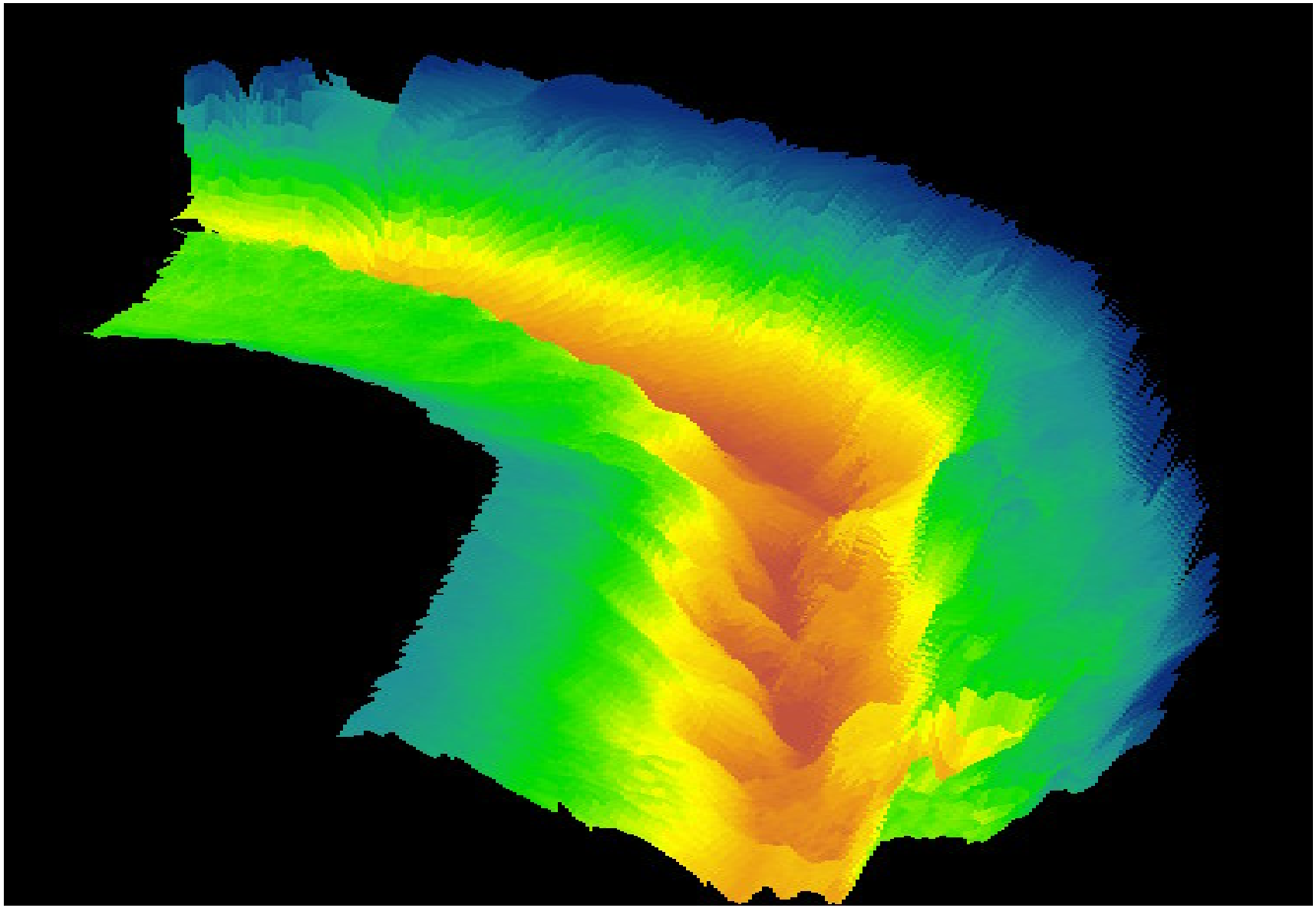

Figure A.31 3D view of multibeam at RM 234.00

VITA

Karim El Kheiashy holds a Bachelor of Science degree from Ain Shams University in Cairo, Egypt and a Masters of Science in Civil Engineering from the University of Louisiana at Lafayette. Mr. El Kheiashy has been employed by Dargroup International for the period of 2000-2001 and C.H. Fenstermaker and Associates for the period of 2002-2007. Mr. El Kheiashy is currently employed by KBR Inc. as a Principal Technical Professional. Mr. El Kheiashy is a licensed professional engineer (PE) in the state of Louisiana. As an experienced engineering professional, he has participated in a wide array of projects for the federal, state and private sector in the fields of water resources and coastal engineering. El Kheiashy is a member of the American Society of Civil Engineering (ASCE), Environmental and Water Resources Institute (EWRI) and the American Water Resources Association (AWRA). Mr. El Kheiashy is expected to finish his Doctorate degree in Civil Engineering from the University of New Orleans and a Masters of Business Administration from the University of Louisiana at Lafayette in May 2007.